ANALYSIS AND VISUALIZATION OF DIGITAL ELEVATION DATA FOR CATCHMENT MANAGEMENT

By

Mesfer Ali M Al-Yami

A thesis submitted for the degree of Doctor of Philosophy

University of East Anglia, Norwich

School of Environmental Sciences

September
2014

ABSTRACT

River catchments are an obvious scale for soil and water resources management, since their shape and characteristics control the pathways and fluxes of water and sediment. Digital Elevation Models (DEMs) are widely used to simulate overland water paths in hydrological models. However, all DEMs are approximations to some degree and it is widely recognised that their characteristics can vary according to attributes such as spatial resolution and data sources (e.g. contours, optical or radar imagery). As a consequence, it is important to assess the 'fitness for purpose' of different DEMs and evaluate how uncertainty in the terrain representation may propagate into hydrological derivatives.

The overall aim of this research was to assess accuracies and uncertainties associated with seven different DEMs (ASTER GDEM1, SRTM, Landform Panorama (OS 50), Landform Profile (OS 10), LandMap, NEXTMap and Bluesky DTMs) and to explore the implications of their use in hydrological analysis and catchment management applications. The research focused on the Wensum catchment in Norfolk, UK. The research initially examined the accuracy of the seven DEMs and, subsequently, a subset of these (SRTM, OS 50, OS10, NEXTMap and Bluesky) were used to evaluate different techniques for determining an appropriate flow accumulation threshold to delineate channel networks in the study catchment. These results were then used to quantitatively compare the positional accuracy of drainage networks derived from different DEMs. The final part of the thesis conducted an assessment of soil erosion and diffuse pollution risk in the study catchment using NEXTMap and OS 50 data with SCIMAP and RUSLE modelling techniques.

Findings from the research demonstrate that a number of nationally available DEMs in the UK are simply not 'fit for purpose' as far as local catchment management is concerned. Results indicate that DEM source and resolution have considerable influence on modelling of

hydrological processes, suggesting that for a lowland catchment the availability of a high resolution DEM (5m or better) is a prerequisite for any reliable assessment of the consequences of implementing particular land management measures.

Several conclusions can be made from the research. (1) From the collection of DEMs used in this study the NEXTMap 5m DTM was found to be the best for representing catchment topography and is likely to prove a superior product for similar applications in other lowland catchments across the UK. (2) It is important that error modelling techniques are more routinely employed by GIS users, particularly where the fitness for purpose of a data source is not well-established. (3) GIS modelling tools that can be used to test and trial alternative management options (e.g. for reducing soil erosion) are particularly helpful in simulating the effect of possible environmental improvement measures.

TABLE OF CONTENTS

Chapter 5:   Threshold Definition

Chapter 6: Comparing automated drainage networks derived from DEMs

Chapter 7: Modelling of Soil Erosion and Diffuse pollution

Chapter 8: Conclusions

LIST OF FIGURES

XII

km², respectively.

correspondence.

XV

assumed to be cultivated with strip tillage.

LIST OF TABLES

XVIII

season 2011/12 and 2012/13.

LIST OF ABBREVIATIONS

ASTER	Advanced Spaceborne Thermal Emission and Reflection Radiometer
CSA	Critical Source Areas
CSF	Catchment Sensitive Farming
CGIAR-CSI	Consultative Group for International Agricultural Research Consortium for Spatial Information
DEFRA	Department of the Environment, Food and Rural Affairs
DEM	Digital Elevation Model
DSM	Digital Surface Model
DTC	Demonstration Test Catchments
DTM	Digital Terrain Model
D8	Deterministic 8-Direction
ERS	European Radar Satellite
ERSDAC	Earth Remote Sensing Data Analysis Centre
FGDC	Federal Geographic Data Committee
GDEM1	Global Digital Elevation Model Version 1
GDEM2	Global Digital Elevation Model Version 2
GIS	Geographical Information Systems
HGCA	Home Grown Cereals Authority
IDB	Internal Drainage Board
IFSAR	Interferometric Synthetic Aperture Radar
InSAR	Interferometric Synthetic Aperture Radar
JAXA	Japan Aerospace Exploration Agency
LCM 2007	Land Cover Map 2007
LiDAR	Light Detection and Ranging
ME	Mean Error
METI	Ministry of Economy, Trade and Industry

MFD	Multiple Flow Direction
NDVI	Normalised Difference Vegetation Index
NSSDA	National Standards for Spatial Data Accuracy
NTU	Nephelometric Turbidity Unit
OMAFRA	Ontario Ministry of Agriculture Food and Rural Affairs
OS	Ordnance Survey
OSGB36	Ordnance Survey Great Britain 1936
RBMP	River Basin Management Planning
RMSE	Root Mean Square Error
RUSLE	Revised Universal Soil Loss Equation
SAC	Special Area of Conservation
SD	Standard Deviation
SCIMAP	Sensitive Catchment Integrated Modelling and Analysis Platform
SRTM	Shuttle Radar Topography Mission
SSSI	Sites of Special Scientific Interest
SWAT	Soil and Water Assessment Tool
TIN	Triangular Irregular Networks
USEPA	US Environmental Protection Agency
USGS	United States Geological Survey
USLE	Universal Soil Loss Equation
WEPP	Water Erosion Prediction Program
WFD	Water Framework Directive
WGS84	World Geodetic System 1984

ACKNOWLEDGEMENT

Chapter 1

Introduction

1.1 Research context

The watershed, also termed catchment or river drainage basin, is a basic environmental unit where all surface water runoff flows downhill to a point on a stream (Gordon et al. 2004; Holden, 2014). It is an area defined naturally by surface water hydrology (Defra, 2013). A catchment is recognized as an appropriate scale for soil and water resources planning and management (Prato and Herath, 2007). Soil erosion and sediment transport, storage, and remobilization are controlled by hydrological and geomorphological processes which operate within the context of a catchment scale. Therefore, catchments are the natural scale for the assessment of soil erosion potential, and consequently water quality, since their shape and characteristics control the pathways and fluxes of water and sediment (Collins and Owens, 2006). It is now increasingly recognised that better coordinated action by all those who use water or influence land management is desirable at the catchment level. This, for instance, is central to the EU Water Framework Directive (WFD), a fundamental feature of which is the use of river catchments as reference units (Volk et al., 2010). The overall purpose of WFD is to achieve good ecological status for all European water bodies from 2015 onwards through the implementation of river basin management planning (RBMP) processes in all EU member states (Smith et al., 2014).

It is clear that catchments are an important functional entity for hydrological and landscape processes. Environmental processes are altered as landscape features are

manipulated and changed by human activities and the catchment is a natural scale to consider this aspect of the environment. In the UK this has been reflected in the promotion of the catchment-based approach to management and planning of the water environment with increasing support for local river trusts and research initiatives such as the Demonstration Test Catchments (DTC) programme (Defra, 2013; McGonigle et al., 2014).

The catchment area is an ideal unit to work with when looking at the land use management issues because everything is linked by water. What happens in one part of a catchment is likely to affect the remainder of the area. For example, a soil erosion problem in a farm in the upper headwaters may lead to diffuse pollution problems in lower parts of the catchment. The extent of such connections will depend on the topography, soil and geology of the catchment (Wu et al., 2007). Where the soil and geology are relatively impermeable the topography will be the key influence on the distribution and flux of water within the catchment landscape. The digital representation of topography is termed a Digital Elevation Model (DEM). A DEM is therefore a core spatial dataset for catchment planning and management (McDougall et al., 2008).

1.1.1 The importance of DEMs

More generally, DEMs are one of the most fundamental types of spatial data used in Geographical Information Systems (GIS) (Li et al., 2005: Zhou et al., 2008). DEMs are a form of surface model widely employed in spatial modelling applications and for environmental modelling in particular. They are essential for a wide range of applications in hydrology, geomorphology, ecology and other related fields (Maune, 2007; Li et al., 2005). These digital representations of topography can be used to perform numerous topographic analyses, such as calculations of slope, aspect, wetness index, topographic roughness and curvature among other topographic attributes (Lyon. 2003; Wilson, 2012; Wilson and Gallant, 2000). An extension of such topographic analysis is hydrographic feature extraction, which

includes delineation of stream profiles and catchments, and derivation of stream networks that represent catchment drainage (Liu and Zhang, 2011; Poggio and Soille, 2011; Gallego et al., 2010; Mantelli et al., 2011; Hengl et al., 2009; Joowon, 2011, Vianello et al., 2009). Many hydrological processes, such as soil erosion and sediment transport are strongly dependent on the landscape topography and linked to catchment as the spatial reference unit.

1.1.2   Sources of DEMs

Terrain data acquisition is the primary stage in digital elevation modelling. DEMs can be created from a number of different data sources as summarised in Table 1.1. Traditionally, these data have been obtained directly from field survey using surveying instruments such as a total station or GPS, digitising information from existing topographic maps, or photogrammetric techniques (Li et al., 2005). These traditional methods can yield highly accurate digital elevation data, but they are also time consuming and labour intensive.

In the UK, Ordnance Survey (OS) DEMs have been a common sources of terrain data. The Ordnance Survey (OS) created 50 m Landform Panorama and 10 m Landform Profile digital terrain models (DTMs) from interpolation of mapped contour lines during the 1980s. These contour data were themselves captured from map series completed during the 1970s and 1980s using photogrammetric techniques (Ordnance Survey, 2010a and b).

During the past decade great progress has been made in more automated methods for DEM generation, particularly over larger regions and at the global scale. Remote sensing from both airborne and spaceborne sensors now provides an excellent source of worldwide DEM coverage (Wilson, 2012). This involves the use of optical satellite sensors, such as the Advanced Spaceborne Thermal Emission and Reflection Radiometer (ASTER) (ASTER Validation Team, 2009) and radar remote sensing sensors, such as the Shuttle Radar Topography Mission (SRTM) (Reuter et al., 2007).

The SRTM was a single pass interferometric synthetic aperture radar (IFSAR) mission conducted in February 2000 (Reuter et al. 2007). It was the first time that a global high-quality DEM was produced with a resolution of 1 arc-second (approx. 30 m) and 3-arc second (90 m), however of these two datasets only 90 m data are available globally, while the 30 m data are restricted to USA territory (Jarvis et al. 2008). The ASTER GDEM is derived from stereo processing of imagery from the ASTER instrument on the Terra satellite. Version 1 of the ASTER GDEM (a global 1 arc-second (30 m) elevation dataset) was released to the public in June 2009 (Hirt et al., 2010). An improved version of ASTER GDEM (ver. 2) was released in October 2011 (ASTER GDEM Validation Team, 2011). Currently there are two new satellite and sensor systems aiming to produce a global DEMs of even higher accuracy. These two missions are TanDEM-X which aims to produce a global 12 m resolution DEM based on IFSAR images, which will be available during 2014 (DLR, 2014), and the JAXA mission aiming to release a global 5 m resolution DEM (PRISM 5m DEM) during 2016 based on three optical systems on the ALOS satellite (JAXA, 2014).

Aerial photogrammetry and airborne radar interferometry have been used commercially to produce national coverage of high resolution DEMs. For example, the Bluesky 5m data were photogrammetrically interpolated from stereoscopic aerial photography and are available for England and Wales from the JISC Landmap service (Landmap 2011). Another example is the NEXTMap 5m data produced using an airborne IFSAR system for the USA, UK and some other countries within Europe and Asia by Intermap Technologies (Intermap, 2011). A further source of DEM information is LiDAR, which uses laser equipment on aircraft and can create very accurate and high spatial resolution representations of topography. At present, LiDAR is more of a local or regional data resource (e.g. for cities or coastal areas), but it is increasing in availability all the time (Goodchild, 2009; Robert et al., 2007). In response to all these advances in the production of DEMs, many studies have investigated the effects of

DEM data sources and resolutions on the creation of an accurate representation of the Earth's

surface and on derived topographic attributes (e.g. McDougall et al., 2008; Vaze et al., 2010).

Table 1.1: Key characteristics of DEM different data sources.

Source	Resolution (m)	Accuracy	Elevation/surface
Ground survey	Variable but usually <5 m	Very high vertical and horizontal	Elevation
GPS	Variable but usually <5 m	Very high vertical and horizontal	Elevation
Topo-map	Depends on map scale and contour interval	Very high vertical and horizontal	Elevation
Ortho-photography	<1	Very high vertical and horizontal	Surface
LiDAR	1-3	0.15-1 m vertical, 1 m horizontal	Surface
InSAR/IfSAR	2.5-5	1-2 m vertical, 2.5-10 m horizontal	Surface
SRTM	90	16 m vertical, 20 m horizontal	Surface
ASTER	30	7-50 m vertical, 7-50 m horizontal	Surface
TanDEM-X	12	2-10 m vertical, ≤10 m horizontal	Surface
JAXA	5	5 m vertical	Surface

Modified from Wilson, 2012; Nelson et al. (2010). TanDEM-X information were taken from Krieger et al., (2007), (DLR, 214) and JAXA DEM from (JAXA, 2014).

1.1.3 Error and uncertainty in DEMs

Whatever the source of data all DEMs contain some inherent errors and these result in uncertainty regarding height values (Liu and Bian, 2008). This uncertainty in the DEM representation of the terrain surface propagates to the hydrological derivatives (e.g. slope, aspect) computed from the DEM (Wechsler, 2007: Wilson, 2012). Accuracy can affect the usefulness of a DEM dataset in hydrological applications, particularly in low relief areas (Chirico, 2004). For example, it can be important to assess the probability of an incorrect output from a hydrological flow model when a particular DEM is used (Darnell et al., 2010). It is common to admit that the accuracy of surface features will depend on the resolution and

vertical accuracy of the DEM being used. However, some research (e.g. Hirt et al., 2010; Li and Wong, 2010; Zandbergen, 2006; Zhou and Liu, 2004) has demonstrated that coarser scale DEMs are sometimes more accurate in their representation of terrain surfaces, and that this can depend on the characteristics of the terrain itself and the nature of the analysis conducted (Wechsler, 2007).

From a practical point of view it is therefore important to regard the quality of a DEM as a combination of DEM accuracy and the suitability for a certain application (e.g. surface water flow path modelling) (Peckham and Jordan, 2007). Knowledge of the source data used to derive a DEM and its impact on hydrological derivatives can help when choosing an elevation dataset for a particular application. In other words, quantification of the accuracy associated with various DEMs (different sources and different resolutions) and subsequent hydrologic derivatives, drainage networks and catchment boundaries would assist other potential users in determining whether or not a specific dataset was appropriate for a particular application at a certain scale (i.e. fit for purpose).

As stated previously in Section 1.1.2, different sources, sensors, and formats with different characteristics like accuracy and spatial resolution have been developed to meet the rising demand for elevation data. Therefore, it is important that a user has an idea of how accurate a DEM that was created with a certain method is going to be used for a particular application (i.e. in catchment management) and the level of accuracy that can reasonably be expected. Numerous approaches have been developed to assess the accuracy of DEM elevation values (Reuter et al., 2009; Wilson, 2012). This includes quantitative assessments of DEM accuracy as well as qualitative assessments of data usefulness (Carrara et al., 1997; Maune, 2007; Wilson and Gallant, 2000).

Many researchers have compared a set of heights extracted from the DEM with reference elevation values taken from a more accurate source of topographic data and then calculate the root mean square error of elevation (RMSE) to represent the differences between the estimated (DEM) and reference values (Hirt et al., 2010; Maune, 2007; Schumann et al., 2008; Wise, 2000; Wu et al., 2008). To fully address the DEM data for overall quality and suitability for an intended product, a qualitative assessment should also be performed. This may involve visually inspecting the spatial pattern of the DEM or its derivatives by means of a variety of rendering tools, such as shaded relief maps or other display techniques (Carrara et al., 1997; Maune, 2007).

1.1.4 Drainage network extraction from DEMs

In hydrology the accurate delineation of surface water drainage networks is a prerequisite for investigation of many catchment-based natural resource management issues (Liu and Zhang, 2011) and is useful, for example, in distributed hydrological modelling, estimation of source areas, drainage density and downslope flow path length (Orlandini et al., 2011; Wilson, 2012). Surface water flow path is one of the most important hydrological parameters and investigation of the location of such networks within a watershed is vital. Ferrier and Jenkins (2010) argued that one of the key principles towards developing sustainable management of catchments is to understand the natural processes occurring within a catchment and in particular, to determine the physical pathways of water movement throughout the catchment landscape. The positive outcome of this will be seen in water management by helping land managers to choose the best management practices for maintaining water quality (Vieux, 2005).

Automated derivation of drainage networks and catchment boundaries from DEMs is a well-established technique used in terrain analysis (Vogt et al., 2003) and is primarily limited by landscape relief and DEM resolution (McMaster, 2002). The most commonly used

approach is based on the deployment of a model for surface water flow accumulation. As the flow of water is traced downhill from a point, flow accumulation is computed for all the downstream points through which the water flows such that an area threshold can be set whereby any points with an accumulation area higher than the threshold are defined as streams (Colombo et al., 2007). This threshold represents the minimum contributing area needed to form and maintain a drainage network. The choice of flow accumulation threshold influences the extracted drainage network (Lin et al., 2006; Orlandini et al., 2011). As the extraction of drainage networks in a catchment is the first step in the simulation of hydrological processes (Paik, 2008), the choice of an appropriate threshold is vital (Colombo et al., 2007; McMaster, 2002; Orlandini et al., 2011; Wilson and Gallant, 2000).

Different DEMs with the same or different resolution will produce different realisations of stream networks and catchment boundaries. Uncertainty (error) exists in all spatial data (Zhang and Goodchild, 2002). However, the extent of differences in the derived stream networks and catchment boundaries will depend on the DEM resolution, technologies and methods used to collect the source data, the processing methods that are applied, and the complexity of the surface itself. Not surprisingly, the horizontal and vertical resolution of a DEM can have a significant influence on the accuracy of hydrologic delineations (i.e. drainage network) that are extracted from the DEM (Wilson, 2012). Therefore, the comparison of stream networks and catchment boundaries derived from different DEMs is an important aspect of quality assessment and can indicate their suitability for a particular application (Charrier and Li, 2012; Hengl et al., 2009; Mantelli et al., 2011; Penas et al., 2011; Poggio and Soille, 2011). The horizontal accuracy of DEMs can be tested by quantifying positional offset distances between the delineated drainage networks from each DEM and a higher accuracy reference stream network, if we assume that the reference data are the best available representation of this particular feature (Goodchild and Hunter, 1997).

The mean of these differences (RMSE) can be used to quantify horizontal offset error between the reference stream channel and the delineated drainage networks. In turn, these errors can be comparatively evaluated to determine which DEM best describes the relative terrain (Mantelli et al., 2011).

1.1.5   Soil erosion modelling

Within a watershed, surface runoff (sometimes termed overland flow) can play a very important role in soil erosion and transport of diffuse pollution (Vieux, 2005; Lane et al., 2006). Within a catchment, soil eroded from agricultural lands is one of the most obvious pollutants (Chapman et al., 2014) and may have other chemical particles (e.g. of phosphorus) associated with it (Haygarth et al., 2005). Hydrological pathways can exert a major control on where soil is eroded within a landscape and whether it is subsequently delivered to watercourses (Ferrier and Jenkins, 2010; Reaney et al., 2011). Surface hydrological connectivity can be assessed through analysis of the potential pattern of soil moisture and saturation within the catchment (Lane et al., 2006). The spatial pattern of soil moisture throughout a catchment depends partly on its landscape topography (Wu et al., 2007). Therefore, DEMs are crucial surface representations in soil erosion modelling.

Digital elevation models have been widely used in a geographical information system (GIS) to extract the topographical and hydrological characteristics of a catchment in soil erosion and diffuse pollution studies (Datta and Schack-Kirchner, 2010; Shen et al., 2013). Estimation of soil erosion loss is often difficult due to the complex interplay of many factors, such as climate, land cover, soil type, topography, and human activities. Accurate estimation of soil erosion loss or evaluation of soil erosion risk at a catchment or river basin scale has become an urgent task (Owens and Collins, 2006). However, in many situations, land managers and policy makers are more interested in the spatial distribution of soil erosion risk than in absolute values of soil erosion loss. To address this need the combined use of

geographical information system (GIS) and erosion models has been shown to be an effective approach in estimating the magnitude and distribution of soil erosion risk (Prasuhn et al., 2013). Studies have also been carried out to evaluate the effect of spatial resolution on the accuracy of soil erosion prediction (Cochrane and Flanagan, 2005; Lee and Lee, 2006; Molnar and Julien, 1998; Rojas et al., 2008; Wu et al., 2005; Zhang et al., 2008).

1.1.6 The role of GIS

Geographical information systems (GIS) are now considered as a key component of many environmental studies and their advantages for watershed studies have been recognised (Lovett and Appleton, 2008; Lyon, 2003). GIS are computer-based tools that facilitate mapping and spatial analysis of the Earth's features and processes. One particularly important role of a GIS in catchment modelling is to provide an environment for the integration of spatial data at multiple scales collected from different sources (e.g. ground, air and space borne sensors) to create spatial datasets of catchment characteristics. Therefore, GIS layers describing topography, land use and land cover, soil types and, rainfall become model parameters or inputs in the simulation of hydrological processes (Vieux, 2005).

1.1.7 Summary

Catchments are increasingly recognised as important units for many types of environmental management and planning. This is particularly true of the water environment, where local catchment-based approaches have become increasingly common in the UK. It is also clear that understanding of many key catchment processes depends on accurate representations of the topography involved. As a consequence, it is important to evaluate the effect of using different DEMs in hydrological analysis and catchment management applications. By doing so, it is hoped that this research will provide guidance to local catchment managers and organisations such as river trusts about the best use of DEM datasets in developing catchment understanding and plans.

1.2 Aims and Objectives

1.2.1 Main aim

Given the above context the overall aim of this research is to understand accuracies and uncertainties associated with different digital elevation datasets derived from different sources and to explore the implications of their use in hydrological analysis and catchment management applications. This will include the assessment of stream networks and catchment boundaries, as well as the implications for soil erosion and diffuse pollution modelling. The latter are particularly important in terms of the effective spatial targeting of catchment management activities.

1.2.2 Objectives

To achieve the general aim stated above, the specific objectives of this research are:

1. To evaluate the accuracy of different DEM datasets representing the same region and surface type but derived from different sources.

2. To determine an appropriate threshold value (flow accumulation threshold) that can be used to accurately delineate channel networks in a study catchment.

3. To quantitatively compare the positional accuracy of drainage networks derived from different DEMs.

4. To conduct an assessment of soil erosion and diffuse pollution risk in the study catchment using different DEMs. A particular focus of this investigation will be to identify the locations (or sub-catchments) of high risk soil erosion areas within the study catchment using RUSLE and SCIMAP modelling techniques.

1.3 Structure of the Thesis

This chapter has described the context of the thesis research and set out the general aim and objectives. Chapter 2 reviews the existing research literature with respect to Digital Elevation Models, drainage network extraction from DEMs and soil loss and diffuse pollution modelling. This leads to a refinement of the research objectives.

Chapter 3 briefly describes the study area (the River Wensum catchment). The descriptive of the elevation datasets (ASTER, SRTM, Landmap, Bluesky, OS Landform Panorama, OS Landform Profile and NEXTMap) as well as the quality assessment of all the elevation datasets used in the study are presented in Chapter 4. Quantitative and qualitative assessments of all DEMs are performed using several different approaches. Firstly, the accuracy of each DEMs is assessed using elevation and slope descriptive statistics and histograms, cross-sectional profiles, and analytical shading images (hillshade). Secondly, an analysis of DEM accuracy against a higher accuracy reference data set is undertaken. Finally, an assessment of whether or not these elevation datasets are of sufficient quality (fitness for purpose) for catchment management studies is made, and five elevation datasets out of seven are selected for further investigation.

Chapter 5 is devoted to the determination of an appropriate supporting area threshold to delineate an adequate channel network in the Blackwater sub-catchment using the selected DEMs from the previous chapter. Three approaches are examined; trial and error, 1% of the maximum flow accumulation value (a rule of thumb), and the area-slope relationship approach. Chapter 6 goes on to compare the extracted stream networks using two different methods. In the first, stream networks are extracted directly from the original DEMs; in the second, an error propagation method (Monte Carlo approach) is used to determine a probabilistic estimation of the stream networks and then identify the most probable stream network. The second part of this chapter investigates the positional accuracy of the predicted

stream networks by comparing them with a higher accuracy reference drainage network using horizontal RMSE and different buffer zones.

Chapter 7 examines soil erosion and diffuse pollution issues within the study catchment using the SCIMAP and RUSLE modelling frameworks. Outputs from the SCIMAP diffuse pollution and fine sediment connectivity model are discussed in the first part of the chapter. The second part outlines the use of the empirical universal soil loss equation (RUSLE) to estimate potential soil loss from fields in the study catchment. Within a GIS environment the RUSLE is then applied to the study catchment for two different farming years using two different DEMs. Results from both SCIMAP and RUSLE are compared to each other and also are validated and compared against water quality data collected across the study catchment. The final chapter (Chapter 8) summarises the main findings of this study, considers the implications for catchment management and discusses future research priorities.

Chapter 2

Literature review

2.1 Introduction

Chapter 1 highlighted how a catchment-based approach has been promoted by a range of organisations and initiatives for effective management of water quality. These include the EU Water Framework Directive (WFD) (Benson et al., 2014), the US Environmental Protection Agency (USEPA) in America (Ferrier and Jenkins, 2010) and the Demonstration Test Catchment (DTC) programme in the UK (McGonigle et al., 2014). The WFD aspires to achieve good ecological and good chemical status for all surface waters through successive six-year cycles of measures (initially 2009-15). A surface water is defined as of good ecological status if there is only slight departure from the biological community that would be expected in conditions of minimal human impact (Kallis and Butler, 2001). It has also been recognised that the key principles towards developing sustainable catchments management are firstly to understand the hydrological processes occurring within the catchment, in particular, to determine the surface pathways of water movement across the catchment landscape. Secondly, to identify possible locations within the catchment landscape where nutrients and pollutants are generated (e.g. hotspots of soil erosion) and how they may be transported to the watercourses. It has been shown that catchment geomorphology and hydrology exert control over the natural processes occurring within the catchment, and DEMs

provide a wealth of information regarding catchment geomorphology and hydrology

(Martinez at al., 2010). Therefore, ensuring that a DEM dataset accurately represents

catchment surface topography is critical to understanding the natural processes occurring

throughout the catchment landscape, which in turn has an important bearing on water quality

management. Hence, this chapter starts (Section 2.2) by providing insight into DEMs

themselves, their sources, structure, associated uncertainty, and their derived topographic

parameters. This leads on to consideration of issues related to drainage network extraction and

diffuse pollution modelling.

2.2 Digital Elevation Models (DEMs)

2.2.1   Concept and definition

Digital elevation data are samples of the Earth's surface elevations stored and handled

in a digital environment, which have been defined by many authors in many different ways.

The simplest definition is the one by Burrough (1986) that the DEM is any digital

representation of the continuous variation of relief over space, or more briefly any digital

representation of the terrain. Based on one of the most widespread definitions, the digital

elevation model is a representation of the Earth's surface excluding natural or artificial

features (Peckham and Jordan, 2007). Also, a DEM is defined as a mathematical model of

the Earth's surface that, at present, is the most powerful method of representing relief. Fisher

and Tate (2006, p.468) have defined a DEM as "a set of elevation values which are recorded

on a regular grid, most commonly in a square form, less frequently in a triangular or

rectangular form". Three types of terrain model are commonly distinguished: digital elevation

model (DEM), digital terrain model (DTM) and digital surface model (DSM) (Maune, 2007).

Maune (2007) stated that, unless specifically referenced as a DSM, the generic DEM normally implies elevations of the bare earth surface void of vegetation and man-made features, and this bare earth DEM is generally synonymous with a DTM. The difference between a DSM and a DTM is that a DTM represents bare ground elevations whereas a DSM contains elevation information about all features in the landscape, such as vegetation, buildings, and other structures (Maune, 2007). Jordan (2007) argued that a DEM is the most basic type of a DTM, and is defined as a spatial distribution of elevations above some arbitrary datum in a landscape. Li et al (2005) reported that a DEM is a subset of a DTM and is the most fundamental component of a DTM. Maune (2007) stated that DTMs may be similar to DEMs, but they may also incorporate the elevation of significant topographic features on the land, plus mass points and break lines that are irregularly spaced, so as to better characterize the true shape of the bare earth terrain. The term DTM is often used because 'terrain' often implies attributes of a landscape beyond just the altitude of the land surface. For the purposes of this research, the term DEM will be used as described above and as used in Maune (2007).

2.2.2 Elevation data structure

A continuous surface, such as that of the Earth's surface, has an infinite number of points. Therefore, it is impossible to record every point, and consequently a sampling method must be used to extract representative points. These discrete points can then be used to build a surface model that approximates the actual surface. The generation of DEMs includes three interrelated tasks: (i) the sampling of the land surface (e.g. the collecting of height measurements); (ii) creating a surface model from the sampled heights; and (iii) correcting errors and artefacts in the surface model (Wilson, 2012). Fisher and Tate (2006) mentioned that a DEM is usually the end result of a number of modelling and processing steps, as illustrated by the flowchart in Figure 2.1 below. Digital elevation data are usually organized

into one of three data structures; regular grid/raster models, triangular irregular networks (TIN), or contour lines, depending on the source and/or preferred method of analysis.

Process		Example
Conceptual Model		The Land Surface
Measurements		Photogrammetric Survey
Intermediate Model		Contour Map
Conversion		Digitization of Contours
Interpolation		TIN Interpolation
Digital Model		DEM
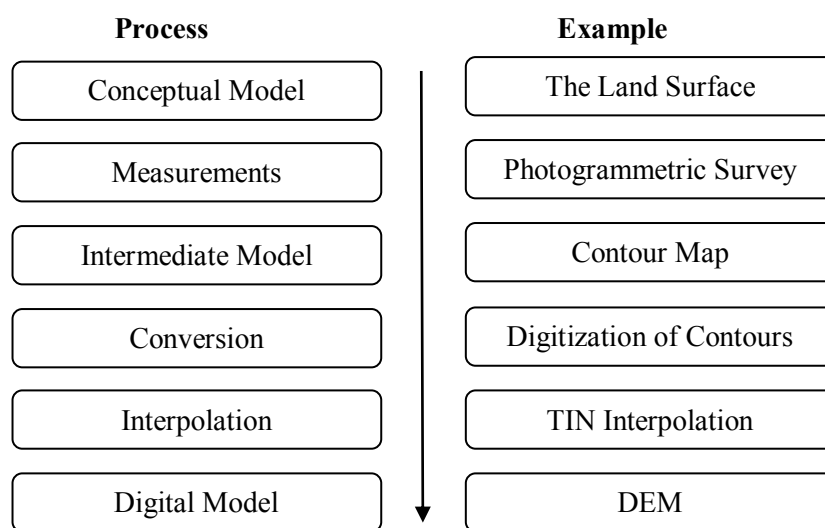
Figure 2.1: A flow chart showing the process of construction of a DEM through the intermediary of a contour map. After Fisher and Tate (2006).

2.2.2.1 Contour lines

Contour lines are defined as a set of lines that connect points of the same elevation value on a surface (Figure 2.2a). Each contour line contains an infinite number of potential sample points which are connected together to draw a continuous line following the contour across the surface. They are an excellent representation of the heights and variations of a surface for a two-dimensional printed map. This is because, with topographic maps, it is easy to interpret the contours since anyone can look at contour lines on a map, can recognize peaks, ridges, valleys, relative slope, aspect, stream direction, and other characteristics that cannot all be easily interpreted from a TIN or a grid (Maune, 2007). Contour accuracy depends upon whether the lines have been generated from primary or derived data. Contours were historically created by manual interpretation of spot heights, but more recently have been derived through a photogrammetric process. When contours have been captured directly

from aerial photographs as primary data using a stereoplotter, the contours are highly accurate (El-Sheimy et al., 2005). If the contours have been generated from point data, the location of the contours must be interpolated between known values. However, contours can be derived from a TIN or grid DEM and vice versa. Jordan (2007) stated that contour lines are the form of topographic surface representation which can be converted to grid DEM by interpolation after contour line digitisation. On the other hand, Maune (2007) mentioned that, today, most contours are derived from a TIN or grid which is already created by other techniques.

The major drawback of contours is that there is no data between contour intervals and they only indicate surface values along the lines. Therefore, once the surface has been represented as contours, interpolation can be used to derive an elevation for locations between contours and may not provide an accurate portrayal of the topography. This phenomenon is particularly apparent when the distance between contours is large, due to either a large elevation interval between contours, or in low relief terrain, where a greater horizontal distance is covered between contour intervals. Contours have often been used by cartographers to represent relief and profiles. However, due to their crude topological structure, they are not particularly suitable for automated spatial analysis of ground morphology. Even the derivation of slope or shaded relief maps from contours is a rather cumbersome operation (Carrara et al., 1997).

(a)   (b)   (c)
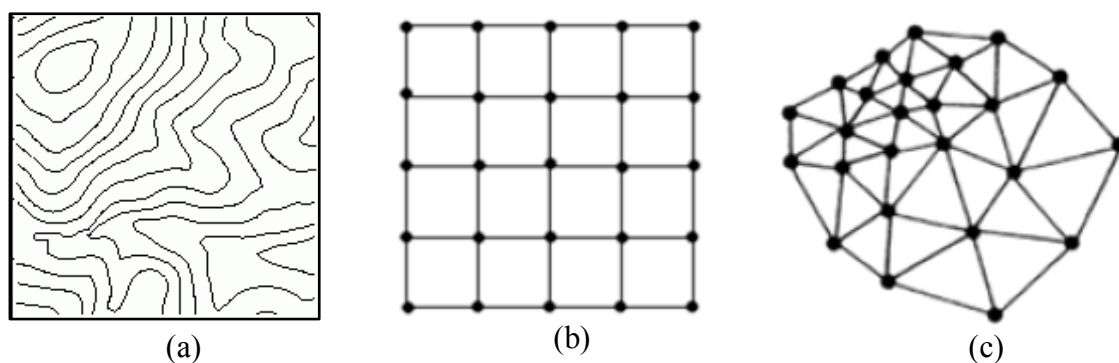
Figure 2.2: Examples of elevation data structure: (a) contour lines; (b) square grid; and (c) triangular irregular network (TIN). Source: Wilson and Gallant (2000).

2.2.2.2 Grid or raster structure

The most common elevation data form is the regular grid DEM, a gridded set of points in Cartesian space attributed with elevation values that describe the Earth's surface (El-Sheimy et al., 2005; Fisher and Tate, 2006; Maune, 2007; Wilson, 2012; Wilson and Gallant, 2000). Grids have a matrix structure of regular grid cells (usually square and known as raster cells) with an average elevation value that is representative for the area that comprises each cell (Figure 2.2b). Spatial resolution in the X and Y directions refers to the cell size or the width and length of a single cell, which determines the precision of the grid representation. The size of a grid cell depends upon the level of detail of the input data used to create the grid and the data resolution required for the most detailed analysis. The smaller the cell size, the higher the resolution of the DEM, which is separate from the quality of the original data. The cell must be small enough to capture the required detail, but large enough so that computer storage and analysis can be performed efficiently. Gridded terrain models are appropriate for small scale mapping applications where absolute positional accuracy is not paramount and where surface features do not need to be characterised exactly (Maune, 2007).

In a GIS environment, square-grid DEMs are the most commonly used data structure because of their simplicity and ease of computer implementation (Wilson and Gallant, 2000), and hence are utilised in the majority of environmental models (Raaflaub and Collins, 2006). A regular grid data structure is needed for spatial data manipulation by GIS (Peckham and Jordan, 2007). Therefore, its widespread use as a model of surface form may be attributed to its easy integration within a GIS environment. Moreover, the simplicity of data handling in surface analysis makes gridded DEMs the most popular among users (Hengl and Reuter, 2008).

Although the grid format is a fast and efficient data structure for analysis algorithms, and is a useful DEM structure to perform numerous topographic analysis - such as

calculations of contours, slopes, aspects, hill shading images as well as delineations of drainage networks and catchment areas - it is not without disadvantages. Maune (2007) argued that the disadvantages of the grid representation are that surface discontinuities such as ridges and stream centrelines are not well represented, and precise locations for features such as peaks are lost in the sampling of the grid. He also mentioned that, for these same reasons, grids are not good for representing man-made objects such as road cuts, buildings, etc., but are good for bare earth terrain models. When information is represented in grid (raster) form, all detail about variation within cells is lost, and instead the cell is given a single value (Longley et al., 2005).

Burrough et al. (1998) and Moore et al. (1991) also stated that a gridded DEM has several weaknesses: (1) inability to adapt to areas of differing relief complexity without changing the grid size; (2) grid spacing needs to be based on the roughest terrain in the catchment, resulting in redundancy in smoother areas; (3) resolution affects the results and computational efficiency; and (4) the computed flow paths tend to zigzag, not follow the drainage lines, and are hence systematically too long.

2.2.2.3 Triangular Irregular Networks (TIN)

A TIN is a digital terrain model that is based on an irregular array of points, which approximates a topographic surface by connecting this set of irregularly spaced elevation vertices into non-overlapping triangular facets (Figure 2.2c). The points used to construct a TIN come from individually sampled locations or from the vertices of linear features. Ideally, these represent a set of critical locations on the surface which defines breaks in slope such as peaks, pits, ridges, valleys, and passes (Maune, 2007).

The accuracy of a TIN is consistent with the degree of variation in the terrain. Therefore, the accuracy of a TIN is limited by the selection of input data points; well-chosen

points will be located so as to capture significant changes in the modelled surface, such as topographical summits, breaks of slope, ridges, points along streams, pits and cols. As the terrain becomes complex, the density of the TIN should be increased accordingly. This occurs because more points are sampled and included in the TIN model in areas of high complexity. This is an advantage of the TIN model over other surface representations since where there is a little variation in the terrain surface only a small amount of data is stored, and where there is much variation, more data is stored. However, TINs have several disadvantages. There are not as many tools to process TINs as with gridded DEMs, and, because of their complex structure, some operations are not as efficient (Maune, 2007).

2.2.3   DEM quality issues

2.2.3.1   Introduction

Data quality assessment has become a core practice in fields such as GIS (Zhang and Goodchild, 2002) and remote sensing (Lunetta and Lyon, 2004). The quality of spatial data means how well these data represent reality and fulfil the requirements of users (Ehlschlaeger and Goodchild, 1994). Digital elevation models (DEMs) are a representation of the Earth's surface but with unavoidable inherent errors, which result in DEM uncertainty (Liu and Bian, 2008). The quality of a DEM, in terms of horizontal and vertical accuracies, is dependent upon a number of interrelated factors, including the methods of data acquisition, the nature of the input data, and the methods employed in generating the DEMs (Weng, 2002; Wilson and Gallant, 2000). As DEM generation goes through a multitude of processes, uncertainties are inherited as early as from the data source and post-processing production methods (Zhang and Goodchild, 2002). For most GIS-based environmental studies, primary topographic indices such as basic descriptive statistics of elevation (e.g. maximum, mean, minimum, and standard deviation), local relief, slope, aspect, curvature and hydrological products such as flow

direction, flow accumulation and watershed boundaries are often required for specific environmental models (Hebeler and Purves, 2009). While derived from the digital elevation model (DEM), these parameters often display noticeable uncertainties due to the accuracy of the DEM (e.g. sample errors, interpolation errors, and representation errors) and to the spatial structure of the DEM (e.g. precision and grid resolution) (Zhou and Liu, 2008).

Authors categorize spatial data quality as a function of three primary components: accuracy, precision and uncertainty (Chrisman, 1991; Maune, 2007). Accuracy refers to the closeness of measured values, observations or estimates to the real or true value (Chrisman, 1991). The accuracy of a DEM is considered critical when the DEM data are used for environmental modelling and for the prediction of the spatial distribution of hydrological, geomorphological, and biological properties (Thompson et al., 2001). The term 'precision' is used to describe random errors; the smaller the random error, the greater the precision (Atkinson and Foody, 2002; Wise, 2000). The difference between accuracy and precision is often not understood (Atkinson and Foody, 2002). Our lack of knowledge about the reliability of a measurement in its representation of the true value is referred to as 'uncertainty'. Uncertainty is a measure of what we do not know and exists in all spatial databases (Longley et al., 2005).

In general, the quality of a DEM determines the quality of the products derived from it (e.g. slope, aspect, flow direction). The methods used to acquire elevation data and the processes or techniques used to transform these data into a digital elevation model have marked impact on the final DEM and, consequently, on the derived products (Wilson and Gallant, 2000; Maune, 2007; Li et al., 2005; El-Sheimy et al., 2005; Wechsler, 2007; Charrier and Li, 2012; Hirt et al., 2010; Hodgson et al., 2003; Rayburg et al., 2009). In many cases, the derived parameters of the Earth's surface models are often in more demand than the DEM itself because they are key components of applied models.

2.2.3.2 Source and type of DEM errors

As mentioned above, DEM accuracy can be defined as the degree of closeness of an observation or estimated value to the true value (Carlisle, 2005). Values which are very close to the true values have higher accuracy and those that are far from the true values have lower accuracy. Sources of DEM error are closely related to DEM production methods. Generally speaking, the accuracy of a DEM depends on (i) elevation source data, including the techniques for measuring elevations either on the ground or remotely, the density of observations, and the location of samples; (ii) the interpolation method used to create the DEM from the raw elevation data; (iii) DEM data structure (e.g. grid, contour, TIN); and (iv) the surface complexity of the landscape being modelled. Therefore, error is implicitly associated with any DEM, but usually the error magnitude and spatial distribution for any particular location are unknown (Hebeler and Purves, 2009). The error from different sources and processing methods can be categorised into three groups namely; gross, systematic and random errors (Fisher and Tate, 2006; Li et al., 2005; Wechsler, 2007). Gross errors are blunders that result from operator error or equipment failure and are easily detected and removed (Fisher and Tate, 2006). Gross errors are, in fact, mistakes (Li et al., 2005). Systematic errors result from the procedures used in the DEM generation process that show some form of dependency or trend that can cause bias or artefacts in the final DEM product, which as such, can be eliminated or reduced (Wechsler, 2007). Random errors occur due to a lack of precision from a variety of operational tasks and are introduced for unknown reasons. They cannot be governed by certain standard rules, thus they remain in the data after gross and systematic errors are removed (Maune, 2007; Wechsler, 2007).

2.2.3.2.1 Errors in contour-based DEMs

The quality of contour-derived DEM is affected by the data source used to create the map, interpolation method, grid cell size selected and the terrain complexity (Fisher and Tate,

2006; Wilson and Gallant, 2000). Errors in the source map data generally come from the process of collection, recording, and generalization inherent in the cartographic process (Fisher and Tate, 2006). The contour interval of topographic maps used to collect elevation data may affect the density and the distribution of data. The elevations can be derived by manually digitizing the contour lines from paper maps or from scanned maps (El-Sheimy et al., 2005). In both techniques, errors can occur during the digitizing/scanning process or in automatically identified contour lines. For example, when obtaining digital elevation data from cartographic contour lines, a vertical error can be caused by the operator tagging the wrong elevation value to a contour line. However, the general quality of the derived DEM is improved if great efforts are made to extract terrain characteristic features and break lines as well (Weng, 2002).

2.2.3.2.2 Errors in passive sensors-based DEMs

DEMs produced from photogrammetric techniques are affected by both human errors and instrumental errors (Hunter and Goodchild, 1995). In photogrammetry these errors arise due to changes in film media, instrument errors, software precision, and interpolation. Fisher and Tate (2006) stated that the production of DEMs from photogrammetry introduces both random and systematic errors. Random errors may accrue through the lack of precision in the identification of target points on a photograph as part of the process of aerial triangulation, and systematic errors may occur from changes in the film media, instrument errors and from human errors. The resulting DEMs often have spikes or pits in places where the algorithm used to generate the DEM incorrectly matches two points from the stereo pair (Nelson et al., 2009).

All aerial and satellite imagery capture Earth's surface cover rather than the bare earth surface, so the resulting DEM will include heights of vegetation and man-made objects which can also result in rough surfaces and high slope values (Reuter et al., 2009). Consequently, the

elevation data produced are more a DSM rather than DTM. Therefore, applications that required bare-earth surface DEMs need to have the surface elevation measurements corrected to bare surface elevations (Hensley et al., 2007). Another serious problem in DEMs derived by this method is the existence of voids or NODATA areas because of cloud contamination in the data. Areas covered by cloud will be obscured in the visible and near-infrared wavelengths, leading to gaps in the data (Nelson et al., 2009). For example, a validation study of the digital elevation data produced from ASTER stereo images (GDEM1) identified a number of artefacts associated with this DEM due to the effect of cloud cover and inland water bodies (ASTER GDEM Validation Team, 2011).

2.2.3.2.3 Errors in active sensors-based DEMs

The quality of elevation information collected by active systems (e.g. LiDAR and IFSAR) is related to sensor and terrain surface characteristics. The data collected by active systems may require not only interpolation, but also considerable processing to obtain the resultant DEM (Fisher and Tate, 2006). Similar to the passive system, radar elevation data usually represent the visible surface rather than the land surface. In radar DEMs, for example, the natural vegetation and man-made objects are seen as small hills, elevated plateaus, escarpments or islands (Reuter et al., 2009). Often in radar-based DEMs, errors were found higher on vegetated areas due to the tendency of the signal to reflect from the canopy (LaLonde et al., 2010), and voids were found over water bodies, in desert and mountain areas (Rodriguez et al., 2006). In general, natural vegetation and man-made objects in radar and LiDAR DEMs can be quite problematic, and often require a number of post-processing and filtering steps (using high resolution auxiliary data) to filter out the impact of these features (i.e. conversion from DSM to DTM) (Reuter et al., 2009). An example of a radar imagery-based DEM is the SRTM DEM (Farr et al., 2007).

2.2.3.3   Measures of DEM accuracy

DEM accuracy has received considerable attention since DEMs came into widespread use in the 1980s. Many studies have sought to quantify DEM accuracy and compare the accuracy of DEMs produced using different data sources and production methods (Carlisle 2005). Different data sources (i.e. radar, optical or contour) and methods incorporate systematic and random errors that can generate bias in elevations which then propagate through derived parameters (slope, aspect, etc.) (Wilson, 2012).   The assessment of errors in DEMs is often complex, since errors can be introduced at many stages of the DEM production process through to the use of the DEM (Figure 2.3). The measurement of errors in DEMs is often impossible because the true value for every geographic feature or phenomenon represented in a geographic data set is rarely determinable (Ravibabu and Jain, 2008). According to Weng (2002), uncertainty may be a better means of describing the quality of a DEM than error.
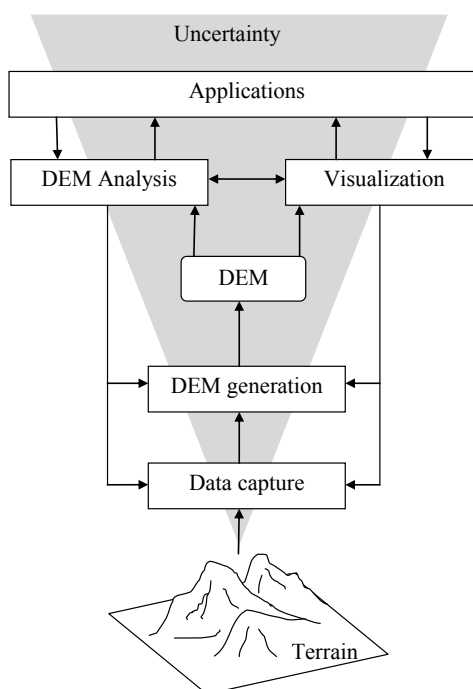
Figure 2.3: Digital elevation model and uncertainty (modified from Wilson, 2012)

Quantifying uncertainty in DEMs can be achieved by comparing the elevations in a DEM surface with sample point measurements known to be of a higher order of accuracy (Hohle and Hohle 2009). Fisher and Tate (2006) also noted that the error of a DEM can be determined by comparing this dataset with other more accurate measurements, known as reference data and assumed to be free of error. Such a comparison results in elevation differences (residuals) at the tested points. This approach is the most common in DEM evaluation studies (Anderson et al., 2005; Li et al., 2005; Wise, 2008). Statistical measures such as Root Mean Square Error (RMSE), Standard Deviation (SD) and Mean Error (ME) are the conventional ways to analyse the deviation between two sets of elevation data. The most widely used measure to represent the difference between the DEM values and the reference values is the Root Mean Square Error, and it is mathematically expressed as follows:

$$\text{RMSE} = \sqrt{\frac{\sum_{i=1}^{n}(Z_{DEM} - Z_{Ref})^2}{n}} \qquad \text{(Equation 2.1)}$$

where Z_{DEM} is the measurement of elevation from the DEM, Z_{Ref} is the corresponding higher accuracy measurment of elevation and n is the number of spot heights.

Published assessments of DEM quality often quote Root Mean Square Error (RMSE) values. For example, the United States Geological Survey (USGS) describes the accuracy of its 7.5 minute DEMs with one RMSE value for each quadrangle or tile. The RMSE calculation for each quadrangle requires a minimum of only 28 points (USGS, 1998). The widely quoted National Standards for Spatial Data Accuracy (NSSDA), given by the Federal Geographic Data Committee (FGDC, 1998), recommend the use of a minimum of 20 checkpoints to reflect geographical area of interest and the error distribution in the dataset. Such standards assume a normal distribution of residuals. In the UK, the Ordnance Survey's

digital contour data have included a single statement of the RMSE (±1.8m) in their products metadata, claiming that it is the same for the whole national dataset (Ordnance Survey). The larger the value of the RMSE, the greater the difference between two sets of measurements of the same phenomenon.

Many studies have been conducted to quantify DEM accuracy and compare the accuracy of DEMs created using different data sources and production methods. Hirt et al. (2010) examined the quality of SRTM version 4 and ASTER version 1 elevation datasets among others over Australia, based on a set of ground control points using the statistical measures stated above (e.g. RMSE, SD and, ME). They found vertical accuracies of approximately 6 m and 15 m for SRTM and ASTER, respectively. Another study conducted by Reuter et al. (2009) evaluated the horizontal and vertical accuracy of ASTER GDEM data and found that the average RMSE values of GDEM were between 18 and 29 m. Nikoloakopoulos et al. (2006) evaluated the elevation differences between SRTM and ASTER products using the root mean square error (RMSE) over regions in the island of Crete, Greece, which was found to be less than 50 m. Hodgson et al. (2003) investigated the elevation accuracy of LiDAR and IfSAR derived DEMs with USGS level 1 and level 2 DEMs using RMSE and other statistical measures. Survey-grade points were used as reference points. They found that the LiDAR and contour to grid derived DEMs exhibited the highest overall absolute elevation accuracies.

The main advantage of RMSE lies in its easy computation and straightforward interpretation. However, a major drawback of the RMSE is that this measure is usually a single global measure of deviation for each DEM based on comparisons with higher accuracy reference data, and thus does not account for the spatial variation of errors over the surface of the DEM (Gonga-Saholiariliva et al., 2011; Fisher and Tate, 2006; Weschsler and Kroll, 2006). The RMSE does not provide an accurate assessment of how well each cell in the DEM

represents the true elevation value and assumes that DEM errors are random (Wechsler and Kroll, 2006). The RMSE is not necessarily a good description of the statistical distribution of the error (Fisher and Tate, 2006). Therefore, assessment of DEM uncertainty requires more definitive information regarding the spatial structure of DEM error beyond that provided by the RMSE. This was the motivation of a large body of research focusing on DEM error modelling (Darnell et al., 2010; Hebeler and Purves, 2009; Hunter and Goodchild, 1997; Oksanen and Sarjakoski, 2005; Raaflaub and Collins, 2006; Wechsler and Kroll, 2006).

As mentioned earlier, in the context of spatial databases, it should be realized that error has a very different meaning to uncertainty (Foody and Atkinson, 2002). The concept of error is, in fact, narrower than that of uncertainty. The former relates to individual measurements; the actual difference between an individual result and the true value. Therefore, error is a single value. On the other hand, uncertainty relates to a measure of what is not known or not known with certainty about the reliability of a measurement in its representation of the true value (Wechsler and Kroll, 2006). Inaccuracy, ambiguity and vagueness all contribute to the notion of uncertainty in the broadest sense (Longley et al., 2005)

In a GIS analysis, the effect of DEM uncertainty is not well understood for all terrain derivatives, in particular the more complex ones. For such a GIS operation, error propagation (uncertainty) to the terrain derivatives can be modelled by the Monte Carlo simulation method (Hunter and Goodchild, 1997). The Monte Carlo method, sometimes called stochastic simulation, is a technique that has been widely used to assess uncertainty in data derived from DEMs by creating a set of potential realisations of the DEM and of the derived features (e.g. Darnell et al., 2010; Darnell et al., 2008; Hengl et al., 2010; Hunder and Goodchild, 1997; Oksanen and Sargakoski, 2005; Poggio and Soille, 2011; Wechsler and Kroll, 2006). The assumption behind it is often based on DEM residuals with a zero mean and normal

distribution (the standard deviation of the distribution being based on RMSE calculated from comparison with a higher accuracy data source), although it is accepted that it can often be unrealistic and should be considered as the worst-case scenario (Hunter and Goodchild, 1997). However, simulation does not ensure that a 'true' map of a derivative (e.g. streams) is generated from the process, but provides a distribution of results within which it can be stated that the 'real' map lies. The high number of studies that use Monte Carlo simulation to assess uncertainty indicates that this is a preferred method for quantifying DEM uncertainty and its propagation to DEM derived derivatives (Wechsler, 2007). Error tends to be spatially autocorrelated, however, this is not always considered in such assessments.

The underlying assumptions of the simulation procedure as applied to DEM uncertainty assessment are as follows: (1) DEM error exists and constitutes uncertainty that is propagated with manipulation of the elevation data; (2) the true nature and extent of these errors are unknown; (3) DEM error can be represented by a distribution of DEM realisations; and (4) the true surface lies somewhere within this distribution (Lindsay and Evans, 2008; Poggio and Soille 2011). Thus, uncertainty characterizes a range of values within which the true value is asserted to lie with some level of confidence.

2.2.4 DEM based topographic parameters

The DEM provides a base dataset from which topographic derivatives are digitally generated. The raster grid structure lends itself well to neighbourhood calculations which are frequently used to derive these parameters (Wechsler, 2007; Wilson, 2012). Topographic parameters may be divided into primary topographic parameters, such as slope, aspect, surface curvature, or catchment area, and secondary parameters, such as the topographic wetness index, or stream-power index (Wilson and Gallant, 2000). The primary attributes are calculated directly from the elevation data or from one of its derivatives, whereas the

secondary attributes are calculated from two or more primary attributes (Oksanen and Sarjakoski, 2005; Wechsler, 2007). These terrain attributes are used extensively in hydrological applications and are derived directly from the DEM. Table 2.1 shows some of these derivatives and their applications. The path of water through the landscape (routing of water) is controlled by topography, and DEMs are the best means of depicting and analysing topography in a GIS (Holmes et al., 2000). Flow direction is derived from slope and aspect. From flow direction, the upslope contributing drainage area that contributes flow to a cell can be calculated, and, from these maps, drainage networks and catchment boundaries can be identified (Do et al., 2011). Wilson and Gallant (2000) provide a detailed review of the DEM-derived primary and secondary topographic attributes.

Table 2.1: DEM derivatives and their application.

Derivative	Description	Applications
Slope	Rate of change of elevation	Overland and sub-surface flow, runoff rate, soil and land capability assessment.
Aspect	Compass direction of steepest downhill gradient	Solar irradiance, evapotranspiration, flow direction.
Profile curvature	Rate of change of gradient	Flow acceleration, erosion/deposition zones.
Plan curvature	Rate of change of aspect	Converging/diverging flow, soil water properties.
Flow direction	Direction of downhill flow	Computing surface topology, material transport.
Upstream area	Number of cells upstream of a given cell	Watershed delineation, volume of material passing through a cell.
Stream length	Length of longest uphill path upstream od a given cell	Flow acceleration, erosion rates, sediment yield.
Stream channel	Cells with upstream area greater than a specified threshold	Location of flow, flow intensity, erosion and sedimentation.
Ridge	Cells with no upstream area	Drainage divides; soil, erosion and geological analysis.
Wetness index	ln(upstream area/tan(slope))	Index of soil saturation potential.
Stream power index	Upstream area*tan(slope)	Index of the erosive power of overland flow.

Source: Modified from Ravibabu and Jain, 2008; Wilson and Gallant, 2000; and Wilson, 2012.

Derivatives derived from DEMs are sensitive to both the quality of the DEMs from which they were generated and the algorithms used to derive them (Wise, 2007). Numerous algorithms have been developed for calculating topographic parameters from DEMs. For example, slope is often calculated for the centre cell of a 3 x 3 matrix from values in the surrounding eight cells. Algorithms behave differently in the way that the surrounding values are selected to calculate change in elevation (Wechsler, 2007). Many different algorithms have also been developed to calculate flow direction from a gridded DEM data and are described as single or multiple flow direction algorithms (Wechsler, 2007). The method most commonly used is the one introduced by O'Callaghan and Mark (1984), which determines the direction that water will flow from a cell to one of its eight neighbouring cells with the lowest elevation; this single flow direction is also referred to as Deterministic 8-Direction (D8) (Wise, 2007). Flow routing is further discussed Section 2.3.4.

2.2.5 DEM resolution for representing topography

The quality of a DEM refers to more than just its vertical accuracy. The spatial resolution is also a very important aspect that has an effect on the DEM accuracy and its derivatives (Wu et al., 2008b). The size of a grid cell is commonly referred to as the DEM resolution, with a smaller grid cell indicating a higher resolution. Smaller grid cell sizes can capture more detail and smaller variations in topography. DEM accuracy decreases with coarser resolutions due to the averaging of elevations (Li, 1992). It is well known that the accuracy of most terrain attributes derived from a DEM is affected by variations in the underlying grid cell size (Kienzle, 2004). Vaze et al. (2010) argued that if a DEM resolution is within the spatial range of the processes that are operating in the landscape of interest, there is no problem. However, if the DEM resolution is coarser than the resolution of landscape processes, any results or attributes derived from DEMs must be treated with caution. They added that in some areas and for some processes a grid size of 25 m or even higher would be

adequate to capture the scale of surface processes whereas in other areas the resolution required may be as small as 1 m.

The sensitivity of topographic derivatives used in hydrologic modelling to DEM resolution has been explored in several studies. Chang and Tsai (1991) examined how spatial resolution affects the accuracy of slope and aspect. Comparison of the results from resolutions of 20 m, 40 m, 60 m and 80 m with those at 8m revealed that the two parameters are less accurate if generated from a DEM of a coarser resolution. Gallant and Hutchinson (1996) found that the grid resolution of DEMs profoundly influences both the spatial pattern and the frequency distribution of derived topographic attributes, such as slope and specific catchment area, and therefore influences environmental models built on such attributes. Warren et al. (2004) compared slopes measured in the field with those derived from different DEMs with different resolutions. They found that a higher resolution DEM (1 m) produced much better results than a lower resolution DEM (12.5 m). They also concluded that errors in slope can lead to widely varying estimates of environmental factors such as soil erosion. Murphy et al. (2008) argued that, when considering hydrologic modelling using DEM data, DEM cell size has a greater impact on results than does the method by which the DEM was generated. Charrier and Li (2012) investigated the resolution and data source effect of DEMs on automated stream network, watershed and floodplain boundaries and found that higher resolution DEMs produced results that more closely match reference data. Kienzle (2004) studied the effect of DEM resolution on first order, second order and compound terrain derivatives and found that the optimum grid cell size is between 5 and 20 m, depending on the terrain complexity. Sorensen and Seibert (2007) investigated the effects of DEM resolution on the calculation of topographical indices and identified that the resolution and information content of a DEM has a great impact on the computed topographic indices.

The impact of DEM spatial resolution on the hydrologic model predications has been shown in the following applications: CASC2D-SED erosion model response to raster-based grid cell sizes (Rojas et al., 2008); RUSLE (Lee and Lee, 2006); USLE (Molnar and Julien, 1998; Wu et al., 2005); erosion relevant topographical parameters, elevation, slope, aspect, LS factor derived from different DEMs (Datta and Schack-Kirchner, 2010); WEPP (Cochrane and Flanagan, 2005; Zhang et al., 2008), TOPMODEL (Lin et al., 2010; Wu et al., 2007); and the SWAT model (Chaubey et al., 2005).

Research has also demonstrated that higher resolution is not usually necessarily better when it comes to the calculation of DEM derived topographic parameters (Zhou and Liu, 2004; Zhang et al., 2008). Higher resolution DEMs tend to generate greater slope values (Wechsler, 2007). Research has also been undertaken (Kienzle, 2004; Sharma et al., 2011a; Zhang and Montgomery, 1994) to determine an appropriate grid cell resolution for particular analysis. However, selection of an appropriate resolution will depend on the characteristics of the study area and the nature of the analysis. In general, the effect of grid cell resolution in various hydrologic features produced from DEMs is an important factor in our understanding, assessment and, quantification of the propagation of DEM errors to hydrologic parameters and the resulting uncertainty in related modelling applications (Wechsler, 2007).

2.3 Drainage network extraction from DEMs

2.3.1 Introduction

In previous sections it has been demonstrated that because topography impacts on hydrological, geomorphological and environmental landscape processes the application potential of DEMs has greatly expanded and become very significant in catchment management. Currently, DEMs are not only used to extract primary topographic attributes

(e.g. elevation, slope, aspect, drainage lines, catchment areas, and others), but also to characterise the spatial variability of complex processes occurring in the landscape (Wilson, 2012). These secondary topographic attributes are used for many types of applications, including the prediction of erosion potential, sedimentation rates, catchment runoff response, non-point source pollution and others.

However, although there is increasing availability of DEM data from remote sensing sources, it remains difficult for users to select an appropriate DEM for a specific application (Lin et al., 2013). It has been acknowledged that accurate delineation of drainage networks and catchment boundaries are critical for many hydrological modelling and watershed resource management. DEMs are used to simulate overland flow paths in hydrological models and the accuracy of these drainage patterns are dependent upon how well the DEM represents the terrain features that control runoff patterns. Therefore, this next part of the chapter (Section 2.3) provides a background regarding automated extraction of stream networks from DEMs using grid-based flow direction algorithms. In addition to the stream extraction methods, a review of the impacts of different sources and different resolutions of input DEMs on the accuracy of derived drainage networks is given.

2.3.2 Background

The value of DEMs in hydrologic applications is growing and has received considerable attention in recent years (Vogt et al., 2003). Hydrologic features produced from DEMs include drainage networks, channel characteristics and watershed boundaries. The extraction of stream networks and catchment boundaries from digital elevation models (DEMs) are common and important hydrology products. The value of these DEM derivative features varies depending upon the purpose and use of the data. Identifying channel networks is important to applications in hydrology, geomorphology, and water resource management

because of the control exerted by topography, soil properties, and other environmental attributes on surface flow paths and erosion properties within a drainage catchment (Wilson et al., 2008). Therefore, runoff modelling is valuable in predicting the movement of water and sediment (route of water flow) on the landscape and as such relies on the accurate delineation of watersheds (Wilson, 2012). Different DEMs with the same or a different resolution will produce different realisations of stream networks and catchment boundaries. As previously mentioned, the amount of difference in the derived stream networks and catchment boundaries will depend on the DEM resolution, technologies and methods used to collect the source data, the processing methods that are applied, and the complexity of the surface itself. The comparison of the stream networks and catchment boundaries derived from different DEMs is an important assessment of their quality and suitability for a particular application.

Automation of the drainage network extraction, catchment boundary delineation and other hydrologic derivatives from digital elevation models (DEMs) has been the subject of much research in recent years (e.g. Colombo et al., 2007; Hengl et al., 2010; Liu and Zhang, 2011; Vogt et al., 2003). The extractions of all these parameters first involves the determination of flow direction and then the calculation of flow accumulation (Do et al., 2011). Many different algorithms have been developed to calculate flow direction from gridded DEM data and are described as single or multiple flow direction algorithms (Wechsler, 2007). These approaches are discussed in Zhou et al (2008). A brief discussion of common flow direction algorithms is given in Section 2.3.4.

For overland flow modelling, it is important that depressionless DEMs are used (i.e. what are also known as hydrologically corrected DEMs). DEMs often contain pits, defined as pixels with no neighbouring pixels of lower elevations. Different methods have been described in the literature for the treatment of spurious depressions in DEMs (see Section 2.3.3).

Generally, the common method of automatic delineation of stream networks and catchment boundaries starts by filling the sinks of the DEM, and then identification of flow direction followed by calculation of flow accumulation and then stream definition by applying a specific threshold value. The density of the drainage network increases as the threshold value decreases. (Liu and Zhang, 2011).

2.3.3 Treatment of depressions in DEMs

Some pits are the result of errors in the source data used to generate the DEM or artefacts arising from the interpolation processes and the limited resolution of the DEM itself (Liu and Zhang, 2011). Other pits, however, represent authentic depressions in the surface. The presence of pits or depressions, whether as real topographical features of terrain or errors resulting from the DEM source data or creation processes, influences drainage network delineation. These depressions affect the prediction of stream network location as it is difficult to ascertain the correct drainage path through them, and the direction of flow through them cannot be resolved. When attempting to extract stream networks from DEMs with numerous and/or large depressions (artificial or natural), the stream extraction algorithm "fills" the depression with "water" and forces flow direction to follow a path around the depression until it finds a downstream pixel with an elevation lower than the depression wall. This results in stream lines being wildly inaccurate in the vicinity of depressions.

Therefore, hydrologic derivatives extracted from DEMs require the prior removal of spurious pits (Poggio and Soille 2011), even though such treatment may also eliminate natural depressions (Peckham and Jordan, 2007). The simplest and earliest method used to remove these pits involved smoothing the DEM (O'Callaghan and Mark, 1984), however, it was found that smoothing tended to alter some elevation values in areas of the DEM not

containing pits (Raaflaub and Collins, 2006). Figure 2.4 illustrates examples of depressions

before and after the process of pit filling.
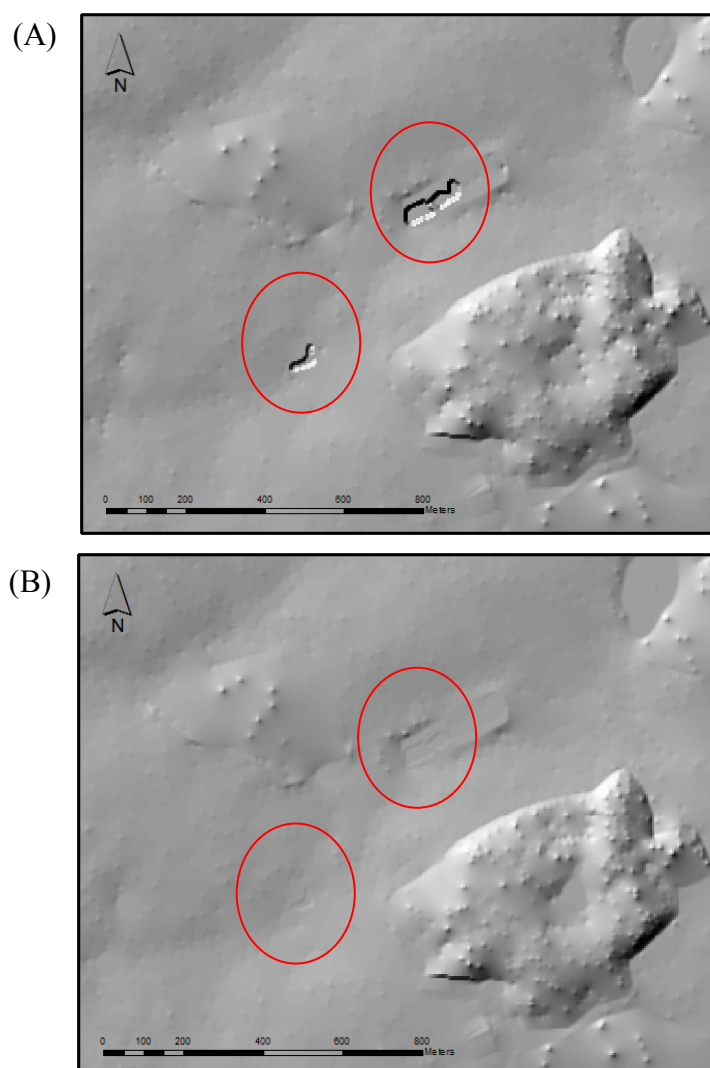
Figure 2.4: Examples of spurious pits treatment using ArcGIS pit filling function (A) snapshot of two pits from NEXTMap DTM shaded relief image (Wensum area) and (B) same area after pits filling treatment.

Depression filling has become by far the most widely used approach and several

different algorithms have been proposed to detect and fill surface depressions (Wang and Liu,

2006). According to Poggio and Soille (2011) the available pit treating methods can be

categorized into three approaches (Figure 2.5): (i) pit filling, whereby the values of cells in

each sink will be filled by the value of the cell with the lowest value on the sink's boundary

(i.e. depression filling by Jenson and Domingue (1988)); (ii) carving, where DEM pixel values (elevation) are lowered from the bottom of the depression, creating a descending path until the nearest point of lower elevation value is reached (i.e. carving by Soille et al. (2003)); (iii) hybrid, an optimal approach combining the first two (filling and carving) in such a way that the pits are filled up to a certain level and then the carving process starts from that level. In general, Jenson and Domingue's (1988) algorithm is best known and is widely used in many GIS software packages (e.g. ESRI) for sink filling (Wechsler, 2007).

(A) Input

(B) Pit filling (raised pixels in) blue

(C) Carving (lowered pixels in orange)

(D) Hybrid (filling and carving)
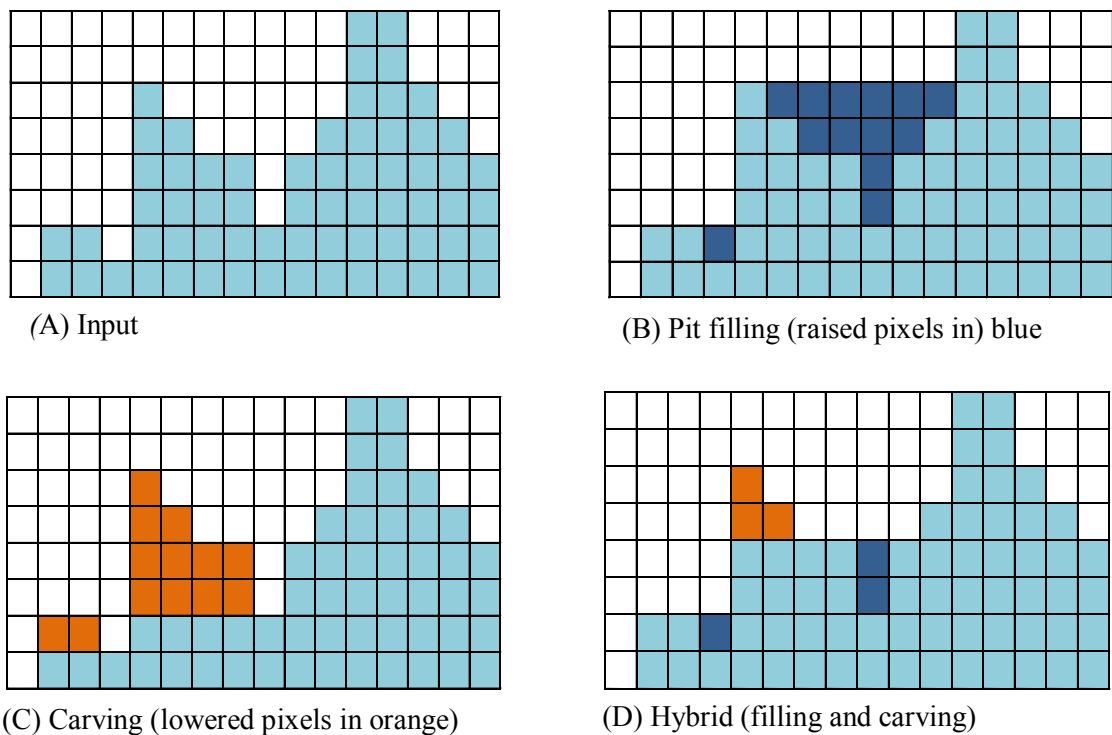
Figure 2.5: Pit removal methods. The spurious pits are the two inner minima in the graph (source: Peckham and Jordan, 2007)

2.3.4 Flow direction

The second step in the process of delineating stream networks from DEMs is assignment of directions. A flow direction raster shows the direction of water flow out of each cell of a DEM. As mentioned earlier, numerous algorithms have been developed to calculate flow direction from digital elevation data. The most popular is the D8 single flow algorithm (O'Callaghan and Mark, 1984), which has been implemented in a lot of commercial GIS software such as ArcView, ArcGIS, IDRISI or GRASS, because of its simple and efficient computation, and strong capability in dealing with spurious depressions and flat areas (Gandolfi and Bischetti, 1997; Lindsay, 2006; Schauble et al 2008; Tarboton 1997). Moreover, the popularity of this algorithm is due to its capacity to generate directly fully connected stream networks and also to the fact that it is based on overland flow simulation, the hydrologic process largely responsible for initiating and maintaining stream networks (Martz and Garbrecht, 1995). The flow of water over a gridded surface is determined by considering the direction of steepest downhill slope of the eight surrounding cells. As shown in Figure 2.6, flow direction is encoded to correspond to the orientation of one of the eight cells surrounding the cell that is located in the middle of a window of 3 x 3 cells (Burrough and McDonnell, 1998; Jenson and Domingue, 1988). However, the D8 flow direction determination method has long been considered to oversimplify the flow process, due to the fact that the flow direction is limited to only one of eight cardinal directions at a time (Kenny and Matthews, 2005; Wise, 2007). Thus, it is not suitable for areas where divergent flow occurs, convex slopes and ridges (Wilson and Gallant, 2000). Another weakness in the D8 is the parallel flow path problem that occurs because flow direction can be assigned only in one of two principal directions: a cardinal or diagonal direction. When the true flow is at an angle or not parallel to the principal direction, errors occur (Wilson et al., 2008).

To overcome the limitation of the D8 algorithm, multiple flow direction algorithms have been developed which distribute flow downslope to one or more neighbouring pixels with weighting by slope. Algorithms such as; Multiple Flow (MFD) (Quinn et al., 1991), DEMON (Costa-Cabral and Burges, 1994), D-Infinity (Tarboton, 1997) have long been used to create multiple flow direction maps from raster DEM datasets. The multiple flow algorithms improve the D8 by distributing multiple stream flows from a grid to its neighbours, eliminating the parallel flow path problem. However, they do not create a single flow path but multiple flow paths from a grid so that they tend to cause considerable dispersions of flow in downstream and even discontinuity in the middle of supposed stream networks (Wilson and Gallant, 2000). Furthermore, according to Wise (2007), some researchers have compared different flow routing algorithms and found that single and multiple flow path algorithms produce significantly different results.

Even though the multiple flow algorithm methods enhance flow direction problems in the D8 method, they still have dispersion and multimodal stream link problems. As Tarboton (1997) concludes, trade-offs take place by selecting one stream mapping method over others. For instance, the D8 method has the advantages of the prevention of the dispersion problem, robustness to manage large data, simplicity and efficiency of computation, and a strong capability in dealing with spurious depressions, whilst it has errors inherent in flow direction determination. In contrast, the alternative methods have more sophisticated flow direction modelling functions in compensation to dispersions and multimodal stream links.

The choice of which flow direction algorithm to use can be quite difficult, where some methods are more suited to certain applications than others. For example, in applications of flow routing that involve the extraction of streams which are used in drainage network analysis (i.e. the analysis of topological and geometric characteristics of the stream networks) or for catchment boundary delineation, a single flow direction algorithm such as D8 is

preferable (Desmet and Govers 1996, Li et al. 2005, Wolock and McCabe 1995, Zhou et al. 2008).

78	72	69	71	58	49
74	67	56	49	46	50
69	53	44	37	38	48
64	58	55	22	31	24
68	61	47	21	16	19
74	53	34	12	11	12

(A) Elevations
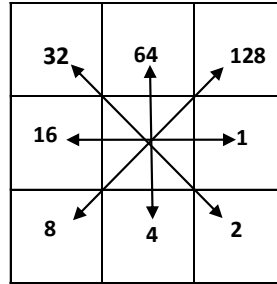
(B) Flow direction codes

32   64   128

16 ←   → 1

8   4   2
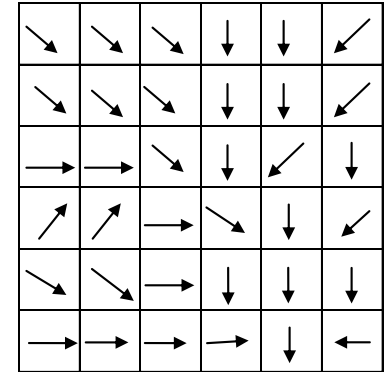
(C) Symbolic representation of flow directions

2	2	2	4	4	8
2	2	2	4	4	8
1	1	2	4	8	4
128	128	1	2	4	8
2	2	1	4	4	4
1	1	1	1	4	16

(D) Flow direction grid values

Figure 2.6: Assignment of flow directions using the D8 model (modified from Li et al. 2005)

2.3.5 Flow accumulation

Using a flow direction surface, a flow accumulation raster can be calculated. The flow accumulation value for a cell represents the number of cells upstream that drain into it (Li et al., 2005) (Figure 2.7). Naturally, water flows in an upslope (catchment area) to downslope (dispersal area) direction accumulatively. Therefore, the lowest area will collect the water flows from all cells in the catchment area. Flow accumulation is considered as a powerful GIS application because calculating the accumulation grid as a spatially distributed quantity

allows determination of drainage area, not just at one point, but also at any point within the

original DEM. A flow accumulation grid can be studied according to each cell's

accumulation value. Cells having high accumulation values generally correspond to stream

channels, whereas cells having zero values - which means no water from other cells flows to

them - must correspond to points at peaks or ridge lines (Jenson and Domingue, 1988). The

cell located at the outlet of the catchment has a value equal to the sum of all of the cells in the

catchment.
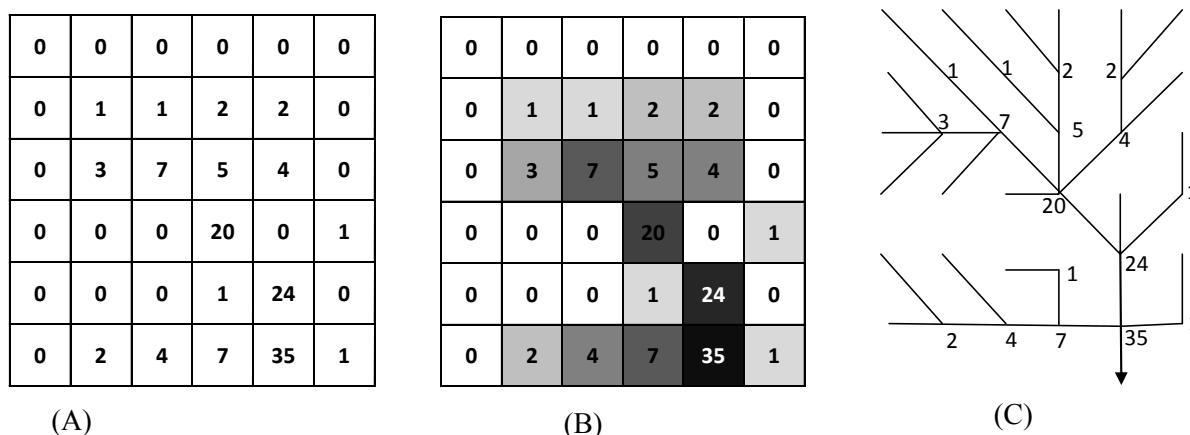
Figure 2.7: Flow accumulation grid (A), flow accumulation with shading (B), and schematic of drainage network (C) (modified from Li et al. 2005).

2.3.6 Channel network identification

As discussed above, once the flow accumulation grid is created, the stream network can

be extracted by applying a threshold value to the flow accumulation grid (Dobos and

Daroussin, 2005; Liu and Zhang, 2011). The threshold value represents the minimum

upstream drainage area that is necessary to delineate an adequate stream network. All those

cells with flow accumulation values greater than this threshold will be linked together and

vectorized to become flow lines. The drainage network will be formed from all these flow

lines and can be represented by a tree structure (Figure 2.7C). The level of detail of the

extracted stream networks depends on the threshold value used for the flow accumulation.

For example, using a smaller threshold value will produce a denser stream network data than using a larger one (Wang and Yin, 1998).

2.3.6.1 Threshold definition

Threshold value is referred to as a critical threshold area that represents the minimum support area required to delineate an adequate channel network (Wilson and Gallant, 2000). This approach is based on the assumption that channels form where the area drained by a given point (called contributing drainage area) exceeds some area threshold (called critical drainage area) (Soille, 2007). Threshold of flow accumulation is a key factor in stream network extraction from DEMs and will strongly influence the results obtained (Lin et al. 2006). However, the selection of an appropriate threshold value is difficult and there is no consensus about how it should be chosen. Nevertheless, the most widely used approaches are the contributing drainage area method and area-slope method (e.g. Montgomery and Foufoula-Georgiou, 1993; Ijjasz-Vasquez and Bras, 1995; Hancock and Evans, 2006; Henkle et al., 2011). The accuracy of delineated drainage networks varies from method to method, and depends on the associated threshold values (Orlandini et al., 2011).

The contributing area method requires a supporting area threshold. The selection of an adequate supporting area threshold is usually a trial and error process until the desired value is reached, and needs to take into account the DEM resolution and terrain characteristics (Dobos and Daroussin, 2005). Selections of different flow accumulation threshold values produce a radically different drainage network in terms of total stream length, stream order, and drainage density. The definition of an adequate threshold value has been the subject of several studies and often the threshold is set to the value that makes the resulting stream network terminate at approximately at the same locations as a reference network obtained from large scale topographic maps (Colombo et al. 2007; Da Ros and Borga, 1997), thus using trial and

error until the desired extent is reached. Experience has also suggested that good results can be achieved if the threshold is set to the value of 1% of the maximum flow accumulation (Maidment, 2002; Tang and Liu, 2009) or the mean accumulation value in all the cells (Li et al., 2005).

Efforts have also been made to obtain an appropriate threshold value by using the log – log linear drainage area-slope relationship as computed from DEMs (Colombo et al. 2007, Da Ros and Borga, 1997; Tarolli and Dalla Fontana, 2009; Henkle et al., 2011). This approach is based on the assumption that different inflection points can be observed in the log-log plot, suggesting that these enable the distinction between various geomorphic and hydrologic regimes (Montgomery and Foufoula-Georgiou, 1993). These drainage and slope regimes include hillslopes, unchanneled valleys, debris flow-dominated channels, and alluvial channels. Figure 2.8 illustrates the hillslope-to-valley transition generated by Montgomery and Foufoula-Georgiou (1993). There are two inflection points in area-slope relationship depicted by the plot, the first infliction is related to the hillslope-to-valley transition, while the second is related to the transition from debris flow-dominated channels to gentler channels (Tarolli and Dalla-Fontana, 2009). For the log – log analysis, a routing algorithm that allows for dispersion of flow such as D-Infinity (Tarboton, 1997) was used for the calculation of the local slope and the contributing area (Colombo et al. 2007). However, as noted already, all these analyses are strongly affected by DEM accuracy and resolution.
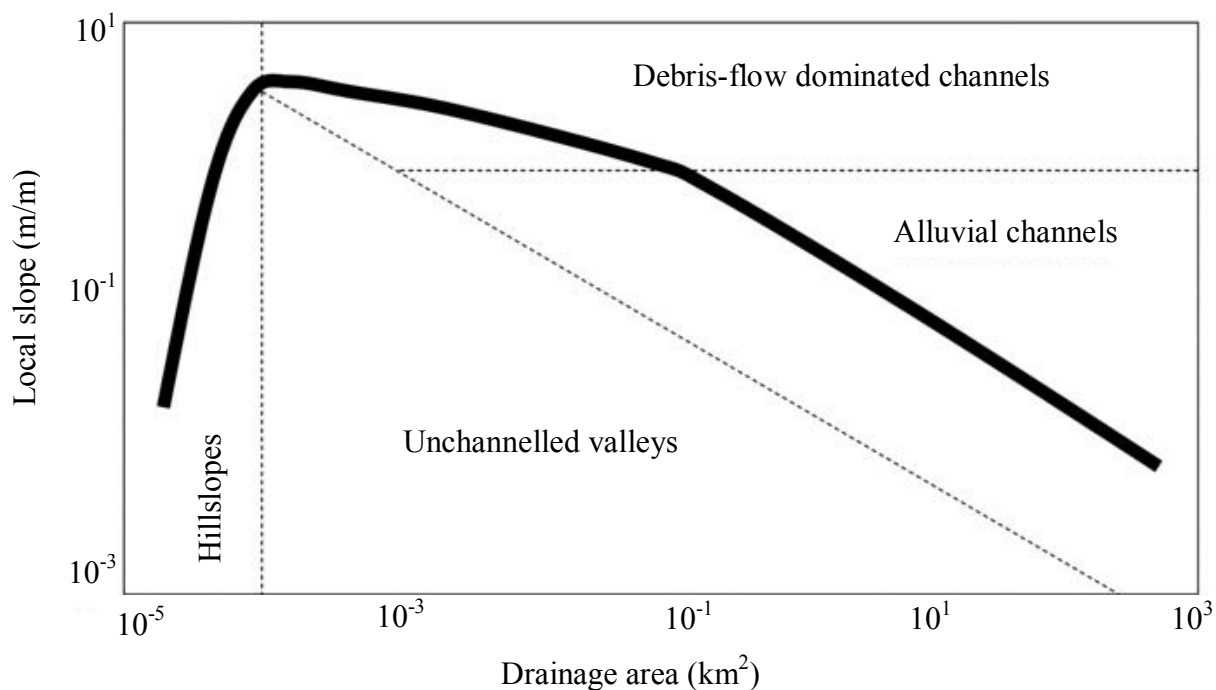
Figure 2.8: Schematic illustration of relations between drainage area and local slope depicting transition from hillslopes to valleys (Montgomery and Foufoula-Georgiou, 1993)

Other researchers, such as Lin et al. (2006), McNamara et al. (2006) and Tribe (1992), have suggested the identification of channel initiations (valley heads) as an alternative to the threshold contributing area for positioning channel sources. The advantage of this approach is the constraining of the drainage network to areas of the digital landscape where there is morphological evidence of a valley head, while retaining the overland flow simulation as the basic approach for the extraction of drainage network below the channel sources (Martz and Garbrecht, 1995).

The identification of the channel networks is therefore a crucial step in catchment management. However, each of the methods presented here has certain requirements and limitations that make their universal applicability limited (Orlandini et al., 2011). There is consequently a need for further research on this issue.

2.3.7 Drainage network comparison

Hydrological modelling and catchment resource management require accurate stream networks and catchment boundaries to understand the flow of water on the land surface. This will help land managers to choose the best management practices for maintaining water quality and quantity. Thus, accuracy assessment or validation of stream networks and catchment boundaries should be a key component of any hydrological modelling project. This is particularly necessary when automatically generating spatial data (in this case stream networks) from computational algorithms or methods using raster data (Zhang and Goodchild, 2002). Such an assessment of accuracy gives researchers the ability to quantitatively compare methods and results and allows decision-makers to be more confident in the use of spatial data analysis results in the decision-making processes.

2.3.7.1 Effect of DEM source and resolution on the accuracy of delineated drainage networks

It has been established that different DEM resolutions and sources, processing steps, and topography lead to differences in the extracted drainage networks and catchment boundaries. These differences can be identified visually and quantitatively, and most techniques rely on measurement of distance between delineated network features and reference features or comparison of attributes such as stream order, stream length, and drainage density. Although stream networks can be assessed qualitatively, based on visual inspection, quantitative methods can improve the accuracy and ease of the comparative analyses.

Lin and Zhang (2011) compared drainage networks extracted from two different DEMs (LiDAR 3m DEM and Vicmap10m) visually and quantitatively in terms of attributes such as stream order and drainage density. Visual validation of the extracted drainage networks was

also carried out using high spatial resolution (0.35 m) aerial photographs with the help of 3D viewing techniques. They used a small threshold value (0.025 km²) in order to delineate detailed drainage networks in flat areas. They found that the LiDAR 3m DEM provided a more detailed drainage network compared with the Vicmap10m DEM.

Poggio and Soille (2011) compared drainage networks extracted from four different DEMs, (ASTER, SRTM, NEXTMap (DSM) and NEXTMap (DTM)). Monte Carlo simulation was used to obtain a probability estimation of the position of the drainage networks using a higher resolution reference data. Results were compared with an independent reference drainage network. The datasets examined were (i) the inverse of the channel probability map *(not channel probability =1 – channel probability value)*; (ii) the average of all the 100 simulated DEMs; (iii) the drainage network extracted from the original dataset; and (iv) the highest overall probability drainage network amongst all the drainage networks that were extracted in the 100 realisations. They compared the stream networks that were extracted from the above four datasets using two methods; (a) calculating the overall probability of the drainage network by summing the values of the probability maps for all the cells belonging to the network considered, and (b) comparing all these networks to the independent reference network using Euclidean distance to assess the spatial match of the extracted drainage networks. They found that the network extracted from NEXTMap DTM, particularly the inverse of the channel probability map, was the closest to the reference network.

Gallego et al. (2010) also studied the uncertainty related to the extraction of stream networks from DEMs. They performed their comparative evaluations by calculating several geomorphologic parameters for each stream network extracted. These parameters were basin area, Horton/Strahler's order, number of stream heads, total stream length, drainage density, highest elevation in basin, elevation at basin pour point, average slope for basin, and basin

perimeter. They found that DEM resolution did not have a great influence on most basin parameters, except for average slope of the basin. On the other hand, resolution had a very significant effect on the accuracy of the stream length in the automatically delineated stream networks.

In order to assess local and regional ecological risk to the landscape in a protected biological resources area, Mantelli et al. (2011) compared automatically extracted drainage networks and watershed boundaries from three different DEMs, SRTM, TOPODATA (obtained from InSAR) and ASTER, to a reference drainage map adopted as a ground truth. They compared each extracted network to a total of 11,581 points, randomly picked from the reference drainage map, where the distances between each drainage reference point and the nearest point from the extracted network were calculated. The extracted watersheds were compared visually and also in terms of area. They found that drainage network generated using TOPODATA (30m) was more similar to the reference network than those extracted using ASTER or SRTM datasets. The network generated using ASTER-DEM produced many commission errors and the one generated using SRTM produced a poor network, less detailed than the others.

Hengl et al. (2009) assessed the spatial accuracy of the derived stream networks by calculating the main distance from point line sets which can be derived by overlaying the delineated stream network over a buffer map generated using the actual stream network. Penas et al. (2011) compared the spatial accuracy of several stream networks extracted from DEMs with different spatial resolutions and different sources ranging from regional (topographic 5 m DEM) to national (topographic 25 m DEM) to global (SRTM 90 m) scales in relation to a reference river network. They assessed the degree of coincidence between each of the extracted stream networks and the reference network by applying buffers of 5, 15, 20, 30, 40, 50, and 60 m to the extracted stream networks and evaluating the percentage of

vertexes from the reference network that fell inside each of the buffers. They found that the 5 and 25 m DEMs generated a more spatially accurate stream network than the 90 m DEM.

Other researchers such as Hengl et al. (2010) and Lindsay (2006) have used geostatistical simulation (Monte Carlo method) to evaluate the uncertainty in derived stream networks from DEMs. A large number of stream network realisations have been compared in terms of the probability of any DEM cell being part of a stream channel. This approach is not a direct comparison of any pair of networks, but it provides a measure of sensitivity to possible stream location error.

2.3.7.2 Measuring the positional accuracy of stream networks

It is important to assess the reliability of stream networks because they are often used in environmental modelling, which in turn is used in water resources and catchment management applications (Lindsay, 2006). One of the most critical attributes of drainage networks is the configuration in terms of spatial locations (Penas et al., 2011). According to Goodchild (1993), all spatial data contains errors. However, if one dataset is assumed to be the best representation of a particular feature, then the error contained within other features can be estimated by comparing them to the reference data. For example, in Figure 2.9, the red lines represent a derived stream network and the blue lines represent the reference stream network. Therefore, the positional accuracy of derived stream network segments can be defined through measures of differences between the locations of these features and locations determined with higher accuracy from the reference dataset. The mean of these differences is used to quantify the horizontal offset error between the reference stream channel and the delineated drainage networks. These errors are comparatively evaluated to determine which DEM best describes the relative terrain when different stream networks extracted from different DEMS are compared to the reference network.
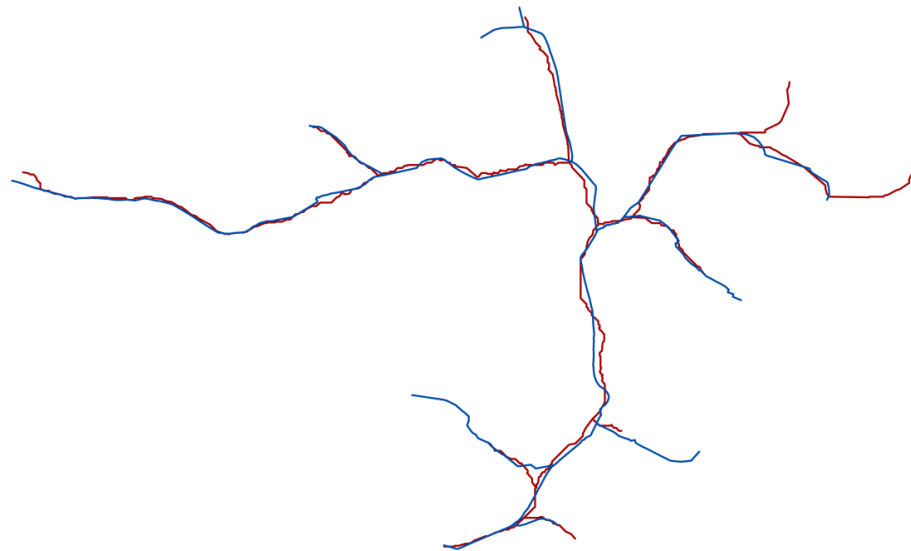
Figure 2.9: Two representations of the stream networks in the Blackwater sub-catchment of the River Wensum, reference network shown in blue and the derived stream network shown in red.

2.3.7.2.1 Root Mean Square Error (RMSE)

Stream segment positional uncertainty can affect the stream network characteristics. Positional difference between an absolute position of a mapped stream segment (polyline) and that in a reference dataset can be used to indicate the stream segment's positional accuracy. RMSE of the positional difference between the delineated and reference stream segment can be computed to indicate stream segment positional accuracy (Anderson and Ames 2011). The FGDC (1998) used RMSE to estimate the positional accuracy of spatial features. Anderson and Ames (2011) used RMSE to compare the degree of matching between a stream network delineated from LiDAR data and a reference network data. Zhang and Goodchild (2002) also discuss using horizontal RMSE as a measure of uncertainty in continuous variables, categorical variables and objects associated with spatial data. Horizontal RMSE is the square root of the average of squared distance differences between extracted dataset coordinate values and coordinate values from a higher accuracy reference data for identical points.

2.3.7.2.2 Epsilon band

The true location of a line can be thought to occur at some displacement from the measured position of the line, lying within a band on either side of the measured position. The

width of the band reflects the standard error, a measure of the uncertainty of the line's location. These bands are sometimes referred to as epsilon bands (Chrisman, 1991). The epsilon error band model has been used to describe the inaccuracy of a modelled line (Zhang and Goodchild, 2002). The band is formed as a constant radius error band around the position of the reference line (Goodchild and Hunter, 1997). Hence, the shape of the band looks like the buffer of a line (Figure 2.10).
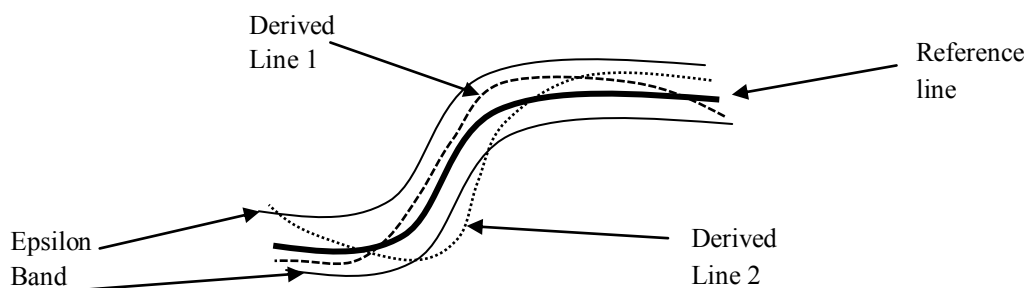
Figure 2.10: The epsilon band concept. The true position of the line (stream) will occur at some displacement from the measured position, between the two parallels of the epsilon band. Modified from Zhang and Goodchild (2002)

The proportion of lines within a specified band's width can be used to assess line accuracy. For example, 95% of the digital line vertexes may be required to be within an epsilon band of a specified distance. According to National Map Accuracy Standards for horizontal accuracy of maps, 95% of errors are expected to lie within 1/30 inch (0.85 mm) for maps at scales of 1:20,000 and finer (Longley et al., 2005). Longley et al. (2005, p.142) proposed a convenient rule of thumb used to provide error estimates for features on maps, in which a typical quality criterion is that "… positions measured from maps are subject to errors of up to 0.5 mm at the scale of the map". Multiplying this 0.5 mm by the scale of the map gives the corresponding distance on the ground, so this 0.5 mm translates to 0.5 m at a scale of 1:1000; 5 m at 1:10,000; 50 m at 1:100,000 and so on (Hunter and Goodchild, 1995; Longley et al., 2005).

2.3.8   Conclusions

Hydrological modelling and catchment resource management require accurate stream networks and catchment boundaries for better understanding of how water is routed across the land surface. Surface water quality is strongly influenced by the hydrological pathways by which water travels through a watershed (Chapman et al., 2014). It is clear from the literature reviewed above that horizontal and vertical DEM resolution is a critical component to terrain modelling and represents the most important consideration in DEM selection. Within a catchment, erosion processes are often a key mechanism in the transport of diffuse pollutants (such as sediment or phosphates) to water bodies, so accurate determination of overland water pathways enables the study of land use impacts on water quality (Evans, 2010: Heathwaite et al., 2005). As discussed previously, the prediction of water flow pathways by topography analysis is controlled by landscape relief and data resolution. Thus, topography is a crucial surface characteristic in soil erosion and diffuse pollution modelling. These models typically use a DEM to derive the topographical characteristics of the study catchment. Therefore, it is necessary to analyse the reliability of erosion assessments at different spatial resolutions. Soil erosion and diffuse pollution modelling within a context of catchment scale are discussed in the following section.

2.4 Soil loss and diffuse pollution modelling

2.4.1 Introduction

A catchment is the natural scale for the assessment of soil erosion potential or risk, since their shape and characteristics control the pathways and fluxes of water and sediment (Collins and Owens, 2006). In the UK, there is strong evidence that agricultural activities are responsible for a large contribution to degradation in land and water quality as a result of soil erosion and diffuse pollution (Evans, 2010; Boardman et al., 2009; Rickson, 2014; Inman, 2006). Rickson (2014) particularly highlights the importance of fine sediment as a diffuse source pollutant in surface waters. Agricultural topsoil provides the largest contribution to sediment that reaches water bodies, which also provides a strong link between estimated soil erosion and sediment yield in rivers. Several studies (Defra, 2009; Environment Agency, 2004) have argued that over 70% of sediment load in UK rivers comes from arable land. Collins et al. (2009) estimated that 76% of sediment delivered to rivers in England and Wales came from agricultural lands, 15% from channel banks, 6% from urban diffuse sources, and 3% from point sources.

The agricultural contribution to diffuse pollution varies widely as a complex function of soil type, topography, climate, hydrology, land use and land management. This complexity hinders accurate identification of pollutant sources and makes their control difficult. Contributing areas of diffuse pollutants (critical source areas-CSAs) from agricultural sources depend on the coincidence of source factors (soil type, local slope, land use, and land management) and transport factors (runoff, erosion, and channel processes) (Heathwaite et al., 2005). Export of eroded soil from a particular point depends on the connectivity further down slope (Lane et al., 2006). According to Hook (2003), gaps in the connectivity or risk re-exportation chain lead to the capturing and disconnection of the risks. Knowledge about the

locations of the important sources and pathways is helpful in developing appropriate management interventions to reduce the risk to rivers (Reany et al., 2011).

As stated previously, DEMs are used to extract topographic parameters in soil erosion modelling. The topographic features of the landscape have a great influence on the amount of soil loss. DEMs from different data sources and with contrasting resolutions may produce different representations of topography that subsequently result in varying erosion predictions.

2.4.2 Soil erosion

Soil erosion is one of the most serious land degradation problems in the world and has a negative impact on agricultural production and water quality. In the UK lowland areas, cases of high water-based soil erosion have largely been associated with arable farming (Boardman, 2013). The degradation of soil involves the processes of physical detachment of soil particles by water and their subsequent transportation to other parts of the catchment, such as watercourses (Stocking et al., 1995). The potential for soil erosion varies from catchment to catchment depending on the characteristics of the catchment (topography, shape), soil properties, the local climatic conditions, cropping and land management practices, control practices and the size of the catchment under consideration (Drzewiecki et al. 2013; Romkens et al. 2002).

In the case of soil erosion by water, soil material can be detached by raindrops or flowing water. Raindrops hitting the surface have enough energy to detach individual soil particles from the soil mass, initiating the erosion process (splash erosion) (Romkens et al., 2002). The soil detachment rate increases rapidly with rainfall intensity. In simple terms, erosion by water proceeds in three stages: (i) separation of soil particles by the energy of raindrop impact; (ii) transportation of these particles by surface runoff along the slope and

(iii) deposition of mobilised sediments when transport energy reaches a low level (Romkens et al., 2002).

Sheet, rill and interrill erosion represent the major sources of soil lost from croplands in the UK (Boardman, 2013). Sheet erosion is a form of surface runoff, where runoff is concentrated in many small ephemeral streams of water (Toy et al., 2002). Overland flow is of very high frequency and very low magnitude, and thus, occurs area-wide between rills (Hogg, 1982). This area is also called the interrill area and erosion occurring here is defined as interrill erosion (Toy et al., 2002). Rill erosion is a process caused by the concentration of surface runoff. This type of erosion is of lesser frequency but higher magnitude than sheet erosion. Areas of both rill erosion and interrill erosion make up the overland flow areas of landscapes (Toy et al., 2002).

Haygarth et al. (2005) have argued that soil erosion by rainfall drops (splash erosion) and overland flow represent the main pathways through which sediments are lost to rivers. In many cases, agricultural erosion occurs when fields are left bare for large parts of the year, so that rainfall is not intercepted by vegetation and raindrops hitting the soil have high erosive powers. Vegetation cover plays a very important role in reducing soil erosion by water. If the rainfall is intercepted by a canopy, the impact of raindrops on the soil is much lower, which will reduce the amount of runoff and consequently the transport capacity (Drzewiecki et al., 2013).

Since croplands in a watershed are a significant source of sediment, a systematic rating of their potential for erosion would be useful in soil conservation planning. Most importantly, mapping and assessment of erosion prone areas enhances soil conservation and watershed management. Identifying the spacial distribution of areas with high risk of erosion is of great

value in water quality and catchment management application, allowing identification of preferential areas where action against soil erosion is more urgent.

As discussed above, using different DEMs in modelling of watershed processes may result in contrasting predictions of soil erosion. Various approaches and equations for risk assessment or predictive evaluation on soil erosion by water have been discussed in the research literature. The Universal Soil Loss Equation (USLE) and its revisions are the most commonly used model to estimate the long-term average annual rate of soil loss (see Section 2.4.3). However, in many studies, a DEM is incorporated into an erosion model as a given parameter without testing its suitability for terrain modelling at the desired scale of the study, in contrast to other parameters related to soil type, land use and climate (Datta and Schack-Krchner, 2010).

DEMs with different source characteristics and resolutions have been used in many parts of the world to produce soil erosion risk maps on the basis of USLE/RUSLE models. Examples of these studies are given by Prasuhn et al. (2013) for Swizerland (2 m x 2 m LiDAR DEM); Lee (2004) for Boun, Korea (5 m x5 m contour based DEM); Bargiel et al. (2013) for south-eastern Poland (21 m x 21 m stereo image-derived DEM); Parveen and Kumar (2012) for South Koel basin, India (ASTER 30 m); Suri et al. (2002) for Slovakia (50 m contour-based DEM); Sharma et al. (2011) for Maithon catchment, India (STRM 90 m). The published literature indicates that the USLE/RUSLE approach has been applied in most European countries (e.g. Austria, Belgium, Germany, Hungary, Poland, Italy, Spain and Switzerland) as well as the USA and Canada. However, it appears to be less common in the UK, highlighting an aspect requiring further research.

2.4.3 Universal Soil Loss Equation model (USLE)

The Universal Soil Loss Equation (USLE) is a popular empirical approach for the prediction of long-term annual soil erosion loss and the designation of potential risk zones for soil erosion (USLE, Wischmeier and Smith, 1978). It was adopted by the Soil Conservation Service in U.S. in 1958 and has become the most widely used and accepted model for long term assessments of soil erosion. The equation predicts the long-term average annual soil loss associated with splash, sheet and rill erosion using six factors that are associated with climate, soil, topography, vegetation and management. The USLE is often given as:

$$A = R * K * LS * C * P \quad \text{(Eq. 2.2)} \quad \text{(Wischmeier and Smith, 1978)}$$

where A is annual average soil loss, in tonnes per hectare, R is the mean rainfall erosivity factor for a defined period, K is the soil erodibility factor, the average soil loss in tonnes/hectare for a particular soil in cultivated, continuous fallow with an arbitrarily selected slope length of 22.13 m (72.6 ft) and slope steepness of 9%, LS is the topographic factor which represent the slope length and slope steepness, C is the cover management factor, which is used to determine the relative effectiveness of soil and crop management systems in terms of preventing soil loss and P is the support practice factor which represents the soil conservation operations or other measures that control the erosion. The L, S, C and P factors are dimensionless parameters and they are normalized relative to standard plot conditions.

The USLE model was developed by Wischmeier and Smith (1978) based on data obtained from more than 10,000 test plots throughout the eastern part of the U.S. in 20 years of field experiments under natural rainfall (Kinnel, 2010). The USLE is currently a globally accepted method for soil erosion prediction in the U.S. and in other countries all over the world. However, the USLE is known to have a few shortcomings. If just one of the input data is not accurately specified, the multiplication of the six factors will lead to a large error in

58

results (Sonneveld and Nearing, 2003). There are also questions about the reliability of the parameter values assigned to the model (Sonneveld and Nearing, 2003). Despite criticisms, limitations and shortcomings, the empirical Universal Soil Loss Equation (USLE) remains the most commonly used soil erosion model worldwide. This popularity of the USLE can be attributed to its minimal data computation requirements as well as to its transparent and robust model structure (Figure 2.11) (Prasuhn et al., 2013).

Additional research and experience have resulted in upgrades of the USLE during the past 30 years. One of the improved equations developed from the USLE model is the Revised Universal Soil Loss Equation (RUSLE) by Renard et al (1997). The RUSLE incorporates improvements in the factors based on new and better data, but keeps the basis of the USLE equation. In many cases, formulae used to determine the values of R, K, L, S, C and P in the USA have been adopted in other countries. RUSLE uses Equation (2.2) with changes in how some of the six factors are determined, in particular, developing a new method to calculate the cover management factor. For example, a sub-factor approach to the determination of C-factor enables the model to be applied to crops and management systems not present in the original experiments used to develop the model (Kinnell, 2010).

Soil erosion risk differs spatially because of heterogeneous topography, soil types, land cover, land use and management. GIS are able to handle these spatially variable data easily and efficiently. Thus, the use of GIS techniques allows spatially variable soil erosion estimates to be made at reasonable costs and better accuracy (Prasuhn et al. 2013; Csafordi et al. 2012). The required data for the estimation of soil loss (rainfall erosivity, soil data, DEM, land use and management data) have to be converted into a GIS format in order to implement the USLE/RUSLE in a GIS (Pandey et al., 2007). The integration of USLE/RUSLE and GIS can be further applied as a core procedure for other geomorphologic and hydrologic applications such as watershed condition analysis, water quality monitoring of agricultural

pollutants in soils, sediment loading of streams and rivers and diffuse pollution (Blaszczynski, 2001). Different authors have used GIS-based techniques to model USLE factors for predicting soil loss on a grid cell basis (e.g. Bargiel et al., 2013; Csafordi et al., 2012; Drzewiecki et al., 2013; Nigel and Rughooputh, 2010; Prasuhn et al., 2013; Tetzlaff et al., 2013; Volk et al., 2010).
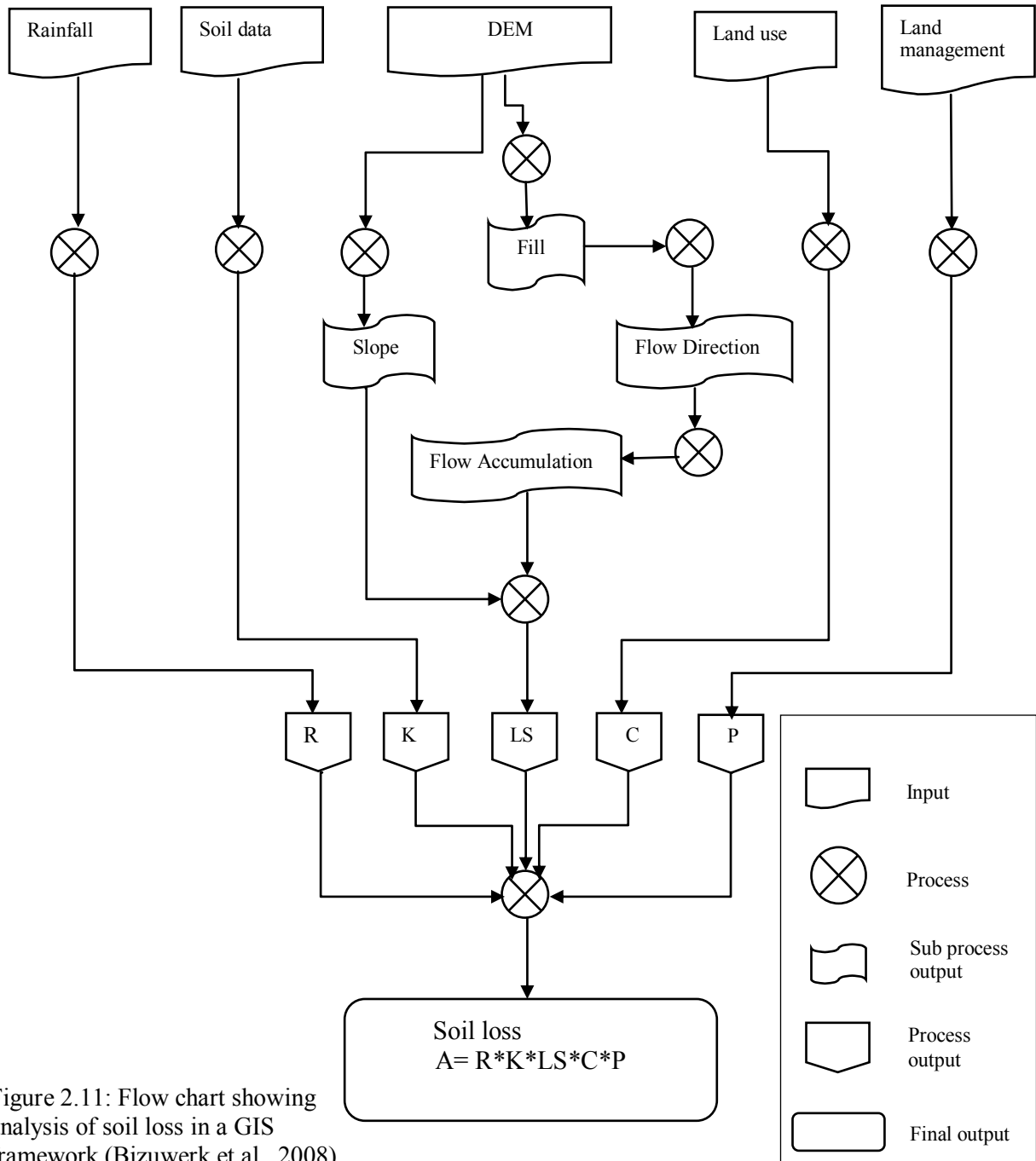
Figure 2.11: Flow chart showing analysis of soil loss in a GIS framework (Bizuwerk et al., 2008)

Despite being used extensively throughout the world, the USLE/RUSLE has been criticized for a number of reasons (Brazier, 2013). For example, in catchments where field sediment losses may be dominated by channel erosion rather than hillslope erosion, the RUSLE is not able to simulate these processes in a meaningful sense, as the empirical basis is limited to hillslope erosion processes and does not account for connectivity and channel or gulley erosion (Csafordi et al., 2012; Evans, 2002; Renard et al., 1991). As mentioned before, the RUSLE is used to predict the long-term average annual soil loss from the study catchment and spatially identify locations with high risk of erosion, however, it does not account for the hydrological connectivity of these locations to rivers. However, other modelling approaches such as SCIMAP do consider this issue and are discussed further below.

2.4.4 Sensitive Catchment Integrated Modelling and Analysis Platform (SCIMAP)

According to Munafo et al. (2005), diffuse pollution is a form of pollution that is not attributable to any one particular source. Diffuse pollution has been conceptualized as consisting of multiple interconnected point sources. The interconnection constitutes a risk (Lane et al., 2006). Not all locations in a catchment contribute equally to the delivery of sediment to the receiving watercourses and hence to water quality degradation (Milledge et al., 2012). This insight has given rise to the concept of critical source areas within a catchment where particular locations contribute disproportionally to in-stream sedimentation and pollution. Critical source areas in catchments are parts of the landscape that have the greatest probability of contributing high sediment loads to receiving waters (Milledge et al., 2012; Reaney et al., 2011). Several modelling approaches have been developed to meet the challenge of identifying these critical source areas within the catchment. According to Lane et al. (2006), Reaney et al. (2011) and Milledge et al. (2012), these can be classified into three

main groups: (i) transport function modelling, (ii) land unit modelling and (iii) land transfer modelling. A detailed description of these models can be found in Lane et al. (2006).

The most developed approach to identifying and modelling the location of critical source areas (CSAs) is the use of a relative risk based approach (Lane et al., 2006). Relative risk based analysis of diffuse pollution risk is a well-established idea and such an approach has already proved to be very effective in diffuse pollution modelling (Munafo et al., 2005). Given an observed change in catchment water quality, the primary challenge is to determine which parts of the landscape are most likely to be contributing to that alteration (Reaney et al,. 2011; Lane et al., 2006), and therefore constitute CSAs. The Sensitive Catchment Integrated Modelling Analysis Platform (SCIMAP) provides a framework for identifying the probable spatial origins of diffuse pollution problems within agricultural catchments. It is based upon a conception of catchments as organising entities: catchments can be conceptualised as a set of flow paths that accumulate distributed sources of possible contaminants from across the landscape into receiving waters, where, for surface waters, diffuse pollution may become visible either through detection of temporal changes in water quality via routine monitoring or through the more limited evidence of physical water quality degradation (e.g. algal blooms) (Lane et al., 2006; Reaney et al., 2011; Milledge et al., 2012). As such, SCIMAP focuses on the question of "where in the catchment is the pollution materials coming from" rather than aiming to produce estimates of the actual pollution load (Lane et al., 2006).

SCIMAP uses three principal inputs: a digital elevation model, land cover and rainfall data. The model combines these three different inputs to determine the probable relative risk of a point in the landscape producing pollution (Figure 2.12). The SCIMAP risk mapping framework comprises two dimensions of analysis: firstly the delimitation of hydrologically connected source areas (CSAs); secondly the accumulation of these CSAs through to the locations of concern (Lane et al., 2006). Surface hydrological connectivity is assessed

through analysis of the potential pattern of soil moisture and saturation within the catchment. The prediction of the spatial pattern of soil moisture is used to assess the ability of each point in the landscape to generate saturated overland flow, which also allows for the probability of continuous flow to the stream network to be assessed. The export of risk in surface flow from a point on the landscape is dependent on each downslope point also being saturated, otherwise the risk will be captured and not reach the stream channel. These risks are accumulated through the catchment from fields through to the receiving water so as to allow for tracing the problem upstream to the locations where the problem is most likely to have originated. A full description of the SCIMAP model is provided in Reaney et al. (2011), who show how it can be used to understand the relationships between land cover, topography (hydrological connectivity) and salmonid fry abundance.
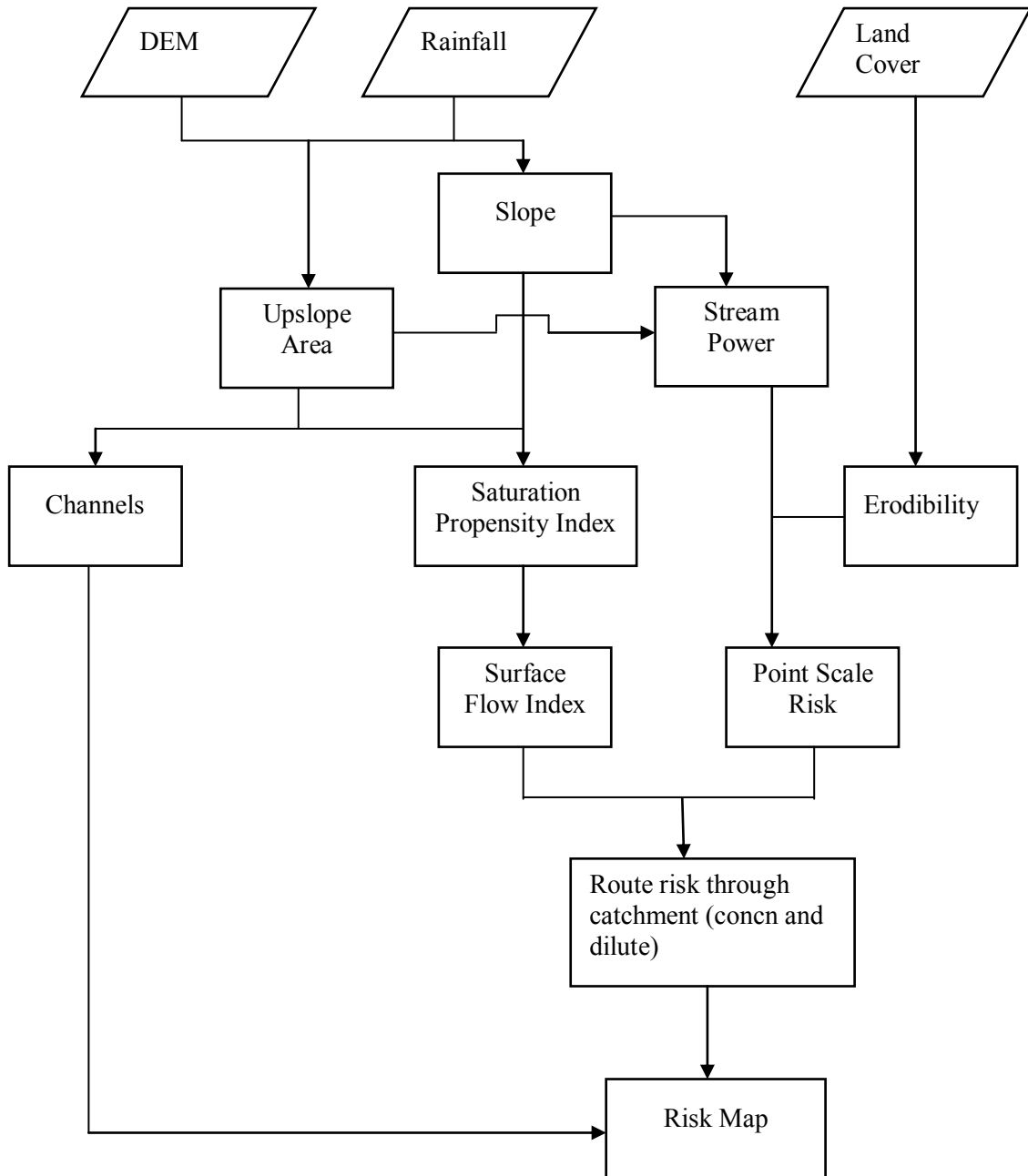
Figure 2.12: SCIMAP model stages (SCIMAP project website: www.scimap.org.uk)

2.5 Chapter conclusions

Water quality and catchment management applications often require detailed terrain data (Lin et al., 2013). Nowadays, DEMs derived from remote sensing form an increasingly important source of information for these applications. However, it is often not easy to decide

what the most suitable source of information is for a specific application. Within a catchment, DEM resolution and data source are sources of uncertainties associated with the prediction of hydrological features such as terrain slope, drainage networks, and catchment boundaries (Wu et al., 2008a). Therefore, the type of DEM needed for a particular application is an important consideration in catchment management.

DEMs derived from optical imagery sources such as ASTER and aerial photography may be negatively affected by the frequency of cloud cover, vegetation, and man-made objects. In contrast, active sensors such as IFSAR (as used for SRTM) penetrate clouds but do not fully penetrate dense vegetation and man-made objects. Data from such sensors can also have voids over water bodies and in desert or mountain areas, which need to be masked or filled to produce a viable DEM. However, for hydrological analysis, these filling methods can over or under-estimate elevation values at the void locations and generate unsatisfactory results (Ling et al., 2005). Nevertheless, airborne radar and LiDAR are rapidly becoming the choice for GIS practitioners and land managers interested in very high resolution DEMs.

From the studies reviewed in this chapter which have evaluated the quality of different DEMs and the effects of DEM source and resolution on the process of drainage network extraction, the following main points can be inferred. The selection of DEMs for hydrological studies is normally focused on those with the highest resolution available, typically on the basis that they avoid more uncertainties (Lin et al., 2013; Liu and Zhang, 2011; Poggio and Soille, 2011). When DEMs with similar resolutions from different sources have been used, IFSAR derived DEMs are often preferred over optical source-derived DEM (Mantelli et al., 2011). In some occasions, even coarser SAR DEMs are more reliable than optical source-derived DEMs. For example, the quality of ASTER 30 m data has been evaluated, and significant anomalies and artefacts noted, even if it has better nominal resolution than 90m SRTM data (Hirt et al., 2010; Huggel et al., 2008; Reuter et al., 2009). All these issues

concerning the accuracy of DEMs, sources, resolutions, and post-processing techniques (e.g. for void filling or converting a DSM to DTM) need to be recognised when selecting a DEM for hydrological analysis within a catchment. In addition, higher resolution data (such as LiDAR) are sometimes only available for limited areas and so another consideration is whether nationally available data sets (such as Ordnance Survey data in the UK) or those with global coverage (e.g. SRTM or ASTER) are suitable for local catchment management applications.

Achieving water quality objectives, such as those set in the WFD, is at risk in many parts of the UK due to the impacts of sediments and associated pollutants from diffuse sources (Tetzlaff et al., 2013). Better decision-making in soil and water resources management to reduce such impacts requires a suitable representation of the catchment topography. However, the literature reviewed in this chapter indicates that the implications of using different DEMs to derive catchment characteristics and in modelling techniques such as RUSLE and SCIMAP are still only partly understood.

The research presented in the remainder of this thesis addresses these issues though a detailed analysis of DEM characteristics, derived parameters and DEM-related modelling outputs for a study catchment in Norfolk. It is intended that the results will help provide guidance to local catchment managers and organisations such as river trusts regarding the best use of DEM datasets in the field of soil and water resource management. Using appropriate DEMs and processing techniques will help identify areas of high soil erosion risk so that preventative practices can be suggested, which in turn will limit amounts of sediment and nutrients entering watercourses and subsequent in-stream sedimentation and water quality degradation.

Chapter 3

Study Area: The River Wensum Catchment

3.1 Overview

This chapter describes the characteristics of the River Wensum catchment in East Anglia, eastern England. The study area is a section of the Wensum catchment. It lies between 1° 15.5′ (605000) and 1° 2.5′ (620000) East Longitude and 52° 41.5′ (315000) and 52° 49.5′ (330000) North Latitude with a total area of 225 km², (15 km x 15 km). Figure 3.1 shows the geographical location of the Wensum study area, including the Blackwater sub-catchment approximately in the middle of the map.

At an early stage in the research (Chapter 4), the whole area illustrated in Figure 3.1 was used as the study area for the general investigation of DEM quality. However, for the rest of the research more focus was given to the Blackwater sub-catchment (Figure 3.1), particularly for the studies of soil loss and diffuse pollution potential risks. Many hydrological processes, such as soil loss, sediment transport and land cover changes, are strongly linked to the catchment level as a spatial reference unit. Moreover, it is necessary to perform soil loss and diffuse pollution studies at catchment or sub-catchment scales so that their results can be compared and validated against water quality data that are usually measured at the outlet of the catchment or its sub-catchments (Walling et al., 2006).

Within the River Wensum area, five priority sub-catchments have been identified by the Catchment Sensitive Farming (CSF) initiative. The Blackwater is one of these and is

intensively monitored as part of the River Wensum Demonstration Test Catchment (DTC) project (Wensum Alliance, 2013) funded by the Department of the Environment, Food and Rural Affairs (hereafter DEFRA). The Blackwater sub-catchment, and the Wensum in general, is a lowland arable catchment typical of much land in eastern England in terms of soil and drainage systems. The Blackwater sub-catchment was therefore selected as the local catchment study for this project. The main reasons for this were the existence of detailed mapping, farm business, meteorological, river flow and water quality data from contacts and infrastructure established as part of the Wensum DTC project. It was necessary to identify the existence of water quality data, both in digital and monitoring data, for the purpose of comparisons to the results from SCIMAP and RUSLE.

3.2 Catchment characteristics

The River Wensum is 78 km long with a catchment area of 593 km². It lies in a rural region with diverse and intense water management interests (Sear et al., 2006), with sites of Special Scientific Interest (SSSI) and European Special Area of Conservation (SAC) status (Cooper et al., 2014). The catchment has very low-relief topography that ranges from approximately 80 metres in the west to a few meters at the confluence with the River Yare near Norwich (Wensum Alliance, 2013). The River Wensum has low channel gradients with shallow and low velocity streams and tributaries. It has a groundwater dominated flow regime, arising from the chalk aquifer (Hiscock et al., 2001).

The climate is relatively dry compared with the west of the British Isles, with an average annual rainfall total of 550 – 750 mm (Mokrech et al, 2008). During the September 2011 to August 2013 DTC monitoring period (our research study period), the average annual rainfall total was 653.6 mm.

Cretaceous Chalk dominates the geology of the catchment, which has influenced the characteristics of the soil. The Wensum catchment is characterised by rich loams, silts and sandy peats, which have a high potential for cultivation (Wensum Alliance, 2013). Soil texture, underlying glacial deposits of clays, sands or gravels strongly influence the hydrological properties of the soil and drainage networks (Sear et al., 2006). In the Blackwater sub-catchment, the west part is dominated by seasonally wet soils that cover chalky boulder clay, whereas central and eastern reaches are predominantly gravels with well drained sandy loam and glacial sands soil. Soils on valley slopes are generally highly permeable and highly fertile sandy loams.

The management of the River Wensum is influenced by the land use of the catchment surface as well as by the modifications made to the channels over time. In the past the channel and floodplain of the River Wensum has been physically modified interrupting the natural flow regime (Collins et al., 2013; Coombes et al., 2007). It is a modified watercourse as it has been altered by the creation of a network of drainage channels (Sear et al., 2006). Activities such as widening, deepening and straightening of tributaries and parts of the main river channels and also construction of embankments have altered natural river network form and processes. Channel management and land use have, therefore, modified the hydrology and channel morphology of the catchment (Coombes et al., 2007; Hiscock et al., 2001).
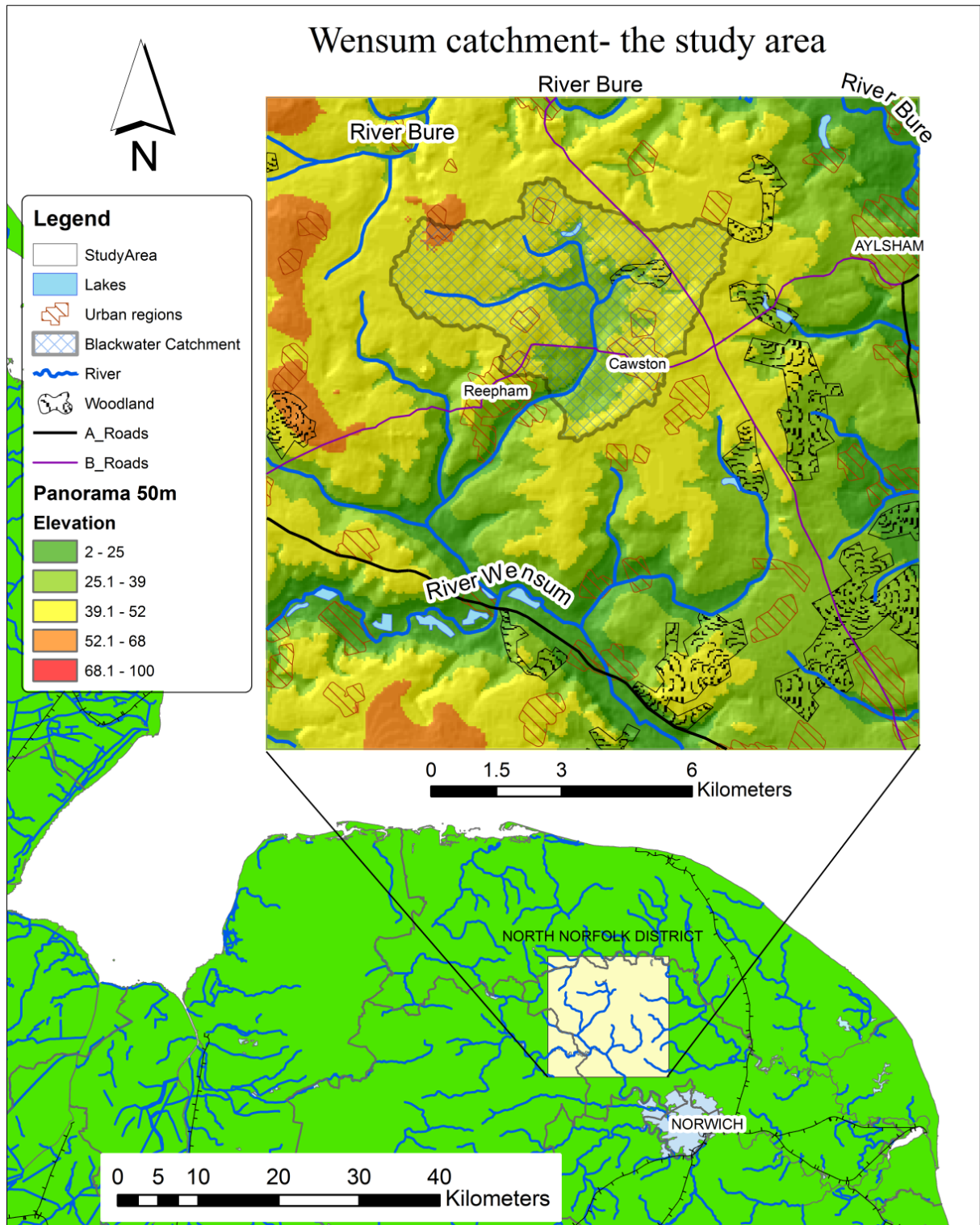
Figure 3.1: Study area.

3.3 Land use and land cover

The Wensum catchment is dominated by intensive arable farming. Intensive arable land use dominates the landscape on the upland areas (plateau) and valley slopes, whereas on the floodplains low intensity grazing has dominated and scattered woodland, scrub and wetlands remain (Sear et al., 2006). On the arable land, cereals, irrigated potatoes and sugar beet are the main crops cultivated (Maréchal and Holman, 2004; Wensum Alliance, 2013). There are also villages and market towns, such as Reepham and Cawston, which the Land Cover Map 2007 (Figure 3.2) shows are also located in the study area.

The Blackwater sub-catchment is used for intensive arable farming. Cereals (wheat and barley), oilseed rape and sugar beet production dominates, although managed grassland pasture also occurs where soils are peaty and poorly drained (Entec, 2012). Farms in the Blackwater sub-catchment are generally capable of having every field cultivated and most of the above mentioned crops as well as, to a lesser extent, potatoes, peas and beans are cultivated in rotations ranging from 3 to 7 years in length across the sub-catchment. As a results of the intensive arable production, streams across the sub-catchment have been identified as having some problems associated with sediment losses from agricultural sources (Rawlins, 2011). Evidence from the detailed flow monitoring measurements also suggests that agricultural pollution has had some detrimental impacts on water ecology in the sub-catchment.
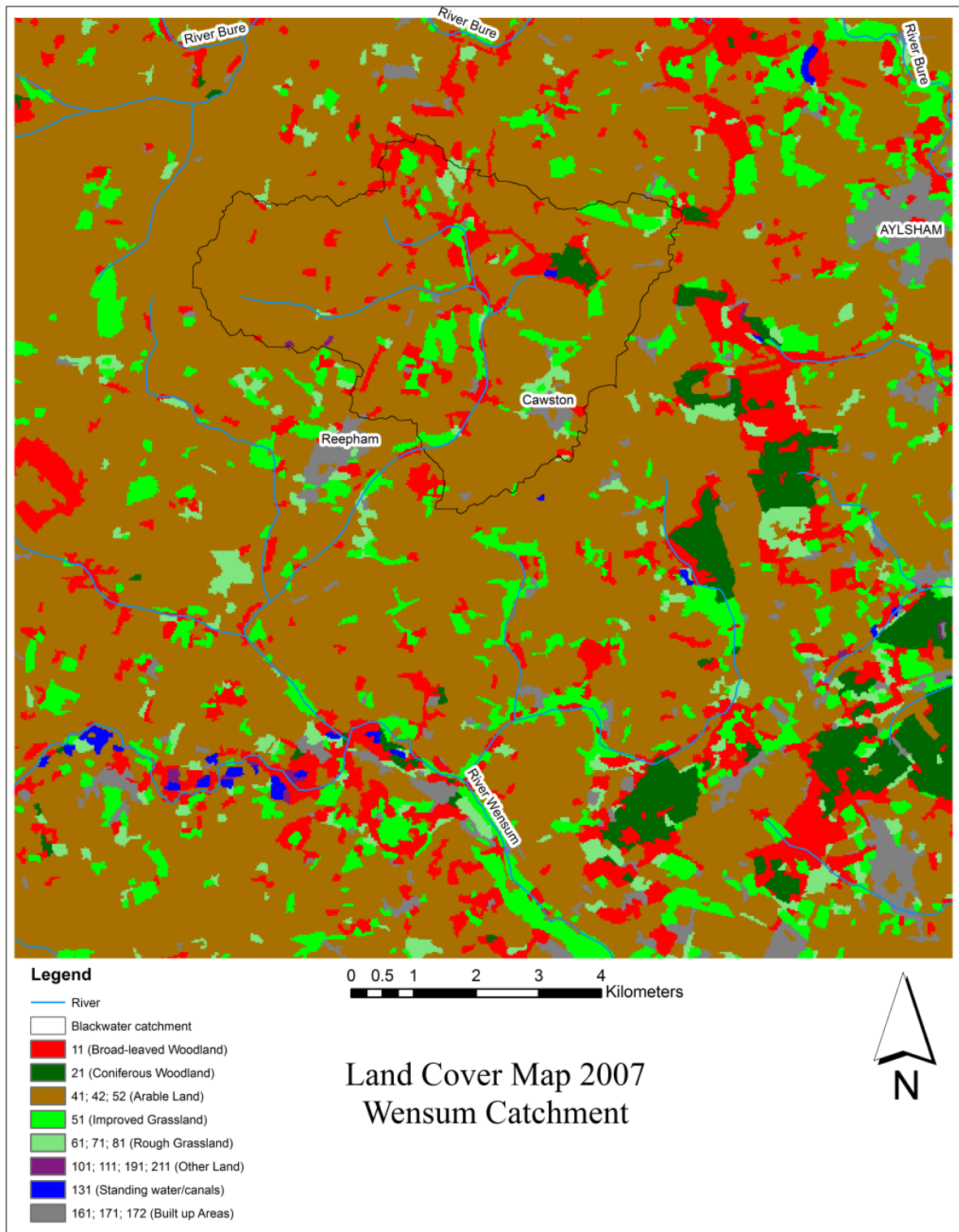
Figure 3.2: Land cover map 2007 for the study area

3.4 The Demonstration Test Catchment (DTC) Programme

In 2010, DEFRA established three Demonstration Test Catchments (DTC) across England to assess whether the implementation of multiple on-farm mitigation measures, targeted to reduce the impact of agricultural diffuse water pollution, could also maintain sustainable food production and environmental benefits (Collins et al., 2013; McGonigle et al., 2014). These catchments were selected for their contrasting natural characteristics, agricultural land use and farming systems, but also reflecting the range of conditions across England (OECD, 2012). As mentioned earlier, one of the three DTCs chosen for study was the Wensum catchment in Norfolk, within which a smaller area – the Blackwater sub-catchment- was subsequently selected for detailed study and intensive monitoring instrumentation. The Blackwater sub-catchment is, in turn, divided into six mini-catchments, labelled A to F, each of which has been equipped with bankside station at its outlet monitoring parameters including turbidity, stage, flow and more at 30 minutes resolution (Wensum Alliance, 2013).

An essential part of the DTC is that data are collected at appropriate temporal and spatial resolutions using a high resolution monitoring infrastructure, where monitoring covers groundwater, surface water, flow and socio-economic aspects of land management. These data are intended to be freely used by others where research is undertaken in a much more collaborative and open way, using the concept of a research platform (McGonigle et al., 2014).

Another important component of the DTC program is to consider new concepts and adopt more integrated management approaches to addressing diffuse source pollution. These approaches recognise the river catchment as the appropriate organising unit for understanding and managing the environment in a context that includes social, economic and political

considerations (McGonigle et al., 2014; OECD, 2012). The outcomes of the DTC research programme are intended to benefit the whole community engaged in land use and water resource management. In general, DTC project is an initiative of DEFRA to provide a research platform from which a number of integrated ways of managing agricultural diffuse source pollution at the river catchment scale can be developed (OECD, 2012).

3.5 Conclusion

The River Wensum catchment, East Anglia was chosen as the study area for this research for reasons explained earlier. As stated above, the River Wensum and its tributaries, particularly the Blackwater sub-catchment, were identified as having high risks from diffuse pollutant substances, including nutrients, heavy metals and pesticides associated with soil loss and sedimentation delivered to the channels (Rawlins, 2011). Therefore, in order to improve the status of the river so it meets the criteria of good water quality and ecological condition under the Water Framework Directive (WFD), problems related to soil loss and diffuse pollution need to be addressed. Sediment mobilized by water from agricultural land and deposited in the rivers is an important component, possibly the most important one, of the turbidity and suspended sediment load in waterways. Thus, as Blackwater sub-catchment is intensively monitored as part of Wensum DTC project it is an ideal testing area for the SCIMAP risk modelling approach for diffuse source of pollution and the RUSLE model for an average annual soil loss estimation within the sub-catchment using different digital elevation models (DEMs), particularly because the results from these two models can be validated and compared with the monitored water quality data.

Chapter 4

DEM quality assessment for the Wensum study area

4.1 Introduction

This chapter begins by describing all the elevation datasets compiled for this study from the perspective of their characteristics and technical specification. The types of the elevation datasets that were selected for this study consist of ASTER 30 m, SRTM 90 m, Landform Panorama, Landform Profile, Landmap DTM, Bluesky DTM and NEXTMap DTM. These types of elevation datasets were selected for this study for their diversities in their resolution, the way they were generated, their source (i.e. contour, optical or radar images) and of course their availability (Table 4.1).

The quality of these elevation datasets is assessed using different approaches. At first, a comparison between the DEMs is performed in terms of slope and elevation descriptive statistics and histograms, cross-sectional profiles, and analytical shading relief images. Then an analysis of all the DEMs against a higher accuracy reference dataset is undertaken. Finally, a statement of whether or not these elevation datasets are of sufficient quality (fit for purpose) for catchment studies is given.

4.2 Elevation dataset characteristics

Different sources and techniques for the generation of DTMs have been developed since their inception in the middle of the 20th century (Maune, 2007; Li et al., 2005). DEMs generated from different sources can be at similar scales but with different characteristics. Traditionally, methods of creating DTMs were from ground survey measurements and the use of vectorized contour lines and spot heights from existing topographic paper maps. Nowadays, significant advances in remote sensing technologies have led to the possibility of a wide variety of higher quality elevation sources (Tighe and Chamberlain, 2009). These regional and global topographic observations are collected by means of optical, radar or laser sensors such as; improved photogrammetric imagery, IFSAR and LiDAR.

Several processing steps needed to be performed before these elevation datasets could be compared. The first is those datasets downloaded in tiles (ASTER and SRTM) covering larger areas needed to be clipped to the study area, while others (Bluesky, NEXTMap and Landform Profile) with smaller tiles were mosaicked into one file covering the whole region. The second was re-projecting the non UK produced data (ASTER and SRTM) from WGS 84 to British National Grid. Moreover, as the assessment of DEM quality often also requires supplementary information about land cover, Land Cover Map 2007 (LCM2007) was downloaded and prepared to help in the analysis process. Below is a brief summary of the technical specifications for all the elevation datasets included in the study.

4.2.1   Remote sensing derived elevation data

4.2.1.1   Shuttle Radar Topography Mission (SRTM)

The Shuttle Radar Topography Mission (SRTM) is a single pass interferometric synthetic aperture (InSAR) mission conducted in February 2000 (Reuter et al. 2007). The

SRTM elevation data cover most of the globe land surface between 60 N and 56 S. It was the first time that a global high-quality DEM was produced with a resolution of 1 arc-second (30 m) and 3-arc second (90 m), however, of these two datasets only 90 m data are available globally, while the 30 m is only for the USA territory (Jarvis et al. 2008). The post-processed SRTM elevation data version 4 has now been released for the entire terrestrial surface and is available at the website of Consultative Group for International Agricultural Research Consortium for Spatial Information (CGIAR-CSI) (Jarvis et al. 2008). It is the latest post-processed SRTM elevation data released, which represent a huge improvement over the previous versions because errors (i.e. voids) were corrected using new interpolation and patching algorithms as well as better auxiliary DEMs (Hirt et al., 2010).

The SRTM DEM was produced using data retrieval technology which is based upon the transmission of one radar signal and reception using two SAR antennas. It can be defined as a "snapshot of the reflective surface of the Earth during the time period of the mission" (Reuter et al. 2007, p. 4). This process produced three dimensional measurements for every single point imaged on the Earth's surface (Weydahl et al. 2007). The SRTM signal measurement resulting from reflective surface elevation is a complicated function of the electromagnetic and structural properties of the scattering surface, and this depends on the terrain type and cover type (Tighe and Chamberlain, 2009). As a result, SRTM data are subject to a number of errors (i.e. voids) due to lack of contrast in the radar image, and because of that a methodology based on spatial filtering was developed to correct this problem (Gorokhovich and Voustianiouk 2006). In general, the error was found to be higher in vegetated areas due to the tree canopy (Sun et al., 2003), and voids were found over water bodies, in mountainous area and in desert areas (Reuter et al., 2007).

The existence of no-data regions initially caused significant problems in using SRTM DEMs, especially in the context of hydrological models and catchment management which

require continuous flow surfaces. For the version used in this study (CGIAR-CSI SRTM data products), CGIAR-CSI applied a hole-filling algorithm to provide a continuous elevation surface (Jarvis et al. 2008). This method involved two steps. First filling small holes iteratively and cleaning the surface to reduce pits and peaks. Secondly, interpolating across large holes using a range of methods, based on the size of the hole and the surrounding landforms. The void-filling process was conducted using a high resolution auxiliary DEM, however, for areas without such details, the SRTM30 data were used (Jarvis et al. 2008).

SRTM data were mosaicked into a number of one degree by one degree tiles. Sample spacing between data points is either 1 arc-second (about 30 m) or 3 arc-second (about 90 m), referred to as SRTM-1 and SRTM-3 respectively. The 3 arc-second DEMs are derived from the 1 arc-second data by averaging of the 9 elevation samples in a 3 x 3 window, and spaced at 3 arc-second intervals. Since the primary error source in the elevation data has random noise characteristics, this error is thus reduced by roughly a factor of three (Gamache, 2004). Each tile is projected in geographic coordinates using WGS84 horizontal datum and the EGM96 vertical datum (Jarvis et al., 2008). The elevation data is provided in meters as 16-bit signed integer data.

Among the elevation data literature, several studies have examined SRTM data quality (Gorokhovich and Voustianiouk, 2006; Rabus et al., 2003; Sun et al., 2003) with different horizontal and vertical accuracy results. In general, the horizontal accuracy has been found to be lower than ± 20 m at 90% confidence level. The DEM vertical errors have been recognized to be ±16 m and ±6 m for absolute and relative accuracy, respectively. Absolute accuracy describes the error throughout the entire mission while relative accuracy stands for the error on a local 200 km-scale.

4.2.1.2 Advanced Spaceborne Thermal Emission and Reflection Radiometer (ASTER)

The Advanced Spaceborne Thermal Emission and Reflection Radiometer (ASTER) is an imaging instrument developed by the Ministry of Economy, Trade and Industry (METI) of Japan, NASA and the Earth Remote Sensing Data Analysis Centre (ERSDAC). Images are acquired by sensors measuring reflectance and radiance in parts of the visible, shortwave infrared and thermal infrared spectrum (ASTER Validation Team, 2009). Amongst these, a near-infrared (NIR) Band 3 is acquired using a nadir and backward looking telescope providing along-track stereo coverage from which high quality DEMs are generated using automated stereo correlation. ASTER GDEM (ver. 1) is a global 1 arc-second elevation dataset which was released to the public in June 2009 by METI, Japan and NASA (Hirt et al., 2010).

The ASTER GDEM data covers the Earth's landmass between 83˚ N and 83˚ S latitudes offering greater coverage over SRTM. The GDEM was created by stereo correlating about 1.3 million scenes, each scene corresponding to about 60 km by 60 km ground area which were collected during an observation period of more than seven years (2000-2007) (Hirt et al., 2010). For the final public release, the data were formatted in 1 x 1 degree tiles as GeoTIFF files with a ground surface distance of 30 m (Tighe and Chamberlain, 2009).

There have been several studies to determine the accuracy of digital elevation data derived from ASTER (ASTER Validation Team, 2009; Goncalves and Oliveira 2004; Hirt et al., 2010; Reuter et al., 2009). The overall vertical accuracy of ASTER elevations is recognized to vary between 10 m and 25 m. Like SRTM, ASTER elevation data are projected to WGS84 horizontal datum and the EGM96 for the vertical datum. ASTER GDEM data were examined in terms of the containment of specific features, such as artifacts and residual anomalies and it was determined that the ASTER GDEM does contain anomalies and artifacts

which affect its overall accuracy and impede its use for certain applications (i.e. hydrological applications) unless external information is used as a supplement (ASTER Validation Team, 2009). There are two main sources of these anomalies and artifacts; one is cloud cover and the other is the algorithm used to generate the final GDEM from the individual ASTER DEMs available. It is important to note that the ASTER GDEM version 1 has no inland water mask applied, consequently the elevations of inland lakes are not accurate. As a result of these shortcomings, ASTER GDEM version 1 was considered to be experimental or research grade (ASTER Validation Team, 2009). A second version of the ASTER GDEM was released in late 2011 which incorporated additional image scenes and improved processing to enhance masking of water bodies and reduce voids (ASTER Validation Team, 2011). However, much of the comparative analysis conducted in this chapter had been completed by then so the results presented here refer to version 1 of the GDEM product.

4.2.1.3 Landmap DTM

The Landmap IFSAR DEM was derived from European Space Agency European Radar Satellite (ERS) data using an interferometry technique which is similar to the photogrammetric process used with stereoscopic aerial photography (Muller et al., 2000). The Landmap project generated a DEM with a 25m cell size for the whole of the UK and Ireland using multi-pass IFSAR based on the ERS satellite 1 and 2 data (Smith et al., 2006). Uniquely, this project employed automated processing of image strips (as opposed to individual image scenes) to produce DEMs at no royalty fee cost for use by the academic community in the UK (Muller et al., 2000; Smith et al., 2006).

IFSAR data can be acquired by single pass or repeat pass techniques. Single pass data are acquired from an aircraft or spacecraft where there are two antenna separated by a known base length, while repeat pass is usually from satellites, where the images are acquired from two passes of the sensor in very similar orbits (Dowman, 2004). The coherence between

IFSAR images is the means by which the suitability of a pair of these images for generating DEMs is measured. It was found that the coherence is usually good on single pass images while it can be poor on repeat pass, especially if the capturing time between the images is significant (Dowman, 2004). An advantage of SRTM data over Landmap is that SRTM DEM was created from single pass data (Nikolakopoulos et al., 2006). In other words, the Landmap DTM product suffers from the problem of poor coherence and atmospheric effects caused by the repeated pass data (Dowman, 2004).

The Landmap data are projected to the British National Grid, and it is believed that the absolute accuracies are better than 30m horizontal and ±20m vertical (Muller et al., 2000). The Landmap DTMs are derived from a DSM product which means that the surface representation could still include man-made objects, such as the upper surface of embankments, bridges, etc. The main problems that been recognized in the IFSAR data are the presence of layover and shadows, the size of footprint and loss of coherence (Dowman, 2004).

4.2.1.4   Bluesky DTM

Bluesky 5m DTM is high resolution elevation data photogrammetrically interpolated from stereoscopic aerial photography collected between 1999 and 2008, where a photogrammetric DSM was produced first then converted to DTM. These data have a cell size of 5m and exist in both integer and float elevation versions, where the elevation value is rounded to the nearest metre and values with potential decimal places, respectively. These data are available for England and Wales from the JISC Landmap service. The Bluesky DTM registered to the British National Grid has 5m and ±2m horizontal and vertical accuracies respectively (Landmap 2011).

4.2.1.5   NEXTMap DTM

NEXTMap is one of the Intermap's core products. Intermap is a global provider of high accuracy, high resolution digital elevation data using airborne single-pass across-track interferometric synthetic aperture radar (IFSAR) X-band data (Smith et al., 2006). The system collects return radar pulses from the X-band twin antenna interferometer, which is separated by a one metre baseline, and the positioning and orientation information are achieved through the use of differential GPS and inertial systems (Intermap, 2011). The IFSAR system has been operated commercially by Intermap since January 1997.

Since this system is a single pass technique, terrain heights (DSM) are collected by trigonometry using the phase difference between signals, the distance between the two antennae and the location of the aircraft (Dowman, 2004). By their nature, the original elevation models provided by the IFSAR system are of the first surface and not the underlying bare earth. The NEXTMap digital terrain model (DTM) is derived from the DSM product by digitally removing vegetation, buildings and other cultural features, leaving the bare Earth's surface dependent on the filtering algorithms that are used and also manual editing efforts (Intermap, 2011).

IFSAR DSM and DTM products are subject to several potential sources of errors which degrade their overall accuracy. The most inherent problems are the altitude and motion of the aircraft, the presence of layover and shadow, footprint and the loss of coherence (Smith et al., 2006). In addition, vegetation cover and severe weather conditions can effect IFSAR product accuracy. Areas covered by vegetation will produce more height measurements error (noise) than other surfaces (specular scatters i.e. bare soil). It is known that in moderate to heavily vegetated areas the elevation measures take place near the canopy top, which produces a noisy pattern over forested areas (Mercuri et al., 2006). As a result, vertical

accuracy of IFSAR DSM and DTM products will be degraded due to the vegetation cover since the radar will penetrate vegetation to some distance near to the canopy top before reflecting, depending on the wavelength.

While IFSAR data can be collected in nearly all kinds of weather conditions, night and day, there still are some cases where data accuracy can be affected. These situations, for example, are air turbulence and clouds with heavy moisture; the former affect the stability of the platform, whilst the latter can absorb the radar energy to some extent (Li et al., 2004).

NEXTMap Britain was implemented in 2002 and was performed in two phases. Phase I covered England, Wales and the southern part of Scotland, while the northern part of Scotland was included in Phase II. A huge effort was made for the validation processes for this programme (Mercer, 2004). NEXTMap DTM data are provided in 5 m cell size grids stored in 32-bit floating format using British National Grid, which is defined by OSGB36 projection. The vertical and horizontal datums are ODN (OSGM91) and ETRS89 respectively. The data have a spatial resolution of 5 m, with a vertical accuracy of 1m (Intermap, 2011).

4.2.2   Ordnance Survey of Great Britain data

4.2.2.1   Landform Panorama (OS 50m)

The Landform Panorama DTM is one of the spatial data products that are provided by Ordnance Survey of Great Britain (OSGB) which is the primary provider of spatial data for the UK. This product is derived from 1:50,000 contour mapping to generate a DEM with a 50 m cell size and an integer elevation value. Landform Panorama DTMs consist of elevation values which have been mathematically interpolated from the contours on the Landranger 1:50,000 scale map series. These height values are located at each intersection of a 50 m

horizontal grid. The Landranger maps were originally generated from stereo aerial photography which was captured during the 1970s (Ordnance Survey, 2010a).

The Landform Panorama data are projected to the National Grid coordinate reference system, which is defined by the OSGB36 datum and distributed in 20 km x 20 km tiles. The elevation values are normally related to mean sea level at Newlyn. There are some variations in the Landform panorama DTM accuracy which depend upon the density of elevation data contained in the contour file and the nature of the terrain. Generally speaking, the vertical accuracy of these data is better than one half of the vertical interval of the source contour data, which is ± 5m. In the flat areas, where there are limited height differences, contours and elevation points may be a great distance apart, this can cause irregularities in the DTM which appear as slight terracing of the terrain (Ordnance Survey, 2010a).

4.2.2.2   Landform Profile

The Landform Profile DTM have been mathematically interpolated from a contour product and has a cell size of 10 m. The contour data that were used to generate this DTM were captured from Ordnance Survey's 1:10,000 scale maps, which have contours spaced at 5 m intervals. These data were supplemented by spot heights (captured by photogrammetric methods in 1987), and high and low water marks from Ordnance Survey 1:250, 1:2500 and 1:10,000 scale digital data. These contour lines, spot heights and tidal lines were converted to a TIN and then to a 10 m regular grid (OS 10m) (Wise, 2007; Ordnance Survey, 2010b). The vertical accuracy of the Landform profile data is believed to be better than or equal to half of the contour interval on the original map, in this case ±2.5m. Landform Profile data is referenced to the Ordnance Survey Great Britain 1936 (OSGB36) datum and projected in British National Grid. These OS elevation data are supplied as OS 5 km x 5 km grid tiles (Ordnance Survey, 2010a).

Table 4.1: Characteristics of DEMs used in this study.

	NEXTMap DTM	Bluesky DTM	Landform Profile	Landmap DTM	ASTER GDEM	Landform Panorama	SRTM
Data source type	Radar images acquired by two IFSAR antennas. Single pass system (X-band)	Aerial photography	Contour data from Ordnance Survey's 1:10,000 scale maps	Radar images using multi-pass IFSAR based on the ERS satellite data	Images acquired by visible and near-infrared (VNIR) bands.	Contour data from Landranger 1:50,000 scale map series	Radar images acquired by two SAR antennas. Single pass system (C-band and X-band)
Processing	Interferometric technique produces DSM which need processing to DTM	Stereoscopic technique produces DSM which need processing to DTM	Elevations mathematically interpolated from contours data	Interferometry technique produces DSM which need processing to DTM	Stereo correlation	Elevations mathematically interpolated from contours data	Interferometric technique using two SAR images
Spatial resolution	5 m	5 m	10 m	25 m	30 m	50 m	90 m
Accuracy	Vertical accuracy of ±1m	Vertical accuracy better than ±2.5m	Half contour interval, in this case ±2.5m	Vertical accuracy better than ±20m	Vertical accuracy vary between 10 m and 25 m	Half contour interval, in this case ± 5m	Vertical accuracy vary between 6 m and 16 m
Coverage	National coverage	England and Wales	National coverage	UK and Ireland	Between 83° N and 83° S	National coverage	Between 60° N and 56° S
Example of problems	Some artifacts that are not completely removed during the process of converting DSM to DTM	Some artifacts that are not completely removed during the process of converting DSM to DTM	Stair-step problem, steep slope between different contours positions and integer rounding problem	Artifacts caused by presence of layover and shadows, the size of footprint and loss of coherence	Contains significant anomalies and artifacts caused by residual clouds and the algorithm used.	Integer rounding problem in flat areas (contour ghosts)	Data holes because of a lack of contrast in radar image, presence of water or excessive atmospheric interference.
Acquisition date	30-Dec-2001 to 13-Oct-2003 (Mercer, 2004; Smith, 2010)	1999-2008 (Bluesky; Landrmap, 2014)	Regularly maintained (Smith, 2010)	1995-96 (Smith et al., 2006)	2000-2008 (Urai et al., 2012)	Maintained until 2002 (Smith, 2010)	02-2000 (Smith et al., 2006; Tighe and Chamberlain, 2009)

4.3 DEM quality assessment

4.3.1 Comparison of elevation and slope descriptive statistics

In this study, seven different DEMs were compared using statistical and graphical techniques (Maune, 2007; Penas et al., 2011). Elevation and slope characteristics were assessed by comparing minimum, maximum, mean and standard deviation values, as shown in Table 4.2 and Table 4.3.

Table 4.2: Elevation descriptive statistics

Statistical Calculation	NEXTMap 5m	Bluesky 5m	OS10m	LandMap 25m	ASTER 30m	OS50m	SRTM 90m
Minimum (m)	7.8	8.3	8	-1	7	8	5
Maximum (m)	75.8	64.6	62	75	61	63	67
Mean (m)	38.3	37.04	37.2	34.5	31.8	36.8	38.1
Standard Deviation (m)	11.1	10.9	10.7	11.3	9.8	10.9	10.6

Table 4.3: Slope descriptive statistics

Statistical Calculation	NEXTMap 5m	Bluesky 5m	OS10m	LandMap 25m	ASTER 30m	OS50m	SRTM 90m
Minimum (°)	0	0		0	0	0	0
Maximum (°)	56.2	31.3	30.4	38.9	27.9	10.3	11.8
Mean (°)	1.7	1.4	1.5	2.97	2.6	1.1	1.3
Standard Deviation (°)	1.99	1.25	1.65	2.3	1.6	0.97	0.97
% of area ≥ 3 (°)	13.7%	9.3%	16.3%	36.5%	37.3%	3.0%	6.1%

From the elevation descriptive statistics (Table 4.2), it can be seen that the ASTER and Landmap DTMs have the lowest mean elevation values, 31.8 m and 34.5 m, respectively. This could indicate that these two datasets do have some accuracy problems, with elevation values usually underestimated. A study by Blanchard et al. (2010) found that compared to SRTM 90 m, ASTER 30 m accuracy was lowest for agricultural and grassland areas. It is clear from the table that the Landmap 25 m has the worst accuracy on most statistical measures; minimum (-1 m), maximum (75 m) and, standard deviation (11.3 m) compared to

results from other datasets. On the other hand, several other datasets (NEXTMap 5 m, Bluesky 5 m, OS10 m, OS50 m and SRTM) produced very similar results.

In the literature, it is common that DEMs with lower resolutions produced lower average slopes (e.g. Kienzle, 2004; Li and Wong, 2010; Wu et al., 2008; Zhang et al., 1999). However, in this study, coarser resolutions, ASTER 30 m and Landmap 25 m DEMs, have higher mean slope measures compared with the higher resolution DEMs, Bluesky 5 m and NEXTMap 5 m, 2.6° for ASTER and almost 3° for Landmap DTM (Table 4.3). This is probably related to the DEM generation process and data source, rather than to DEM spatial resolution or vertical accuracy.

4.3.2   Elevation histograms

It is clear from the histograms in Figure 4.1 below, that the elevation data derived from remote sensing sources (i.e. ASTER, SRTM ,Landmap DTM, Bluesky DTM and NEXTMap DTM) are, to some extent, distributed as normal bell-curves around values relatively close to the mean elevation value of each dataset. On the other hand, histograms of DEMs generated from contour data show some diagnostic peaks (spikes) indicating over-representation of the contour lines (Fisher and Tate, 2006). From histograms it can be seen that most of the distributions are negatively skewed (Lee and Wong, 2001), which mean that most of the elevation values in each dataset are greater than the corresponding mean, the exception being the ASTER dataset which has more of a positive skew where its histogram shows a normal distribution around the value of 28 while its mean value is 31.8.
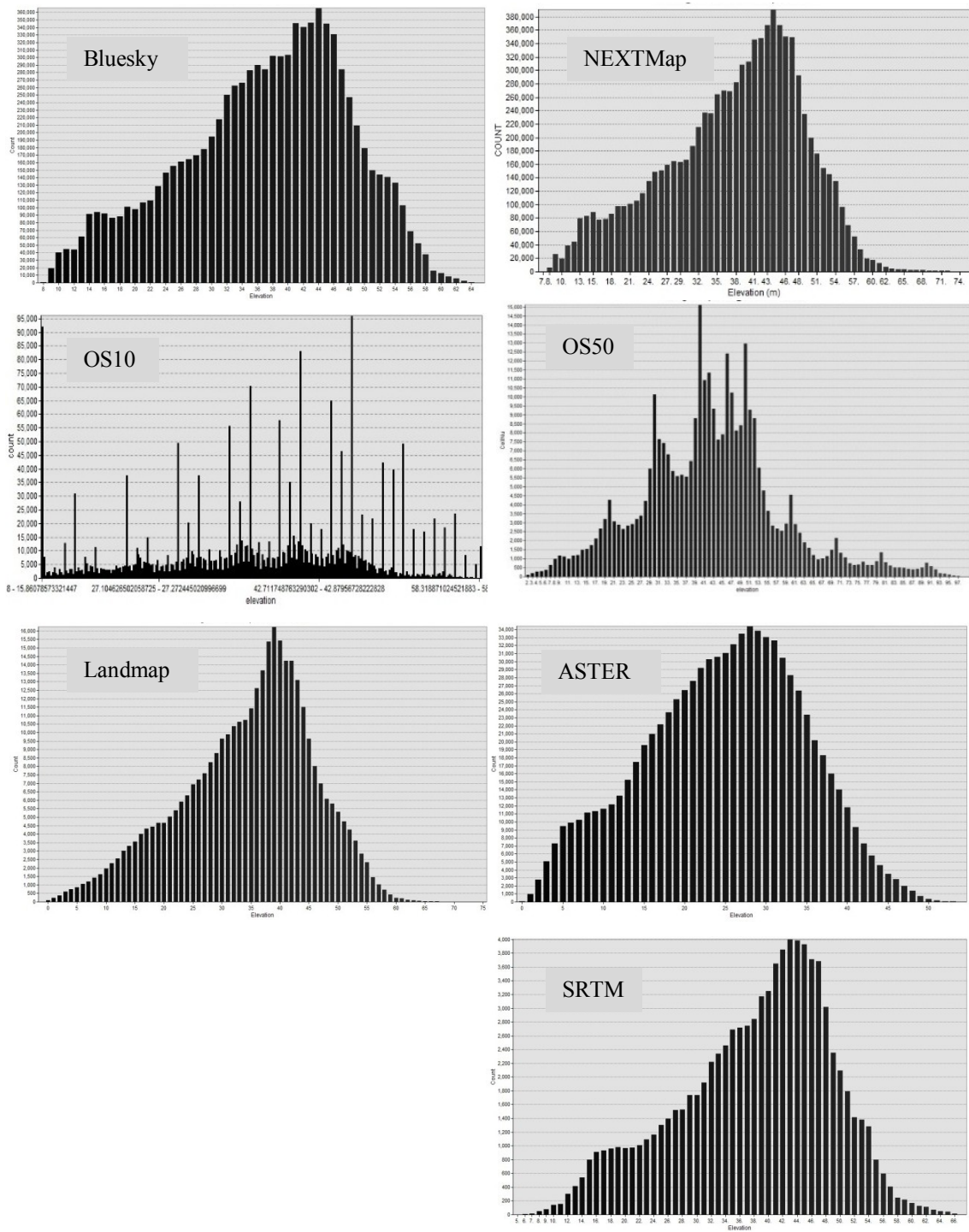
Figure 4.1: Histograms of the elevation values for each dataset.

4.3.3 Cross-sectional profiles

Two cross-sections from West to East were generated and used to visually compare the elevation profile for each DEM in the whole dataset (Figure 4.2). Transect one was selected to pass through the upper part of the Wensum tributary, the area where the catchment management studies are focusing (*Blackwater sub-Catchment*), and lies between these two points *(X1=610187, Y1=325756, X2=614550, Y2=325756).* The other transect *(between X1=608200, Y1=323070, X2=612560, Y2=323070)* was selected to pass through the town of Reepham where the river goes through an built-up area (Figure 4.2).
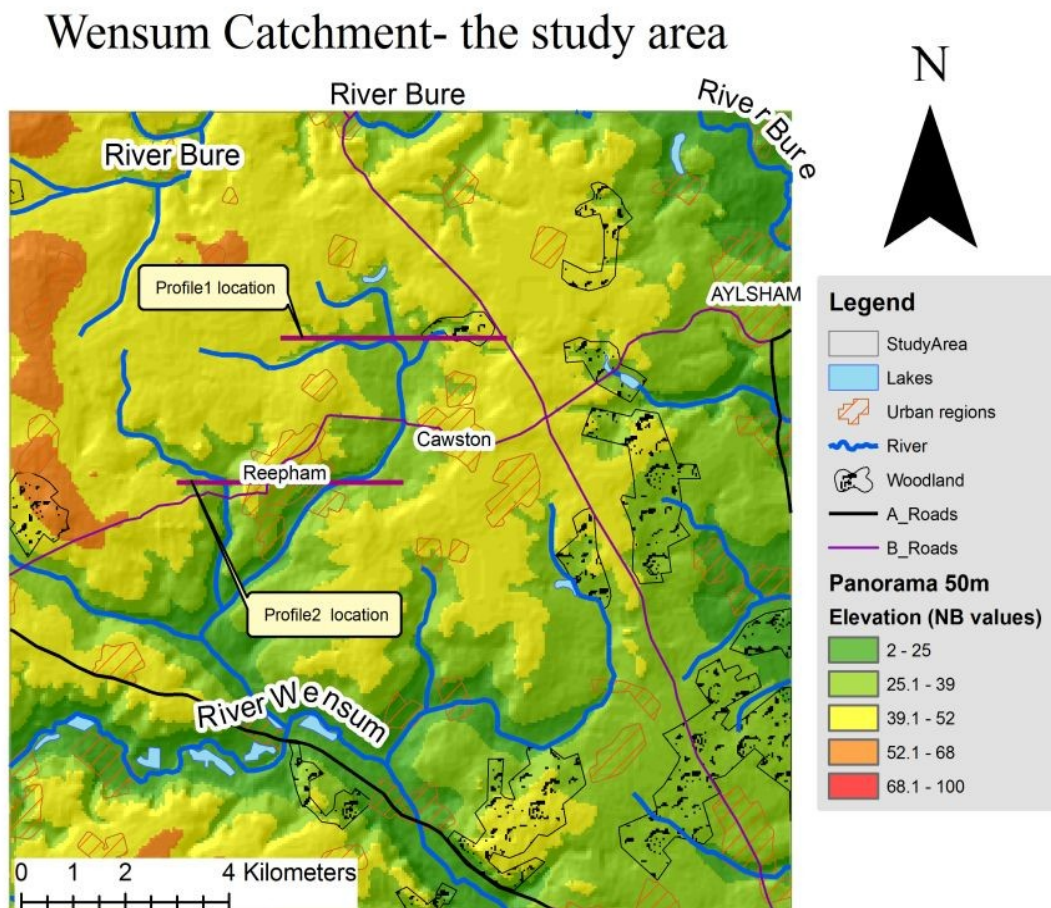
Figure 4.2: Locations of the cross-sectional lines.

4.3.3.1   Cross-sectional elevation profile 1

Figure 4.3 shows cross-section 1 overlaid on top of the land cover map which was used to help in the interpretation of the elevation profile results. It is clear from the illustration that the first profile passed over an area mainly consisting of arable and horticultural land cover with some broad-leaved woodland in the middle and coniferous woodland to the far east of the area.
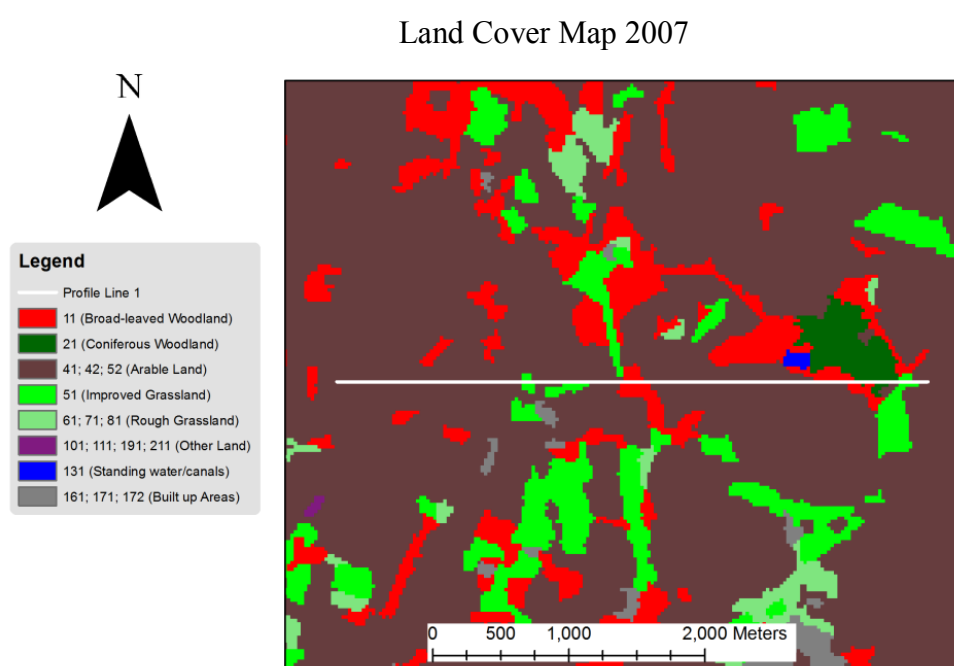
Land Cover Map 2007

Figure 4.3: Location of cross-sectional line 1 overlaid on the land cover map (source: DTC).

For the analysis, elevation values were plotted on the vertical axis whereas distance along the cross profile was along the horizontal axis as shown in Figure 4.4 below.

A visual interpretation of Figure 4.4 shows that Landmap DTM (E) behaves as a noisy dataset. It is clear that this data contains a lot of spurious sinks and peaks where the elevation is considerable lower or higher than the surrounding terrain. This could be due to the fact that this elevation data was created using IFSAR repeat pass data, which has been reported as

suffering from poor coherence, the interval between acquisition of the two images and the weather conditions (Dowman, 2004).

By looking at the elevation profiles for the Ordnance Survey (Figure 4.4C and D) products which were created from contour data, common problems associated with the creation of DTM from contour data are obvious in these two examples. It is clear from profile (C) (Landform profile 10m) that this data is suffering from the stair-step problem, steep slopes between different contours positions and an integer rounding problem (the elevation value is rounded to the nearest metre), where the transect line represents the same elevation value for a long distance (i.e. the value of 34 m between 1700 m and 2300 m from the start of the profile, (profile C)). It has been noted that rounding off elevations to the nearest metre can cause a significant error into the DEM (Fisher and Tate, 2006).

Land cover is a very important factor which affects the calculation of elevation when optical or radar sensors are used, where near top of canopy and man-made objects are measured not the bare earth (ASTER Validation Team, 2009; Liu, 2008; Reuter et al., 2007). This fact is clear on both ASTER, and SRTM cross-section examples below (F and G) where the elevation increased sharply at the far east of these transects, due to a coniferous woodland covering that part of this area (Figure 4.4). Hebeler and Purves (2009) reported that SRTM data appear to be sensitive to overestimating terrain elevation in densely vegetated areas.

Figure 4.5 shows that the Landmap 25 m and ASTER data are below the other DEMs, underestimating elevation values along almost the entire transect line by a few meters. On the other hand, SRTM, the coarsest DEM among all those examined, exhibits almost the same elevation profile pattern as the Bluesky, NEXTMap and OS datasets.
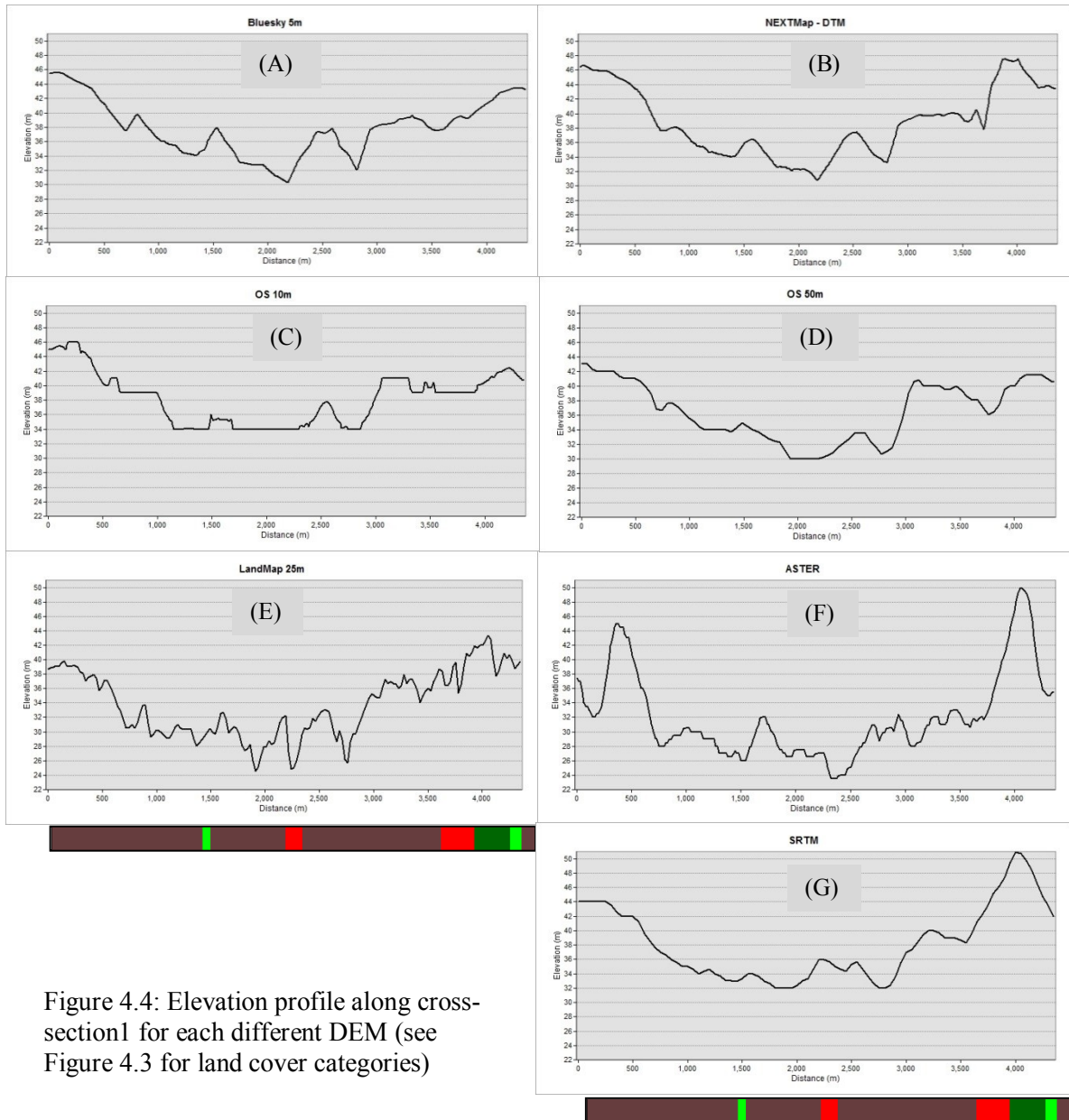
Figure 4.4: Elevation profile along cross-section1 for each different DEM (see Figure 4.3 for land cover categories)
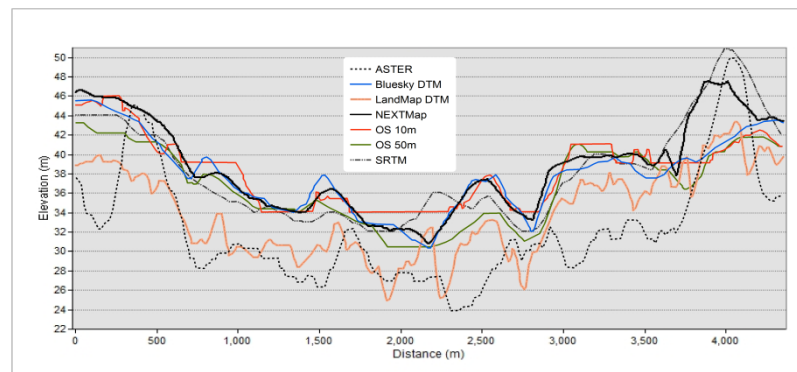
Figure 4.5: Cross-section 1 showing difference between all the seven DEMs used in this study.

4.3.3.2 Cross-sectional elevation profile 2

As can be seen from the map below (Figure 4.6), cross section 2 has an urban area in the middle, with arable land covering much of the rest of the area with some improved grassland and broad-leaved woodland.
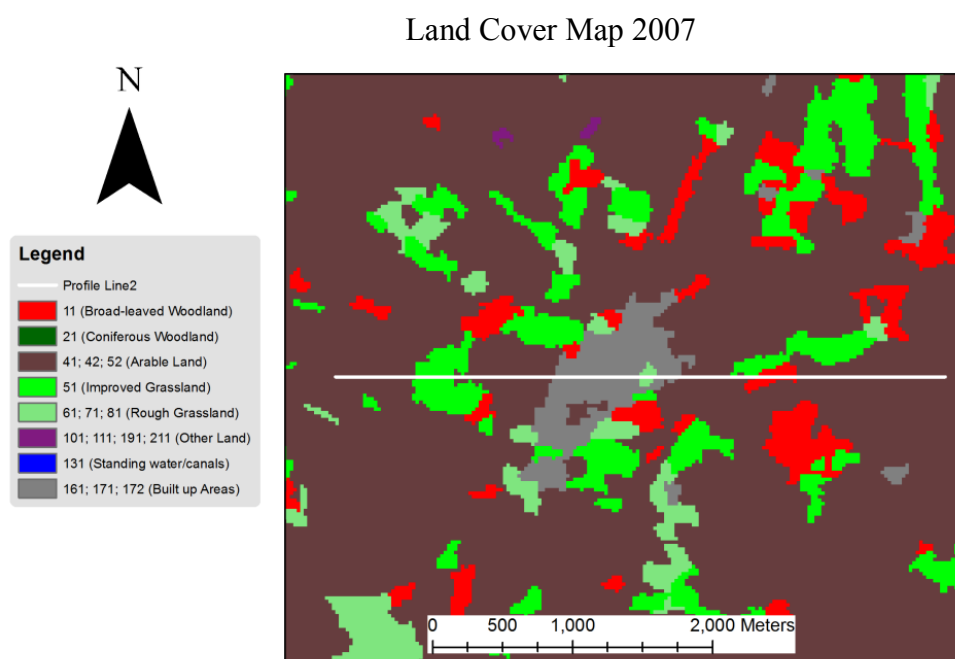
Land Cover Map 2007

Figure 4.6: Location of the cross-sectional line 2 overlaid on the land cover map (Source: DTC).

Comparisons made between all the elevation profiles generated from each elevation dataset using cross-section 2 showed that the effect of land cover type when optical or radar sensors were used. As highlighted in Figure 4.7, there are identifiable false peaks in the ASTER, SRTM and LandMap DTM elevation datasets (see small red circles) compared with the others used in this study. This error was caused by broad-leaved woodland covering that part of the cross-section area (Figure 4.6). Ordnance Survey, Bluesky, NEXTMap and SRTM elevation datasets behave quite similarly over the transect area while ASTER and LandMap appear very rough containing many gross errors affecting their overall quality. It is clear that these two datasets undulate on short lags, while other datasets show less variability.
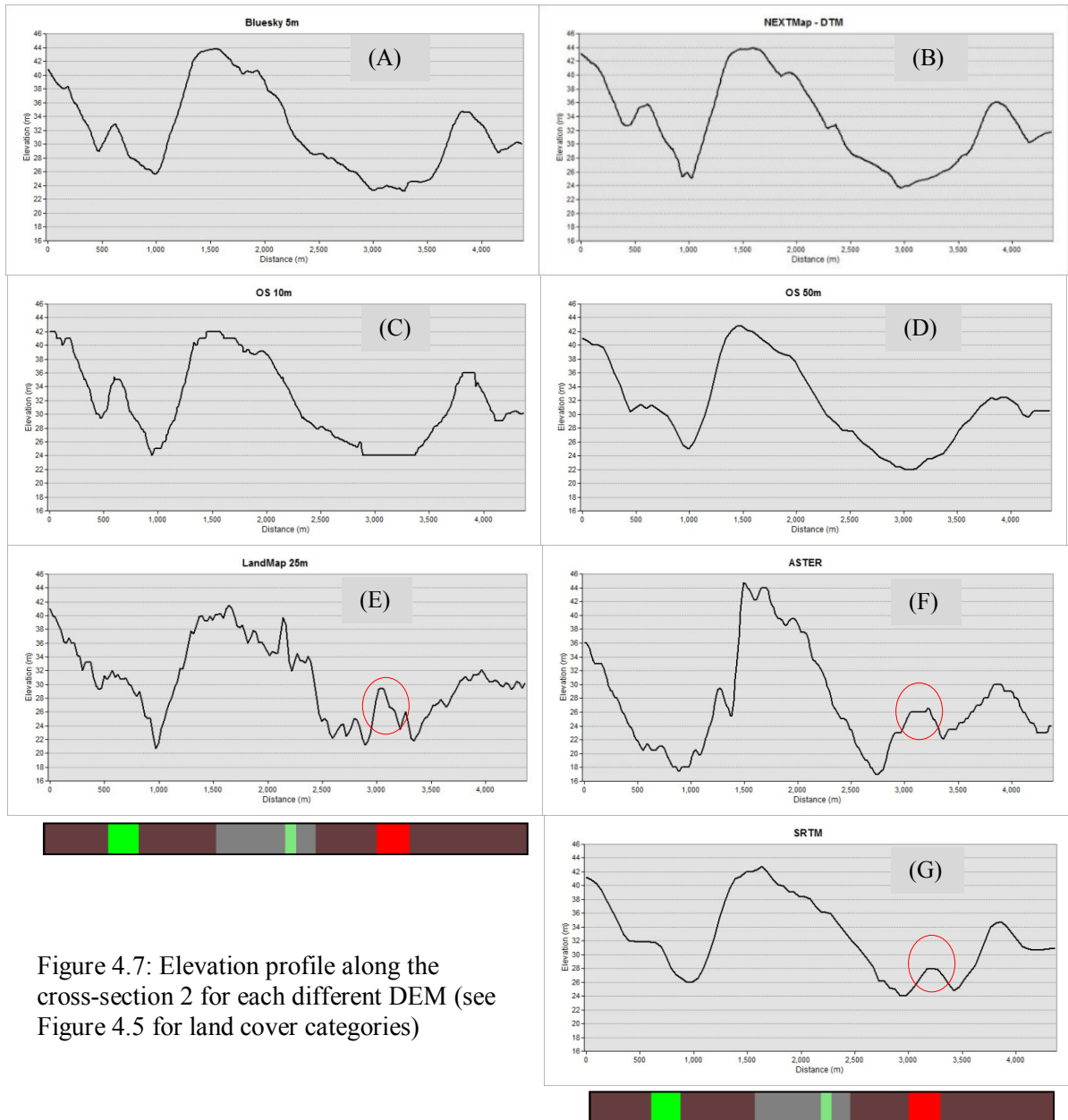
Figure 4.7: Elevation profile along the cross-section 2 for each different DEM (see Figure 4.5 for land cover categories)
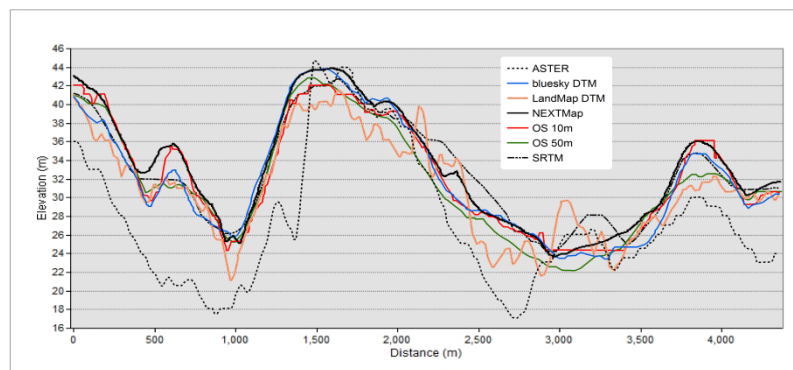
Figure 4.8: Cross-section 2 showing difference between all the seven DEMs used in this study.

Additionally, the effect of the small woodland, which can be seen clearly in the other optical and radar remote sensing generated DEMs (see red circles), does not exist in NEXTMap DTM elevation profile example above (Figure 4.7B). This could be due to the fact that as reported by Intermap, "trees that stand alone, in clumps, rows and areas that are fully encompassed in a circle of radius 50 metres or less will be removed" (Intermap, 2011). Similar to the Bluesky, NEXTMap, OS10m and OS50m profiles, along the two transect lines, SRTM data provides a fairly consistent profile across the various land covers except for forest areas, where it does provide higher elevation values (Figure 4.8). This result is consistent with Blanchard et al. (2010) who reported that, compared to ASTER 30 m, SRTM 90 m vertical accuracies were the highest for built-up areas and bare soils, and lower for forest areas.

Contour derived DEMs provide a consistent surface profile in all land covers which mean that these products provide a reasonable accuracy regardless of land cover. In contrast, remote sensing-derived DEMs, especially SRTM, provide a consistent surface profile in all land covers except woodland where the elevations are too high (Figures 4.5 and 4.8).

4.3.4   Common problems

Along with statistical comparisons, visually inspecting the spatial pattern of the DEMs through a variety of rendering tools such as shaded relief maps can help to fully address overall quality (Carrara et al., 1997). Visual methods can offer an initial assessment, benefitting from the huge improvements in digital data visualisation capabilities (Podobnikar, 2009). Analytical shading with different parameters is an extremely effective way to examine and identify any artifacts and anomalies that an elevation dataset may contain. The shaded relief image (hillshade), is a technique that has been used to determine the hypothetical illumination of a surface for either an analysis or a graphical display (Maune, 2007).

Hillshade images were therefore created for each elevation dataset and examined for any errors (i.e. anomalies, artifacts, etc).
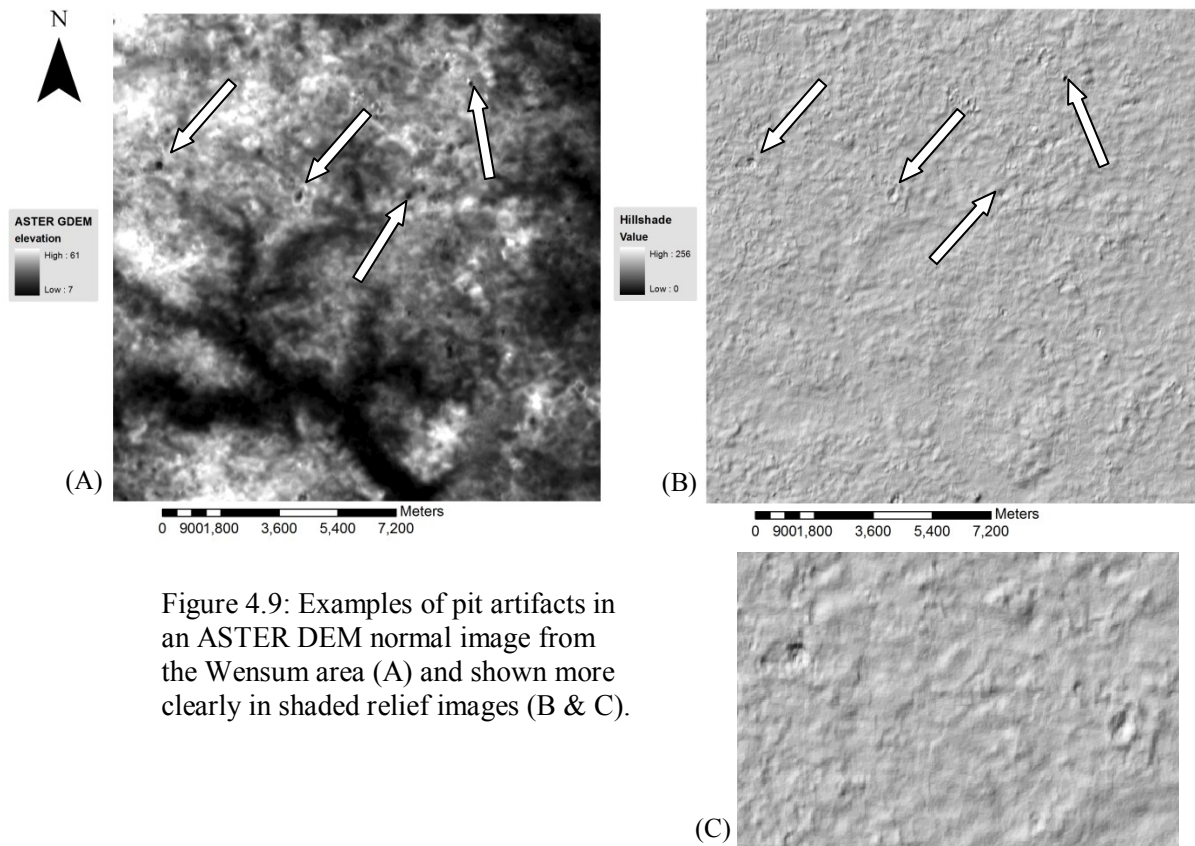
Figure 4.9: Examples of pit artifacts in an ASTER DEM normal image from the Wensum area (A) and shown more clearly in shaded relief images (B & C).

It is clear from Figure 4.9 above that the ASTER elevation data reflects the comment in the ASTER GDEM Validation Summary Report stating that anomalies and artifacts occur with regularity and often high frequency within the ASTER GDEM. Figure 4.9 illustrates some pit artifacts (see white arrows) where the elevation is considerably lower than the surrounding terrain. It has been suggested that this kind of artefact is related to irregular stack number boundaries caused by the linear boundaries that exist between swath-oriented zones of two different stack numbers (ASTER Validation Team, 2009).
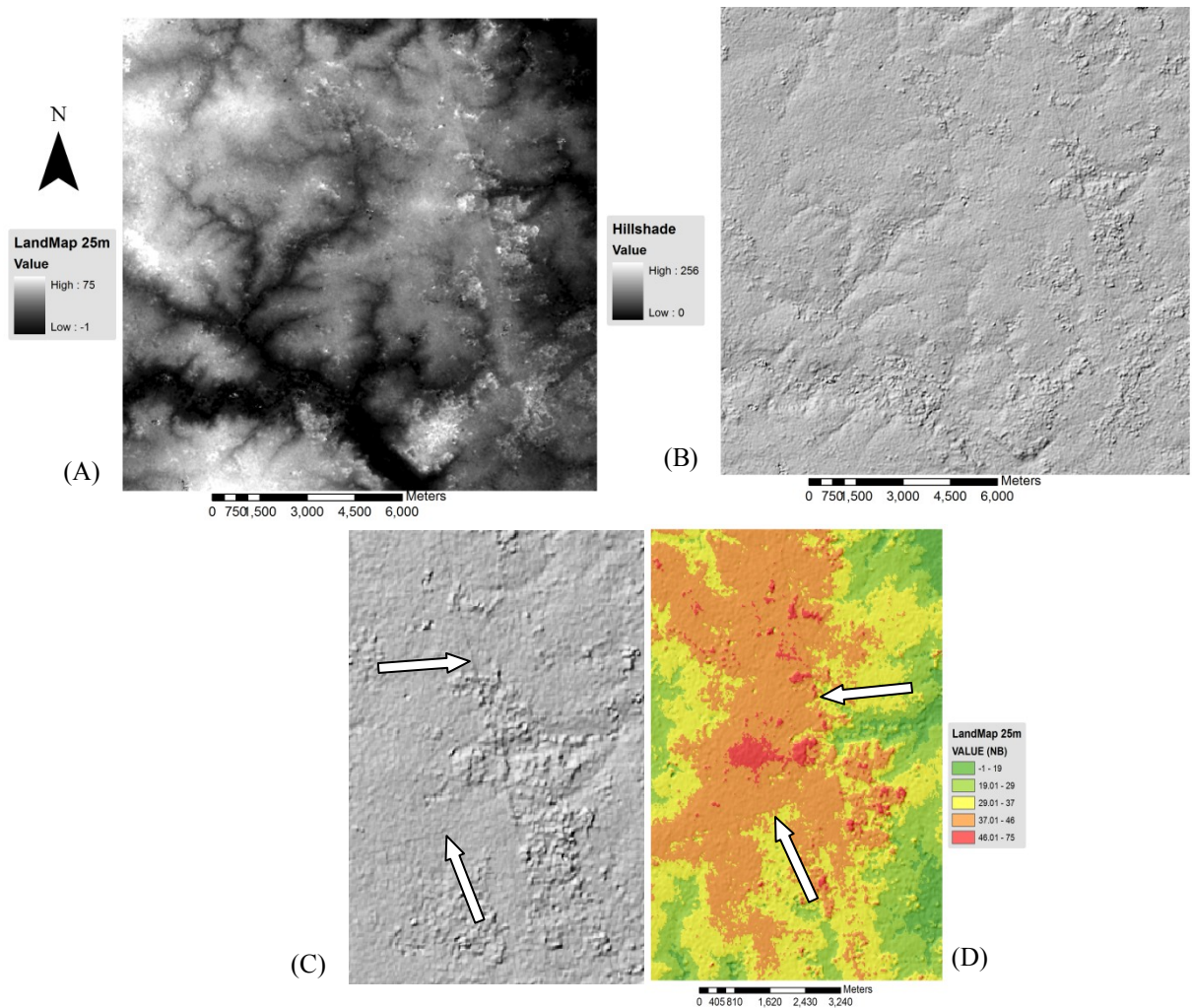
Figure 4.10: Stripe effects (linear boundaries) in the LandMap dataset (A) and the associated abnormal elevation change is clear in the shaded relief images (B&C) and the elevation colour scheme image (D).

From the images shown in Figure 4.10 above, it appears that the Landmap dataset suffers from stripe-effects in the elevation values. Striping is usually caused by some sensors that are out of alignment, defective or not calibrated correctly. Moreover, as this elevation dataset was generated from SAR data using an interferometry technique, the effect of woodland cover type on the calculation of elevation is of great impact. As can be seen from the Figure 4.11 below, the areas with higher estimated elevation are covered by broad leaved and coniferous woodlands. It is known that area with dense vegetation obstruct the radar

irradiance which results in higher estimation of elevation than the true value (Liu, 2008). This also could indicate that vegetation cover may not have been classified correctly to produce a bare-earth data during the process of converting from DSM to DTM (Bandara et al., 2011)
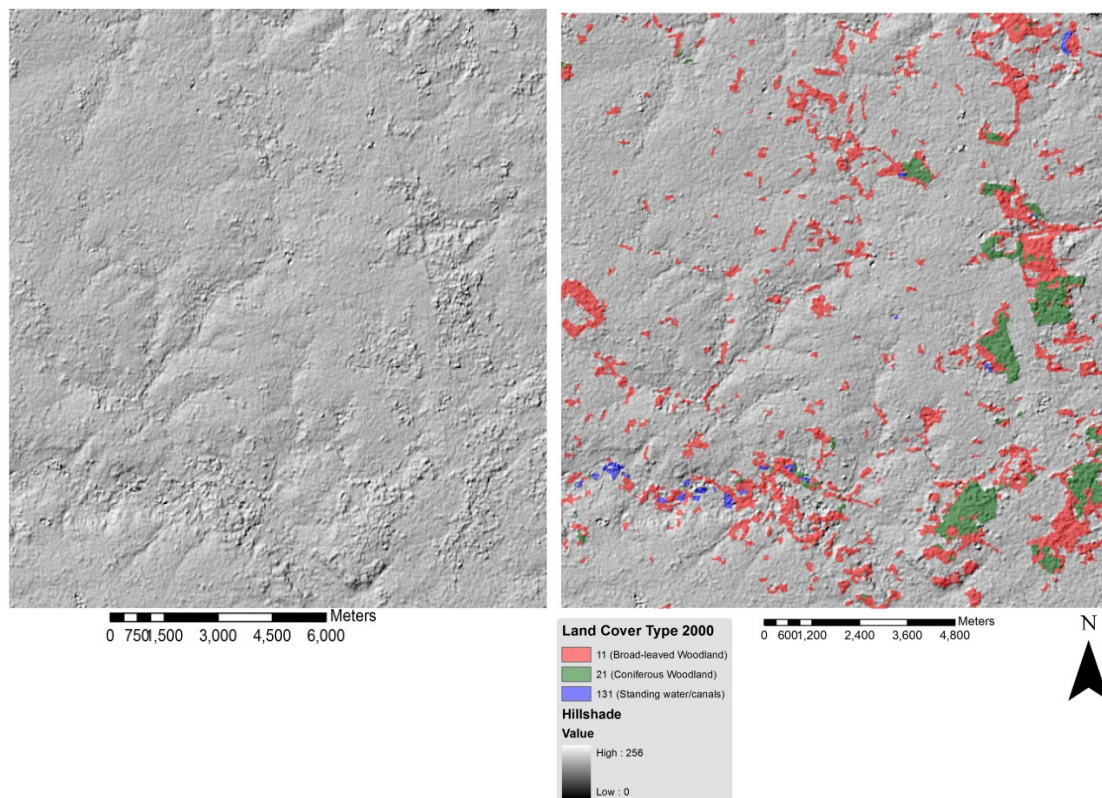
Figure 4.11: Land cover map 2007 (only three categories) overlaid on top of shaded relief image of the LandMap DTM form the River Wensum study area illustrating the effect of woodlands on the data.

More generally, it is clear that this elevation dataset contains a lot of artifacts (i.e. pits, bumps and stripes) which give the product a noisy and blemished appearance. This could be due to the fact that this elevation data was created using IFSAR repeat pass data, which has been proven to suffer from poor coherence, the interval between acquisition of the two images and the weather conditions (Dowman, 2004).
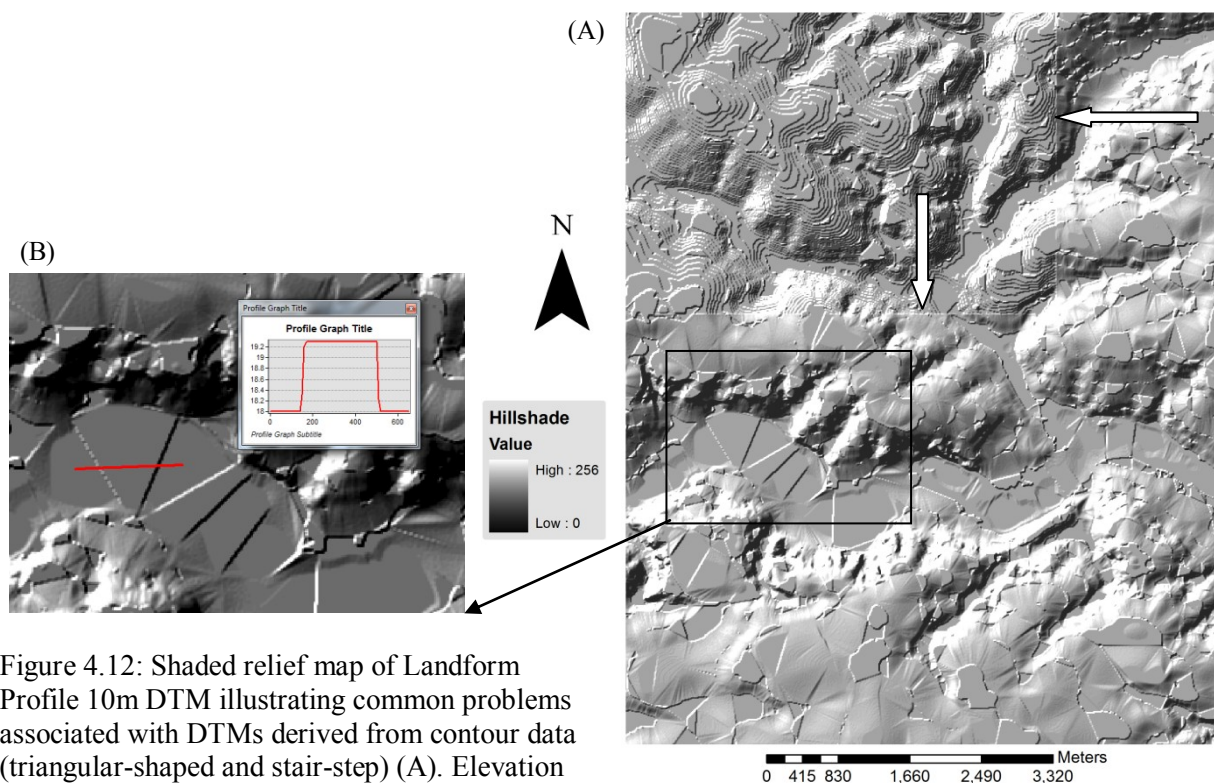
Figure 4.12: Shaded relief map of Landform Profile 10m DTM illustrating common problems associated with DTMs derived from contour data (triangular-shaped and stair-step) (A). Elevation profile indicates abnormal elevation change (2.3 meters) caused by unrealistic triangular-shaped relief (B).

Figure 4.12 above reveals some common interpolation artifacts that are associated with elevation datasets that are produced using contour data. Peckham and Jordan (2007) stated that DEMs derived from contour data often display bias towards contour elevations and the curvature parameters can appear as waves over the landscape. These errors are evident in the illustrations above as sudden slope changes and flat areas between contour lines. It is also apparent that the flat river plain is covered by an unrealistic relief pattern consisting of triangular-shaped surfaces at which elevation values are slightly different (i.e. 2.3 metre in the example Fig. 4.12B). Moreover, by inspecting the image carefully, it is apparent that this elevation dataset is affected by stair-step artifacts along contour lines positions. In addition, this shaded-relief image of the OS 10 m contour based DTM illustrates large areas of similar values (the flattening of hilltops and valley bottoms) which is probably due to horizontally flat regions induced by TIN to grid conversion (Wise, 2007). Artificial horizontally flat surfaces occur within in valley floors and on hill-tops where no additional data were available (e.g.

spot heights, break lines) (Figure 4.12). Other problem can be clearly witnessed by the relief

pattern in the north-west portion of Figure 4.12A, where the surface appears noisy giving

more details of the contours position, while it is much smoother in the other parts of the

dataset. This is believed to be a systematic error caused by the process of mosaicking the

elevation data tiles (5 km x 5 km grid tiles).
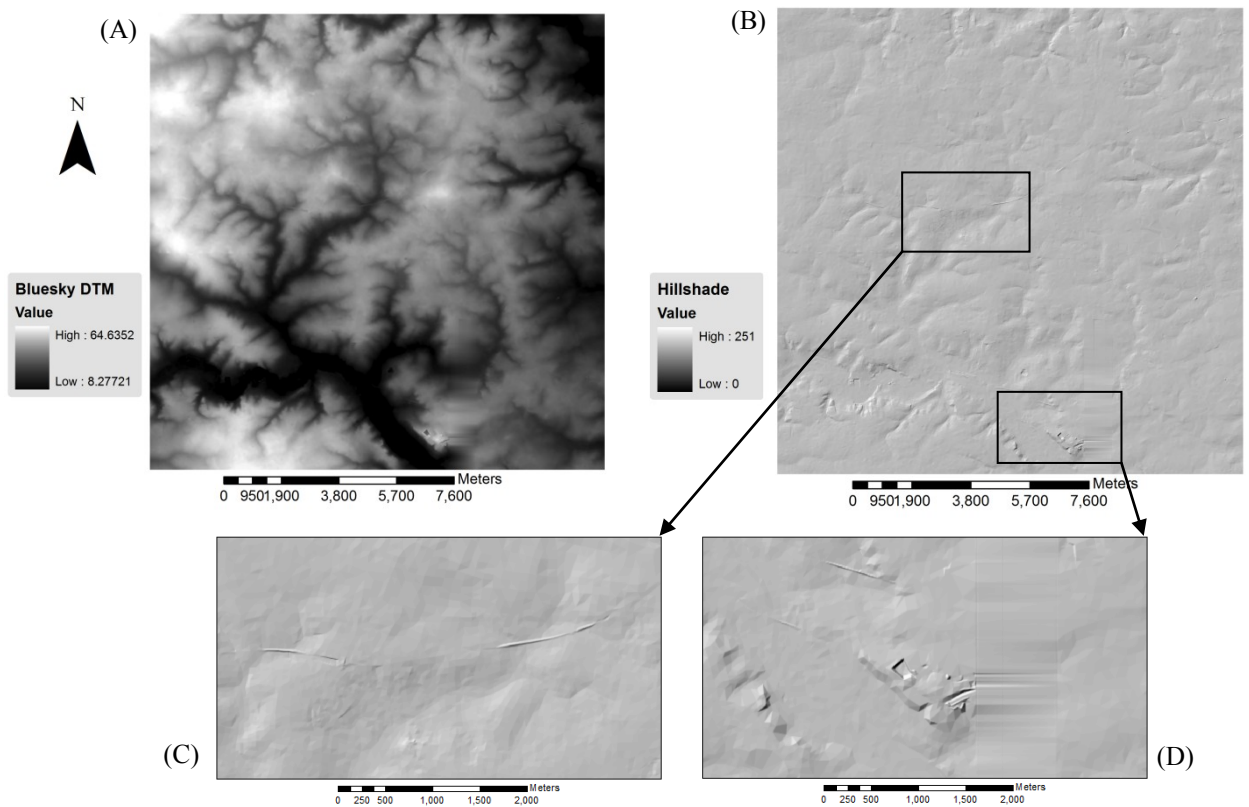
Figure 4.13: Examples of artifacts in a Bluesky DTM shaded-relief image (River
Wensum area) that illustrate problems associated with DTMs derived from DSM data.

As noted earlier, the Bluesky DTM was generated from photogrammetrically derived

digital surface models (DSM). A DSM represents earth topography along with the elevated

features such as vegetation and man-made objects on it. As DTM generation goes through

many processes, errors are inherited from the source data and before production processes.

Therefore, errors are propagated in the DTM if not identified and removed from the DSM.

The Bluesky DTM relief-shaded image above (Figure 4.13) reveals some artifacts that are not

completely removed during the process of converting from DSM to DTM. As can be seen from image (C) above, there are dam-shape artifacts that can be easily identified in the middle of the image, which might be related to features such as elevated roads, embankments or dams. Shaded-relief image (D) shows some other artifacts which appear like buildings. In addition, a horizontal smearing is clearly noticeable. This kind of artifact is likely to be a result of errors during the collection of the source data, such as unstable remote sensing equipment or image processing (Gehrke and Uebbing, 2011). All these quality problems indicate that man-made structures and vegetation effects have not been completely removed from the data during the process of converting from DSM product to a bare-earth DTM, a common problem in remote sensing-derived DEMs (ASTER Validation Team, 2009; Dowman, 2004; Hodgson et al., 2003; Jordan, 2007).
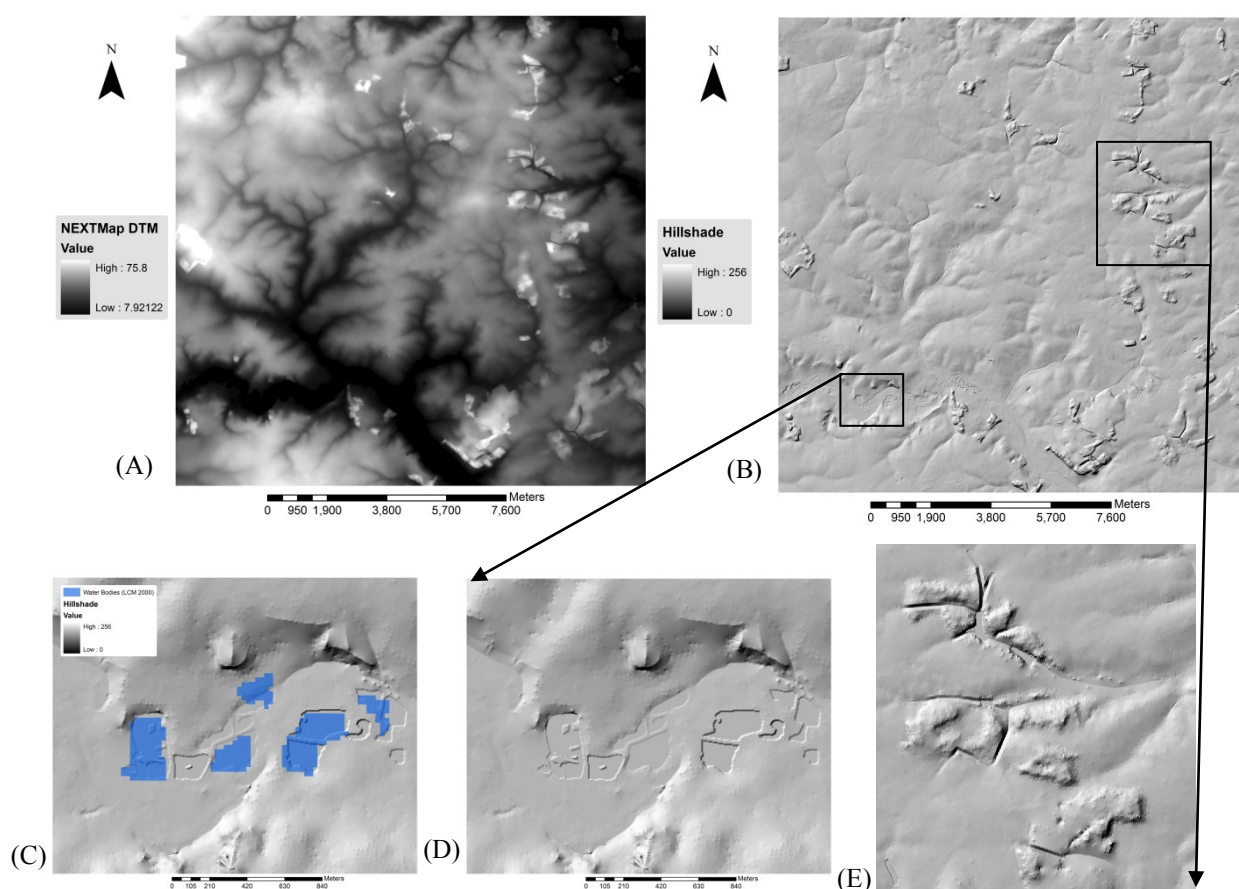
Figure 4.14: Examples of artifacts in the NEXTMap DTM shaded-relief image of Wensum area that illustrate problems associated with DTMs derived from DSM data.

NEXTMap DTM is a single-pass IFSAR product. It was derived from DSM data, which represents surfaces that are visible to the radar signal, after the automatic processing and manual editing to remove vegetation, buildings and other man-made features leaving just the bald-earth (Intermap, 2011). However, as can be seen from Figure 4.14 above, the canopy cover problem still exists in the NEXTMap data from the River Wensum catchment area. Intermap's Products Handbook (2004) indicates that any woodland region covering an area that exceeds fifty metres in all directions will not be removed from the DTM product. This can be seen clearly in the shaded relief image Figure 4.14E where elevation values represent the canopy heights not the bare earth. The presence of these artifacts also influences the character of the DEM surface and distorts derived parameters, in particular applications that are based on neighbourhood analysis such as upslope contributing area (Schwanghart et al., 2013).

Intermap also edits and modifies features such as lakes and streams in the DTM product. The Intermap Products Handbook (2004) reports that elevations along streams less than 20 metres in width and greater than one kilometre in length will be modified to maintain the monotonic flow within the vertical accuracy limit of radar elevation data. Figure 4.14E illustrates modified streams where the narrow drainage canals are preserved through the woodland area. This helps to ensure that water flow paths through the woodland area are uninterrupted.

Figure 4.14C and D demonstrates how water bodies are represented in the NEXTMap data, where lakes greater than 400 square metres in area are levelled to a single elevation value (expressed to the nearest 0.1 m) based on the water elevations and the surrounding shoreline (Intermap, 2011). This process produced water bodies as depression artifacts, where the elevation values are lower than surrounding terrain (Figure 4.15).
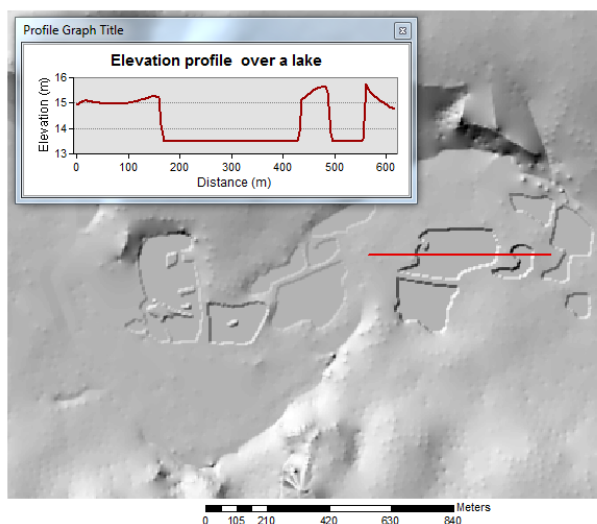
Figure 4.15: Elevation profile transect over a lake (Wensum River area) illustrating elevation differences between the lake and the surrounding terrain.

4.3.5   Assessing DEMs against higher accuracy reference data

A dataset of higher accuracy can be used to quantify the accuracy of other datasets (FGDC, 1998; Hohle and Hohle, 2009). In this situation of determining the accuracy of DEMs, reference data are needed which provide accuracy sufficient to serve as statistical control. Therefore, the accuracy of the different available DEMs was assessed against the spot heights collected from Ordnance Survey 1:1000 MasterMap (Section 4.3.5.1). Such a comparison results in elevation differences (residuals) at the tested points. Statistical measures such as Root Mean Square Error (RMSE), Standard Deviation (SD) and Mean Error (ME) are the conventional ways to analyse the differences between the DEM elevations and reference data.

4.3.5.1   Reference data description

The reference data were a set of spot heights collected from Ordnance Survey 1:1000 MasterMap data (Figure 4.16). The altitude of these points was determined by levelling techniques, and recorded to one decimal place of a metre (Ordnance Survey, 2009a).

According to the OS technical documents, it is believed that these data offer a horizontal and vertical accuracy better than a metre (tens of centimetres). These spot heights were therefore selected to serve as ground control points because of their higher order accuracy of the height component, and also because of their precise horizontal positions (Ordnance Survey, 2009a). The spot heights dataset comprised 963 levelling points collected from 250 (1 km x 1 km) Ordnance Survey MasterMap tiles covering the Wensum study area (Figure 4.17).

Figure 4.16: Examples of the spot heights used in this study as reference data (see red circles).
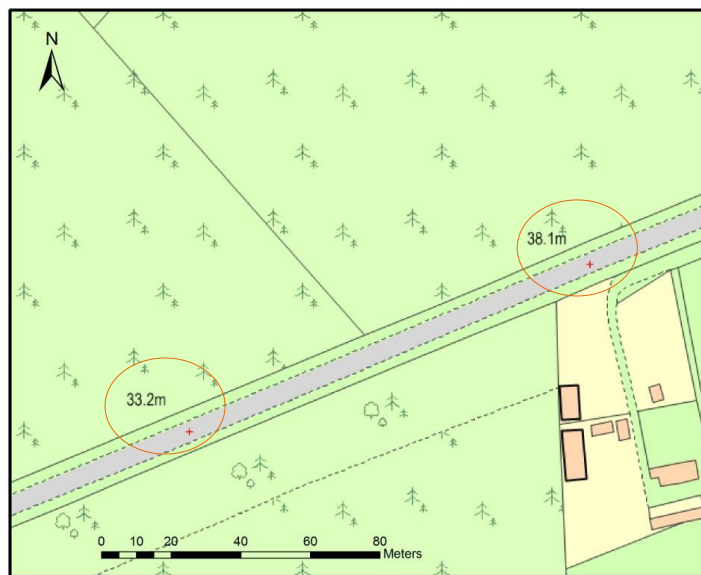
Figure 4.17: Distribution of the spot heights in the study area.
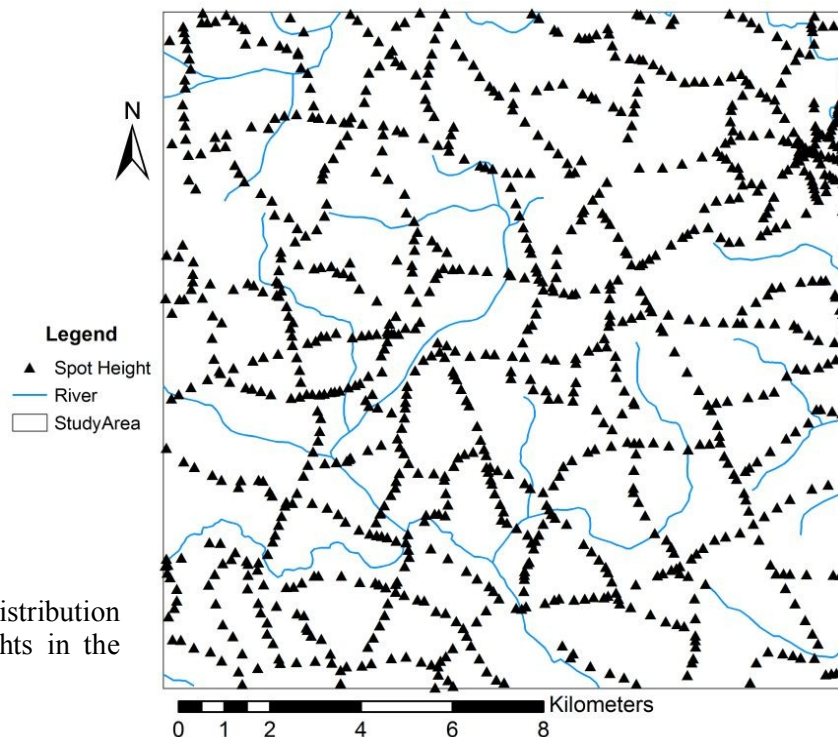
4.3.5.2   Test of normality

As the accuracy assessment of the DEMs will involve comparisons with the reference data (spot heights), it is important to examine the underlying distribution of this dataset. This can be done using both graphical (i.e. histogram and normality plot) and statistical (i.e. mean, standard deviation, skewness and kurtosis) methods of evaluating normality (Hohle and Hohle, 2009). SPSS statistical software was used to determine normality of the reference data. According to Field (2009) if you want to test whether or not data are normally distributed, three interrelated approaches should be conducted. First, a histogram with the normal curve superimposed should be drawn so that the data can be compared to the normal curve. Second, the level of normality can be determined by drawing a quantile-quantile 'Q-Q Plot' and examining how close the data points are to the straight line to check the deviation from the normal distribution. Finally, statistical descriptives such as; Skewness and Kurtosis, mean, standard deviation etc, should be calculated.

(A)   (B)
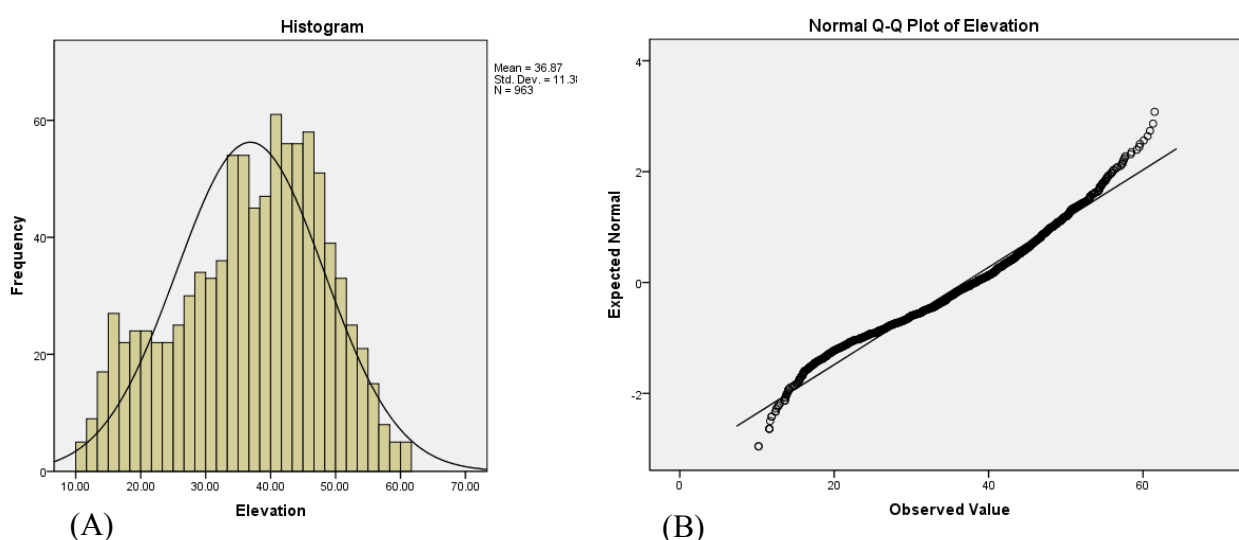
Figure 4.18: Histogram of the reference data with the normal curve superimposed (A), and Normal Q – Q Plot for the reference data (B).

Descriptive statistics and histograms are a useful way of generating a picture of the data distribution (Field, 2009). Figure 4.18A depicts the histogram of the reference data distribution. In order to compare with normality, the figure contains the normal distribution curve superimposed. By examining the histogram graph visually and comparing the real data distribution to the normal curve, it can be seen that the histogram shows a fairly normal distribution even if it looks slightly negatively skewed. The first thing that can be inferred from the graph is that there are no values at the extremes of the normal curve. It is also clear from the histogram that the peak is not completely symmetrical, and what that seems to suggest is that elevation values were more clustered around the values ranging from 40m to 50m. It can be noticed that there is a group of values at around a value of 15m making a small peak out of the normal curve, which could be a contour artifact problem.

By looking at the Q-Q plot (Figure 4.18B) it can be noticed that the data points fall very close to the ideal diagonal line. However, there are some data values in the upper and lower end of the chart deviating away from the diagonal (S-shaped), which is an indication of small skewness problem (Field, 2009), and this is consistent with the results obtained from the histogram.

Table 4.4: Descriptive statistics for the reference data

			Statistic	Std. Error
Elevation	Mean		36.8722	.36678
	95% Confidence Interval for Mean	Lower Bound	36.1524	
		Upper Bound	37.5920	
	5% Trimmed Mean		37.0567	
	Median		38.3000	
	Variance		129.552	
	Std. Deviation		11.38210	
	Minimum		10.20	
	Maximum		61.50	
	Range		51.30	
	Interquartile Range		16.30	
	Skewness		-.331	.079
	Kurtosis		-.655	.157

SPSS outputs in Table 4.4 shows the descriptive statistics for the reference data. From this table, it can be seen that the mean value of the higher accuracy reference data is 36.8722, and by looking back to the mean measure for each DEM in our dataset (Table 4.2), this value falls in the middle (which is good). However, the standard deviation (11.38210) for the reference data is larger than those for all DEMs (ranging from 9.8 for the ASTER to 11.3 for LandMap (Table 4.2)), this could be due to the fact that a DEM is a smooth continuous surface created from discreet features by interpolation. The values of skewness and kurtosis should be zero in a normal distribution (Field, 2009). From the table above, the negative values of skewness indicate a slight bias in the peak to the right, and that also clear from the histogram too, as it is slightly negatively skewed.

The Kolmogorov-Smirnov test (or simply the K-S test) can be used to test the hypothesis that data comes from a normal distribution (Field, 2009; Illian et al., 2008; Lee and Wong 2001). It is a statistical test to assess how closely an observed distribution matches an expected distribution. The K-S test is always testing what is called the null hypothesis, which states that there is no significant difference between the expected and observed result. Therefore, the K-S distribution can be used to test whether or not that the data as a whole deviates from a comparable normal distribution, with the same mean and standard deviation (Field, 2009).

The K-S test was used to test the null hypothesis that the spot height elevation data follow a normal distribution. K-S test of normality results for the reference spot heights are reported in Table 4.5. Traditionally, in a K-S test, to compare two probability distributions, the distribution have to be converted into cumulative probability distribution (Ebdon, 1978), columns (e) and (f) of Table 4.5 show these cumulative probabilities and they are also illustrated in Figure 4.19. The right-hand column (f) lists the absolute differences between the two columns of cumulative probabilities. The largest absolute difference is 0.05, and this is

therefore the value of the K-S statistic, D. The critical value of D ($p = 0.05$) can be calculated as follows:

$$D (p = 0.05) = 1.36 * \sqrt{(963+963)/(963*963)} = 0.0620 \qquad \text{(Lee and Wong, 2001)}$$

Table 4.5: K-S test statistics output table

Elevation categories	Frequency		Probabilities		Cumulative probabilities		
	Observed (a)	Expected (b)	Observed (c)	Expected (d)	Observed (e)	Expected (f)	Difference (g)
10.2-15.2	31	18.19	0.032	0.019	0.032	0.019	0.013
15.2-20.2	76	41.45	0.079	0.043	0.111	0.062	0.049
20.2-25.2	67	78.09	0.070	0.081	0.181	0.143	0.038
25.2-30.2	93	121.66	0.097	0.126	0.277	0.269	0.008
30.2-35.2	124	156.74	0.129	0.163	0.406	0.432	0.026
35.2-40.2	144	167.01	0.150	0.173	0.556	0.606	**0.050**
40.2-45.2	174	147.16	0.181	0.153	0.736	0.759	0.022
45.2-50.2	143	109.24	0.148	0.113	0.885	0.872	0.013
50.2-55.2	81	77.64	0.084	0.081	0.969	0.953	0.016
55.2-60.2	26	32.21	0.027	0.033	0.996	0.986	0.010
60.2-65.2	4	13.27	0.004	0.014	1.000	1.000	0.000
	963	962.66	1.00	1.00			
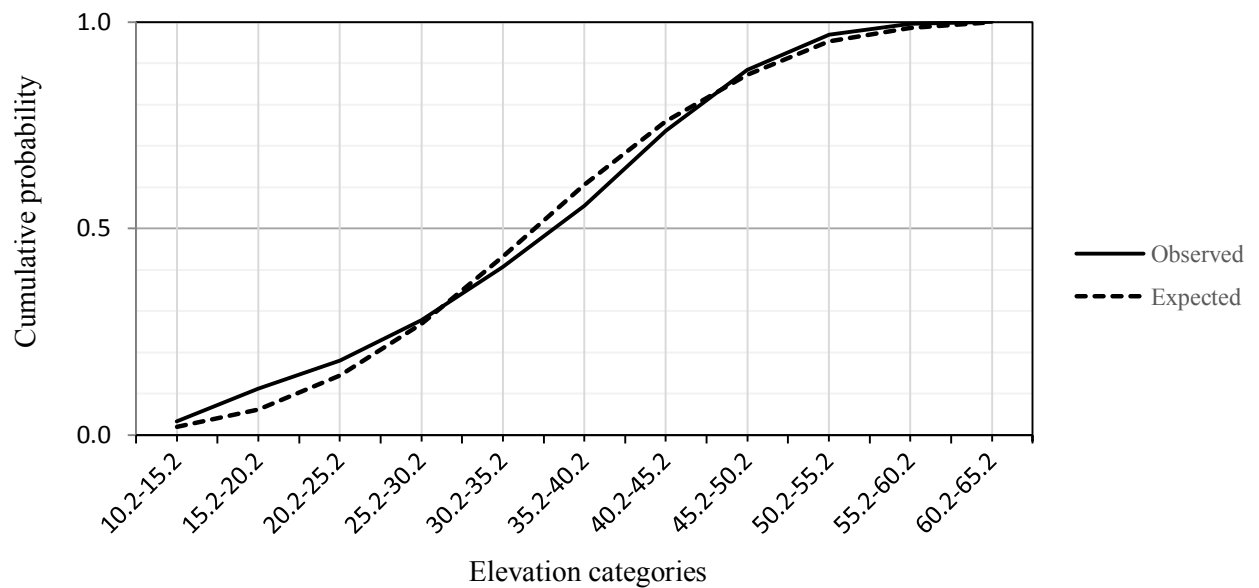
Figure 4.19: Cumulative probability distributions for K-S test.

Since the K-S test calculated value of D is 0.05, which is smaller than the critical value (0.062), the test is not a statistically significant and hence we can accept the null hypothesis that the data follow a normal distribution. In other word, the test does not indicate that the data distribution is significantly different from normality.

In general and based on the normality distribution tests discussed above, it will be assumed that the reference data have a normal distribution, and the accuracy measures for the DEMs will be applied using these spot heights as a higher accuracy reference data. The elevation error will be computed as the differences between the seven considered DEMs and the reference data and then will be used to calculate accuracy measures like Root Mean Square Error (RMSE), mean and standard deviation for each DEM. The RMSE for each DEM will be used later as an input for Monte Carlo simulations to obtain a probability estimation (uncertainly) of the position of a river network extracted from each DEM (Chapter 6).

4.3.5.3 DEM comparisons with reference data (ground truth)

DEM accuracy assessment using reference data can deliver reasonable accuracy estimates, provided that the reference data are independent and sufficiently precise (Hirt et al., 2010). For assessment purposes, the elevation of each spot height was compared with the elevation of the respective DEM pixel. 963 points spread over the study area were used in this comparison. Using ArcGIS 9.3, the corresponding DEM pixel value with each spot height point was extracted, and then the differences between all DEM values and the reference data were calculated. Statistical parameters such as; minimum, maximum, mean, standard deviation and RMSE values for each DEM against the spot height reference values were calculated. The differences for each DEM against the spot heights are reported in Table 4.6 and Figures 4.20. In addition, cross-plots (Bland and Altman, 1986; Thomas et al., 2014) of reference data versus elevations from each DEM were used to demonstrate the degree of

agreement between reference heights and the corresponding heights from each DEM (Figure 4.21).

Table 4.6: Statistics of DEMs comparison with 963 spot heights (units are in metres).

Comparison	Resolution (m)	Min	Max	Mean	RMSE	Std.dev
Bluesky-GCPs	5	-7.2272	4.5777	-0.4116	0.91969	0.8225
NEXTMap-GCPs	5	-4.6274	14.3092	0.6751	2.03168	1.9163
OS10-GCPs	10	-6.8	2.9	-0.1396	0.5987	0.5822
Landmap-GCPs	25	-13.1	13.3	-2.5222	4.1885	3.3439
ASTER-GCPs	30	-22.40	13.20	-5.24	6.8387	4.392
OS50-GCPs	50	-7.1	6.8	-0.6365	1.9962	1.8921
SRTM-GCPs	90	-5.9	15.2	0.8983	2.6259	2.4675

The statistical parameters for the elevation differences between the seven DEMs and the relative points of the reference data were examined. As can be observed from the table above, the mean value of the differences between each DEM and the reference data is less than one metre except for the ASTER and Landmap DEMS which present bigger differences of 5.24m and 2.52m respectively. The mean values of ASTER and Landmap differences reflect that these two datasets are underestimating the elevation values (Figure 4.20). Bluesky and Landform Profile (OS10) elevation datasets produce low residual errors with RMSE of 0.9m and 0.568m, respectively, and also low standard deviations of 0.8m and 0.58m, respectively, compared to the other elevation datasets. In contrast, the accuracies of ASTER and Landmap are the lowest with 6.8 m and 4.18 m for the RMSE and 4.39m and 3.34m for the standard deviation, respectively.

NEXTMap data were assessed in the UK by UCL (Dowman, 2004). It was found that when comparing the NEXTMap DTM with photogrammetric checkpoints, the RMSE was

0.83 m, and when compared with a LiDAR DTM the resultant RMSE was 1.013 m. The NEXTMap data were also compared with detailed GPS measurements and it was found that over mixed terrain (hilly, flat) a RMSE of 1.67 m was obtained (Dowman, 2004). Over several study sites in the United States and using extensive ground control (NGS), Tighe and Chamberlain (2009) reported that the vertical accuracy of NEXTMap data is about 2.05 m (RMSE) which is in agreement with the result obtained here.

The Landform Profile elevation dataset shows better values in most statistical parameters (maximum, mean, RMSE, and standard deviation) in comparison with the other elevation datasets (Figuers 4.20 and 4.21). This good agreement between Landform Profile and the spot heights data can be explained as that the spot heights are more consistent with the Ordnance Survey products than with the remote sensing-based ASTER, Bluesky, SRTM, Landmap and NEXTMap models. On the other hand, ASTER and Landmap present the worst values on most statistical measures (minimum, mean, RMSE and standard deviation) compared to the output statistical results from the other datasets. The cross-plots of reference data versus elevations from each DEM also clearly illustrate that the elevation values from these two data sets, ASTER and Landmap, were generally underestimated (Figure 4.21)
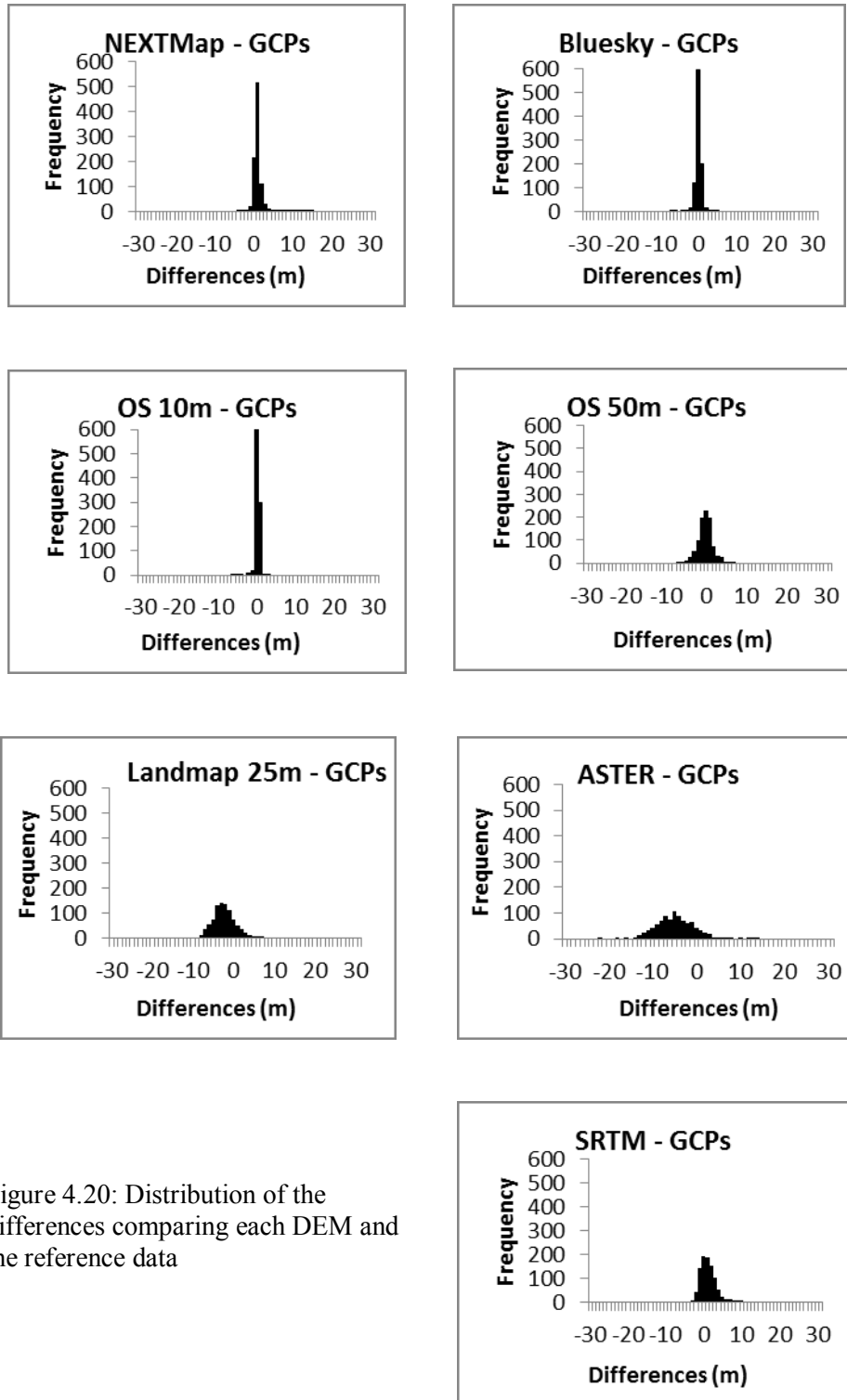
Figure 4.20: Distribution of the differences comparing each DEM and the reference data
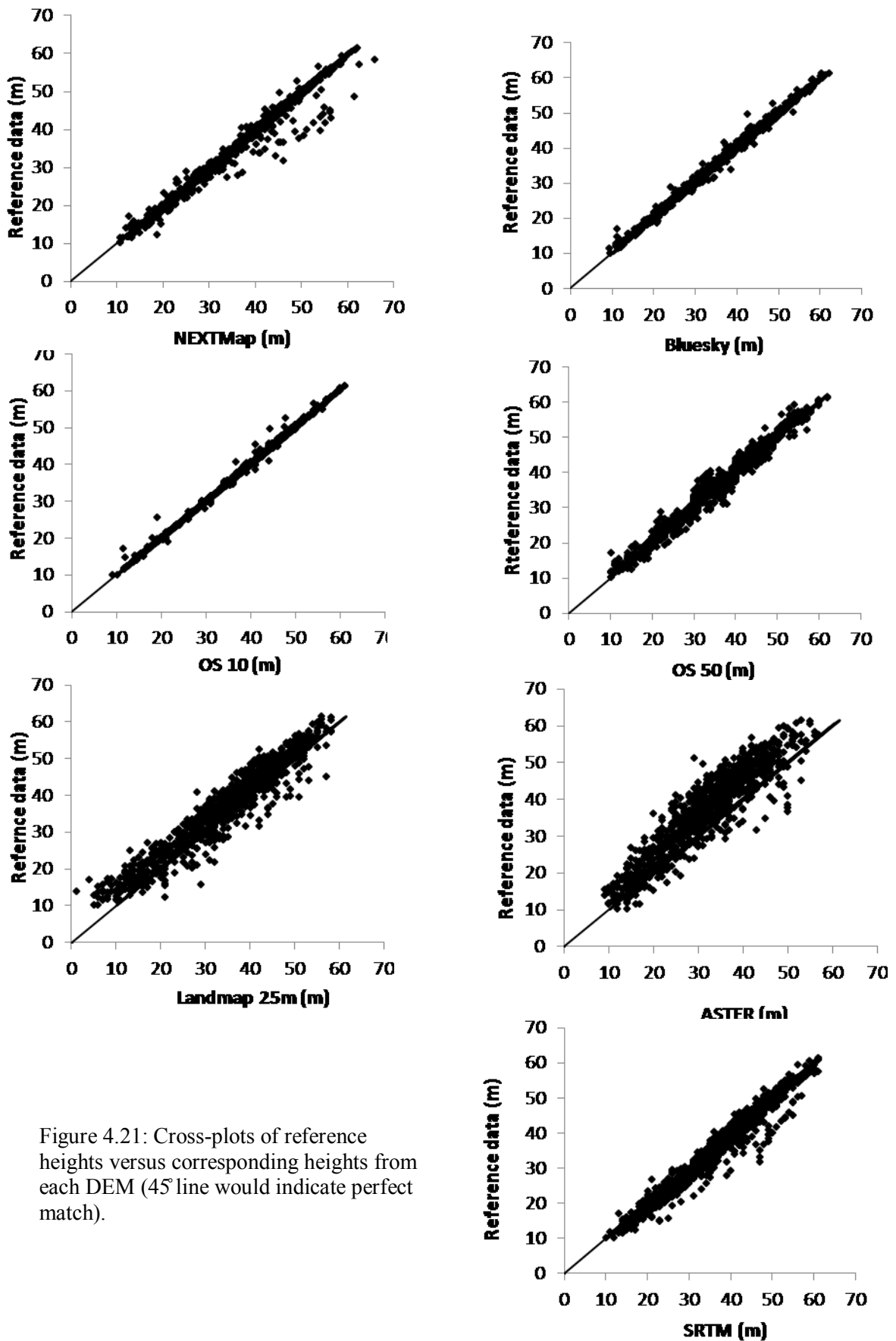
Figure 4.21: Cross-plots of reference heights versus corresponding heights from each DEM (45° line would indicate perfect match).

4.3.5.4 Reference data limitation

The relatively good agreement between the DEMs from the Ordnance Survey (OS 10 m and OS 50 m) and the reference data may partly reflect the fact that all three are products of the same organisation. Therefore, the reference data cannot be considered completely independent of the OS 10 m and OS 50 m elevation datasets. This likely explains the good results from OS 10 m dataset which on visual inspection is clearly poor quality. In their study of DEM resolution and data source effects on automated floodplain delineation Charrier and Li (2012) also noted that elevation data derived from similar sources tends to produce similar results regardless of DEM resolution. They noted that similar levels of uncertainty were observed for different USGS DEM resolutions.

In addition, even though the reference spot heights are located broadly across the study area, the distribution of these heights within the study area is not completely representative of the terrain topography. This stands to reason, as collected spot heights are generally located on the existing road network across the study area, which contributes to the limitations in the spatial distribution of these heights. This problem could be minimised by collecting additional control points (GCPs) using positioning devices (e.g. GPS) in open, accessible areas across the study area. It would also have been appropriate to have reference data created using techniques such as high resolution LiDAR data (i.e. 2 metre LiDAR data).

4.3.6 Statement about fitness for purpose

This study has investigated the quality of seven elevation datasets ASTER, SRTM, Bluesky DTM, Landmap DTM, NEXTMap DTM, Ordnance Survey Landform and Ordnance Survey Panorama over an area of 225 sq km of the River Wensum catchment (Figure 4.2). The assessment begin by describing the main characteristics of these elevation datasets. The quality of each DEM was then quantitatively and qualitatively evaluated. The results of this

assessment revealed a number of interesting outcomes which are relevant to what of these elevation datasets can be used for in catchment management studies. Upon examination of the results it is apparent that the ASTER GDEM 1 elevation dataset contains anomalies and artifacts that degrade its overall accuracy, which is why METI and NASA consider it to be research-grade only (ASTER Validation Team, 2009). These results are consistent with results from previous studies (e.g. Hirt et al. 2010, Reuter et al. 2009).

Moreover, the ASTER elevations showed the lowest elevation mean value (Table 4.2) compared with the other datasets. This agrees with the result from cross-sections profiles (Figures 4.5 and 4.8), as it can be seen from these two elevation profiles that the ASTER elevation values were generally underestimated in the open arable land and overestimated in areas covered by woodlands in comparison with the other elevation datasets. In a study over Western Australia, Hirt et al. (2010) reported that the vertical accuracy of ASTER 30 m was 15 m (RMSE) whereas that for SRTM 90 m was 6 m. Chrysoulakis et al. (2011) stated that, in Greece, the accuracy of ASTER is more than 16.1 m (RMSE).

The Landmap DTM elevation dataset from IFSAR observations comes at 25 m resolution. It performs as a noisy elevation dataset. The model contains a lot of spurious pits and spikes artifacts occurred with high frequency as well as stripe-effects. It is clear that this data suffered from the problem of poor coherence and atmospheric effects caused by the repeated pass data (Dowman, 2004) which degrade the output accuracy. In the case of SRTM, it performs better than both Landmap and ASTER apart from the fact that elevation values are overestimated in areas covered by high canopy trees (Blanchard et al., 2010; Lalonde et al., 2010). SRTM gave quite similar results to the Bluesky, NEXTMap , Ordnance Survey Profile and Ordnance Survey Panorama along the two transects for all land cover types, but if significant vegetation is present the elevation values are usually overestimated.

On this basis, Bluesky, NEXTMap, Ordnance Survey Profile, Ordnance Survey Panorama and SRTM are preferred over ASTER and Landmap DTM for further investigation of their suitability (fitness for use) for hydrologic analysis and other catchment management applications.

4.4 Summary

In this chapter a range of available digital elevation models (DEMs) for the study area have been described. DEMs quality has been extensively evaluated using a wide range of quantitative and qualitative accuracy assessment procedures. In general, the results of this analysis revealed that both ASTER and Landmap elevation datasets performed very poorly in this area. Therefore, these two elevation datasets were considered unsuitable for inclusion in further stages of this research.

Chapter 5

Threshold Definition

5.1 Introduction

At the end of Chapter 4 five elevation datasets (NEXTMap, Bluesky, OS10, OS50 and, SRTM) were selected for further assessment of their suitability for catchment management applications. Literature reviewed in Chapter 2 indicated that the locations and extents of DEM-derived stream networks vary with the method of calculation (e.g. flow accumulation threshold value) and the source and spatial resolution of the DEM used. In this chapter, the five selected DEMs were used to identify the most appropriate contributing drainage area threshold for the study catchment using three different methods and to investigate how sensitive each method was to the input DEM source and resolution. Another objective of this part of research was to evaluate the performance of each different threshold for deriving channel networks in the study area.

5.2 Determining an adequate threshold

Stream channels are rarely singular in form and tend instead to be part of branching networks. A stream network is composed of channel and overland flow elements that represent flow over the terrain (Vieux, 2005). Stream order is a way of categorising the network so that headwater streams (ephemeral streams) are denoted as first-order streams and when two first-order streams meet they produce a second-order stream. Where two second-

order streams meet that produces a third-order stream, and so on (Holden, 2014). Ephemeral stream networks serve as a critical hydrologic link between the surrounding landscape and the larger, connecting stream outflows within a catchment. These networks drain extensive surface areas within the catchment that are not directly in contact with higher order stream channels. The ephemeral channels of any catchment are the overland flow of water during, and often after, a precipitation event (Desmet et al., 1999; Sheshukov, 2015).

It has been acknowledged that for many catchment-based natural resource management issues an accurate delineation of the surface pathways of water movement on the catchment landscape is a prerequisite. Accurate determination of channel network locations and shapes is important for many hydrological and environmental applications at the catchment scale, including diffuse pollution and water quality issues. For modelling purposes, neglecting lower order streams can result in variations of hillslope flow length and drainage density, features that all control how water is routed through the landscape (Zhang and Montgomery, 1994). Channel network extraction models often simulate transitions from hillslope to channelized flow based on a contributing area threshold calculated from a DEM. Therefore, this point of transition is important because it represents a geomorphic threshold point within the catchment where enough surface water has accumulated to cause erosion (McNamara et al., 2006).

Different values of the contributing drainage area threshold can produce radically different stream network in terms of total stream length, stream order and, drainage density. The ideal threshold is at the point where diffuse (hillside) erosion terminates and fluvial (stream) erosion initiates as a result of concentrated surface flow. Several methods have been proposed for threshold value estimation (Colombo et al., 2007; Hancock and Evans, 2006; Ijjasz-Vasquez and Bras, 1995; Montgomery and Foufoula-Georgiou, 1993; Orlandini et al., 2011; Tang and Liu, 2009; Wilson and Gallant, 2000) three of which are widely used: the

area-slope relationships method, a trial and error approach (comparing the derived network with a reference network), and using the 1% value of the maximum flow accumulation. These three approaches have been chosen for further investigation since they are among the most common approaches found in the literature about how to select an appropriate threshold value that will produce a representative depiction of the stream network. Therefore, flow accumulation thresholds were identified and analysed using these three different methods.

First, a trial and error approach was conducted until the extracted network was consistent with a reference stream network obtained from OS VectorMap™ Local at 1:10000 scale and modified using OS 1:1000 MasterMap raster data (Section 5.2.1). Secondly, the 1% of the maximum flow accumulation value approach, as a simple rule of thumb for stream determination threshold was examined. Finally, the area-slope relationship was employed, where thresholds are determined by evaluating distributions of surface slope and drainage area calculated from a DEM. It has been claimed that examining the association between these two variables can help identify a threshold that represents the mean drainage area which distinguishes between hillslope and channel flow in hydrologic modelling (Tarboton et al., 1992). All three threshold methods were used to extract stream networks and these were assessed to find out which threshold(s) can be considered as an appropriate support area threshold in the study area.

5.2.1   Reference river network

The reference network is a modified river network created using the water surface line and area layer products obtained from OS VectorMap™ Local, a GML vector dataset at a nominal scale of 1: 10000 covering the whole of Great Britain. The main characteristics of the dataset is representation of real world features (e.g. roads, railways, buildings, vegetation, surface water lines and areas, boundaries and urban extents) as points, lines, polygons, and

text. According to the OS VectorMap™ Local's user guide and technical specification document, rivers and streams narrower than 5 m are represented as a single line, whereas those wider than this are illustrated as polygons. Lakes and ponds greater than 100 m² are shown as flat water polygons. Water feature such as rivers and lakes are broken into sections by features such as bridges, tunnels, dams, and culverts (Regnauld and Mackaness, 2006). The resolution of this data is believed to be two decimal places of a meter. OS VectorMap Local data are projected to the National Grid coordinate reference system, which is defined by the OSGB36 datum and distributed in 5 km x 5 km tiles (Ordnance Survey, 2009b).

The reference network was obtained from the surface water line layer for the study area and was enhanced using OS 1:1000 MasterMap and Google Earth. As mentioned above, there is no representation of water features where they are obscured by other objects such as bridges. These unconnected water features that are passing under bridges or tunnels were connected to each other to produce a completely connected river network. It was possible to infer the correctness of the connectivity results using the OS 1:1000 MasterMap by overlying the stream network on these high detailed topographic maps (Figure 5.1). Google Earth was used for visual inspection of the correctness of the resultant fully connected river network. In addition, the surface water data included information on man-made ditches and artificial drainage lines which were eliminated. The centre lines of rivers and streams that are shown in a polygonal form were then created and joined to the other linear representations of the river. The centreline representation of rivers and streams was created using the Cartography tools in ArcGIS 10.

This river network was adopted as a reference stream network for the purpose of comparison with the modelled stream networks in the following sections (see the reference network for the whole of the study area in Figure 5.2). Turcotte et al. (2001) argued that river network which was extracted from large scale topographic maps with the help of high

resolution satellite images used for a visual inspection was found to represent a better

accuracy in terms of horizontal location.
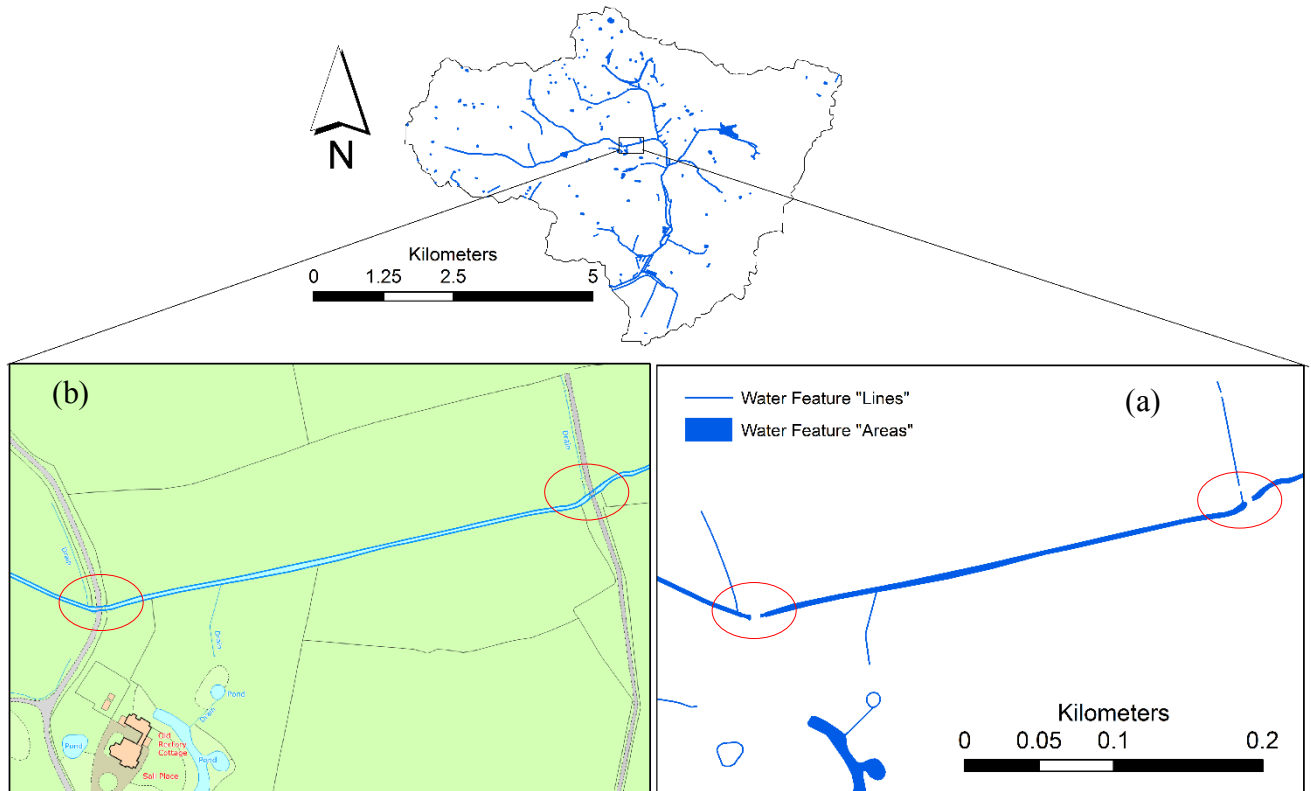
Figure 5.1: Example of OS VectorMap™ water feature data for Blackwater study area, (a) shows the breaks in the river segments (see red circles), and in (b) part of OS 1:1000 MasterMap illustrates that these breaks are indicative of road features intersecting the river, also in this figure the connected river segments are overlaid on the topographic map. Source: Ordnance Survey.
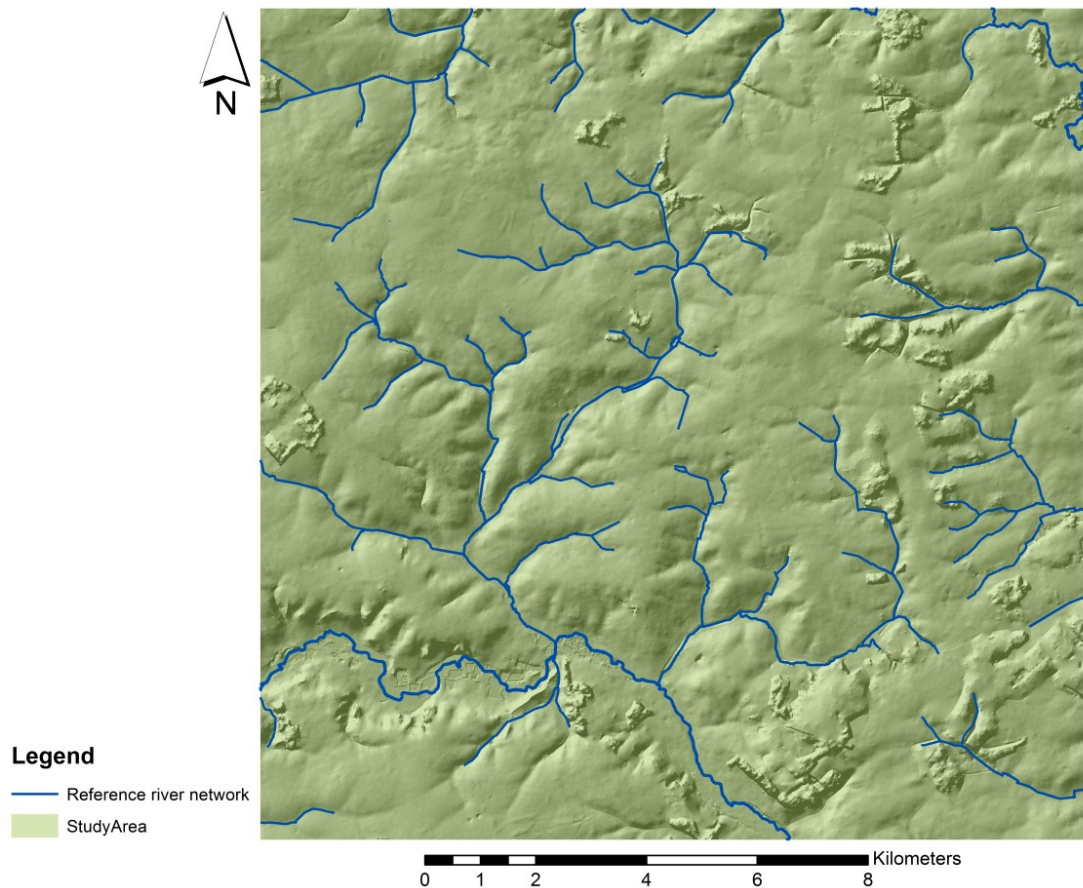
Figure 5.2: Reference river network for the Wensum study area. The underlying terrain is represented using NEXTMap elevation data.

5.2.2 Trial and error approach (method 1)

As mentioned above, the choice of the threshold value obviously influences the generated stream network. Generally, a threshold value is established by visual comparison of the generated network with a reference network obtained from large scale topographic maps, using a trial and error approach until a certain threshold value makes the resulting stream network terminate at approximately the same locations as the reference network (Gandolfi and Bischetti, 1997; Heine et al., 2004). NEXTMap DTM data were used for this trial and error process of determining the ideal threshold value. This DTM was selected because of its higher resolution (5m) and also because during the process of converting NEXTMap

elevation data from a DSM to DTM product the narrow drainage channels were preserved

through woodland areas, as described in the Intermap Product Handbook (Intermap

Technologies, 2011). This was an advantage of NEXTMap data compared to the other 5m

resolution elevation dataset (Bluesky) considered in this study.

After several iterations, it was found that the flow accumulation threshold value that

generated a stream network which had the best match to the reference river network (see

reference network in Figure 5.2) was 25,000 cells (equal to an area of 0.625 km²). It should be

pointed out that this method is based on some assumptions such as; the study area is small and

has a homogeneous landscape (Tang and Liu 2009). However, it is still not a perfect fit with

the reference river network, especially for the first order streams where it was difficult to have

a good match between the reference and the extracted network in terms of channel heads. In

the literature it has been reported that accurate identification of stream initiation locations

requires more than elevation data as it is often influenced by local characteristics of climate,

geology, groundwater level, land cover and land use (Metz et al. 2011).

In order to compare the drainage networks extracted from the different elevation

datasets, the same threshold value was applied to facilitate the comparison (Li and Wong

2010; Liu and Zhang, 2011). Therefore, as a first step, the flow accumulation threshold values

were calculated for the other DEM datasets using Eq. 5.1 and are reported in Table 5.1 below;

$$FA_i = \frac{FA_a \times C_a}{C_i} \qquad \text{Eq. 5.1 (Wang and Yin 1998)}$$

where FA_i is the flow accumulation threshold value needs to be determined for a

DEM, FA_a is the calculated flow accumulation threshold value for DEM_a (i.e. NEXTMap in

this study), and C_a and C_i are the cell areas of each corresponding DEM.

The contributing drainage area can be computed using Eq. 5.2 below;

$$CDA = \frac{FA \times (Cellsize)^2}{1000,000} \qquad km^2 \qquad (Eq.\ 5.2)$$

where FA is the flow accumulation threshold value (count of pixels), CDA is the corresponding contributing drainage area and cell size is the DEM resolution.

Table 5.1: Flow accumulation threshold values for each different DEM

DEM	Calculated FA threshold (count of cells)	CDA (km²)
NEXTMap (5m)	25000	0.625
Bluesky (5m)	25000	0.625
OS 10m	6250	0.625
OS 50m	250	0.625
SRTM (90m)	77	0.625

The hydrology analysis extension within ArcGIS 10 was used to calculate the flow accumulation raster for each DTM using the D8 flow accumulation method, following the basic steps of pit filling, identification of flow direction followed by the calculation of a flow accumulation raster as described in Chapter 2. Stream networks were then identified by applying the same contributing area threshold (0.625 km²) to the flow accumulation matrix of each different DEM. All the grid cells with an accumulation value greater than the threshold were regarded as the potential surface flow path. Stream networks are formed by these flow paths. All streams were further ordered according to the Strahler system, a stream ordering method proposed by Strahler in 1952 (Strahler 1952) which introduces a hierarchy into the river system, where stream order only increases when streams of the same order intersect

(Poggio and Soille, 2008). In this study, the Strahler hierarchy arrives at an order of four for all the extracted stream networks from each DEM.

Stream networks extracted from each DEM using the same threshold value are shown in Figure 5.3. The figure illustrates that all the DEMs are able to capture the general pattern of the drainage networks in the study area compared to the reference river network. It is clear that all the derived stream networks are broadly similar for lower channel reaches. Channels derived from SRTM data have unnaturally straight sections and angular features. This is most likely a result of the lower resolution (90 m). Moreover, visual inspection of the extracted stream networks at the circled locations in Figure 5.3 suggests that none of the five DEMs used was able to capture the real shape of the River Wensum in that part of the study area. This could be due to the existence of large water bodies (lakes) in that area (Figure 5.3), which are represented by the DEM as flat areas. By definition, DEMs do not contain information about lakes or ponds, and it is difficult to determine if an area of equal elevation is either a lake or a flat area (Turcotte et al. 2001).
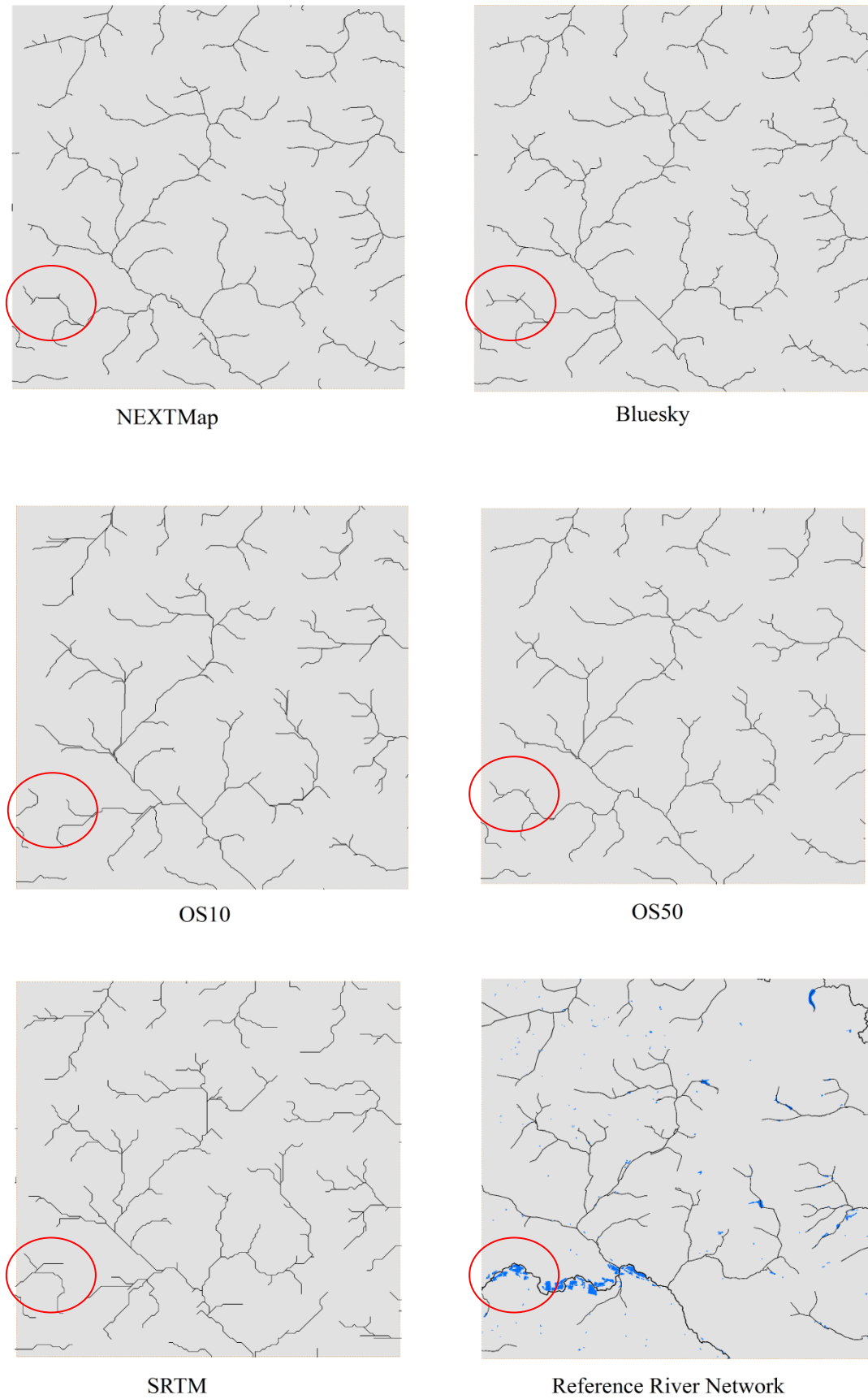
Figure 5.3: The stream networks extracted from each DEM using the selected threshold value (0.625 km²). The reference river network is also illustrated.

The number of streams within different stream orders obtained from each DEM using the same threshold value (0.625 km²) in the study area is summarised in Table 5.2, and illustrated in Figure 5.4. In this study, the Strahler hierarchy arrived at an order of four for all the extracted stream networks. However, there are some differences in the number of streams within different orders obtained from each DEM especially for the first and third order streams, where the Bluesky dataset estimates greater stream numbers than the others, 110 for the first order and 23 for the third order. On the other hand, Landform Panorama (OS 50m) generates the lowest number of streams with 90 streams for the first order and 12 for the third order. Despite the fact that SRTM has the largest pixel size (90m), the number of streams within each order obtained from SRTM is greater than that from Landform Panorama (50m), with the exception of the number of streams within order four.

Generally speaking, the use of a high-resolution DEM should result in more detailed delineated low-order streams (Liu and Zhang, 2011). However, as can be seen from Table 5.2 there is no great differences in the number of first order streams obtained from each DEM, while the resolution of the DEMs varies from 5m for NEXTMap and Bluesky to 90m for the SRTM. This could be due to the relatively large contributing area threshold that has been used, where only recognizable (true) channels were mapped. Finally, all the DEMs produced the same number of streams within the highest stream order, nine streams, except SRTM data with four streams only (Figure 5.4).

Table 5.2: The numbers of streams within each stream order from each DEM

Stream order	NEXTMap (5m)	Bluesky (5m)	OS 10m	OS 50m	SRTM
	Number of streams				
1	103	110	107	90	107
2	54	54	57	48	51
3	18	23	20	12	21
4	9	9	8	9	4
Total	184	196	192	159	183
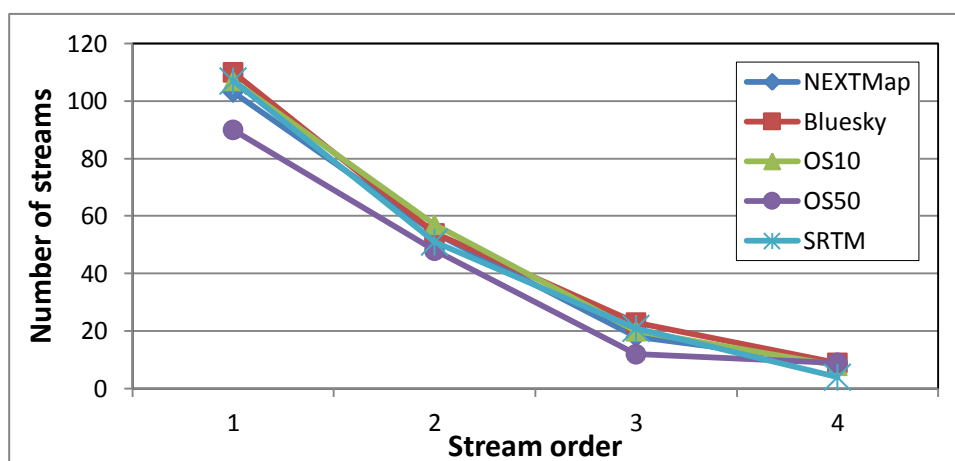
Figure 5.4: The numbers of streams within each stream order from each DEM

5.2.3 1% of the maximum accumulation value approach (method 2)

As stated previously, the use of the 1% value of the maximum flow accumulation value, as a simple rule of thumb for stream determination threshold, has been proposed as resulting in an adequately delineated stream network (Arc Hydro tool documentation, Tang and Liu 2009). The hydrology analysis extension within ArcGIS 10 was used to calculate the flow accumulation raster for each DTM using the D8 flow accumulation method, following the basic steps of pit filling, identification of flow direction followed by the calculation of the flow accumulation raster (the same approach as in the previous method). The threshold values for all the DTMs, selected as the value of 1% of the maximum flow accumulation, are reported in Table 5.3 below.

Table 5.3: Flow accumulation threshold as a 1% of the maximum flow accumulation value for each DTM.

DEM	1% of the max FA	CDA (km²)
NEXTMap (5m)	48666	$1.22 \approx 1.2$
Bluesky (5m)	48666	$1.22 \approx 1.2$
OS 10m	11613	$1.16 \approx 1.2$
OS 50m	482	$1.21 \approx 1.2$
SRTM (90m)	140	$1.134 \approx 1.2$

As can be seen from Table 5.3, the contributing drainage area thresholds obtained from the DTMs are all approximately the same (1.2 km²). This threshold was applied to the flow accumulation raster of each different DEM using the Con function of ArcGIS 10, where all cells with a contributing drainage area larger than the threshold were included as part of the identified stream networks (Figure 5.5). All streams were further ordered according to the Strahler ordering system.

Figure 5.5 below shows a comparison of the streams derived from each DEM when the threshold value is 1.2 km² (1% of the maximum flow accumulation value) with the reference stream network. As can be seen from the maps, the delineated streams match quite closely with the reference network. However, it is clear from Figures 5.3 and 5.5 that stream network with a threshold of 0.625 km² has many small streams that do not appear in the stream network with a threshold value of 1.2 km², hence, the former stream network (method 1) extends farther headward than the latter one (method 2) (see example from Bluesky data in Figure 5.7). In addition, the effect of the water bodies is apparent at the circled locations, as discussed with the previous method.
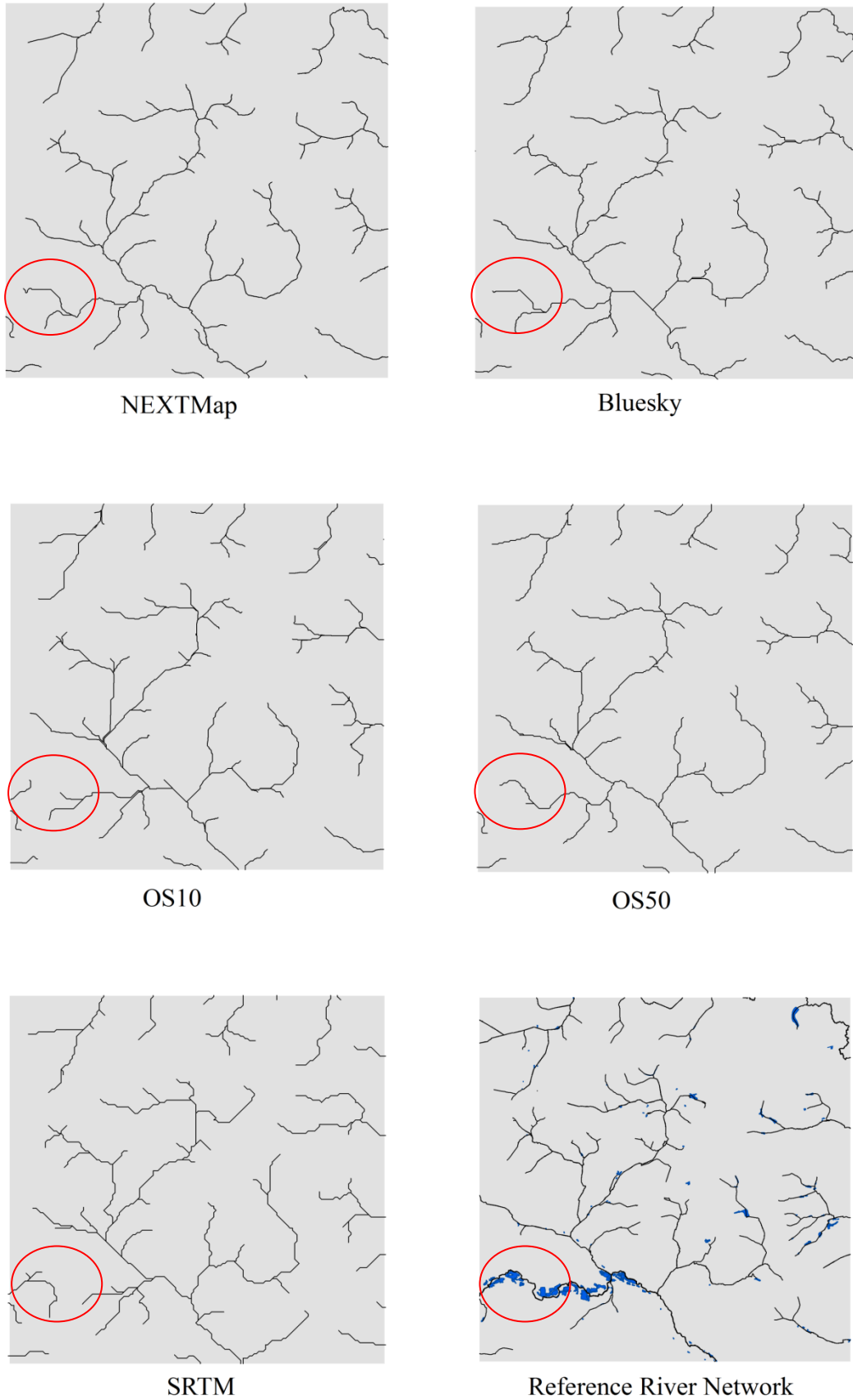
Figure 5.5: The stream networks extracted from each DEM using 1% of the maximum flow accumulation value as the threshold (1.2 km²). The reference river network is also presented including the lakes layer.

Table 5.4: The numbers of streams within each stream order from each DEM

Stream order	NEXTMap (5m)	Bluesky (5m)	OS 10m	OS 50m	SRTM
	Number of streams				
1	61	56	64	56	59
2	32	27	31	34	25
3	9	9	10	7	13
4	5	5	7	0	0
Total	107	97	112	97	97

With the same contributing area threshold (1.2 km²), the Strahler hierarchy arrives at an order of three for two delineations (OS 50m and SRTM) and an order of four for the other three datasets (NEXTMap, Bluesky and OS 10m), (Table 5.4 and Figure 5.6). As expected, it is clear from the figure and the table that with the increase in the threshold value the total stream number and the stream orders decrease. Table 5.5 shows that with the increase in the threshold value from 0.625 to 1.2 km² the number of streams considerably declines by about 80 streams for each elevation dataset.
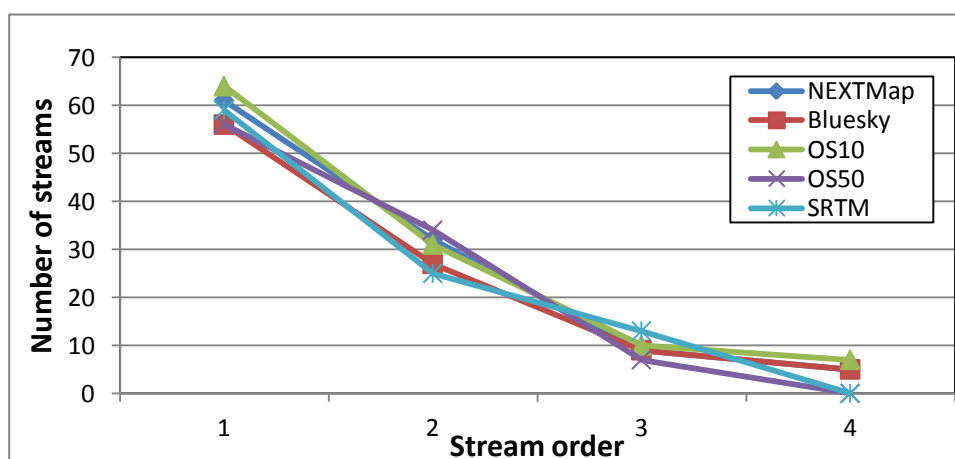
Figure 5.6: Number of streams within each stream order from each DEM

Figure 5.7: The differences between stream networks with 0.625 and 1.2 km² thresholds.
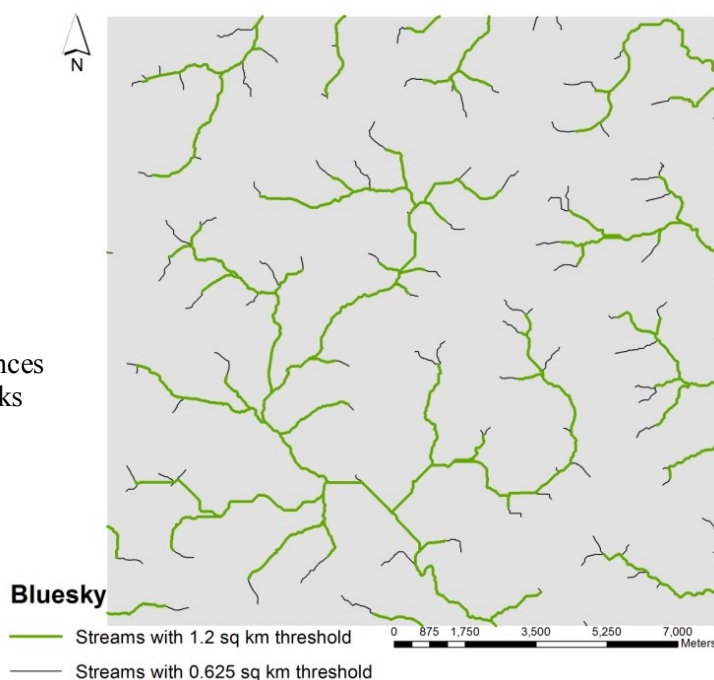
Table 5.5: Comparison of total numbers of streams and highest stream order from each DEM using 0.625km² (visual judgment) and 1.2km² (%1 of the maximum flow accumulation value) threshold values.

	NEXTMap			Bluesky			OS10m			OS50m			SRTM		
	Total stream number	Highest stream order	CDA km² (threshold)	Total stream number	Highest stream order	CDA km² (threshold)	Total stream number	Highest stream order	CDA km² (threshold)	Total stream number	Highest stream order	CDA km² (threshold)	Total stream number	Highest stream order	CDA km² (threshold)
Method 1	184	4	0.625	196	4	0.625	192	4	0.625	159	4	0.625	183	4	0.625
Method 2	107	4	1.2	97	4	1.2	112	4	1.2	97	3	1.2	97	3	1.2

5.2.4 Area–slope relationship approach (method 3)

In order to investigate the critical contributing drainage area threshold some geomorphological descriptors such as area-slope relationship and cumulative area distribution can be used (Hancock and Evans, 2006; Khan et al., 2009; Khan et al., 2013). This approach is based on the assumption that there will be some inflection points in the longitudinal area-slope profile which enable a distinction between various geomorphic and hydrologic regimes (Colombo et al., 2007). Typically, the channel head location is defined as the area where the

132

hillslope ends and channel begins. Downstream of the channel head, the channel takes its proper shape as the surface water flow concentrates, and then stream network formation starts. The underlying hypothesis of these approaches states that channel heads are located in the transition zone which exists between the diffusive and fluvial zones and it is argued that the value of the contributing drainage area at this point of transition represents the critical value (Hancock and Evans, 2006). In other words, the threshold is the point where diffusive (hillslope) processes terminate and fluvial (channel) ones initiate as a result of concentrated surface flow.

Many studies have computed these descriptors from DEMs in order to infer an adequate threshold (e.g Hancock and Evans, 2006; Henkle et al., 2011; Khan et al., 2009; McNamara et al., 2006; Tarboton et al., 1991; Tarolli and Dalla-Fontana, 2009). The area–slope relationship is the relationship between upslope contributing area draining through a point versus the slope at the point. The cumulative distribution of drainage area is the proportion of the catchment that has a drainage area draining through a point which is greater than or equal to a given drainage area.

Hancock and Evans (2006) worked on two small catchments (20 ha and 50 ha) of uniform geology located in Tin Camp Creek, Northern Territory, Australia. The two catchments consisted of closely dissected short, steep slopes (10 – 100 m long) and gradients generally between 15 and 50 per cent. They were able to distinctly differentiate between diffusion dominated areas (hillslope) and those areas dominated by fluvial process (channel) on the basis of area-slope relationship and cumulative area distribution plots. An example is shown in Figure 5.8. In this study of part of the Wensum catchment, a relatively flat and low-lying area, with altitude ranging from few metres to maximum elevation of less than 80 metres above mean sea level and a slope of 1.5 degrees on average and about 30 degrees at maximum has been explored. The catchment is dominated by arable farming with some

scattered woodlands. Moreover, the catchment of the Wensum is known as a modified

catchment due to the creation of a network of drainage channels (reaches) that extend over

some of the Wensum area and drain via gravity into the main River Wensum (Sear et al.,

2006). Thus, the topography of the Wensum catchment is rather different from that for the

two catchments used by Hancock and Evans.
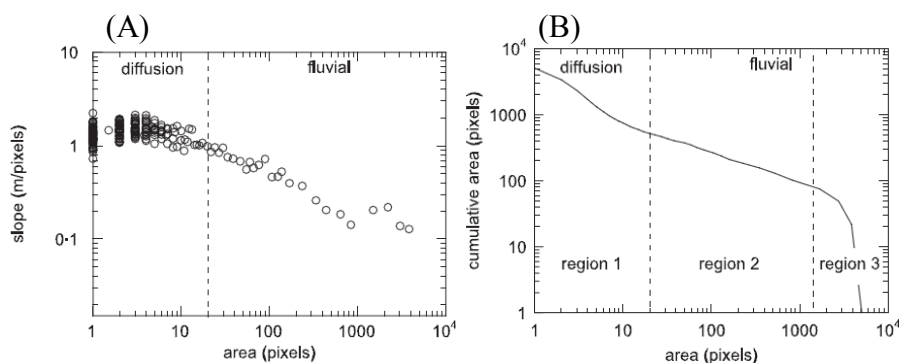
Figure 4.8: Area-slope relationship with each data point being an average of 20 surrounding points (A), and cumulative area distribution (B) plots depicting the hillslope-to-valley transition (Hancock and Evans, 2006).

The area-slope relationship plots generated from all DEMs show considerable scatter

(Figure 5.9). Initially it was thought that the main reason for this scatter was the fact that all

the DEMs used, apart from the Ordnance Survey datasets, were generated by remote sensing

technologies such as IFSAR, where the mapped elevation surfaces include the top of

woodland trees, as well as anthropogenic features rather than the bare ground surface.

However, the area-slope relationship of the areas covered by only the arable and grass land

cover types for the Bluesky DTM (as defined by LCM 2007) was also explored and again

showed considerable scatter (Figure 5.10). Furthermore, a tremendous scatter is also apparent

in the plots from OS DEMs that were generated from contour data. This suggests that the

types of data sources and techniques that were used to generate the DEMs are not major

factors affecting scatter in the area-slope relationship.
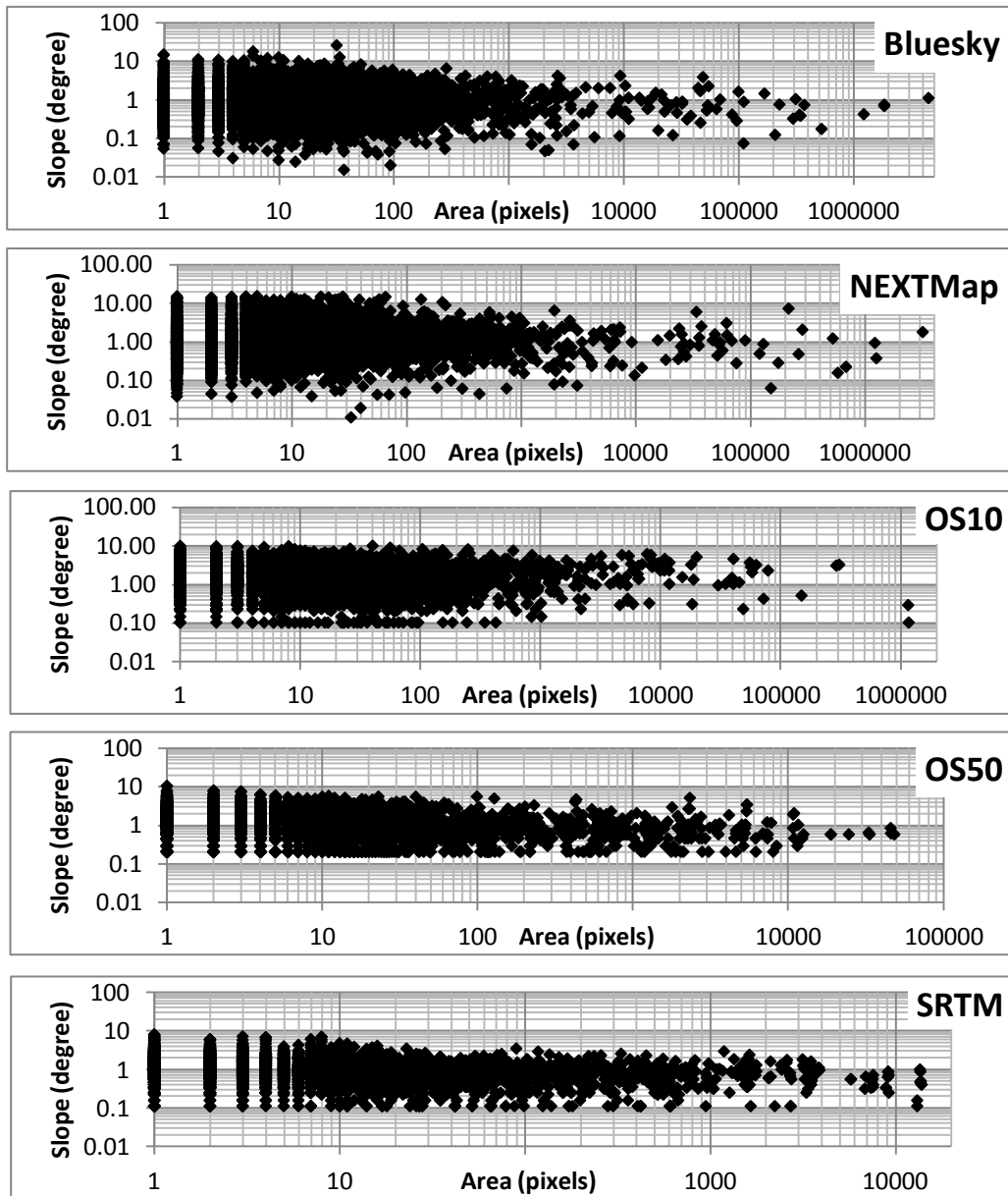
Figure 5.9: Area-slope relationship for Wensum study area
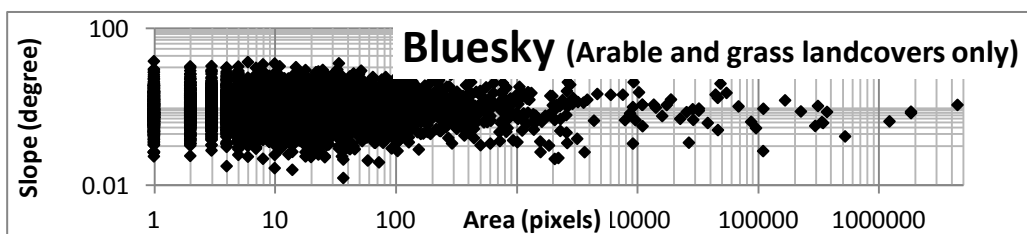
Figure 5.10: Area-slope relationship for Wensum study area using Bluesky data
(arable and grass land cover categories only)

As it was very difficult to distinguish diffusive (hillslope) from fluvial (channel) zones from the plots of area-slope relationship, the concept of area-aggregated slope relationship, introduced by Khan et al. (2009), was investigated. The aggregated slope of an area is the average slope of all the pixels having contributing area greater than or equal to that area (Khan et al., 2009; Ijjasz-Vasquez and Bras, 1995). Conceptually, it represents the variation in average slope of all downslope pixels from the given point (corresponding to the upslope area on x-axis), as we move progressively from upper parts of the catchment to catchment outlet. Unlike the area- slope relationship, the area- aggregated slope relationship is much more stable and it represents change in catchment slope at a macroscopic scale (personal communication to the author). As can be seen from an example using the Bluesky DTM in Figure 5.11 below, this approach is better at defining different regions of area-slope regimes, which makes the data more interpretable. The area-aggregated slope relationship and cumulative area distribution in semi-log plots were therefore generated for all the DEMs.
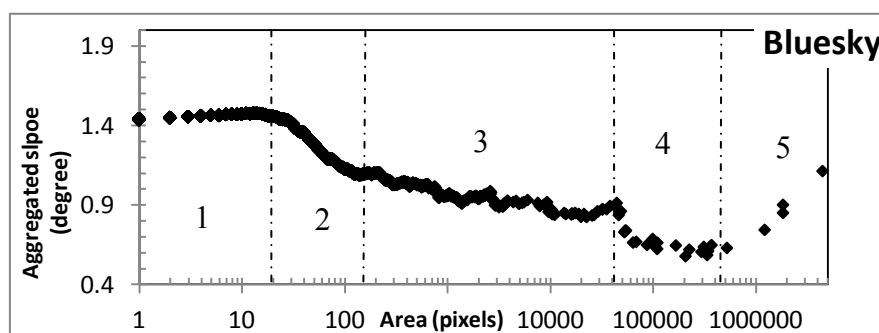
Figure 5.11: Area-aggregated slope relationship on semi-log scale separated into regions based on scaling response. Vertical lines signify transitions between regions denoted by inflictions in the curve.
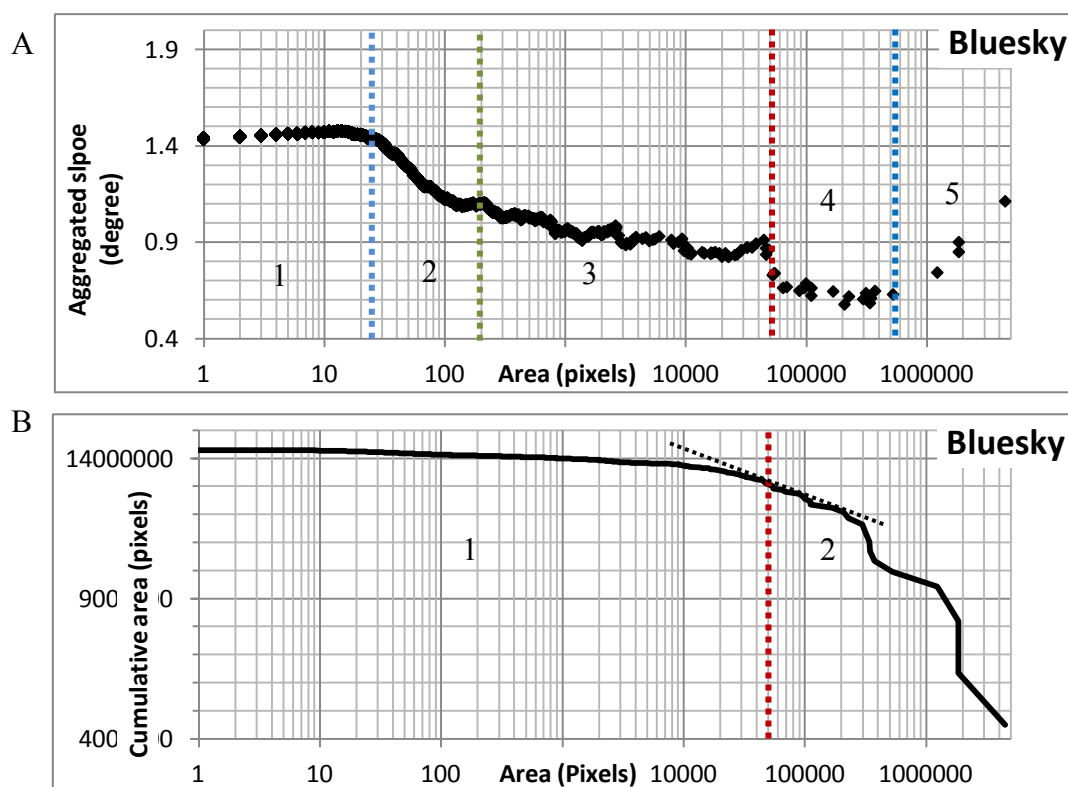
Figure 5.12: Area-aggregated slope relationship in semi-log scale (A) and cumulative area distribution (B) for the entire study area using Bluesky data.

From Figure 5.12A, the area-aggregated slope relationship from the Bluesky (5m) DTM shows five regions with different scaling responses. In region 1, at a very small contributing area (25 pixels), the area-aggregated slope relationship has a positive gradient but it becomes negative in region 2. This positive to negative inflection has been said to represent a transition from convex to concave slope profile, or from hillslopes to valleys. Here, this corresponds to a contributing area of 0.005 km². The negative trend becomes weaker with some fluctuating values in region 3, but it becomes very distinct beyond a sharp inflection point in region 4 at a contributing area equal to 50,000 pixels. This plot of area-aggregated slope relationship for the River Wensum study area (Figure 5.12A) appears similar to the area-slope relationships described by Ijjasz-Vasquez and Bras (1995) and McNamara et al. (1999), where the gradient is positive in region 1, becomes negative in region 2, is less negative in region 3, and returns to steeply negative in region 4. A fifth region appears at larger drainage areas. These four scaling responses are similar to those observed in

two recent studies conducted by Henkle et al. (2011) and Tarolli and Dalla-Fontana (2009).

However, the cumulative area distribution graph (Figure 5.12B) exhibits only two regions. A

point in the middle of a transition zone at approximately 50,000 pixels in the cumulative area

distribution matches the inflection point at 50,000 pixels that was observed in the area-

aggregated slope relationship plot. Similar results were found from the other five metre

resolution data (NEXTMap DTM) for the study area (Figure 5.13).
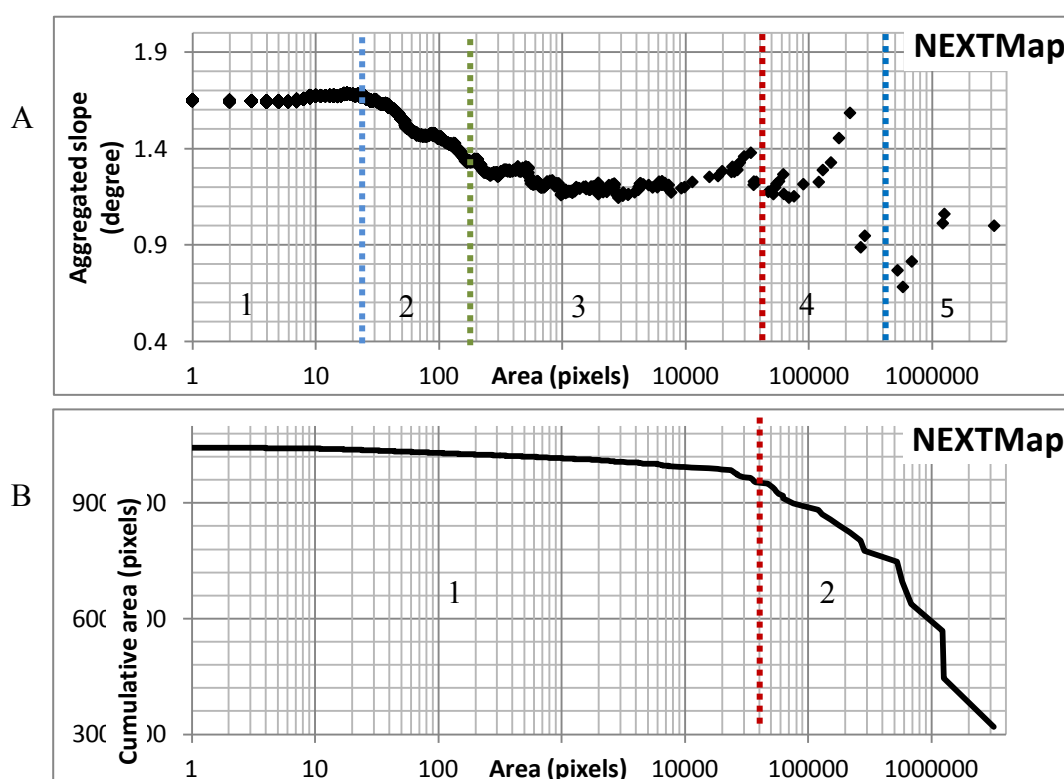
Figure 5.13: Area-aggregated slope relationship in semi-log scale (A) and cumulative
area distribution (B) for the entire study area using NEXTMap data.

In order to better understand the implications of each threshold value obtained at each

transition point observed in the area-aggregated slope diagram presented in Figure 5.12A,

stream networks were delineated and analysed. Four stream networks were delineated using

the contributing drainage area at each inflection point observed on the area-aggregated slope

relationship graph from the Bluesky dataset as threshold values (i.e. 25, 200, 50,000 and

540,000 pixels) (Figure 5.12A) for the Blackwater sub-catchment (Figures 5.14, 15, 16 and

17).
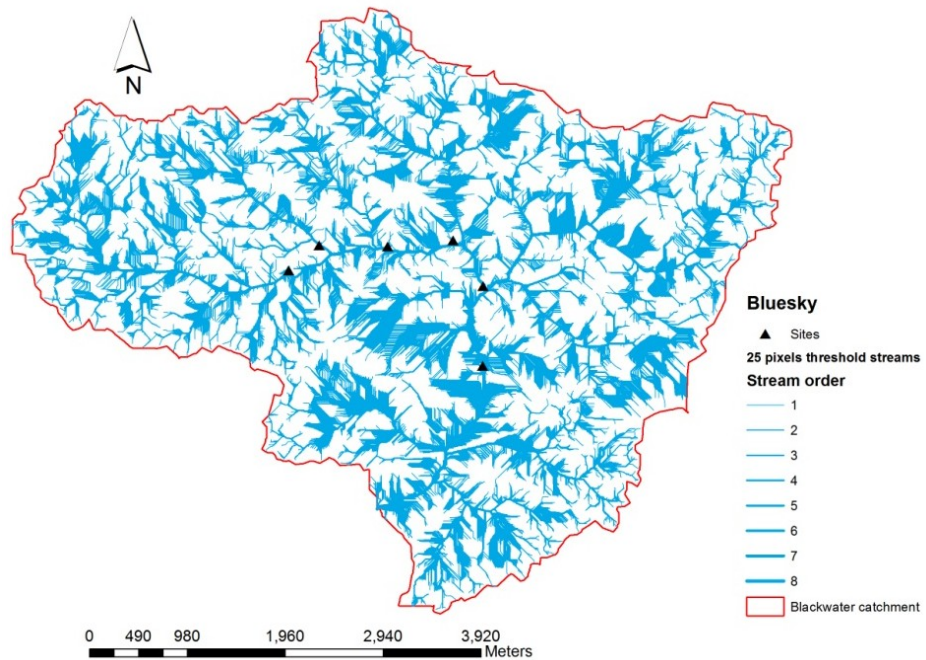
Figure 5.14: Stream networks extracted from Bluesky DTM in Blackwater catchment at a contributing area of 25 pixels (0.000625 km²), transition between regions 1 and 2.
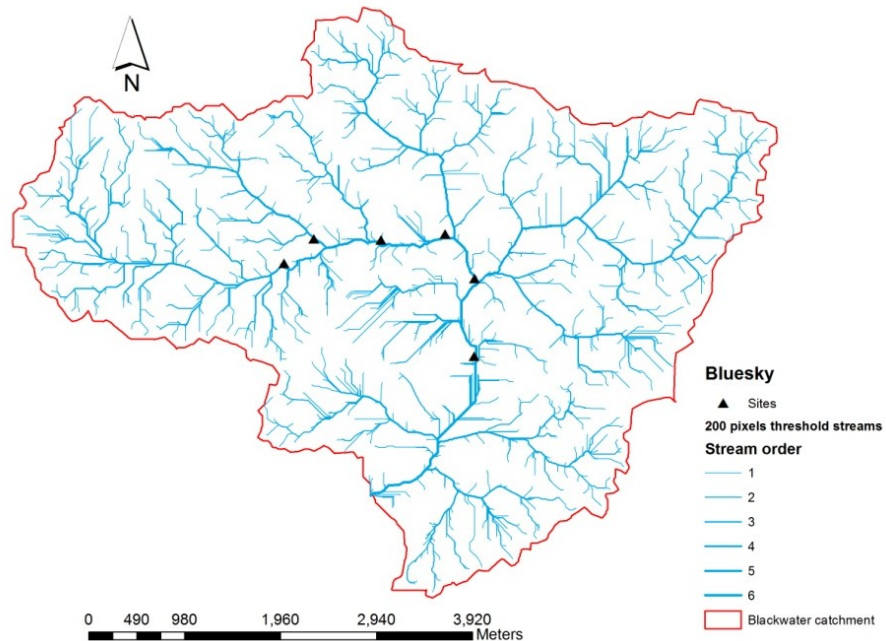
Figure 5.15: Stream networks extracted from Bluesky DTM in Blackwater catchment at a contributing area of 200 pixels (0.005km²), transition between regions 2 and 3.
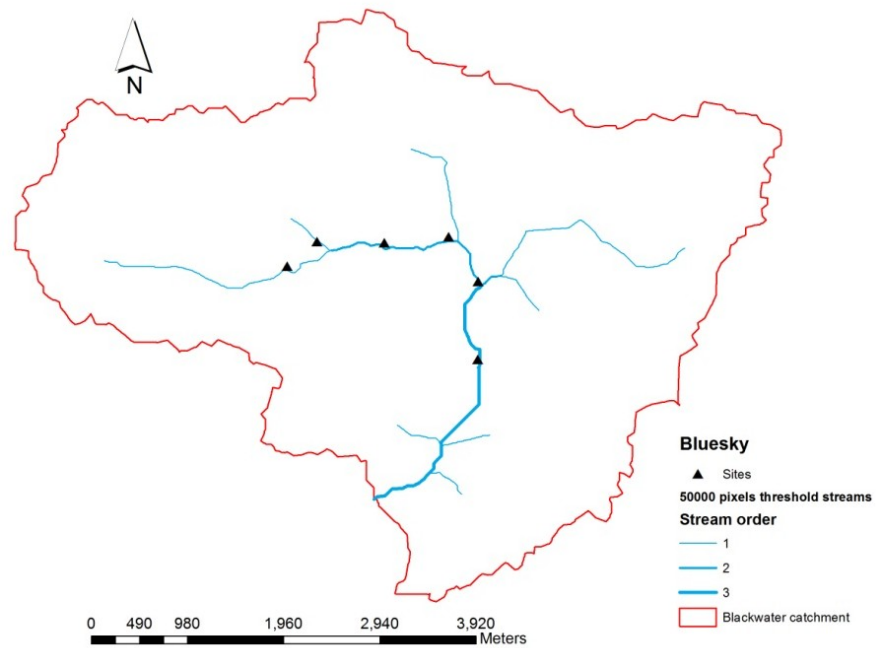
Figure 5.16: Stream networks extracted from Bluesky DTM in Blackwater catchment at a contributing area of 50,000 pixels (1.25 km²), transition between regions 3 and 4.
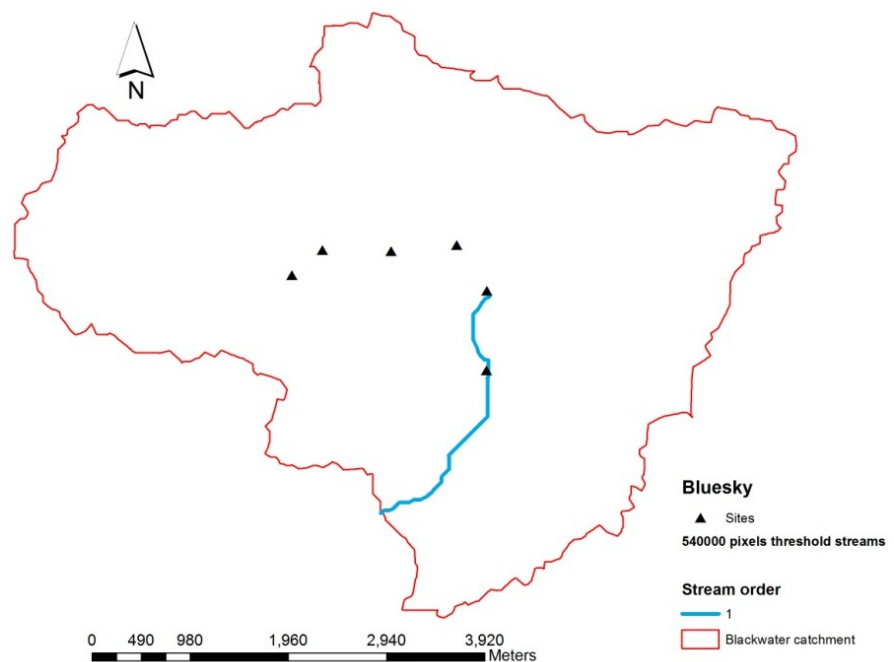
Figure 5.17: Stream networks extracted from Bluesky DTM in Blackwater catchment at a contributing area of 540,000 pixels (13.5 km²), transition between regions 4 and 5.

In order to study these stream networks and to help interpret each threshold value (the four regions observed in the area-aggregated slop relationship profile (Figure 5.11)) a field trip was made to the Blackwater sub-catchment area (Figure 5.20). In region 1, where slope increases with the drainage area until the first inflection point is reached at a very small contributing drainage area of 25 pixels, the stream network extracted at this threshold value (0.000625 km²) shows a very high level of detail (Figure 5.14). This region represents the convex topography (hillslope) that is typically controlled by diffusive processes.

It is clear from Figure 5.14 and Table 5.6 that choosing the threshold value at the transition between regions 1 and 2 would underestimate the minimum drainage contributing area (threshold area) and overestimate the length of channel networks. In many cases, as is clear from Figure 5.14, lower-order streams are represented as a whole series of parallel lines going down the field indicating that the variation in slope is in one direction. In other words, the low-order streams in Figure 5.14 can be interpreted as no more than showing the slope direction across the field (see Figures 5.18 and 5.19 for more illustrations). According to Montgomery and Foufoula-Georgiou (1993) the change between regions 1 and 2 is related to the change between hillslope with diffuse sediment transport and concave unchanneled valleys (see Figure 2.8, Chapter 2 for more illustration from Montgomery and Foufoula-Georgiou, 1993).
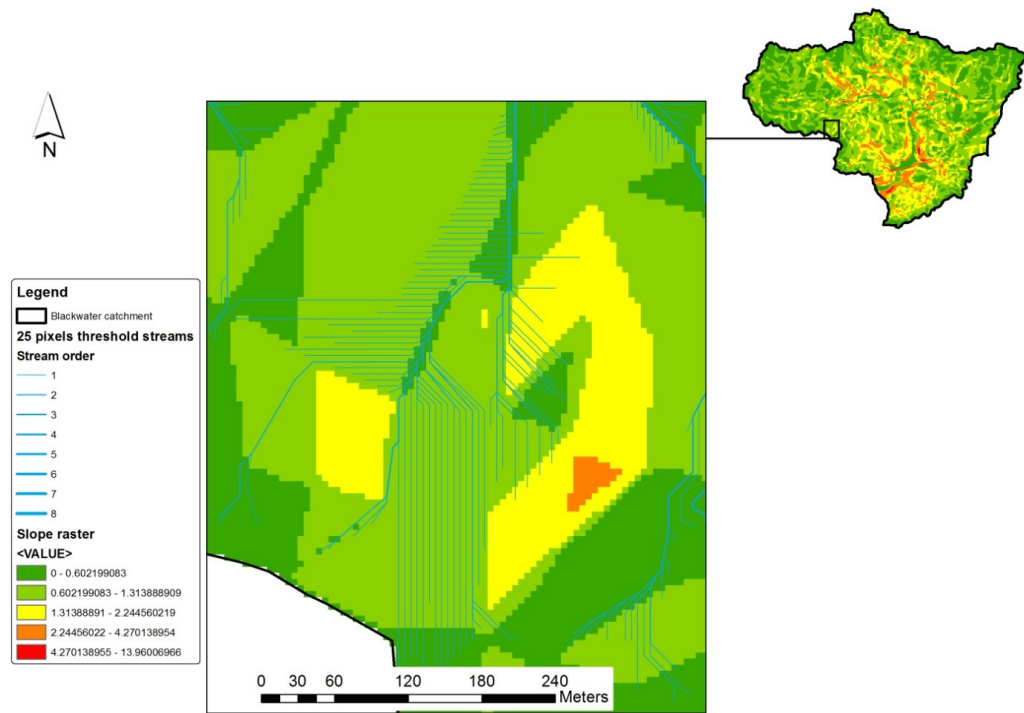
Figure 5.18: Streams obtained using 25pixels threshold are laid over the slope raster map. It is clear that low-order streams are a whole series of parallel lines going down the field when the variation in slope is in one direction.
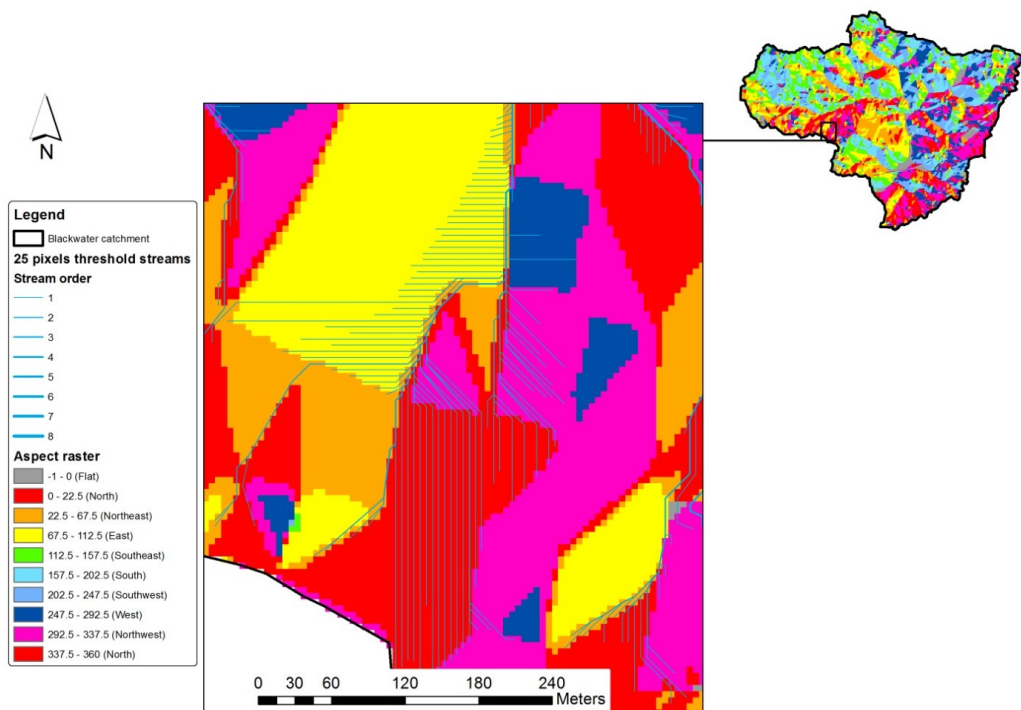
Figure 5.19: Streams obtained using 25pixels threshold are laid over the aspect raster map.

Stream networks obtained using the value of the contributing drainage area at the transition point between regions 2 and 3 (200 pixels) are illustrated in Figure 5.15. In region 2 slope decreases with drainage area, which implies concave topography, until the second turnover point is reached at 200 pixels. In order to examine the stream network that was obtained using the minimum contributing drainage area threshold of 200 pixels, several locations in the Blackwater catchment were visited (Figure 5.20) and some pictures were taken (Figures 5.21, 22 and 23). The field work consisted of exploring the landscape setting for the lower-order streams. At the three locations that were examined, it was found that first, second and third-order streams tend to correspond with the areas where flow accruing across fields could be seen, where there are sufficient variations in slope to concentrate surface drainage across the field. The variations in slope in two directions are evident and during the field investigation there were physical signs indicating that the water accumulated in some areas at the bottom of each field before draining to the main stream (Figure 5.22B). These streams can be defined as ephemeral streams which result from a surface water accumulation process during and following a period of heavy rainfall. In addition, these results also indicate that 5 m resolution DTMs are able to capture the small variations in the topography, which consequently allow these ephemeral streams to be accurately mapped during the process of flow accumulation.
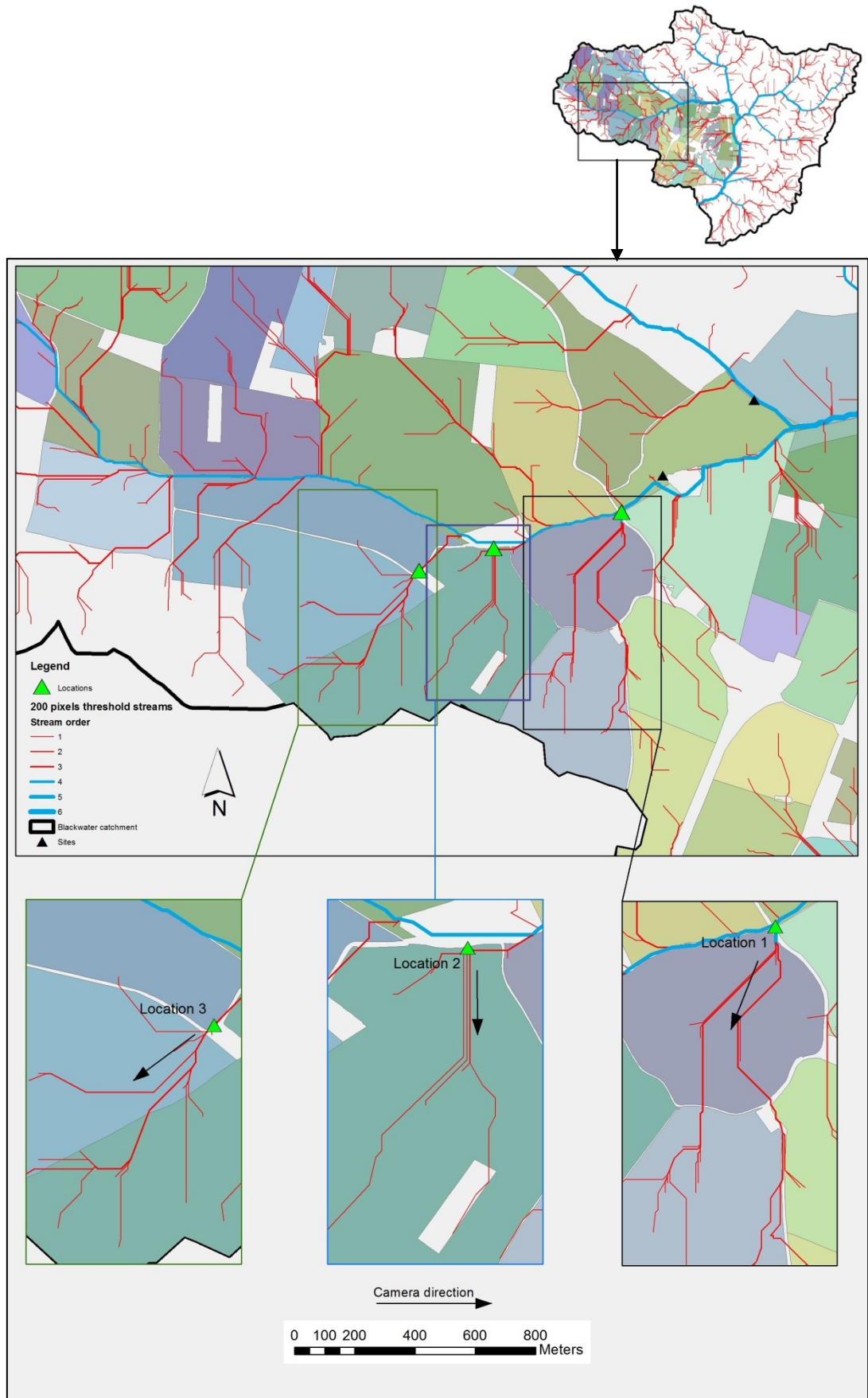
Figure 5.20: The three locations investigated in the sub-catchment of the Blackwater. The little arrows are indicate the directions of the camera when photos were taken.

Table 5.6: The numbers of streams within each stream order from Bluesky DTM using the four threshold values obtained using method 3.

		Streams Number		
		Bluesky DTM		
		Method 3		
Stream order	Threshold 1 (0.000625 km²)	Threshold 2 (0.005 km²)	Threshold 3 (1.25 km²)	Threshold 4 (13.5 km²)
1	131415	10825	55	6
2	59253	4806	27	3
3	26472	2637	9	0
4	14508	1552	4	0
5	9908	828	0	0
6	6338	436	0	0
7	2987	173	0	0
8	1031	0	0	0
9	726	0	0	0
Total	252638	21257	95	9

Figure 5.21: Landscape of location 1. Overland surface water accumulates to the bare part of this field as accurately captured by the DEM.

Figure 5.22: Landscape of location 2 (A). The arrow in image (B) indicates the place at the edge of the field where the surface water accumulates before draining to the main stream just behind the long grass.

Figure 5.23: Landscape of location 3.

Figure 5.16 illustrates the stream networks obtained using the flow accumulation value (50,000 pixels) at the transition point between regions 3 and 4. In region 3 the slope remains relatively constant until the third inflection point is reached at a contributing drainage area of 50,000 pixels (1.25 km²). A contributing drainage area threshold of this magnitude has been suggested in prior studies to represents channelized areas (Montgomery and Foufoula-Georgiou, 1993; Ijjasz-Vasquez and Bras, 1995; Tarolli and Dalla-Fontana, 2009). In our study, the stream networks that were obtained using this contributing area threshold were found to be representing recognisable channels (Figure 5.16). A validation process was carried out by directly observing the true streams in the field at the visited locations. As can be seen from Figure 5.24, the delineated streams using the threshold value of 50,000 pixels match quite closely with the reference network. Therefore, it is very clear that using a threshold value around 50,000 pixels (1.25 km²) will result in a delineated stream network that only reflects as much of the known stream channels as possible.
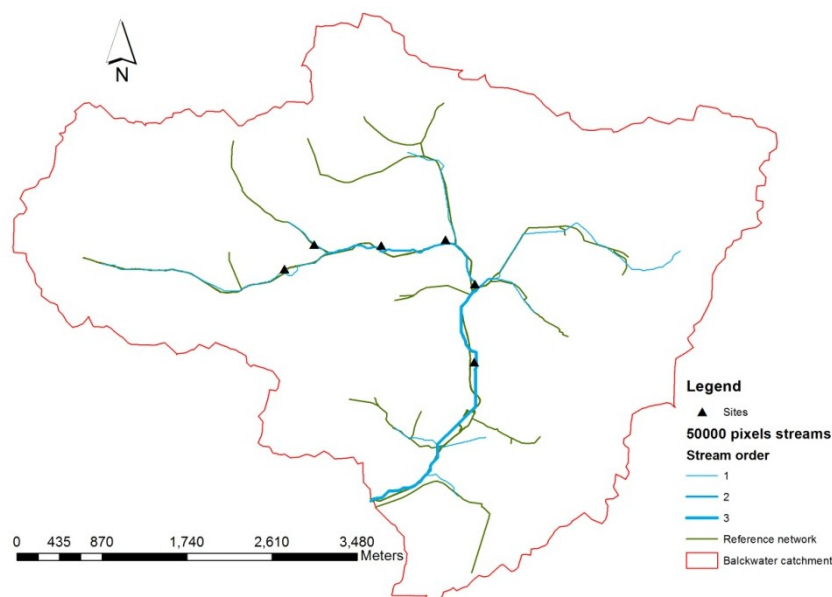
Figure 5.24: Comparison of the 50,000 pixels threshold delineated streams and the reference network.

Figure 5.17 shows that choosing the value of the contributing area threshold at the transition point between regions 4 and 5 will overestimate the threshold value and as a consequence, the derived stream networks are too short (start too late), as is clear from the map where network starts only on the main channel in the middle of the sub-catchment.

In summary, for the entire Blackwater catchment and using the 5 m resolution Bluesky DTM, the contributing drainage area thresholds ranging from 25 to less than 200 pixels produce stream networks where lower-order streams represent parallel lines going down to the bottom of slopes (diffusive processes, surface wash on one direction slopes). Stream networks corresponding to threshold areas of 200 to less than 50,000 pixels represent a mixture of where it possible to get a concentration of surface flow across a field and the edge of the field drains, whereas those corresponding to contributing drainage area thresholds of 50,000 pixels or more depict the recognisable (true) channels (Figure 5.25). This finding is consistent with Montgomery and Foufoula-Georgiou (1993) who have reported that a break from less negative to more negative gradient is found at larger contributing areas (transition

between regions 3 and 4 in our study), attributed to where alluvial channel processes begin to persist.
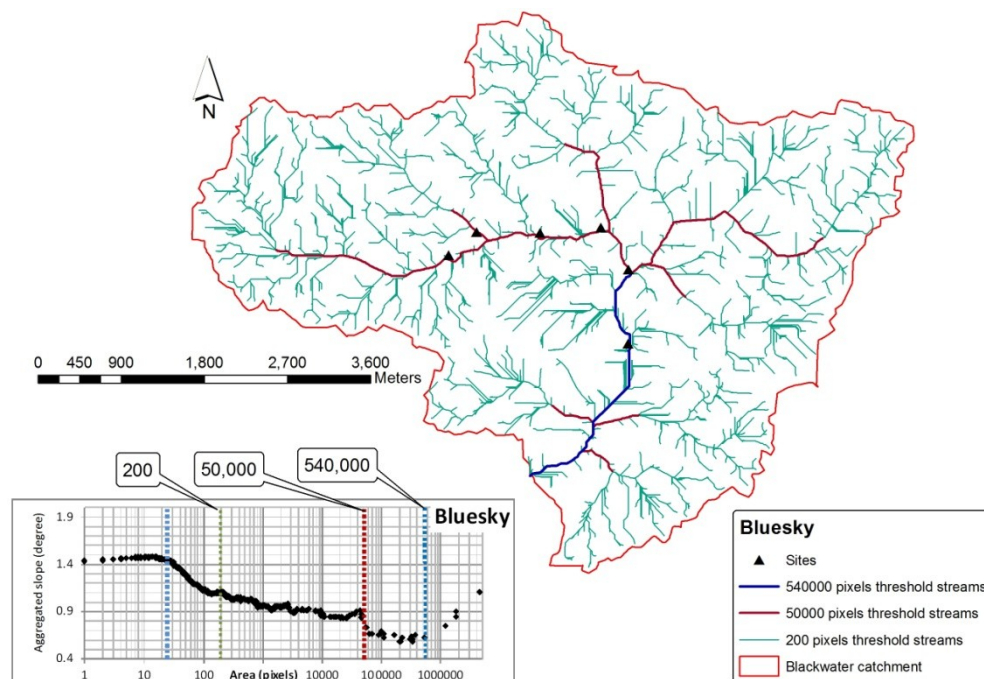
Figure 5.25: Stream networks determined for the Blackwater catchment at contributing areas of 200, 50,000 and 540,000 pixels, 0.005, 1.25, 13.5 km², respectively.

5.2.5 Threshold values for other elevation datasets based on Bluesky results

Flow accumulation threshold values were calculated for the other DEM datasets using Eq. 5.1 and those values obtained from Bluesky data using the area-aggregated slope relationship method. They are reported in Table 5.7 and are also shown on each corresponding area-aggregated slope plot in Figure 5.26.

The analysis of the area-aggregated slope relationship plots (Figure 5.26) shows the capability of high-resolution DTMs to depict the detailed changes in the gradient during the process of flow accumulation. Tarolli and Dalla-Fontana (2009) argued that only DEMs finer than 5 m allow the correct identification of dominant geomorphic process in relation to channel initiation location. Bluesky and NEXTMap DTMs behave very similar since the four

scaling regimes were identically picked out in both of them. Moreover, of the five DTMs, there is strong evidence that the third threshold (1.25 km²) can be picked out very well in three of them (Bluesky, NEXTMap, and OS50m), where it is almost identical in the first two DEMs and in the other one (OS50m) there is a similar sort of threshold but it is to some extent smaller (1.125 km²). Landform Profile (OS10m) DTM does not appear capable of picking up any threshold although there is an inflection point just smaller than the third threshold (1.25 km²) at about a contributing drainage area of 0.8 km². This could be related to the stepping artefacts (stair-step) problem related to the contour origin of this DTM.

Figure 5.26E shows that the four scaling regimes (thresholds) that were picked out by the 5 metre resolution DTMs (Bluesky and NEXTMap) do not exist in the SRTM area-aggregated slope relationship plot although there are two inflection points which can be interpreted as a displacement of the third and fourth thresholds, this is likely to be related to the lower resolution of the SRTM DEM (90 m).

Figures 26D and E demonstrate that the first and second regions that were observed by the finest DTM resolution (5 m) are not detectable by the courser resolution DTMs (OS50m and SRTM), this level of detail is lost (Martinez et al., 2010). However, the 50 m resolution DTM (OS50m) is capable of picking up the third and fourth scaling regimes (thresholds) that were picked up by the finest DTM (5 m). These results indicate that as grid size increases some details are lost (Hancock and Evans, 2006). Tarolli and Dalla-Fontana (2009) found that in a typical steep alpine catchment, a DEM finer that 10 m is required to better recognize local morphology and provide interpretation of the hillslope-to-valley transition based on the slope-area relationship. They also concluded that these scaling regimes, to some extent, disappear in 20 or 30 m DEMs. Montgomery and Foufoula-Georgiou (1993) reported that in moderately steep topography, a DEM finer than 30 m resolution is required to accurately identify the hillslope-to-valley transition.
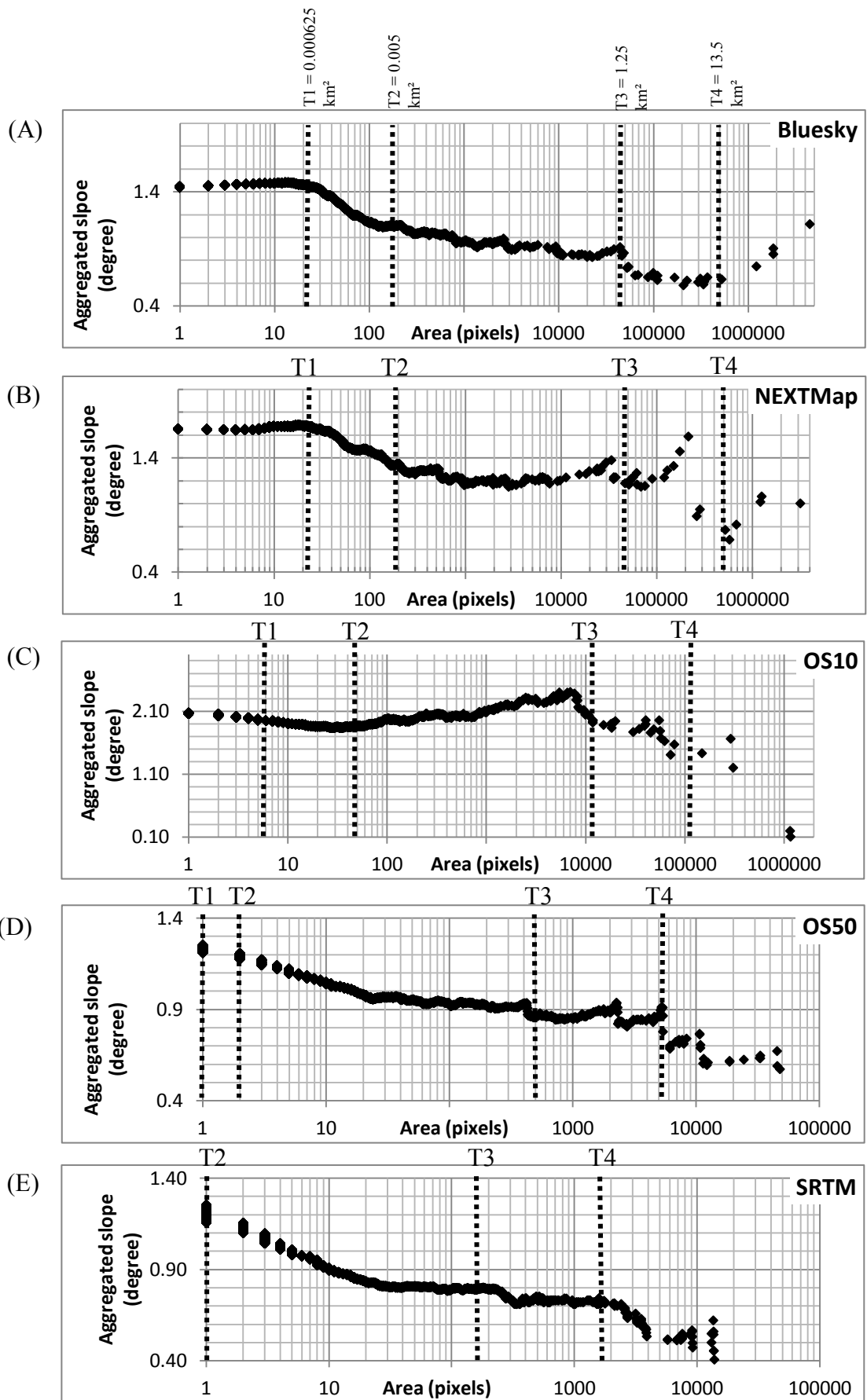
Figure 5.26: Area-aggregated slope plot for each DTM. The vertical dashed lines show the scaling regimes with respect to the four drainage area thresholds (25, 200, 50000 and 540000 pixels) that obtained using Bluesky DTM.

Table 5.7: The number of pixels from each DEM corresponding to each contributing drainage area (thresholds) that were obtained from Bluesky.

		Bluesky	NEXTMap	OS10	OS50	SRTM
Threshold 1	Pixels	25	25	6.25	0.25	0.07716
	Area (km²)	0.000625	0.000625	0.000625	0.000625	0.000625
Threshold 2	Pixels	200	200	50	2	0.617284
	Area (km²)	0.005	0.005	0.005	0.005	0.005
Threshold 3	Pixels	50000	50000	12500	500	154.321
	Area (km²)	1.25	1.25	1.25	1.25	1.25
Threshold 4	Pixels	540000	540000	135000	5400	1666.667
	Area (km²)	13.5	13.5	13.5	13.5	13.5

5.2.6   The suitable threshold for stream delineation

Stream networks have been delineated using various threshold values (method 1 = 0.625 km², method 2 = 1.2 km² and method 3 = 0.000625, 0.005, 1.25 and 13.5 km²). As expected, selection of different threshold values produces radically different stream networks in terms of numbers of streams, the stream orders and the stream lengths (Table 5.8). This shows that with the increase in the threshold values these other parameters gradually decrease.

Comparing the extracted stream networks obtained from all the three methods with each other and with the reference network reveals that networks extracted using the 1% value of the maximum flow accumulation (method 2) and the third threshold from the area-slope relationship (method 3) produce almost the same stream networks. This is because the two threshold support areas are almost the same, 1.2 and 1.25 km² respectively. These findings also indicate that the value that represents 1% of the maximum flow accumulation coincides with an inflection point in the area-aggregated slope relationship diagram (threshold 3) that represents the transition from the unchanneled valley (ephemeral streams) to the start of alluvial channels (recognizable channels). Overall, these results suggest that the use of the value that represents 1% of the maximum flow accumulation: as a simple rule of thumb for

stream determination threshold will result on an extracted stream network that reflects as much of the known stream channels as possible.

Table 5.8: Streams order, numbers of streams and streams lengths obtained from BlueskyDTM using different threshold values.

Stream order	Method 1 (trial and error) CDA = 0.625km²		Method 2 (1% of MFA) CDA = 1.2km²		Method 3 (Area-slope relationship)							
					CDA = 0.000625km²		CDA = 0.005km²		CDA = 1.25km²		CDA = 13.5km²	
	Number of Streams	Streams Length (m²)	Number of streams	Streams Length (m²)	Number of streams	Streams Length (m²)	Number of streams	Streams Length (m²)	Number of streams	Streams Length (m²)	Number of streams	Streams Length (m²)
1	110	93638	56	69261	131415	17766897	10825	1142380	55	67107	6	15601
2	54	52154	27	37419	59253	2610924	4806	426041	27	37419	3	10026
3	23	24558	9	10554	26472	852279	2637	188633	9	10554		
4	9	10169	5	6805	14508	348688	1552	106295	4	6805		
5					9908	185938	828	52631				
6					6338	97782	436	26121				
7					2987	52021	173	10010				
8					1031	18820						
9					726	13887						

Ijjasz-Vasquez and Bras (1995) suggested that the transition between the hillslope and channel regimes begins in region 3 and is completed at the beginning of region 4, as observed from the area-slope relationship (Figure 5.27). Similar findings were reported by McNamara et al. (1999), where they observed three distinct flow path regimes, and the fluvial channel regime is at drainage areas above 0.015 km², which is the value of the contributing drainage area at the boundary between regions 3 and 4 (Figure 5.28). In our study, the stream network that was extracted using a threshold value equal to the contributing drainage area at the boundary between regions 3 and 4 (50,000 pixels = 1.25 km²) represents the recognisable (true) channels.
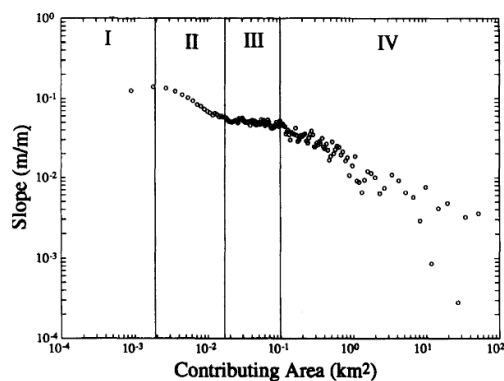
Figure 5.27: Area-local slope plot for the Brushy Creek basin (Alabama, USA). Four regions with different scaling response can be identified (Ijjasz-Vasquez and Bras, 1995).
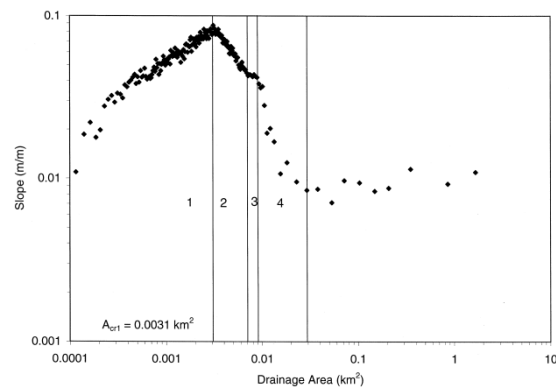
Figure 5.28: Area-local slope plot for the Imnavait Creek Basin (Alaska, USA). Four regions with different scaling response can be identified (McNamara et al. 1999).

To conclude, the response of contributing areas versus aggregated slopes was examined in DEM data from a relatively flat and low-lying area of the River Wensum catchment. Four regions with different scaling response were identified in the area-aggregated slope diagram. The existence of these regions in the DEM data, suggests the existence of different threshold values (Ijjasz-Vasquez and Bras, 1995). The actual concentrated surface flow initiation locations across the catchment landscape is better represented by the first inflection point after the gradient reversal (Henkle et al. 2011; Montgomery and Foufoula-Georgiou, 1993), which would be the transition between regions 2 and 3 (see Figure 5.11 for the scaling response regions and Figure 5.15 for the resultant stream network using the value at the transition between regions 2 and 3).   The transition between regions 3 and 4 is related to the change of dominance from the unchanneled valley (ephemeral streams) to the start of alluvial channels (true channels). Similar findings have been reported by other researchers (e.g. Henkle et al., 2011; Ijjasz-Vasquez and Bras, 1995; McNamara et al., 1999; Tarolli and Dalla-Fontana, 2009)

Since the area-aggregated slope relationship is a quantitative analysis method, the calculated stream threshold area should be more objective and accurate than a visual judgment or arbitrary chosen threshold value. Comparing various results, and according to our study purposes, the second and third thresholds, 0.005 and 1.25 km² respectively, that were obtained from the Bluesky DTM area-aggregated slope relationship graph will be used for the subsequent stream network uncertainty analysis. In addition, because the shape of the area-aggregated slope relationship is similar to those identified in previous studies for different study areas, the thresholds obtained in this study may be of significance for understanding hydrologic and geomorphic processes with the study catchment in relation to sediment transporting and surface water quality.

5.3 Conclusions

In this chapter, the performance of different contributing drainage area thresholds obtained by three different methods for channel network extraction using DEMs was evaluated. The first two methods (trial-and-error method and 1% of the maximum flow accumulation value) are straightforward processes and the flow accumulation area thresholds obtained produced stream networks that match to some extent the length of the reference network (true streams). When examining the relationship between contributing area and local slope, the data for the Blackwater catchment exhibit the systematic relationship identified in studies of other landscapes. Three distinct process domains defined by the area-slope plot have been identified, similar to those previous researchers have attributed to hillslopes, unchannelized, and channelized domains. Three different contributing drainage area thresholds were identified according to these distinct scaling regimes; 0.000625 km² (hillslope diffuse process), 0.005 km² (unchanneled valleys), and 1.25 km² (true streams). In the next

chapter (Chapter 6), the third threshold value is used to address how DEM sources and resolutions influence the positional accuracy of extracted stream networks.

The results of this study suggest that, in a landscape like the Wensum catchment, from the five DEMs examined a 5 m resolution is most appropriate when extracting geomorphic process domains from DEMs. It was clear from the area-slope plots for the different five DEMs that only Bluesky and NEXTMap DEMs were able to depict the different inflection points that enable the distinction between the above mentioned various geomorphic and hydrologic regimes. The examination of the area-slope data for the different DEMs demonstrates that as cell size increases, detail in the area-slope relationship is lost. At a grid spacing of 50 m and 90 m, the curvature in the diffusive region is lost and the area-slope relationship is generally linear for its entire domain (Figure 5.26).

Chapter 6

Comparing automated drainage networks derived from DEMs

6.1 Introduction

Earlier in this research the importance of the accurate delineation of stream networks and catchment boundaries for hydrological modelling and catchment resource management was acknowledged and reviewed. In the previous chapter (Chapter 5), breakpoints in the area-slope gradient were identified for the Blackwater sub-catchment and used to partition the landscape into three distinct flow path regimes: hillslope regimes at drainage area of 0.000625 km², unchanneled valley regimes above 0.005 km², and fluvial channel (true streams) regimes at or above 1.25 km². Two of these thresholds (0.005 and 1.25 km²) are used here for an assessment of extracted stream networks in terms of stream order, number of streams and stream lengths. However, setting different flow accumulation thresholds for a given DEM resolution results in differences of headward extent (lower order streams) of the mapped networks but not in the locations (positional accuracy) of the channels. Thus, the focus of this part of the research is not on assessing performance of these thresholds but rather addressing how DEM sources and resolutions influence the positional accuracy of modelled stream networks in the Blackwater sub-catchment.

Therefore, in the next part of this chapter, quantitative comparisons of the closeness of fit (horizontal accuracy) between derived stream network from different DEMs and reference data (reference network was discussed in Section 5.2.1) are performed, evaluated and

presented using two methods: horizontal RMSE and the Epsilon error band (see Chapter 2, Section 2.3.7.2). As discussed previously in Chapter 2 (Section 2.3.4) in applications of flow routing that involve the extraction of streams which are intended to be used in drainage network analysis or catchment boundary delineation, the use of a single flow direction algorithm such as D8 is preferable (Li et al. 2005; Zhou et al. 2008). In this study, therefore, the D8 was selected as a convenient DEM-based stream network generating method for the purpose of stream network comparison. The comparison of the stream networks and catchment boundaries derived from different DEMs for the Blackwater sub-catchment is believed to be an important aspect of DEM quality and can indicate the suitability of a DEM for local catchment management applications.

6.2 Comparing stream networks to each other and to reference data

Previous research has been undertaken on the quantitative assessment of stream networks in terms of attributes such as stream order, stream length and drainage density (Lin et al., 2010). RMSE has also been used for the assessment of the positional accuracy of spatial features (Shi, 2010; Zhang and Goodchild, 2002). Both in horizontal and vertical measurements, the RMSE has been adopted as a standard method by the Federal Geographic Data Committee (FGDC), in its National Standard for Spatial Data Accuracy (FGDC, 1998). In addition, several studies have been conducted on the positional accuracy of DEM-delineated stream networks, relative to a reference network, by applying a buffer zone to the reference network or vice versa and then evaluating the degree of coincidence between extracted networks and the reference data (e.g. Clarke and Burnett, 2003; Goodchild and Hunter, 1997; Penas et al., 2011; Vogt et al., 2003).

All of these assessment criteria, some selected hydrographical parameters (stream order, number of streams in each order, stream lengths and catchment area), horizontal RMSE and defining a buffer zone around the reference network approaches, were used as methods for quantitatively assessing the quality of extracted stream networks from several different DEMs, NEXTMap (5m), Bluesky (5m), Ordnance Survey Landform Panorama (OS50 m) and SRTM (90m). In this assessment the effect of DEM resolution and type of data source on the derived stream network were investigated as they were believed to be the major factors affecting the positional accuracy of stream networks derived from these DEMs (e.g. Charrier and Li, 2012; Penas et al., 2011; Wang and Yin, 1998). Two methods for stream extraction from the DEMs were used; (1) from the original DEM and (2) from the DEM after an error modelling process (error propagation method).

6.2.1 Stream extraction from original DEMs

As previously indicated, the horizontal and vertical resolution of a DEM can have a significant influence on the accuracy of the hydrological derived surface parameters (i.e. flow direction) that are computed from it (Wilson, 2012). This is likely to be particularly important in low relief areas (Chirico, 2004). It has also been recognised that different DEM sources, processing steps, and topography can lead to differences in the extracted drainage networks and catchment boundaries. These differences can be identified visually and quantitatively, and most studies rely on comparing parameters describing stream network composition, including the stream orders, numbers of streams, stream lengths and catchment areas (Liu and Zhang, 2011; Gallego et al., 2010).

6.2.1.1 Methods

Stream networks were extracted from each DEM using the two threshold values that were obtained using the area-aggregated slope method (see Chapter 5). The smaller threshold (0.005 km²) was found to produce a detailed description of the stream networks, where it possible to get a concentration of surface flow across fields and to the edge of the field drains, whereas the second threshold (1.25 km²) produced a stream network representing the recognisable (true) channels. The resultant stream networks derived using each threshold with each DEM were compared in terms of the stream network parameters mentioned above and also to the reference network.

The extraction of the stream networks and the catchment boundaries was carried out using the hydrology analysis extension within ArcGIS 10, following the basic steps of pit filling, identification of flow direction followed by the calculation of flow accumulation rasters. Stream networks were identified by applying the same contributing area thresholds (0.005 and 1.25 km²) in turn to the flow accumulation values of each different DEM. All the grid cells with an accumulation value greater than the threshold were regarded as potential surface flow paths. Stream networks are formed by these flow paths. All streams were further ordered according to the Strahler system, a stream ordering method proposed by Strahler in 1952 which introduces a hierarchy into the river system, where stream order only increases when streams of the same order intersect (Poggio and Soille, 2008). The length of streams of each order was obtained by measuring all the drainage within the catchment of a given order (Liu and Zhang, 2011). All these geoprocessing tools were combined using ArcGIS Model Builder. Raster to Vector conversions were used to convert stream network and catchment boundaries into a vector data format for the purpose of comparison between each other and to the reference data.

6.2.1.2 Results

Tables 6.1 and 6.2 and Figure 6.1 show the maximum stream order, the number of stream segments and the total stream length using the 0.005 km^2 threshold for each DEM. The NEXTMap DEM generated the highest number of stream segments with 3145 segments, as compared to 2322 from Bluesky, 1174 from OS50 and 706 from the SRTM data. In addition, the total stream length and the maximum stream order of the NEXTMap derived network were 251.193 km and 7, as opposed to 213.766 km and 6 from Bluesky, 206.342 km and 6 from OS50 and 155.895 km and 5 from SRTM, respectively. This ordering of the number of segments and their structure by Strahler order is what would be expected, a function of resolution. It was observed that there is a decreasing trend in the maximum stream order, number of stream segments and the total stream lengths as a function of cell size (see Figure 6.1, Table 6.1 and Table 6.2). These results are consistent with those of Paz et al. (2008) who found that total stream length and the number of segments were underestimated when DEMs with lower spatial resolution were used, as they could not detect some small streams because of reduced vertical resolution. Table 6.2 also shows that the greatest differences associated with resolution are at the lower orders, where at Strahler level 1 NEXTMap generated 1612 segments, in contrast to 1178 modelled by Bluesky, 598 by OS50 and 393 by SRTM. Furthermore, it is clear from Table 6.2, as would be expected, among the different resolutions there is less difference as the stream order increases.

With the same contributing area threshold (0.005 km²), the results indicate that NEXTMap can produce a more detailed delineation of the stream network, as the number of streams and their lengths within each stream order was the greatest for all the five DEMs (Table 6.2). Although Bluesky exhibited a similar resolution to NEXTMap, the latter produced a more detailed stream network. This was attributed to the data source type and

techniques used to generate the DEM and also to the methods used to filter the DSM to

generate a bare-earth data – DTM.

Table 6.1: The number of streams, total stream lengths and the total catchment area for the Blackwater sub-catchment from each DEM using the threshold value of 0.005 km².

DEM	Maximum Stream order	Total N of stream segments	Total stream lengths (km)	Total catchment area (Km²)
Reference Network	3	19	19.198	
NEXTMap	**7**	**3145**	**251.193**	25.484
Bluesky	6	2322	213.766	25.279
OS50	6	1174	206.342	25.568
SRTM	5	706	155.895	**25.790**

Table 6.2: The number of streams and the stream lengths within each stream order for the Blackwater catchment from each DEM using the threshold value of 0.005 km².

Stream order	Reference Network		NEXTMap (5m)		Bluesky (5m)		OS50 (50m)		SRTM (90m)	
	Number of streams	Stream lengths (km)	Number of streams	Stream lengths (km)	Number of streams	Stream lengths (km)	Number of streams	Stream lengths (km)	Number of streams	Stream lengths (km)
1	10	13.061	**1612**	**150.083**	1178	124.033	598	125.383	393	98.785
2	4	2.761	630	51.586	510	44.236	307	50.098	166	29.569
3	5	3.375	356	21.377	307	21.926	102	13.501	76	14.873
4			287	15.973	183	12.906	94	9.972	53	9.425
5			173	9.324	79	5.797	33	4.082	18	3.244
6			11	0.744	65	4.868	40	3.307		
7			79	2.995						
Total	19	19.198	**3145**	**251.193**	2322	213.766	1174	206.342	706	155.895

Table 6.1 also shows the area of the Blackwater sub-catchment determined using each

DEM. From the table it is clear that there is a slight tendency for the area of the catchment to

increase with cell size. This can be attributed to the fact that grid cells of different sizes

cannot consistently cover the irregular shape of the catchment (Wu et al., 2008a). However,

others have also examined the effect of grid size change on the catchment area determined from DEM, and no consistent trend was observed (Vieux, 1993; Wu et al., 2008a). Total length of all stream segments and the area of the catchment often play a critical role in determining catchment hydrologic characteristics for water resource management (Callow et al., 2007; Wu et al., 2008b). The assumption is that longer stream lengths, greater stream orders and higher number of stream segments imply greater accuracy (Paz et al., 2008; Liu and Zhang, 2011; Murphy et al., 2008; Penas et al., 2011). In this regard, it was hypothesized that the relationship between these parameters and the cell size would be linear such that higher resolution DEMs would result in longer stream length, greater stream order and higher number of stream segments. Therefore, the results clearly indicate that the NEXTMap elevation data are preferred over the other elevation datasets used in this study. From comparing these parameters of the stream networks, this study showed that with the same contributing drainage area threshold (0.005 km²) NEXTMap offers a delineated stream network with more detail compared to what can be achieved using the other elevation datasets.
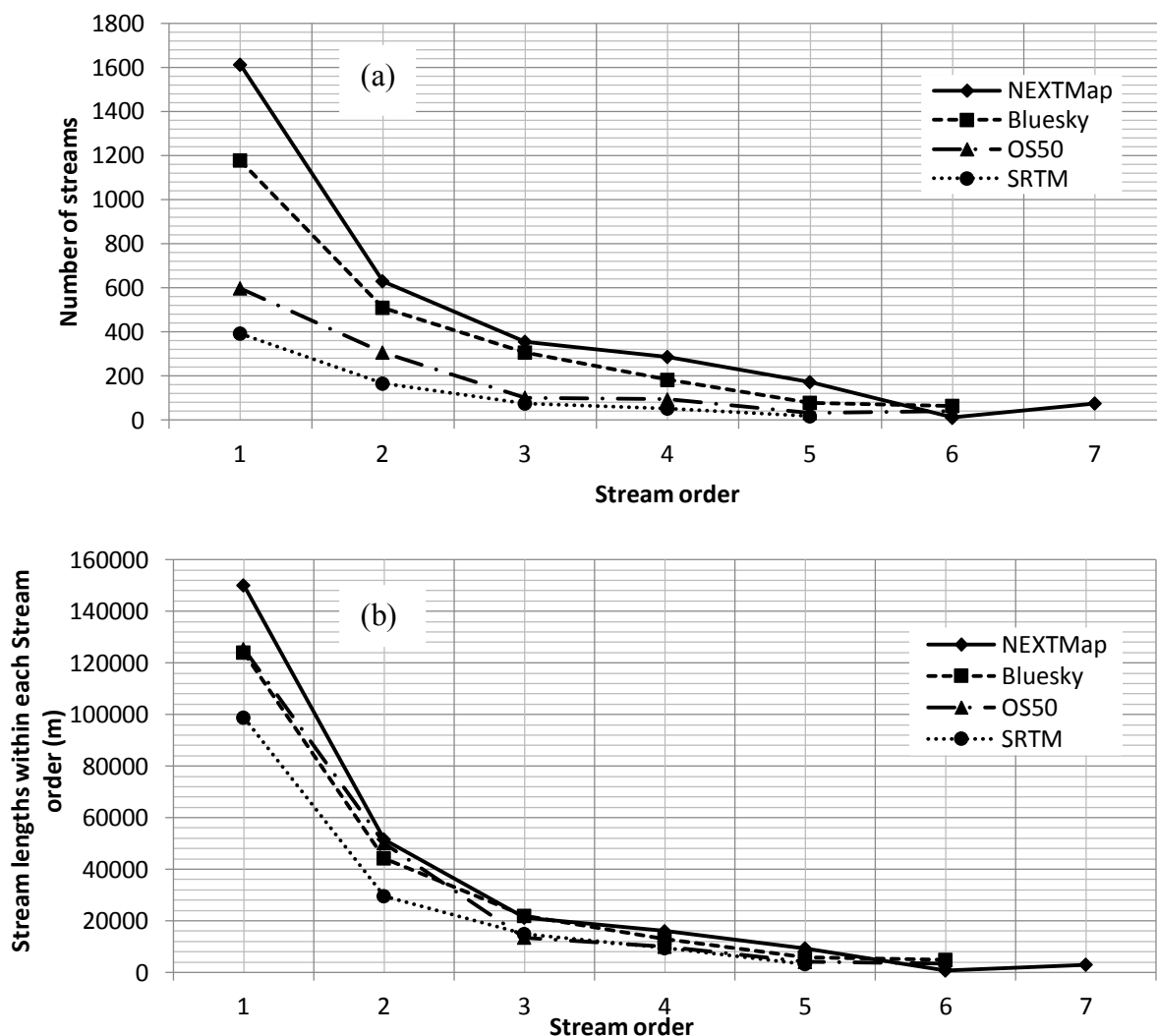
Figure 6.1: The number of streams within each stream order from each DEM (a) and the stream lengths (metre) within each stream order from each DEM (b) using the threshold value of 0.005 km²   for the Blackwater sub-catchment.

In Tables 6.1 and 6.2 the values for the derived stream networks are all appreciably higher than for the reference network since the latter only represents the recognisable channels. The second comparison used a threshold of 1.25 km² which previous analysis in Chapter 5 suggested was the transition point from shallow concentrated flows (ephemeral) to channelized flows.

Results from applying this larger threshold to each of the DEMs are presented as maximum stream order, number of stream segments and total stream length in Table 6.3, and number of stream segments within each order and stream lengths for each stream order in Table 6.4 and Figure 6.2. As expected, the values of all these parameters decrease with the larger threshold and those for the derived network are similar to those for the reference data. As can be seen from Table 6.3, the NEXTMap and Bluesky networks showed the best agreement with the reference network, generating the same maximum stream order of 3, compared to 2 from the other two elevation datasets, OS50 and SRTM. Moreover, the total stream length of the reference network is 19.198 km, while that derived from NEXTMap is 14.672 km, Bluesky 14.407 km, OS50 13.828 km and SRTM 13.200 km. Assuming the distances derived from the reference network are correct, the NEXTMap stream length is an underestimate by 23.57%, 24.96% for Bluesky, 27.97% for OS50 and 31.24% for SRTM. These results suggest that there was a tendency to underestimate the river length as the cell size increased.

Table 6.3: The number of streams, total stream lengths and the total catchment area for the Blackwater catchment from each DEM using the threshold value of 1.25 km².

DEM	Maximum Stream order	Total N of Stream segments	Total stream lengths (km)	Total catchment area (km²)
Reference Network	3	**19**	**19.198**	
NEXTMap	3	**17**	**14.672**	25.484
Bluesky	**3**	15	14.407	25.279
OS50	2	13	13.828	25.568
SRTM	2	13	13.200	**25.790**

Table 6.4: The number of streams and the stream lengths within each stream order for the Blackwater catchment from each DEM using the threshold value of 1.25 km².

Stream order	Reference Network		NEXTMap		Bluesky		OS50		SRTM	
	Number of streams	Stream lengths (km)	Number of streams	Stream lengths (km)	Number of streams	Stream lengths (km)	Number of streams	Stream lengths (km)	Number of streams	Stream lengths (km)
1	**10**	**13.061**	9	8.373	8	9.227	7	8.940	7	8.636
2	4	2.761	4	3.313	3	2.205	6	4.888	6	4.565
3	5	3.375	4	2.987	4	2.975				
Total	**19**	**19.198**	17	14.672	15	14.407	13	13.828	13	13.200
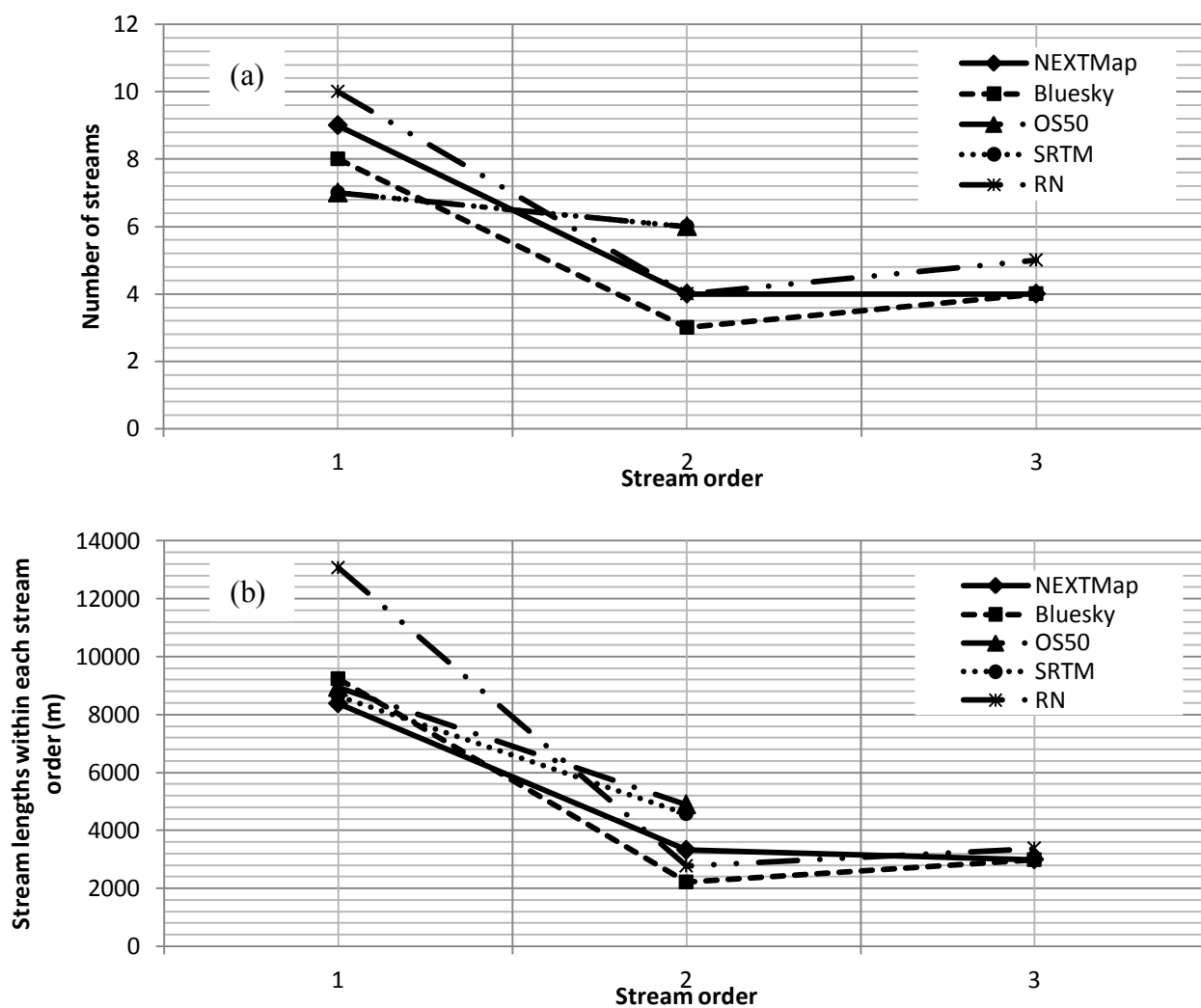
Figure 6.2: The number of streams within each stream order from each DEM (a) and the stream lengths (metre) within each stream order from each DEM (b) using the threshold value of 1.25 km² for the Blackwater sub-catchment.

Overall, these comparisons suggest that the use of increased DEM resolution improved the modelling of stream networks. Other authors have drawn similar conclusions (Paz et al., 2008; Liu and Zhang, 2011; Murphy et al., 2008; Penas et al., 2011). In this study, however, although NEXTMap and Bluesky have similar resolutions, the results indicated that NEXTMap produces a more detailed delineation of the stream network. As noted previously this is most probably due to data source type, techniques used to generate the DEM and also to the methods used to convert from DSM to DTM.

6.2.2 Extracting streams from DEMs after error modelling

6.2.2.1 Introduction

Uncertainty exists in all spatial data, such as elevation datasets. In catchment resource management and modelling applications, any uncertainty within the DEM will be propagated to derived products such as stream networks (Wechsler and Kroll, 2006; Wu et al., 2008a and b). In a GIS analysis such propagation can be modelled by the Monte Carlo simulation method (Hunter and Goodchild, 1997). As stated in Chapter 2 (Section 2.2.3.3) the underlying assumptions of the Monte Carlo simulation procedure as applied to DEM uncertainty assessment are as follows: (i) DEM error exists and constitutes uncertainty that is propagated with manipulation of the elevation data; (ii) the true nature and extent of these errors are unknown; (iii) DEM error can be represented by a distribution of DEM realisations; and (iv) the true surface lies somewhere within this distribution (Lindsay and Evans, 2008; Poggio and Soille 2011). Thus, these models of uncertainty produce a range of values within which the true value is believed to lie with some level of confidence.

Figure 6.3 illustrates the Monte Carlo simulation procedure that was used in this study. This technique is based on performing the GIS operation a number of times, where

each iteration is referred to as a simulation. In each simulation a random error field was first

created. This error surface was then added to the original DEM and the model was run using

the resultant new DEM as the input and derivatives such as the stream network extracted. The

entire procedure was repeated for a hundred iterations. Each iteration generated an alternative

realization of the extracted information that was equally probable. A frequency distribution of

the extracted derivatives is built up over the course of simulation, given the degree of

uncertainty in the terrain model (Lindsay and Evans, 2008). This method offers flexibility

although it also involves relatively heavy computation and calculations.
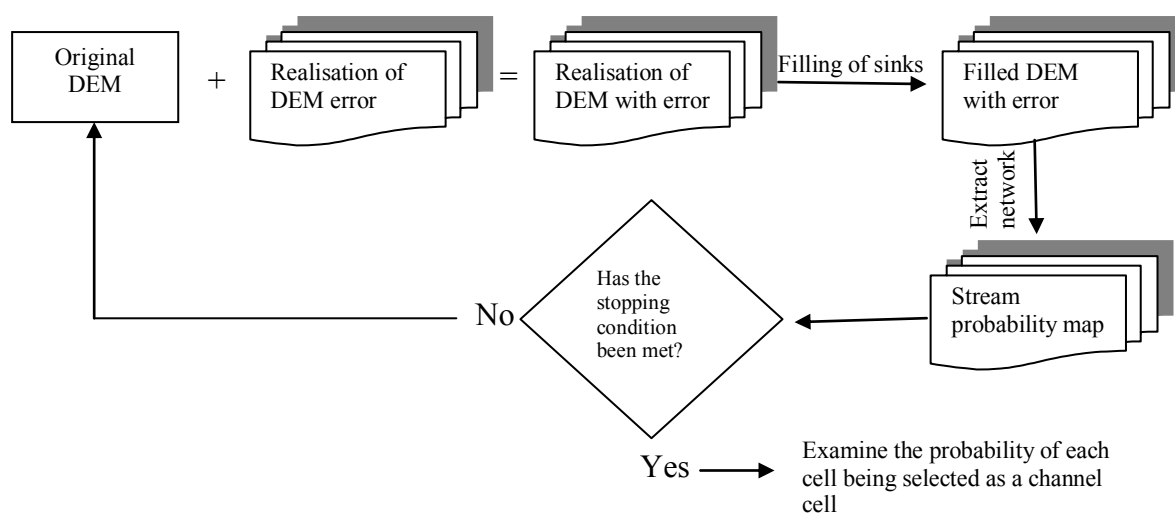
Figure 6.3: Monte Carlo simulation procedure used to produce stream probability maps
from each DEM used in the study (modified from Lindsay, 2006)

The Mont Carlo approach has become popular due to its ease of implementation and

its general applicability. When compared to other error propagation techniques, the technique

is not affected by the exact formulation or model of the spatial operator (Raaflaub and

Collins, 2006). This makes it suitable for global GIS operations, though in such cases its use

requires the simulation of correlated random fields which can be generated by simple first

order autoregressive models on regular grids. However, in this study, the unfiltered random

field method was used. This random field method assumes that errors in the DEM are

completely random and not spatially autocorrelated, with a mean of zero and a standard deviation equal to the RMSE (Lindsay and Evans, 2008). Darnell et al (2010) applied the two methods, spatially dependent and independent, to investigate flow path sensitivity to correlation between errors and found that there was no great difference, concluding that spatially independent errors were therefore fit for purpose.

6.2.2.2 Modelling DEM error propagation to the stream network

To simulate the error over the whole surface of the DEM, the Monte Carlo method was used to generate a grid of random errors which was then added to the original DEM to create a DEM realization. In this study, a spatially independent errors model was used, assuming that the error had a mean of zero and standard deviation equivalent to the RMSE (Wechsler, 2007). These multiple realisations of the DEM produce a Gaussian distribution that better represents the DEM under uncertain conditions (Hunter and Goodchild, 1997; Fisher, 1998; Wechsler and Kroll, 2006). The random fields were created with same geospatial extent of the DEM and with the properties based on the statistics obtained from the DEM accuracy studies (see Chapter 4 Section 4.3.5); mean = 0 and standard deviation = RMSE obtained for each DEM (Wechsler and Kroll, 2006; Widayati et al., 2004). As a rule of thumb, 100 simulations is taken as being enough, and everything below 20 as insufficient (Hengl et al., 2010). Therefore, the random fields were created 100 times to generate DEM perturbations.

ArcGIS Modelbuilder was used to create the error propagation model for the terrain analysis (Figure 6.4). The process begins with the generation of random error grids that have the same dimensions as the original DEM. The values in the error grids were generated from a normal probability distribution with a mean of zero and standard deviation equal to the RMSE of the original DEMs; 2.0317, 0.9197, 1.9962 and 2.6259 m for NEXTMap, Bluesky, OS50

and SRTM, respectively (Table 4.5 in Chapter 4). These RMSE values were obtained from a

local DEM accuracy study conducted using a set of spot heights recorded at a higher degree

of accuracy for the study area (see Section 4.3.5.3). The error grid was then added to the

original DEM to create a new terrain realization. This new DEM became the input into the

stream extraction model (Figure 6.4).
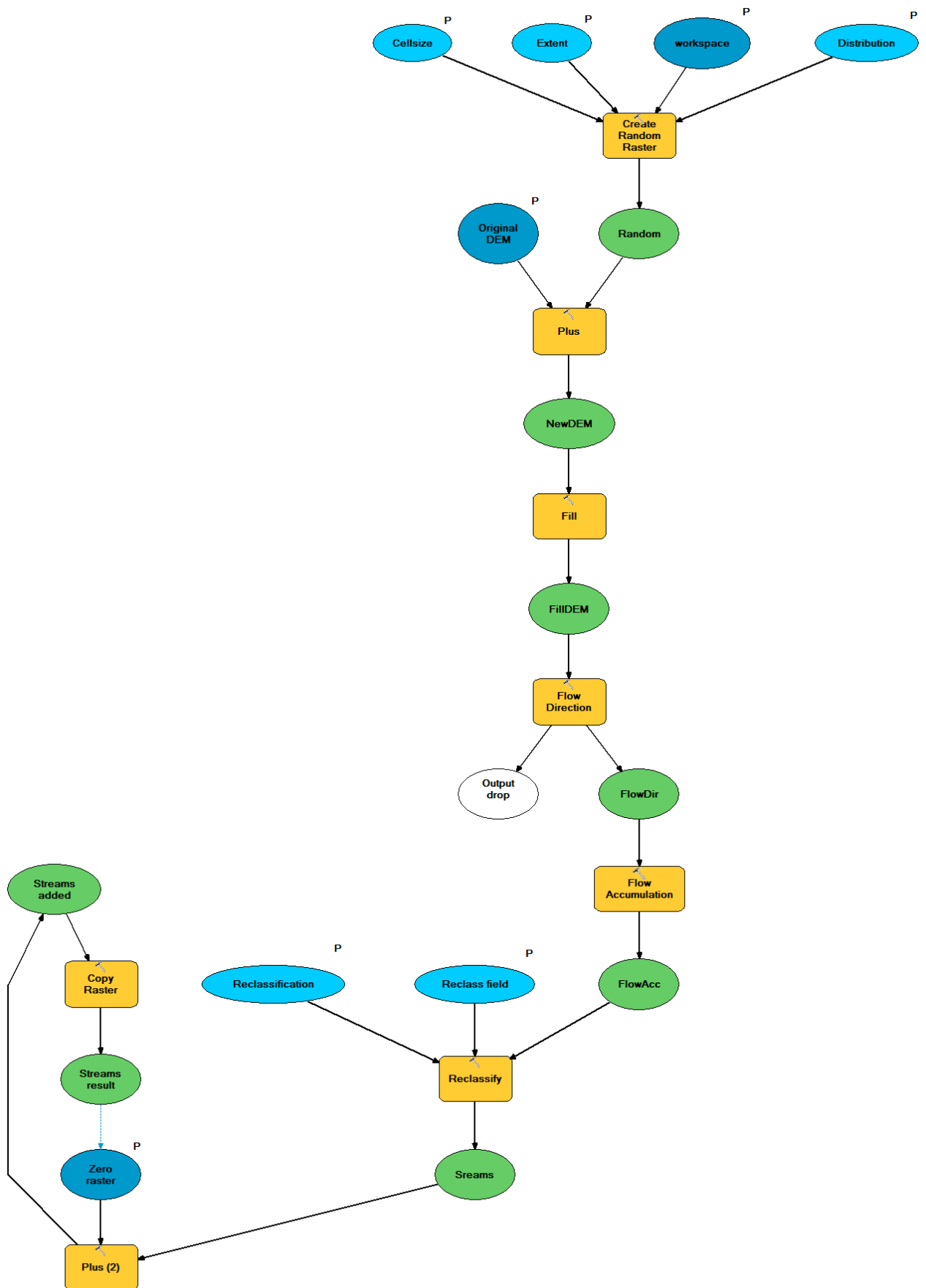
Figure 6.4: ArcGIS Modelbuilder flowchart for the error propagation model used to produce a stream probability map for each DEM used in the study.

The model then created the stream networks: sinks were filled, flow direction and flow accumulation were derived from the DEM and streams were delineated based on a flow accumulation threshold of 1.25 km². The stream network was then added to an accumulating total raster, with cell size same as the DEM and initial values of zero. This raster was copied and from the results a feedback loop was created. As the model ran multiple times, the stream network from each run was added as cells with a value of one to the accumulating total. This ultimately generated a cumulative probability surface, where the value for each cell identified how many times a stream network passed through it. The more times a cell was selected, the higher the probability that the stream network passed through the cell. Figure 6.5 shows the results for the four DEMs.

(b)

(c)
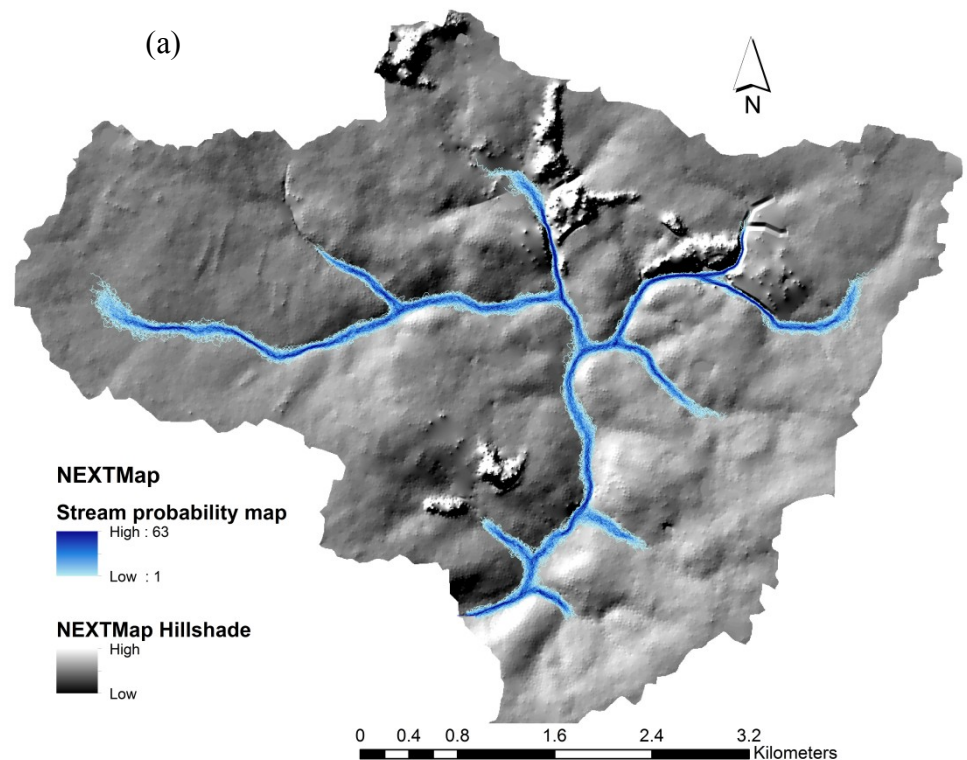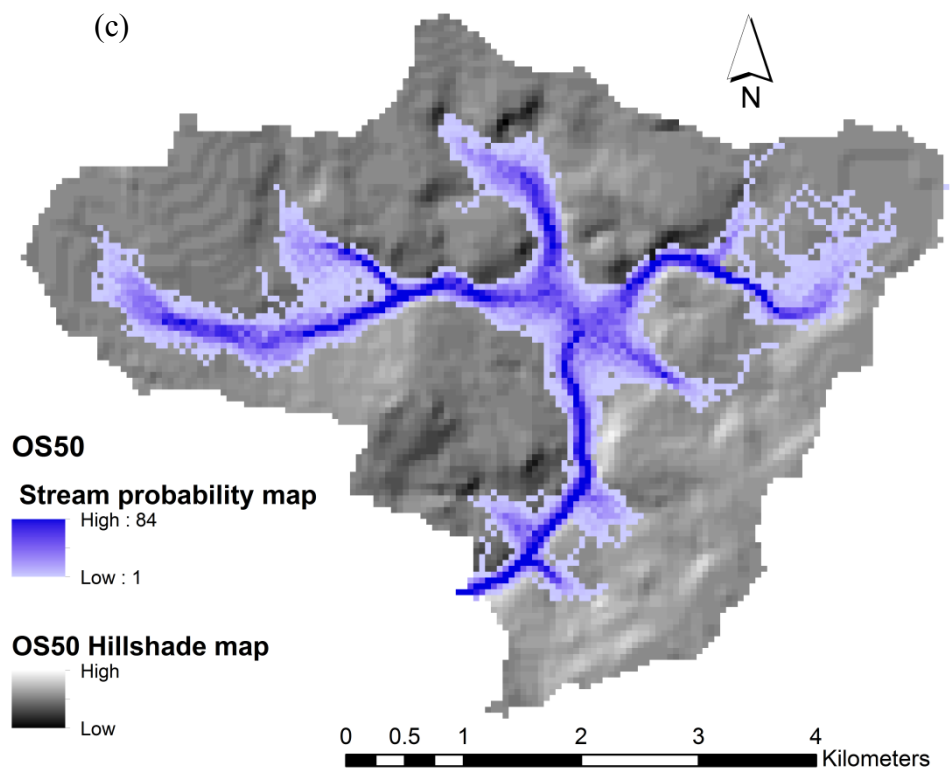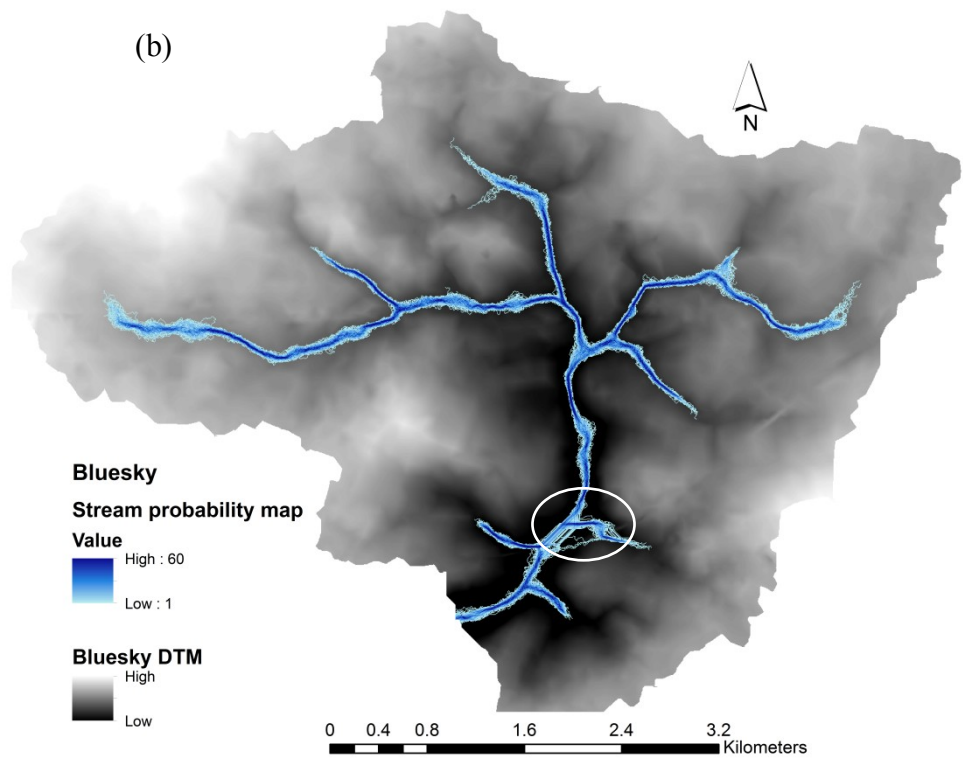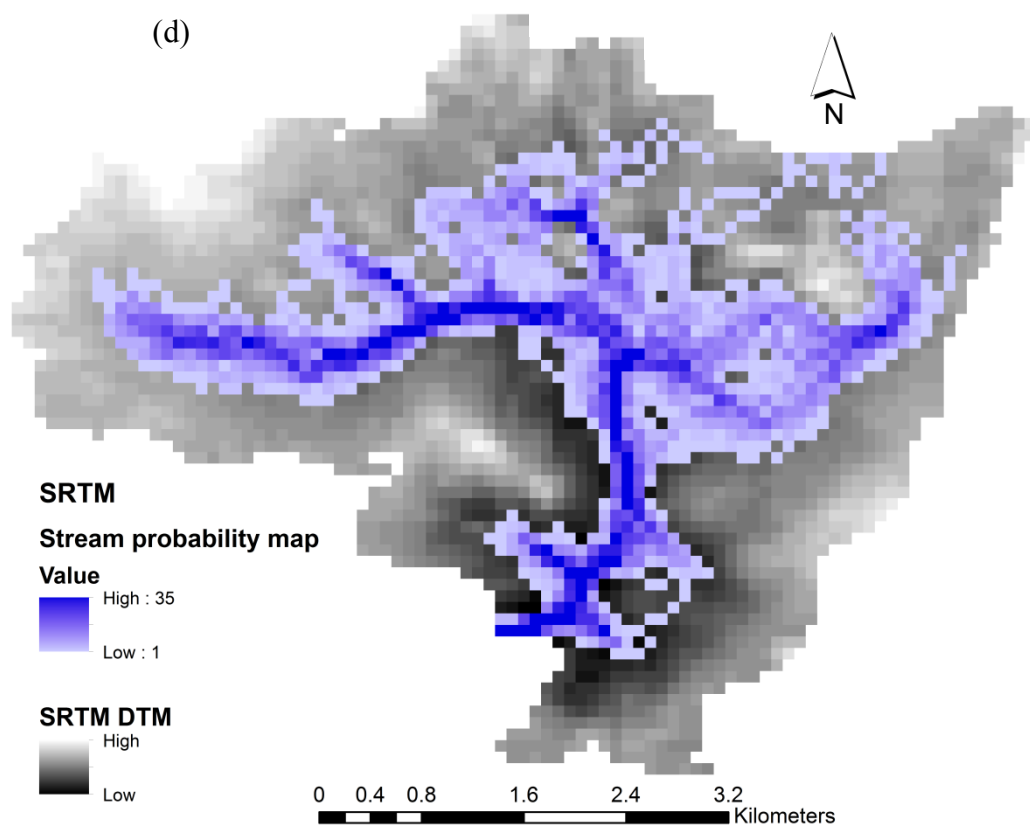
Figure 6.5: Results of the error propagation analysis for stream delineation from (a) NEXTMap with RMSE of 2.032 m, (b) Bluesky with RMSE of 0.92 m, (c) OS50 with RMSE of 1.996 m and (d) SRTM with RMSE of 2.626 m. The model run for 100 iterations.

The model results provide an indication of uncertainty in the stream delineations. The visualisation of the density of streams clearly illustrates the concept of propagated uncertainty. In contrast to running the analysis with just the original DEM, the Monte Carlo modelling identifies areas where there is substantial uncertainty over the location of the streams.

The outcomes of 100 realizations of stream networks for each DEM are shown in Figure 6.5. It is clear from the maps that the stream networks were most affected by error in the headwater reaches (lower order streams). There are also a few places where uncertainty is quite substantial, as a result of a flat area problem or other artefacts existing in the DEM. In

some areas streams are isolated and seem to be very improbable (see circled area in Figure 6.5b).

The influence of DEM resolution is evident in all maps. The maps in Figure 6.5 provide evidence that when coarser resolution DEMs were used, the probable streams appeared as very wide zones as a result of the larger cell size, but inside these zones higher probabilities were present indicating the most likely locations of the streams. However, the overall purpose of this error propagation study is to determine a probability estimation of the position of the stream network from each DEM and then extract the most probable stream network for comparison with the reference network in terms of positional accuracy. This is discussed in the following sections.

6.2.2.3   Selecting the most probable stream network

ArcGIS Cost Surface and Cost Path functions were used to identify the most probable stream network from each probability raster. Cost path analysis is one of the spatial optimization techniques usually used in GIS and is considered as a very useful method in determining the optimal path from one or more origins to one or more destination targets (Choi et al., 2009). The Cost Path function determines a one cell wide least-cost path from a destination to a source relative to the minimum accumulative cost distance over a cost surface raster (Atkinson et al., 2005). A cost surface raster is one whose cells are assigned values representing the 'cost' of passing through them. The accumulative cost surface is generated from the cost surface, by calculating the cumulative cost of reaching each cell from the start point (Lee and Stucky, 1998). Methodologies for the calculation of an accumulated cost raster map and then extraction of the lowest score paths are well implemented and documented in ArcGIS (Collischonn and Pilar, 2000).

To create a cost raster from each probability map a raster with the same geospatial extent, cell size and with a pixel value of 100 (equal to the number of iterations) was first created for each elevation dataset. Each probability map was then subtracted from the corresponding 100 value raster. Each resulting grid was simply the inverse of each probability map. The Cost Path tool was then used to generate the most probable stream network by tracing cells with the minimum accumulative values between start and end points (Figure 6.6). The start point was selected to be the catchment outlet and the destination points were the possible headwaters for each stream segment.
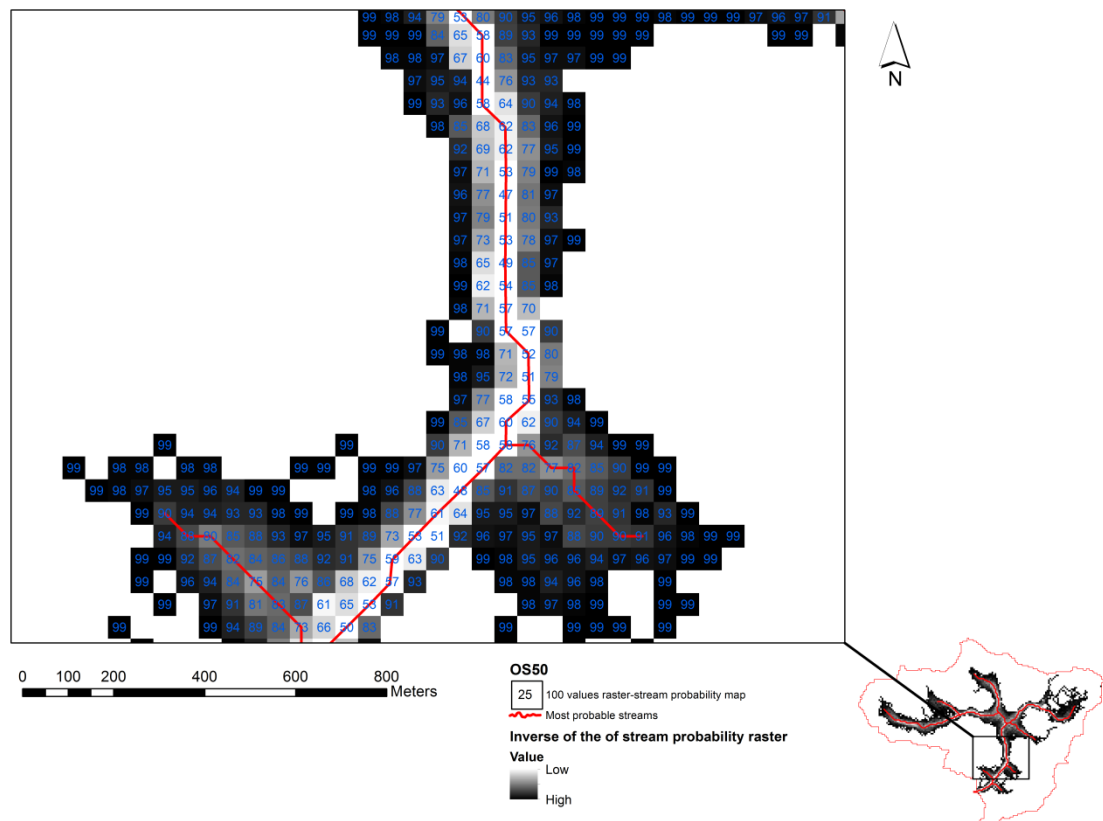
Figure 6.6: Example from OS50 data for the most probable stream created using the cost path method.

The outputs from the cost path processes are the most probable stream networks, identifying locations on each DEM where there are the highest probabilities of finding streams on the terrain (Figure 6.7).
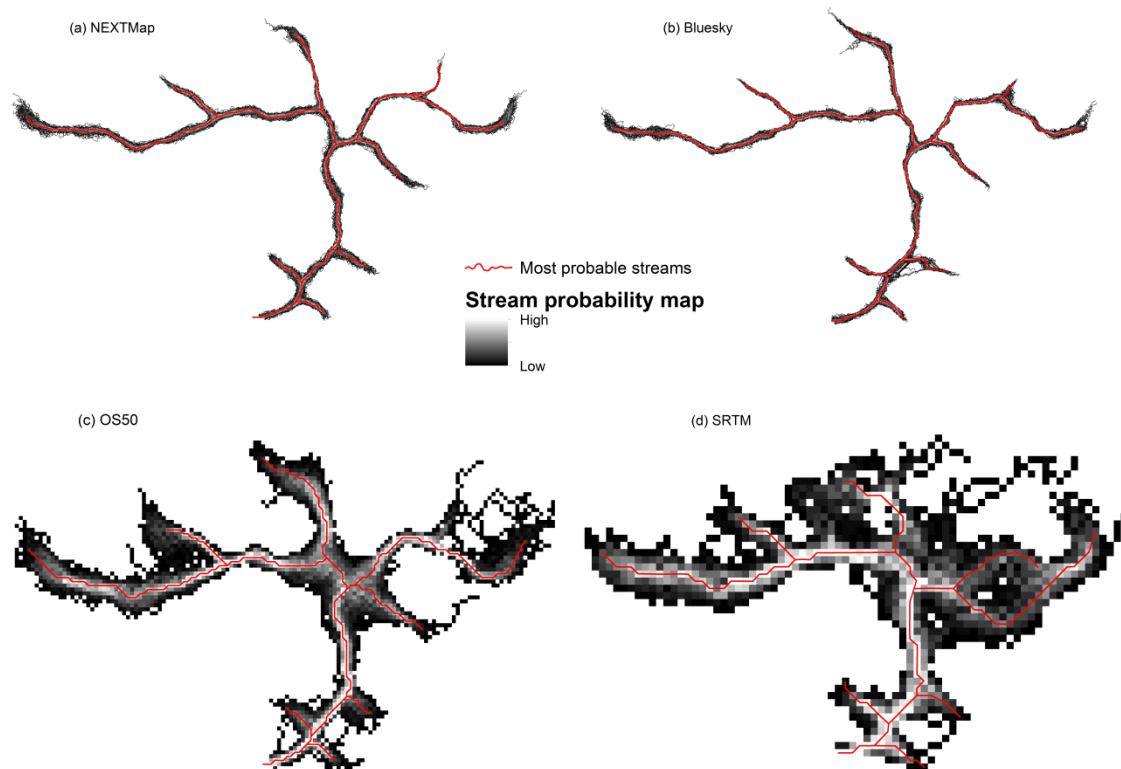
Figure 6.7: Maps of the most probable stream network for each DEM.

6.3 Stream network positional accuracy analysis

6.3.1   Root Mean Square Error (RMSE)

As noted in Chapter 2, the positional accuracies of modelled stream network can be tested by measuring the distance between each derived stream point and its corresponding point from an independent reference data of higher accuracy (FGDC, 1998). RMSE is widely used as a summary measure of such distances (FGDC, 1998; Zhang and Goodchild, 2002). RMSE require the computation of distances between two points on a map which can be calculated using the common equation based on Pythagorean's Theorem (also called the Euclidean distance):

$$d = \sqrt{(x_2 - x_1)^2 + (y_2 - y_1)^2} \qquad (6.1)$$

for n points with di ($i = 1, 2,....., n$), observed as the differences in coordinates between the modelled data and the more accurate reference data, the RMSE is

$$RMSE = \sqrt{\frac{\sum_{i=1}^{n} di^2}{n}} \qquad (6.2)$$

where the di is the distance between a modeled stream point (X_{mi}, Y_{mi}), and a corresponding reference data point (X_{ri}, Y_{ri}). In other words, the di using the Cartesian coordinates is

$$di = \sqrt{(x_{ri} - x_{mi})^2 + (y_{ri} - y_{mi})^2} \qquad (6.3)$$

Thus, the horizontal RMSE computed between a number of paired sets of points located along both delineated and reference stream network segments (polylines) is

$$RMSE = \sqrt{\frac{\sum_{i=1}^{n}(x_{ri} - x_{mi})^2 + (y_{ri} - y_{mi})^2}{n}} \qquad (6.4)$$

RMSE can therefore be used as a measure of how accurately the derived stream network matches the reference network. The smaller the RMSE, the closer the fit between the derived stream network and the reference network.

6.3.1.1   Work process steps

To derive horizontal RMSE values two stream network datasets were considered: one being the derived stream network from each DEM using the 1.25 km² threshold and the other was the reference stream network. This threshold produced stream networks roughly similar in detail to the reference data, easing the comparison of positional accuracy between each pair. For each stream segment in the reference network, the Construct Points function in ArcGIS 10 was used to create points spaced 100 m apart (the analysis was repeated with the stream segments densified to 5 m point spacing for the purpose of results comparison) along each polyline starting from the upstream end point of each stream segment. This was done for the whole of the test area (Blackwater sub-catchment). Then, for each reference point, the nearest location on each of the derived stream polylines was identified using the Near Point to Line function and then the distance (d_i) from that point on the extracted polyline to the corresponding point on the reference polyline was calculated (Figure 6.8). The horizontal RMSE was calculated using equation 6.4, where n is the number of paired points.
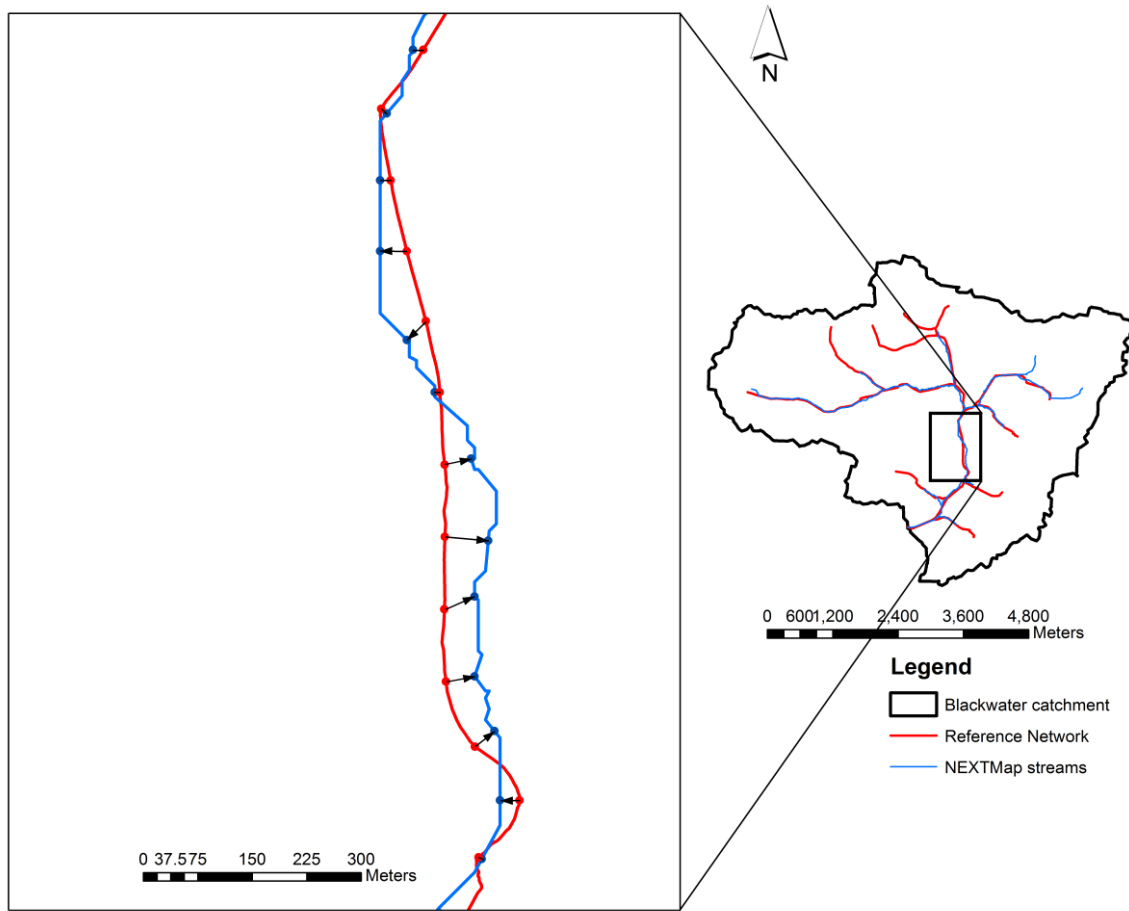
Figure 6.8: Computation of horizontal RMSE between derived stream network from NEXTMap data and the reference stream network for the Blackwater sub-catchment.

6.3.1.2 Some special considerations

There are several considerations that apply when using these methods with vector stream polylines particularly when implemented in a GIS environment using shapefile formatted data. First, a visual quality check was needed to ensure that there was a one-to-one correspondence between stream polyline segments in both derived and reference networks. This does not mean that there has to be a polyline in the extracted network for every polyline in the reference network. If the extracted stream network was missing a stream segment, then the reference segment was ignored (Figure 6.9). In other words, all of the segments in the refrence network that were not included in the derived stream network were ignored.
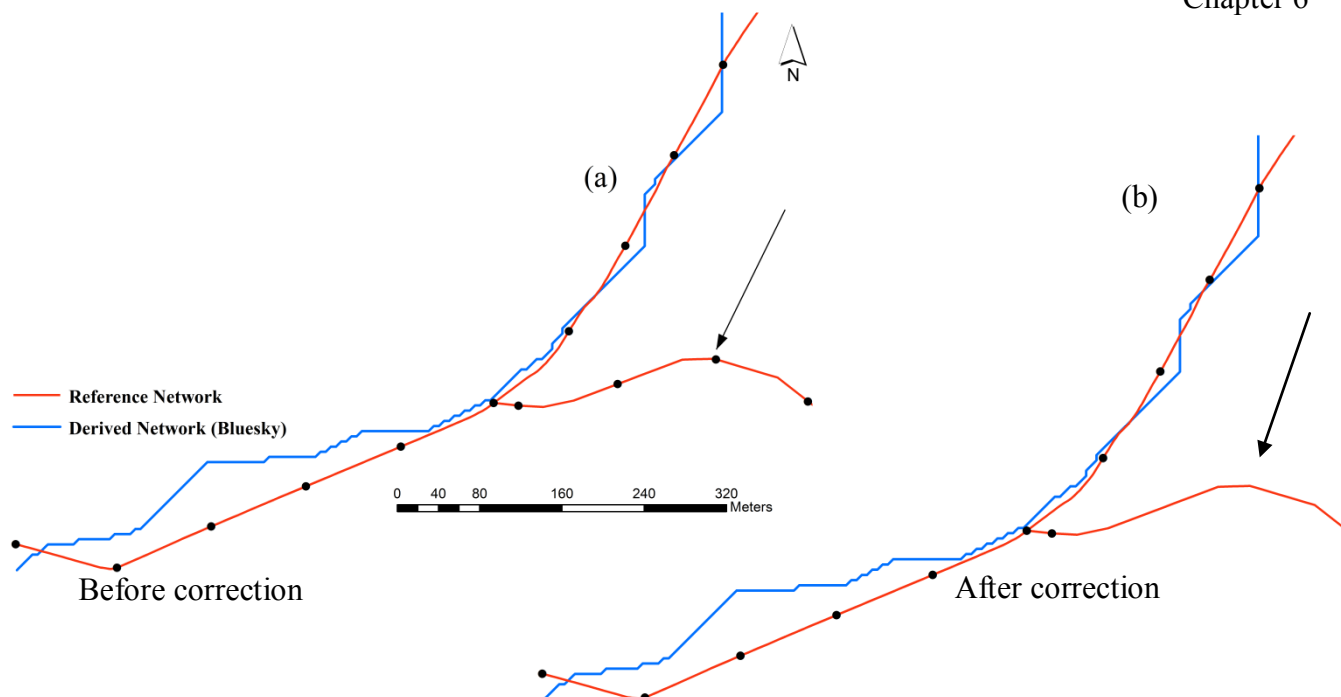
Figure 6.9: Illustration showing that the derived stream network was missing a stream segment compared to the reference network. Points on the reference segment (indicated with small arrow) in (a) were manually removed (b) before the calculation process to ensure one-to-one correspondence.

Secondly, the stream segments under comparison needed to flow in the same direction. This meant that any two stream segments, in different stream networks that were being compared, needed to be constructed in the same order, upstream end to downstream end. So, flow direction was checked and, if necessary, a point that could not be matched to the correct stream segment was removed.

Finally, the third consideration was that the extent of the reference stream segments needed to be visually checked against the extracted network ones. If the reference polyline segment was much longer than the extracted polyline, all points on the reference polyline that were beyond the end of the extracted polyline were ignored for fair comparison of the common segments (Figure 6.10). Therefore, for each comparision, reference stream network against each derived stream network, the total number of paired points varies due to the

removal of points that could not be matched to the correct stream segment or extended

beyond the extent of the derived network polylines.
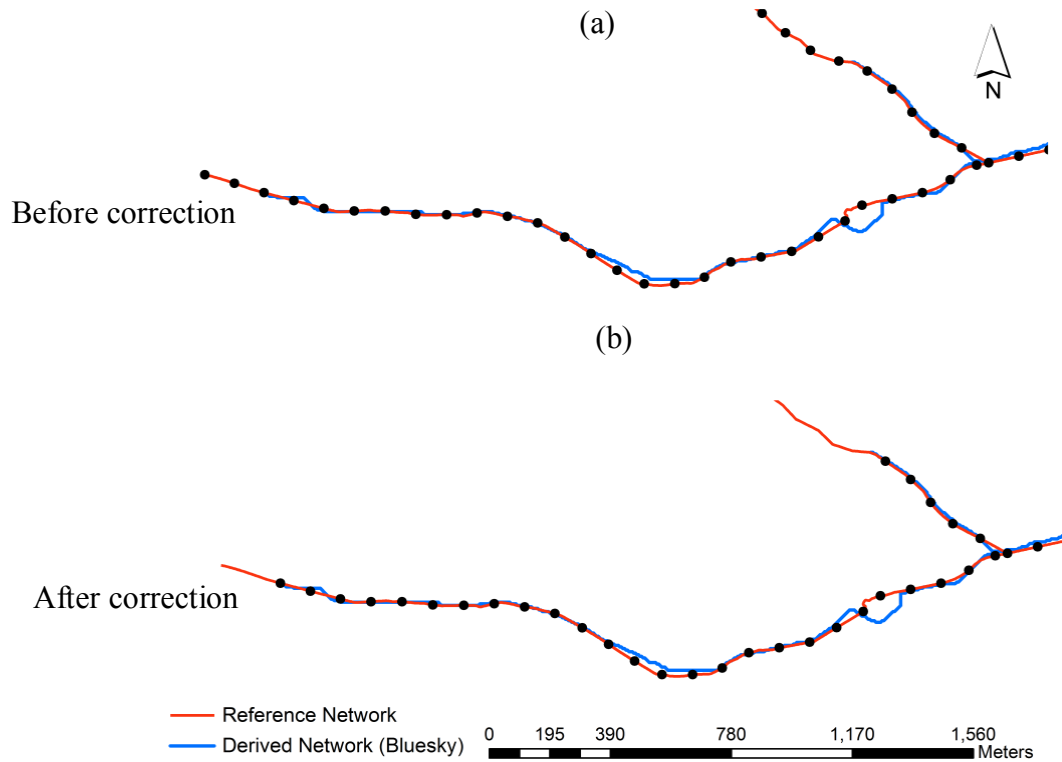
Figure 6.10: Illustration showing that all points on the reference polyline that were beyond the end of the derived polyline (a) were manually removed (b).

6.3.1.3 Results

Horizontal RMSE was computed between the paired sets of points located along both

the reference and extracted stream networks. The smaller the RMSE, the closer the fit

between derived and reference stream networks.

6.3.1.3.1 Stream networks extracted from original DEMs

Resulting RMSE values and other statistical measures, as computed between each

derived stream network and the reference stream network, are shown in Table 6.5.

Table 6.5: Minimum, maximum, mean, median, standard deviation and RMSE values for the distance differences between the derived stream networks and the reference network. The percentage of the distance differences that are equal or less than 10 and 20 metres is also reported. Results when 5 m spacing was used are reported inside the brackets.

DEM	Minimum (m)	Maximum (m)	Mean (m)	Median (m)	Standard Deviation	% within 10m	% within 20m	RMSE (m)
NEXTMap(5m)	0.27 (0.001)	**66.52** **(70.05)**	**17.15** **(17.41)**	13.31 (13.63)	**14.41** **(14.55)**	41.04 (36.7)	**69.40** **(66.91)**	**22.36** **(22.69)**
Bluesky (5m)	**0.02** **(0.001)**	85.45 (87.93)	21.33 (20.45)	**12.67** **(12.20)**	21.18 (20.48)	**44.60** **(45.27)**	63.08 (63.19)	30.01 (28.94)
OS50 (50m)	0.24 (0.027)	139.15 (146.84)	35.24 (36.35)	27.45 (27.21)	30.31 (30.28)	21.80 (18.87)	37.59 (35.92)	46.40 (47.31)
SRTM (90m)	0.55 (0.021)	222.72 (222.72)	50.78 (50.2)	39.25 (38.95)	45.37 (43.41)	15.91 (14.7)	28.79 (26.87)	67.98 (66.37)

As can be seen from the table, the RMSE value increases as cell size increases, with the 5 m resolution DEM producing the best RMSE. The NEXTMap dataset has better values for most statistical parameters in comparison with the other elevation datasets; maximum, mean, standard deviation and RMSE are 66.52, 17.15, 14.41 and 22.36 m respectively. On the other hand, SRTM derived stream network, on the whole, gives the worst results of all extracted networks; minimum, maximum, mean, standard deviation and RMSE are 0.55, 222.72, 50.78, 45.37 and 67.98 m respectively. Therefore, and not surprisingly, there is a considerable resolution effect on the RMSE and other statistical indicators. These results are consistent with Clarke and Burnett (2003) who identified DEM resolution as one of the major factors affecting the accuracy of stream network extraction. Although there is a slight improvement in the RMSE values when the point spacing is densified to 5m, overall the values of all statistical parameters were very similar to those obtained with 100 m point spacing (Table 5.6).

Although NEXTMap has the same resolution as Bluesky, differences in RMSE values and other statistical measures are clearly discernible. According to the descriptive statistics reported in Table 6.5, the comparison between NEXTMap and Bluesky highlights that the stream network obtained from NEXTMap data was the closest to the reference network. Thus, it can be argued that for automatically extracted stream networks those created using radar interferometry produce better results (Mantelli et al., 2011). In addition, the DSM to DTM conversion can be important. The Intermap Products Handbook (2004: p.60) reports that elevations along streams less than 20 metres in width and greater than one kilometre in length 'will be modified to maintain the monotonic flow within the vertical accuracy limit of radar elevation data'. An example illustrating modified streams where the narrow drainage canals are preserved through the woodland area is shown in Figure 6.11.
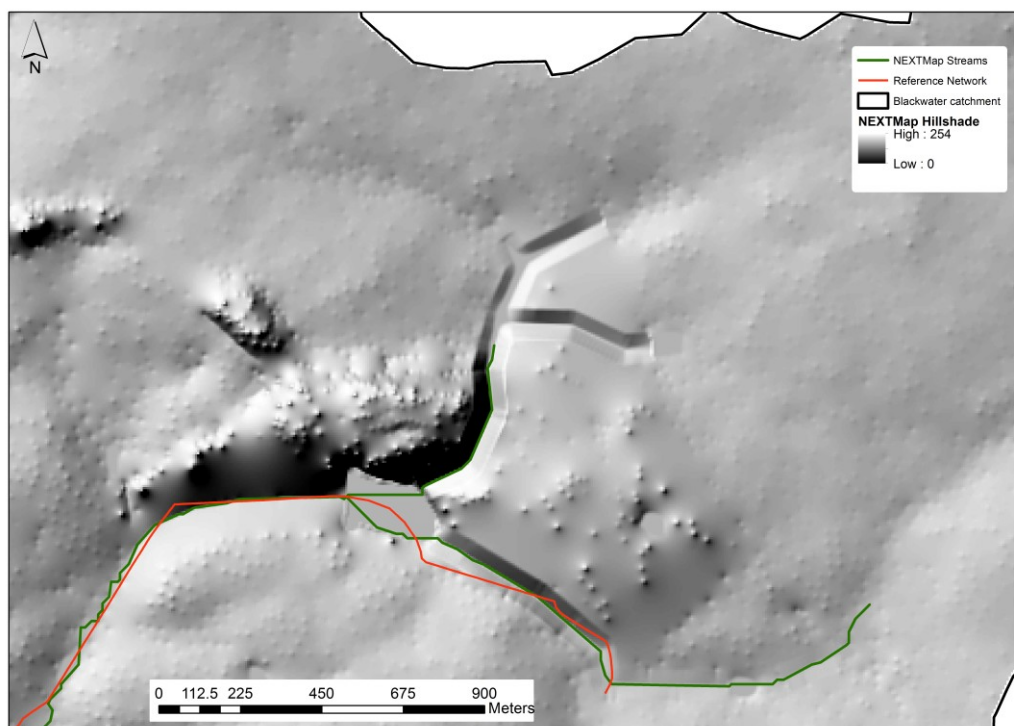
Figure 6.11: Illustration showing modified streams locations where the narrow drainage channels are preserved through the woodland area, NEXTMap example from Blackwater catchment.

On the other hand, as shown in Table 6.5 and Figure 6.12, the percentage of the distance differences within ten metres is slightly higher for the Bluesky data than NEXTMap, 44.6% and 41.04%, respectively. However, this order reverses to 69.4% for NEXTMap and 63.08% for Bluesky when the distance differences are within 20 metres.
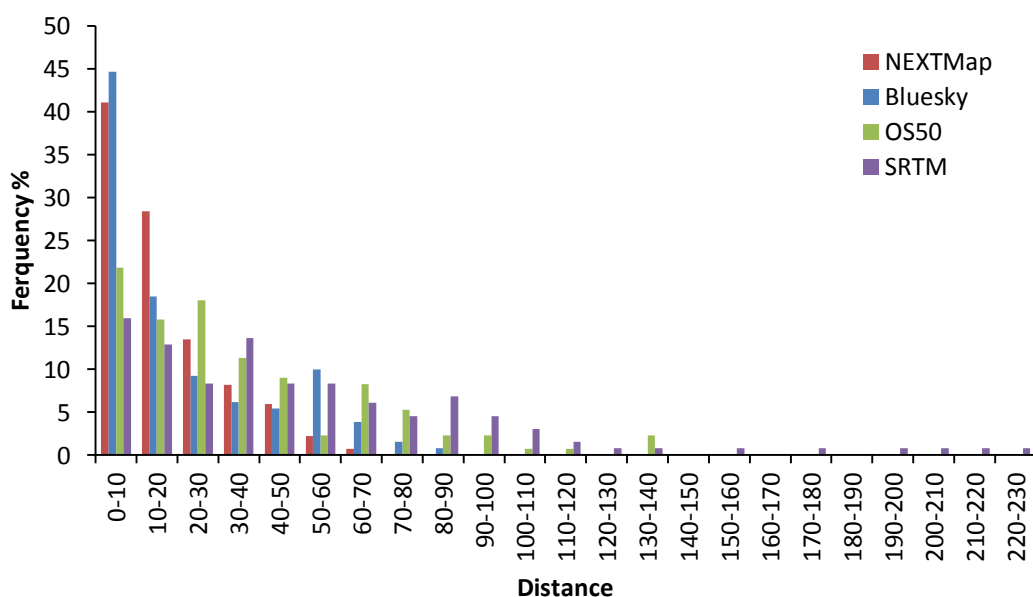
Figure 6.12: Frequency distribution of the distance differences between each derived stream network and the reference network within 10m,20m, 30m, ..., and 230m.

This contrast is further illustrated by the cumulative frequency distribution of distance differences presented in Figure 6.13. The Bluesky data performed equally as well as the NEXTMap data at shorter distance differences (from 0 to 10 m). However, there is a more obvious divergence from 20 m onwards, with the cumulative frequency reaching 100% at about 66 m for NEXTMap and 85 m for the Bluesky data.
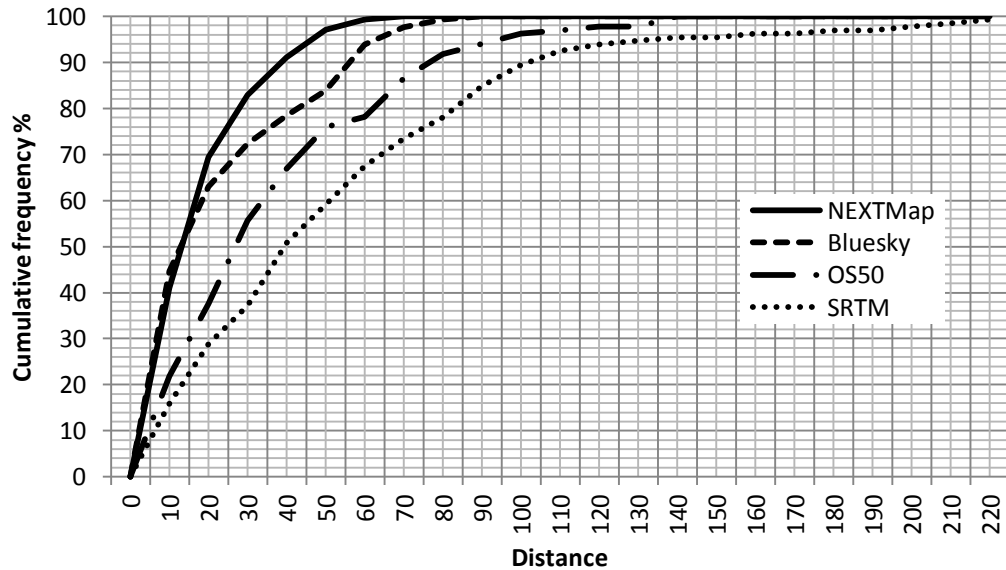
Figure 6.13: Cumulative frequency of the distance differences between each derived stream network and the reference network.

To find those areas where Bluesky was performing noticeably worse than NEXTMap, the study area was investigated carefully. It was found that the longer distance differences between the Bluesky derived stream network and the reference network occurred in an area just upstream of an artefact behaving as a dam, which is believed to be a man-made object was not completely removed during the process of converting the Bluesky data from a DSM to DTM (Figure 6.14). A visual inspection of a hillshade map of the Bluesky data indicated that the pit filling stage in the process of stream extraction generated a very big flat area just upstream the artefact, where the D8 algorithm then produced oversimplified straight stream segments. As a result, the Bluesky derived stream network has a poor match with the reference network in this area, with the maximum distance difference being 85.45 m.
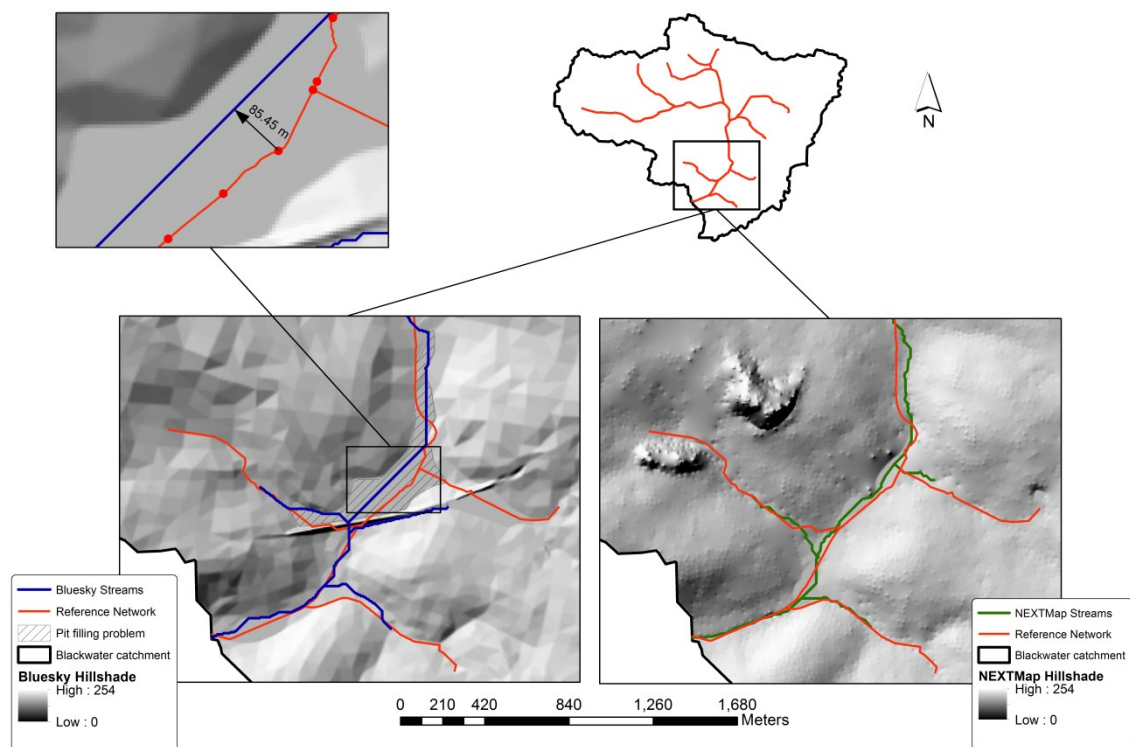
Figure 6.14: Reference network and NEXTMap stream network overlying a NEXTMap hillshade model (right) and Bluesky stream network overlying a Bluesky hillshade model (left). Note the big flat area in the Bluesky image resulting from the pit filling algorithm during the process of filling a huge sink created by an artifact behaving as a dam.

6.3.1.3.2   Stream networks extracted from DEMs after error modelling

The stream network delineated from a single elevation realization is just one out of an infinite number of possible alternative depictions. Thus, it has limited chance of a perfect match to the reference network. The Monte Carlo method employed in this study was used to generate a channel probability map and the most probable stream network was defined as the one passing through the highest frequency cells. The positional accuracy of the most probable stream network extracted from each DEM using the error propagation method was assessed relative to the reference network. The overall positional accuracy of the stream networks extracted from DEMs after the error propagation modelling was found to be slightly better than the values obtained for the networks extracted directly from the original DEMs.

Table 6.6: Minimum, maximum, mean, median, standard deviation and RMSE for the distance differences between the most probable stream networks and the reference network. The percentage of the distance differences that are equal or less than 10 and 20 metres is also reported.

DEM	Minimum (m)	Maximum (m)	Mean (m)	Median (m)	Standard Deviation	% within 10m	% within 20m	RMSE (m)
NEXTMap(5m)	**0.03**	**53.27**	**14.70**	10.93	**12.96**	45.5	**73.1**	**19.57**
Bluesky (5m)	0.16	69.61	18.60	**10.54**	18.07	**46.2**	66.9	25.88
OS50 (50m)	0.61	123.27	33.60	25.97	29.54	24.1	42.1	44.66
SRTM (90m)	0.83	209.67	39.72	28.36	41.69	22.0	37.1	57.47

Resulting RMSE values and other statistical measures, as computed between each most probable stream network and the reference data are shown in Table 6.6. As reported previously, the horizontal RMSE value increases as cell size increases, with the 5 m resolution DEM producing the lowest (best) RMSE. The NEXTMap dataset still shows better results in most statistical parameters in comparison with the other elevation datasets. Nevertheless, as can be seen from the table, all the statistical measures reported here for the most probable streams extracted from the DEMs after the error propagation analysis are slightly better than that were reported in Table 6.5 for the stream networks extracted directly from original DEMs. There is a reduction of about 13% in the RMSE values (better results) for all the stream networks, except for OS50 with only 3% improvement compared to the horizontal RMSE values for the streams obtained from the original DEMs. These results are consistent with Poggio and Soille (2011) who proposed that the overall probability of the stream networks extracted from DEMs after error propagation modelling is significantly higher than those obtained for the networks extracted directly from the original DEMs. They also concluded that the use of the inverse of the channel probability map to extract stream network maximises the probabilities of having a river, according to the simulations of DEM errors.
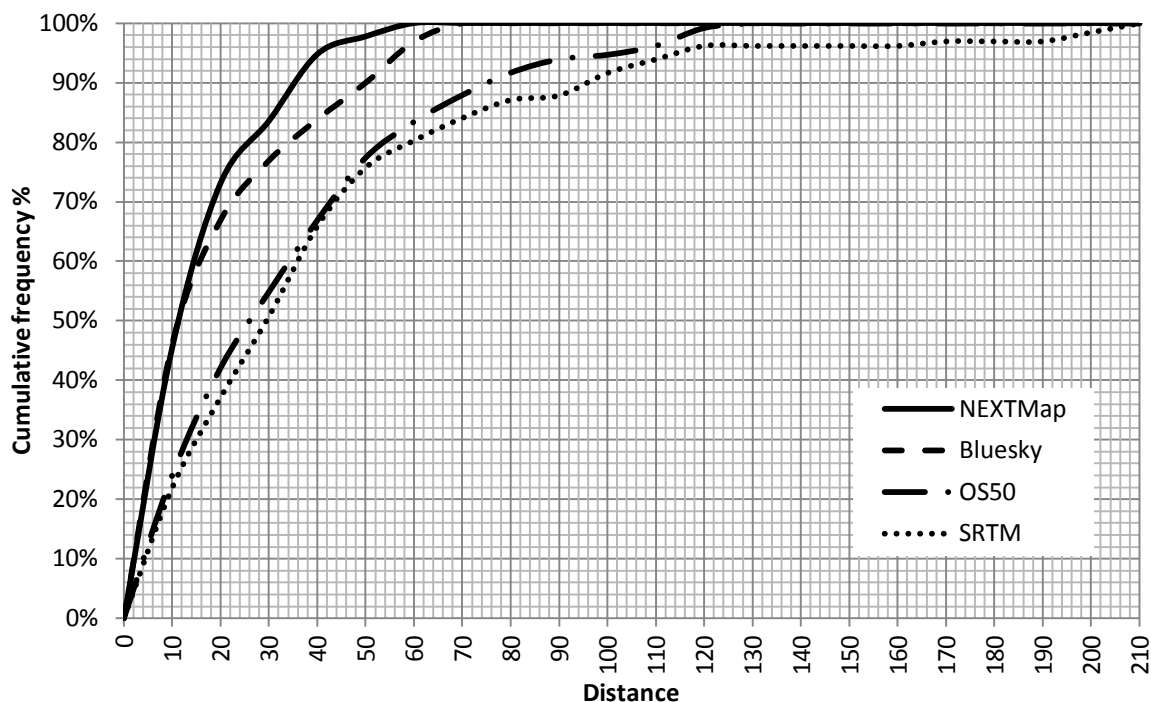
Figure 6.15: Cumulative frequency of the distance differences between the most probable stream networks and the reference network.

According to the cumulative frequency distribution of distance in Figure 6.15, it is clear that the uncertainty for the SRTM derived stream network was minimised when the error propagation method was used. It can be seen from Figures 6.15 and 6.16 that the SRTM derived stream network extracted after error modelling performed almost as well as the OS50 data, especially for short distance differences (from 0 to 60 m), a notable change from when the original DEMs were used (see Figure 6.13). Therefore, Monte Carlo simulations with alternative DEM realizations produced by adding random error surfaces onto the original DEM show potential for improving the fidelity of extracted stream networks.
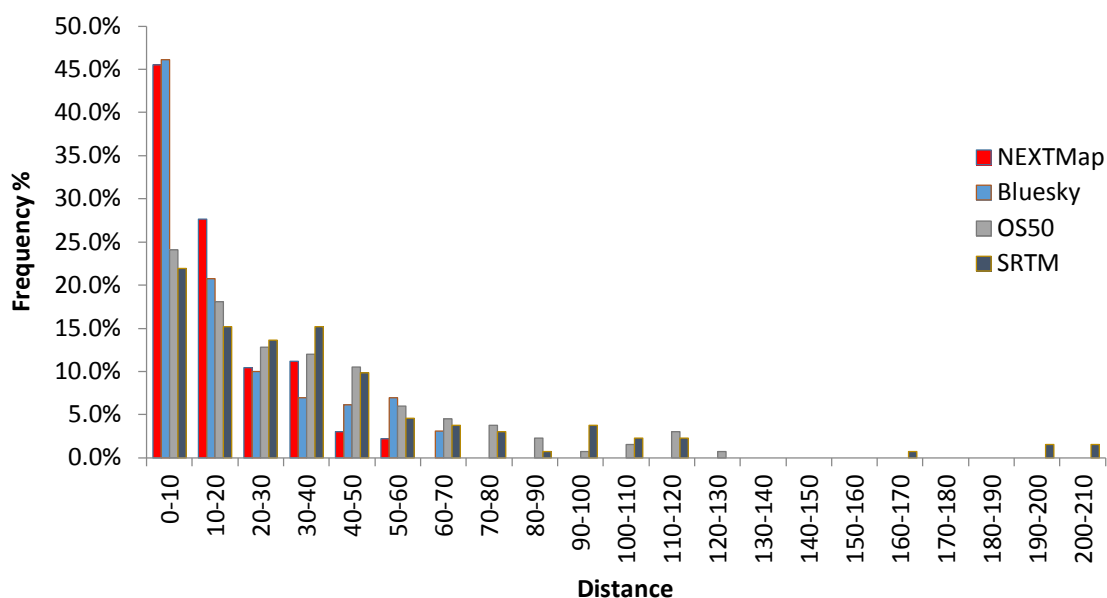
Figure 6.16: Frequency distribution of the distance differences between the most probable stream networks and the reference network within 10m ,20m, 30m, ..., and 210m.

Overall, the positional accuracy of stream lines extracted from DEMs was significantly affected by the DEM resolution. The results showed that the distance differences between the reference and extracted stream networks tended to be smaller with finer resolution. Thus, it can be concluded that DEM resolution is the major factor affecting the positional accuracy of streams derived from DEMs. However, despite the fact that NEXTMap and Bluesky have the same resolution (5 m), the stream network obtained from the NEXTMap product was the closest to the reference network, based on the horizontal RMSE and other statistical measures. This was believed to be related to the type of source data and also to the methods used to create a DTM from a DSM. It was also found that using Monte Carlo simulations to generate alternative DEM realizations and then deriving the most probable stream networks improved their positional accuracy relative to reference data.

6.3.2   Measuring positional accuracy by applying different buffer zones

The second method of measuring positional accuracy for derived stream networks was that described in Goodchild and Hunter (1997). This method calculates the percentage of the total length of the derived stream network that lies within a specified buffer distance of the reference network. The concept of an epsilon band (Figure 6.17) was used to calculate the buffer width (Chrisman, 1982; Goodchild and Hunter, 1997; Longley et al., 2005). Epsilon bands were discussed in detail in Chapter 2 Section 2.3.7.2.2. The rule of thumb proposed by Longley et al. (2005), in which features measured from maps are subject to positional errors of up to 0.5 mm at the scale of the map, was used to define epsilon bands. As the reference network used was obtained from OS VectorMap™ Local, which is a GML vector dataset at a nominal scale of 1: 10,000 the epsilon distance was calculated to be 5 m.
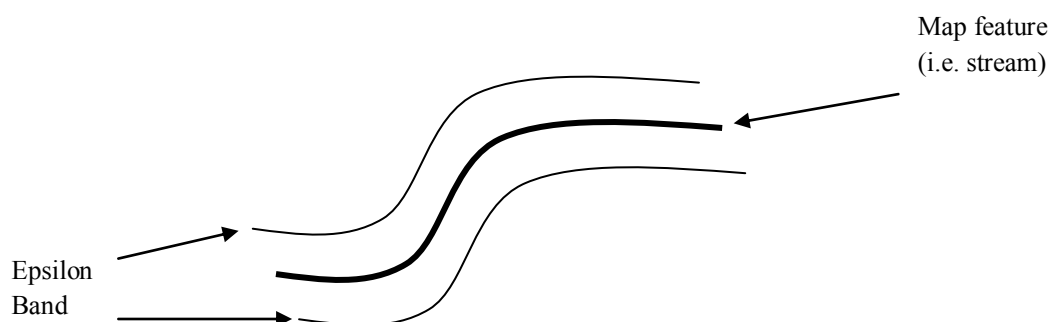
Figure 6.17: The epsilon band concept. The true position of the line (stream) will occur at some displacement from the measured position, between the two parallels of the epsilon band.

The degree of coincidence between each of the extracted stream networks and the reference network was evaluated by applying buffers of 5, 10, 20, 30, 40, 50, 60 and 70 m to the reference network and then calculating the percentage of each derived stream network that fell inside each of the buffers. It was considered that a higher percentage of the total length of a derived stream network in narrower buffers was indicative of a greater spatial accuracy (Penas et al., 2011). Buffer and Clip tools in ArcGIS 10 were used to carry out the analysis.

The principle of this approach is shown in Figure 6.18, and the proportions of the NEXTMap

derived stream network lying inside each different buffer width are illustrated in Figure 6.19.

Figure 6.18: A buffer of width 70m placed around the reference network, and the position of the NEXTMap derived stream network relative to the buffer. This illustration is shown as an example.

(a)

(b)

(c)

(d)

(e)

(f)

(g)

(h)

(i)
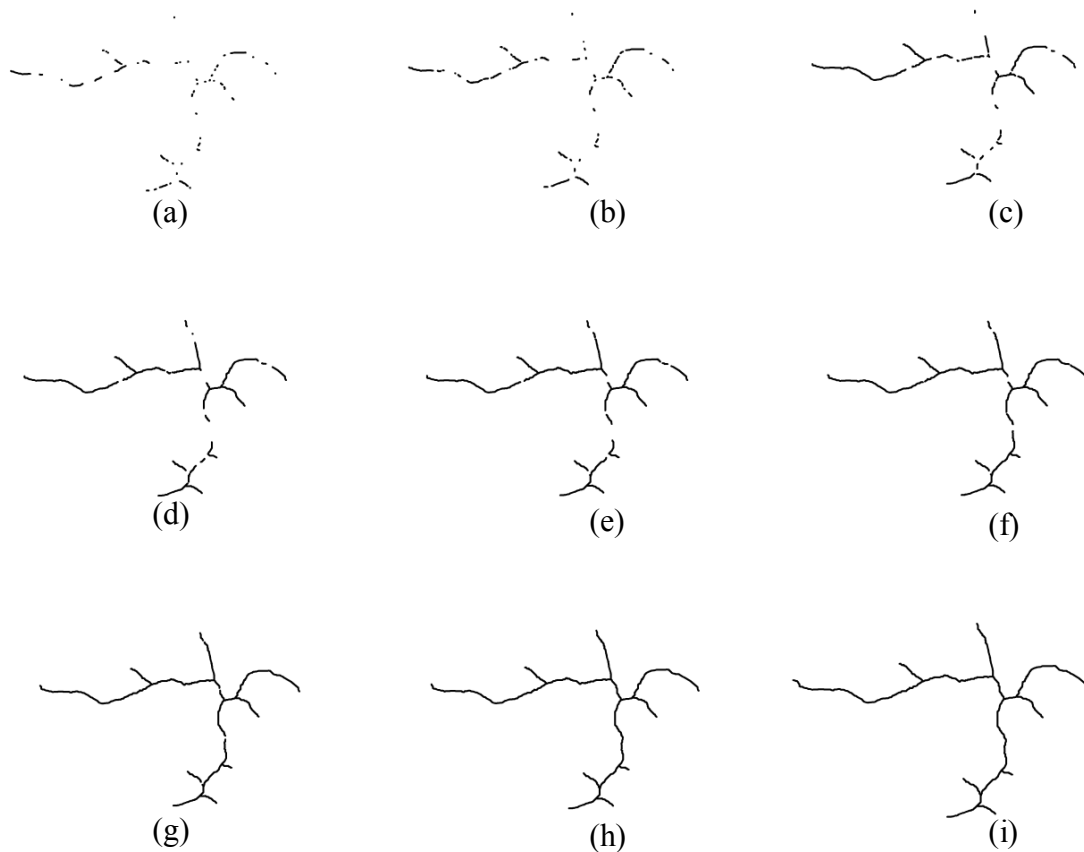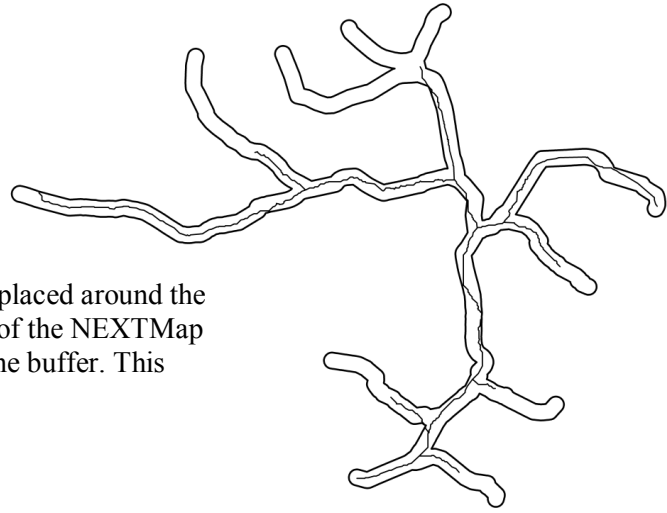
Figure 6.19: Illustrations of the portions of the NEXTMap derived stream network lying inside the buffer for width of (a) 5m (20.99 %), (b) 10m (35.78 %), (c) 20 m (65.09 %), (d) 30 m (79.58 %), (e) 40 m (88.84 %), (f) 50 m (93.71 %), (g) 60 m (97.18 %), (h) 70 m (98.97 %) and (i) the original NEXTMap streams (100 %).

6.3.2.1 Results

6.3.2.1.1 Stream networks extracted from original DEMs

As can be seen from Table 6.7 and Figure 6.20 it is very clear that DEM spatial resolution had large effects on the positional accuracy of the extracted stream networks. The extracted stream networks from the finer resolution DEMs (NEXTMap and Bluesky) have a higher level of agreement with the reference stream network. As would be expected, the percentage of each extracted stream network that lies within each buffer region (from 5 to 70 m) is considerably affected by the cell size of the DEM being used, as the cell size increases this percentage decreases. For the narrower buffers (5 and 10 m), the stream network extracted from Bluesky data was the best overall, with 24.91% and 43.39% of the total stream length falling inside each buffer, respectively. However, the NEXTMap derived stream network gives the best result of all extracted stream networks when applying buffers of 20 m and wider. The least accurate stream network was obtained when using the 90 m SRTM elevation data, showing the lowest percentage of the total stream length within each different buffer region. This could be related to the poorer spatial resolution of the SRTM data (90 m). Similar to these findings, Wang and Yin (1998) identified DEM resolution and the terrain complexity as the two major factors affecting the positional accuracy of stream networks derived from DEMs.

As was pointed out in discussion of the previous method (horizontal RMSE), stream networks extracted from NEXTMap and Bluesky elevation datasets showed significantly higher overall positional accuracy than stream networks extracted from the other two datasets (OS50 and SRTM). However, when compared to each other, for the narrower buffers (5 and 10 m), Bluesky extracted stream network produced better results while for the buffers of 20 m and above, results obtained from the NEXTMap data showed a higher agreement with the reference network. As discussed previously, this could be related to data source type,

techniques used to generate the DEM and also to the methods used to convert from DSM to

DTM (Figure 6.20 and Table 6.7).
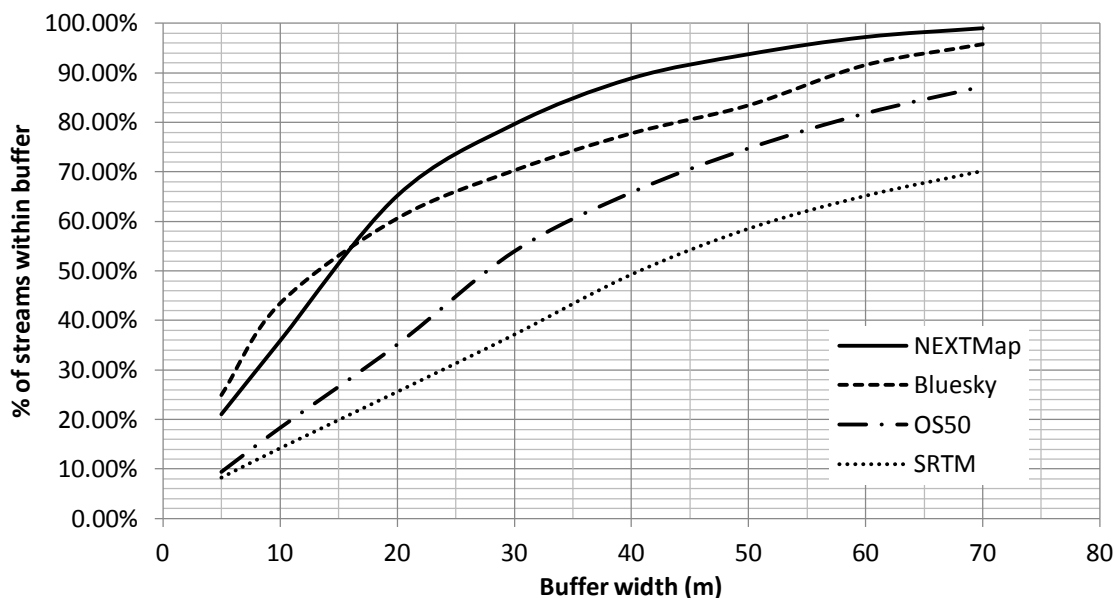
Figure 6.20: An illustration of the percentage of each extracted stream network lying within the buffer versus the buffer width.

From Table 6.7 it can be seen that stream network extracted from Bluesky provided almost three times more of the percentage of stream network features lying within 5 m of the reference network (24.91%) than that extracted from SRTM (8.21%). However, the resolution of the SRTM data is 18 times coarser than Bluesky. In addition, streams extracted from the 5 m resolution NEXTMap data exhibited only double the length of streams lying within 5 m of the reference network (20.99%) than those derived from the 50 m OS50 data (9.43%). This represents a kind of diminishing return in terms of the cell size, as the DEM cell size can be made finer and finer but the percentage of streams feature lying within the 5 m of the reference network might not increase much. Charrier and Li (2012) concluded that stream networks extracted using 3 and 5 m resolution DEMs still produce >95% stream length match compared to the reference streams delineated by a 1 m LiDAR DEM. They also reported that a coarser resolution DEM (such as 10 m LiDAR DEM) is more appropriate to delineate

194

watershed boundaries compared to the results from 1 , 3 or 5 m resolution LiDAR DEMs.

Therefore, although high resolution DEMs may prove more advantageous for certain

applications, the use of such data may not necessarily result in a better positional accuracy in

respect to stream network delineation.

Table 6.7: Results showing the length and percentage of each DEM extracted stream network for the Blackwater sub-catchment inside the buffer in terms of its width.

Buffer width (m)	NEXTMap		Bluesky		OS50		SRTM	
	Length of stream network within buffer(m)	% of stream network within buffer	Length of stream network within buffer(m)	% of stream network within buffer	Length of stream network within buffer(m)	% of stream network within buffer	Length of stream network within buffer(m)	% of stream network within buffer
5	2812.03	20.99	3353.55	24.91	1235.24	9.43	1081.93	8.21
10	4793.17	35.78	5841.56	43.39	2398.27	18.30	1865.22	14.15
20	8718.54	65.09	8152.47	60.56	4604.31	35.13	3368.47	25.55
30	10659.79	79.58	9458.59	70.26	7071.96	53.96	4894.56	37.12
40	11900.80	88.84	10465.62	77.74	8633.01	65.88	6497.61	49.28
50	12553.50	93.71	11228.88	83.41	9801.09	74.79	7719.12	58.55
60	13018.39	97.18	12324.24	91.55	10729.03	81.87	8596.64	65.20
70	13257.28	98.97	12889.85	95.75	11441.33	87.31	9258.68	70.22

Notes:

The highest percentages of stream networks within each buffer region from all the DEMs are highlighted (gray cells). Note that Bluesky data allowed a much accurate delineation of stream network when applying buffers of 5 and 10 m, while NEXTMap produced the best results when applying buffers from 20 m and above. Stream network obtained from SRTM product yielded the lowest percentage of streams within each buffer zone (underlined values). Stream network obtained from OS50 presented slightly better results than that from SRTM, but these results are twice smaller than that from NEXTMap in most cases. However, the differences between the stream networks were greatly reduced when applying 60 and 70 m buffers, indicating that stream networks delineated from OS50 and SRTM were not very far from the reference network
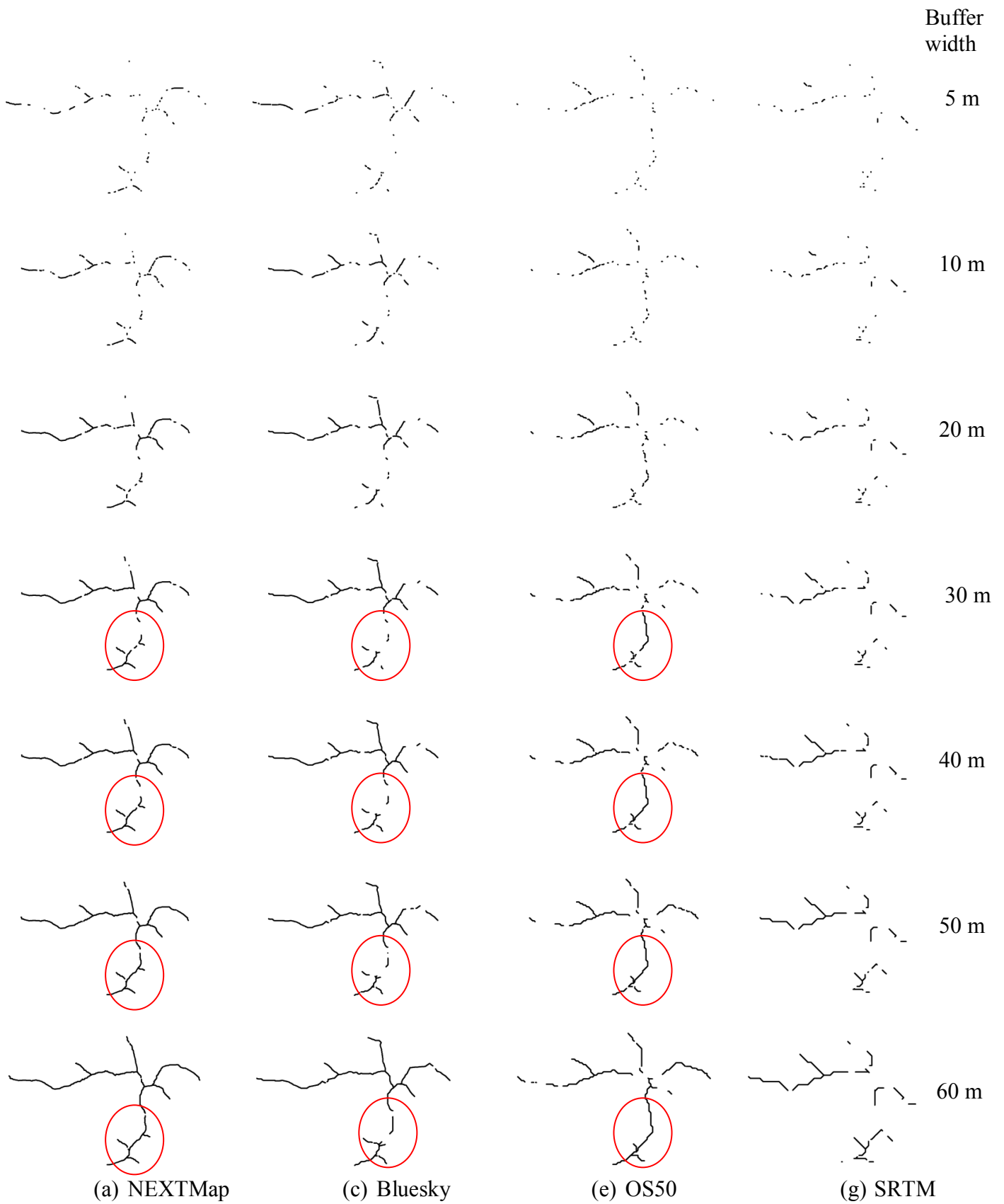
Figure 6.21: Illustrations of the portions of each derived stream network lying inside each buffer width. Line breaks depict sections of each stream network lying outside the buffer.

Another interesting finding related to the use of different data sources is that, in general, the OS50 derived stream network coincides very well with the reference network in terms of the main stretches of the lower reaches of the network (see circled locations in Figure 6.21). Almost the whole lower reaches of the OS50 derived stream network were captured when applying a buffer of 30 m. In contrast, however, in the case of streams extracted from finer resolution datasets, NEXTMap and Bluesky, large sections of the main river stretches lay outside the 30 m buffer compared to the results from the coarser resolution OS50 (Figure 6.21). The good agreement between streams extracted from the Ordnance Survey OS50 m and the reference network in the area of the lower reaches is probably due to the fact that the latter was obtained from OS VectorMap™ Local dataset and was modified using the OS 1:1000 MasterMap raster dataset (i.e sources from the same organisation). In further support to this finding, Charrier and Li (2012) investigated the effect of DEM different data sources and they suggested that different data sources can introduce significant uncertainties and may have different relationships between uncertainties and DEM resolutions due to the inherited resolution of their original data sources. They found that USGS DEMs, which were constructed from similar topographic maps, tend to produce similar results in automated floodplain delineation regardless of DEM resolutions.

6.3.2.1.2 Stream networks extracted from DEMs after error modelling

All the results regarding the percentage of each extracted stream network within each buffer region (from 5 to 70 m) are summarised in Table 6.8 and illustrated in Figure 6.22. It is clear from these findings that the NEXTMap derived stream network gives the best result of all extracted stream networks for all the buffer ranges, a difference from what was obtained when the original DEMs were used (Table 6.7), where for the narrower buffers (5 and 10 m), the Bluesky extracted stream network produced better results. The least accurate stream

network was again obtained when using SRTM elevation data, showing the lowest percentage

of the total stream length within each different buffer region, although these results have

improved to some extent through use of the error modelling method (see Table 6.8). In

general, compared to what was achieved when the original DEMs were used, the percentage

of each extracted stream network that lies within each buffer region (from 5 to 70 m) is

improved when extracted from the DEMs after error modelling.
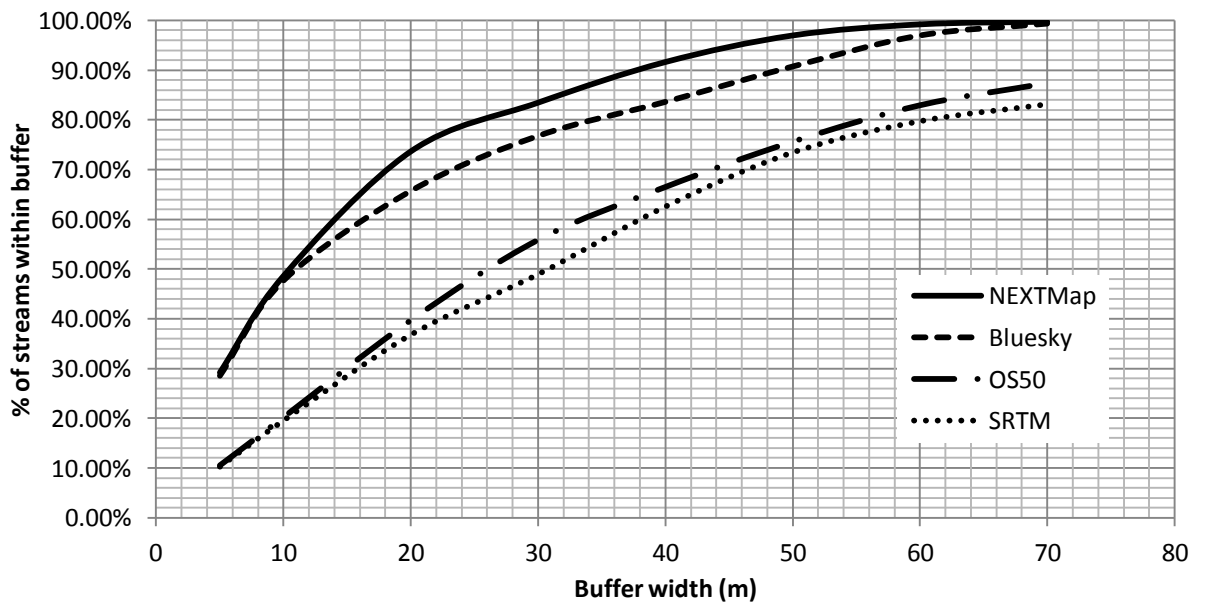
Figure 6.22: An illustration of the percentage of each extracted most probable stream
network lying within the buffer versus the buffer width.

Table 6.8: Results showing the length and percentage of each DEM extracted most probable stream network for the Blackwater sub-catchment inside the buffer in terms of its width.

Buffer width (m)	NEXTMap		Bluesky		OS50		SRTM	
	Length of stream network within buffer(m)	% of stream network within buffer	Length of stream network within buffer(m)	% of stream network within buffer	Length of stream network within buffer(m)	% of stream network within buffer	Length of stream network within buffer(m)	% of stream network within buffer
5	3993.57	29.21	3828.86	28.54	1439.88	10.52	1333.86	10.29
10	6649.79	48.64	6399.63	47.70	2764.18	20.20	2536.18	19.57
20	10074.33	73.68	8819.46	65.74	5431.17	39.69	4770.86	36.82
30	11415.37	83.49	10305.00	76.81	7641.26	55.84	6348.18	48.99
40	12532.23	91.66	11223.98	83.66	9096.32	66.47	8111.43	62.60
50	13262.58	97.00	12178.90	90.77	10342.05	75.58	9522.07	73.49
60	13568.12	99.23	13017.52	97.03	11343.61	82.90	10336.99	79.78
70	13641.39	99.77	13337.27	99.41	11951.93	87.34	10779.19	83.19

There are possible alternative methods of determining the positional accuracy of the extracted stream networks that have been reported in the literature. Li and Wong (2010) adopted a raster approach to evaluate the accuracy of extracted stream networks. Both the modelled and the reference networks were converted into raster layers for comparison. In order to evaluate how well the extracted network can replicate the reference network they used two method of comparison. The first one is called the correctness index and is defined as

$$C = \frac{N_{(A \cap B)}}{N_B}$$

Where N_B is the number of cells representing the reference network and $N_{(A \cap B)}$ is the number of cells representing the extracted stream network, but the cells are also found in the reference network. The second method called Figure of Merit (FM) which is the ratio between the number of cells found in both extracted and reference networks, and the number of cells in the two networks combined, but overlapping cells are counted only once. If $N_{(A \cup B)}$ is the number of unique cells found in either network A or B, the ration is defined as

$$FM = \frac{N_{(A \cap B)}}{N_{(A \cup B)}}$$

Li and Wong (2010) believed that these raster approaches of stream network comparison had advantages over vector-based comparison. They argued that vector-based comparison evaluates only certain parts of the drainage network, but not the entire network, it does not offer a comprehensive assessment of similarity between the extracted and reference networks.

Another method which can be used to quantify the positional accuracy of stream networks is the Digital Shoreline Analysis System (DSAS). DSAS is a software extension to ArcGIS that calculates shoreline change statistics from multiple historic shoreline positions (Thieler et al., 2009). Although DSAS was made to calculate the rate of coastline movement

and changes, it can be also used to obtain distance offsets, or error of any other data, such as stream networks, that incorporate identifying feature positions based of a baseline or reference network (Thieler et al., 2009; Trowbridge, 2014). DSAS generates transects that are cast perpendicular to the baseline at a user-specified spacing. Distance measurements are obtained by calculating distances from the baseline to the points where transects intersected shorelines (which could be the derived stream channels in our case) and then used to calculate the rate-of-change statistics (Kuleli, 2009). Anderson and Ames (2011) have used sinuosity as one measure of detail and closeness of fit between derived and reference stream networks, where the absolute value of sinuosity differences can be used as a measure of derived stream network accuracy.

6.4 Conclusions

The results obtained from all the methods used in this study, the assessment of some selected hydrographical parameters (stream order, number of streams in each order, stream lengths and catchment area), RMSE and percentage length within buffers, reveal that DEM spatial resolution and data source type were important factors that influenced the extracted stream networks positional accuracy. The DEMs employed in this study were derived from different remote sensing sensors (passive and active) as well as different topographic data sources, and consequently, it was anticipated that they would produce different results.

From the results, the effect of DEM resolution on hydrological feature derivation is clearly evident. Among all the different DEMs used, the total stream length, the maximum stream order and the total stream segments had the highest values from the highest resolution DEMs, and there was a descending trend with increasing cell size. While using the same contributing drainage area threshold, the results showed that higher resolution DEMs (NEXTMap and Bluesky) produced more detailed stream networks. However, among the two 5 m resolution DEMs, results from NEXTMap were better than those from Bluesky. This is

attributed to the combined effect of the original data source, DEM generating techniques and the DSM to DTM conversion process, while they have the same resolution NEXTMap provides a more accurate and detailed drainage network. These results are consistent with Charrier and Li (2012) who proposed that re-sampled lower resolution LiDAR DEM generated more accurate and detailed floodplain outputs when compared with outputs from same resolution USGS DEMs, attributing these differences to the type of the original data source.

It was observed that the density of stream networks with a threshold value of 0.005 km² was significantly greater than that of stream network with a threshold of 1.25 km². So it is very clear that a smaller threshold value will result in a denser stream network. It was also found that the best fit between the modelled stream networks and the reference network in respect to the hydrological parameters comparisons occurred with the use of a 1.25 km² threshold value. In the regard to catchment area, although there was a minor tendency to increase with cell size, others have also examined the effect of grid size change on the catchment area determined from DEM, and no consistent trend was observed (Vieux, 1993; Wu et al., 2008a).

The horizontal RMSE was found to increase with the cell size. The difference between extracted stream networks and the reference network increased as DEM resolution decreased. The results showed that distance differences between the modelled stream network and the reference network tended to be smaller with a finer resolution. Nevertheless, the effect of data source and processing methods for generating DEMs is apparent here too, where the 5 m resolution NEXTMap data offered a better horizontal RMSE value of 22.36 m, as opposed to 30.01 m from the other 5m resolution data, Bluesky. It was also observed that the percentage of the modelled streams that fell inside each of the buffers, when the buffer method was used, increased as the DEM resolution increased. This is also consistent with Penas et al. (2011)

who concluded that 5 and 25 m DEMs generated a more spatially accurate drainage network than the 90 m DEM.

It was also observed that using the error modelling method and then extracting stream networks for a specified number (100 in our study) of realizations and then selecting the most probable stream network produced more robust results compared to the networks extracted from the original DEMs. The derivation of the most probable stream networks shows a better spatial matching between these networks and the reference network. Thus, the use of some DEM realizations with modelled error seems to give more reliable results that minimise the uncertainty due to errors in the original DEM (Gatziolis and Fried, 2004; Poggio and Soille, 2011: Raaflaub and Collins, 2006)

Overall, DEMs with higher spatial resolution improved the modelling of stream networks, their structure and spatial accuracy. The process of DEM generation from raw data, the DEM original data source and also the technique used to convert from DSM to DTM also affect the positional accuracy of the modelled stream networks. However, in this study, it was observed that the major factor affecting the positional accuracy of stream networks derived from all the DEMs in our study is the DEM resolution. In further support of this conclusion, several authors have concluded that DEM resolution is the most important factor influencing its derived products (e.g. Charrier and Li, 2012; Paz et al., 2008; Oksanen and Sargakoski, 2005; Penas et al., 2011; Vaze et al., 2010; Wang and Yin, 1998). It should be noted that the choice of datasets does not allow the effects of resolution to be separated from those of data source type. The effect of resolution on the positional accuracy of the derived streams could be examined if the resolution, for example, of the NEXTMap or Bluesky datasets was reduced (re-sampled to a lower resolution).   In a study by Vaz et al. (2010) they investigated the impact of using different resolution DEMs on hydrologically important derived indices. They concluded that the loss of details by re-sampling the higher resolution DEM to coarser

resolution are much less compared to the details captured in the commonly available coarse resolution DEM derived from contour maps. The same conclusion was drawn by Charrier and Li (2012) as they found that DEMs from more detailed original data source, such as LiDAR data, provided more accurate and detailed stream networks even when using re-sampled lower resolutions DEMs.

From comparing several network parameters including the stream orders, the number of the stream segments, the total stream length and the catchment area as well as the results from horizontal RMSE and the buffer methods, this study showed that the NEXTMap elevation data offer better results compared with what can be achieved using the other elevation datasets. However, the differences between NEXTMap and Bluesky derived stream networks were not substantial, in some respects the Bluesky data performed well and similar to NEXTMap. These results suggest that if NEXTMap and Bluesky data are available, NEXTMap is suggested to be used instead of Bluesky, at least according to the results obtained so far and for an area with similar topography to our study area. In addition, the study revealed that it is worth investigating in error propagation to stream network. Comparing to the reference network, the derived most probable stream networks from the multiple equally likely realisations produced more accurate result compared to the networks extracted directly from the original DEM.

Chapter 7

Modelling of Soil Erosion and Diffuse pollution

7.1 Introduction

In many agricultural catchments the problem of soil erosion and diffuse pollution is an important environmental concern (Posen et al., 2011). Soil erosion can cause significant damage to productivity of agricultural lands and when it leads to increased sedimentation in waterways, can have negative effects on drinking water quality (Mainston et al., 2008). For the implementation of the Water Framework Directive (WFD), which came into force in 2003, EU member states must meet good chemical and ecological standards in water bodies by 2015. Research has shown that agricultural activities are responsible for a large contribution to degradation in water quality as a result of soil erosion and diffuse pollution (Harris and Heathwaite, 2005; Rickson, 2014; Boardman et al. 2009) which are consequently a major barrier to meeting these standards (Defra, 2002). Therefore, in order to effectively apply mitigation measures and best practice land management techniques it is necessary to prioritise which areas in the landscape of catchment should be targeted.

As has been mentioned earlier in this research, DEM-based modelling of watershed processes has become increasingly popular in environmental research due to the advances in availability and efficiency of DEMs in acquiring topographic properties of catchments, such as slope, field slope length, and channel network. Within a catchment, hydrological pathways

can play a very important role in soil erosion and transport of diffuse pollution (Lane et al., 2006) by exerting a major control on where soil is eroded within a landscape and whether it is subsequently delivered to watercourses (Ferrier and Jenkins, 2010; Reaney et al., 2011).

As indicated above, a key issue in diffuse pollution management is the concept of Critical Source Areas (CSAs). CSAs are any piece of land where source factors (soil type, local slope, land use, and land management) combine with the local hydrological characteristics (i.e. flow from land is directly connected to streams) (Heathwaite et al., 2005). Connectivity throughout a catchment depends partly on its landscape topography (Wu et al., 2007) which is represented by DEMs. In Chapter 6 it was concluded that, among the four elevation datasets investigated, the NEXTMap data were found to be the best to represent Blackwater sub-catchment topography in relation to drainage network modelling. Therefore, NEXTMap dataset was used here to investigate soil erosion and diffuse pollution problems in the study catchment. Furthermore, for comparison purposes and for evaluation of the DEM uncertainty caused by grid size and data source on the model parameters and results the contour-based OS50 m DEM was also used.

Overall, the concern of this chapter is three-fold. Firstly, SCIMAP modelling is applied and evaluated for the Blackwater sub-catchment within the River Wensum catchment. SCIMAP provides a framework for identifying the probable spatial locations of diffuse pollution problems within the catchment as well as the risk of these areas being hydrologically connected to rivers and streams (Reaney et al., 2011) (see Section 2.4.4 for more details). Secondly, this study attempts to validate the SCIMAP results by comparing the outputs to water quality measurements in the catchment. Finally, the omission of the effects of soil type on diffuse pollution modelling by SCIMAP is perhaps the area where the model may be best improved. Therefore, for the purpose of model comparison, the RUSLE was used in an attempt to account for the considerable effect of soil type on soil erosion estimation

process (see Section 2.4.3). Two mini-catchments (A and B) were selected that were deemed to be representative of those found in the Blackwater sub-catchment and the results from RUSLE were discussed in relation to both water quality measurements and results from SCIMAP. Additionally, in an attempt to demonstrate the effect of changes in the RUSLE factors (such as crop management (C) and support practice (P) factors) on the assessment of soil erosion risk, different scenarios were considered and the results were compared to those that were obtained when the original factors were used.

Resulting from increased levels of environmental degradation in rivers efforts have been made to account and monitor the sources and pathways of diffuse pollution on a catchment level. One such monitoring strategy in the UK was the establishment of the River Wensum Demonstration Test Catchment project, which is part of the UK-wide Demonstration Test Catchment (DTC) programme. As a result of a joint DEFRA and Environment Agency initiative the Wensum DTC was established where issues (hypotheses) relating to diffuse pollution and improved agricultural practices can be tested and evaluated (McGonigle et al., 2014; Wensum Alliance, 2013). The main aim of the project is to work towards reducing the impact of diffuse pollution to the Wensum without impairing agricultural productivity (Wensum Alliance, 2013). In this regard, using SCIMAP and RUSLE in the Blackwater sub-catchment seeks to identify areas of high soil erosion risk so that preventative practices can be suggested, which in turn will limit amounts of sediment and nutrients entering watercourses and subsequent in-stream sedimentation and water quality degradation.

7.2 SCIMAP

7.2.1 Introduction

The Sensitive Catchment Integrated Modelling Analysis Platform (SCIMAP) provides a framework for identifying the probable spatial origins of diffuse pollution problems within agricultural catchments. It is based upon a conception of that sources of risk are thought to be distributed across the river catchment and that a catchment can be regarded as a set of flow paths that accumulate these distributed sources of risk from across the landscape into receiving waters where, for surface waters, diffuse pollution may become visible either through detection of temporal changes in water quality via routine monitoring or through the more limited evidence of physical water quality degradation (e.g. algal blooms) (Lane et al., 2006; Reaney et al., 2011; Milledge et al., 2012). As such, SCIMAP focuses on identifying where in the catchment pollution materials come from rather than aiming to produce estimates of the actual pollution load (Lane et al., 2006). Hence, the result of SCIMAP is a method for determining where in the catchment management resources should be concentrated in order to achieve optimum environmental protection (Lane et al., 2006).

The model first considers the areas in which surface flow will accumulate based upon topography and rainfall inputs to generate a map of the stream network. The erodibility of a given surface, derived from land cover data, is subsequently determined to produce a map of erosion risk across the whole catchment. Each land cover category is assigned a risk value, parameterised by expert judgement (Reaney et al., 2011), which is scaled between 0 (low risk of erosion) and 1 (high risk of erosion). The erosion risk map is then combined with hydrological data to identify those areas in which fine sediment will accumulate due to hillslope and hydrological process. The final stage of the SCIMAP framework is that the accumulated erosion risk map is superimposed upon the stream network map to produce a

weighted output map of sediment risk in channels (in-stream risk concentration). The risk concentration is deemed to be the sum of all upstream contributing risks and by dividing it by the upslope contributing area dilution processes can be accounted for (Lane et al., 2006).

7.2.2 Methods

Within this study the SCIMAP framework was applied at two different scales of topographic data: NEXTMap 5m resolution DTM and OS 50m panorama DEM. The SCIMAP diffuse pollution risk mapping was conducted using two geographical information systems. ArcGIS provided the tools to organise, modify and ultimately display outputs, whilst SAGA 2.0 was used to run the SCIMAP fine sediment risk model. SCIMAP has been developed as a joint project between Durham and Lancaster Universities and takes the form of a custom module in the SAGA GIS framework (SCIMAP, 2013).

As mentioned previously, in order for SCIMAP to compute the relative risk of an area producing a diffuse sediment pollution risk three layers of data are required, topographic, land cover and rainfall (Reaney et al., 2011). Because the study area is small, the rainfall data were assumed to be spatially uniform over the whole catchment. The land cover data was based on the Land Cover Map 2007 (LCM2007) but has been updated using farm records by the Wensum DTC project so that more recent changes in land management are represented across the study area.

It is a prerequisite of the SCIMAP model that all input data exist in the same grid system, with the same extent and spatial resolution. Using the ArcGIS Resample tool the land cover map and the rainfall data were downscaled onto the topographic data resolutions used in this study; 5m for NEXTMap and 50m for the OS 50m data. In SCIMAP it was necessary to reclassify each land cover category from the LCM2007 data into values between 0 (low risk) and 1 (high risk) to produce an erodibility index. In this regard, the literature was consulted

and the land cover risk values based upon the categorisations by Reaney et al. (2011) were used. The land cover weightings used within SCIMAP in this study are shown in Table 7.1.

Once pre-processing of the three data layers has been completed, the SCIMAP model then uses these initial three layers to produce a selection of new layers. SCIMAP modelling produced intermediate maps before the final stage of the modelling process was accomplished. These intermediate layers are: the slope, stream network, network index and erosion risk. The erosion risk map allows areas susceptible to erosion and locations with highly erosive rainfall to be identified. For a particular area in the landscape, the surface flow index map (network index) represents the likelihood of sediments that are mobilised from that area to make their way through to the channel network. Once these intermediate modelling layers have been combined together SCIMAP makes predictions, based on topographic controls, of in-situ soil erosion risk at each location across the catchment. By combining this risk with land cover risk weightings the important role played by different land covers in either increasing or decreasing erosion risk can be identified. The final stage of the SCIMAP modelling process is to incorporate the effects of dilution to the accumulated risk to effectively give a risk concentration (Reaney et al., 2011). Of these layers, erosion risk, network index and in-stream risk concentration maps were then exported back into ArcGIS to manipulate the data for display purposes.

Table 7.1: Default land cover risk weighting used in the SCIMAP framework.

Land Cover	Assigned Risk Value
Arable	1.0
Improved grassland	0.20
Rough grassland	0.10
Woodland	0.05
Urban/Other	0.00
Water	0.00

After Reaney et al. (2011) and SCIMAP final report.

7.2.3 SCIMAP results

The results of applying the SCIMAP model to the Blackwater sub-catchment are presented in this section. Maps of slope, the surface wetness index, erosion risk and erosion risk in channels were produced, amongst other outputs. The key output and the one used most in the subsequent discussion is the concentrated erosion risk in channels map. This map allows hot spot mini-catchments and tributaries within the sub-catchment to be identified.

It should be noted at this point that due to the overall poor performance of the SCIMAP model when the lower resolution OS data was used, the subsequent discussion concentrates on the results from NEXTMap data. The results from SCIMAP model when the OS data were used were unrealistic (Figure 7.1). Visual inspection of the map indicates that the information derived from this DEM shows an unrealistic stream network. It is clear from the map that there are some disconnected stream reaches (mini-catchment D), also some streams that initiate in one mini-catchment end up pouring into a different one (in mini-catchment C; notably the stream is erroneously diverted to the west). This appears to be a consequence of the DEM's coarser resolution where the flow routes were poorly defined. These results suggest that the OS 50m resolution DEM is not suitable for applying SCIMAP for diffuse pollution modelling in the Blackwater sub-catchment. Reaney (2014) has argued that SCIMAP works best with 5m resolution data (or finer data such as LiDAR) as the standard topography data source, however, OS 10m profile DEM can be used but care must be taken to check the results.
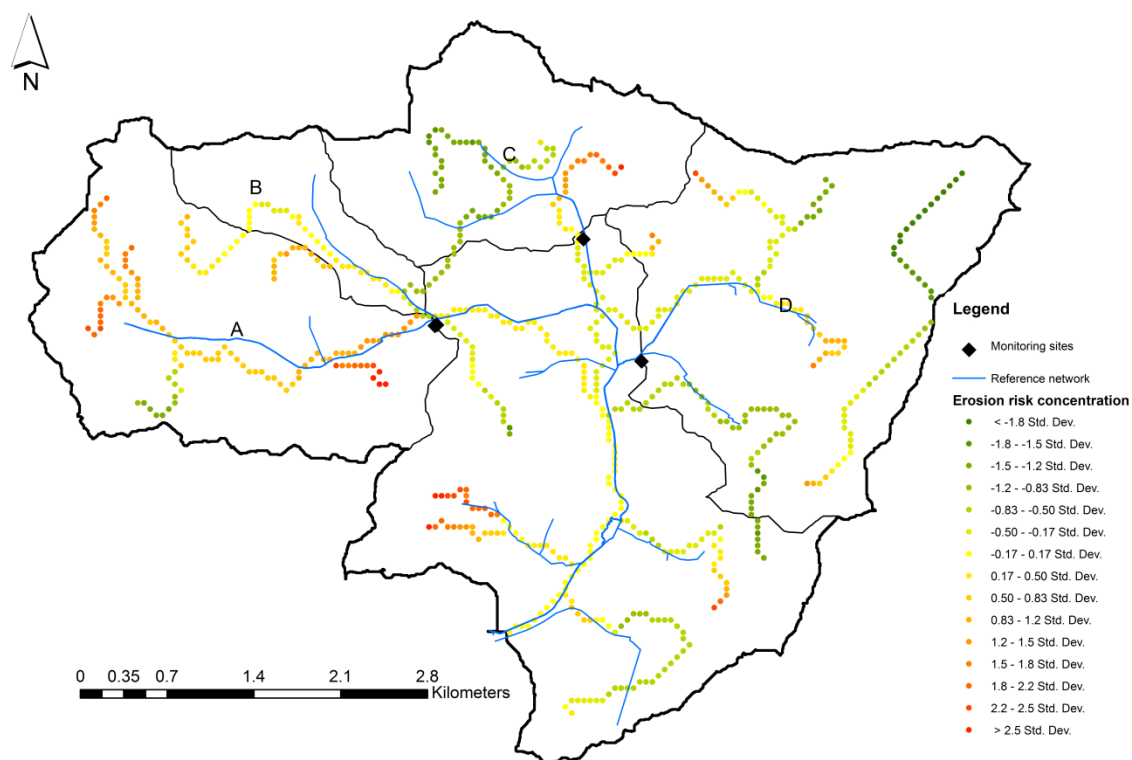
Figure 7.1: In channel risk mapping for the Blackwater sub-catchment using OS 50m DEM, the accumulated risk weighted by the dilution potential. Areas in red show where there is more diffuse pollution risk than water to dilute the risk and green areas show where there is less risk.

7.2.3.1 SCIMAP risk maps using NEXTMap data

Initially the intermediate layers of the SCIMAP modelling process were analysed independently. The following figures are example outputs from different stages of SCIMAP modelling framework; Figure 7.2 shows the network index map, Figure 7.3 erosion risk map and Figure 7.4 is the final output from the model. These intermediate SCIMAP layers will be discussed briefly below and more discussion will be devoted to the final stage result.

Before the final outputs from the SCIMAP modelling process are examined it is possible to use information from the intermediate layers to infer some of the properties of the catchment which might make certain areas more likely to be responsible for generating and transmitting diffuse pollution around the catchment. The likelihood of places to become

connected is demonstrated by the network index (Figure 7.2), where places in the landscape with a higher network index represent a high surface flow connection risk (Reaney et al., 2011). It is clear from the figure that the most highly connected areas are in the gently sloping landscape of the western side of the sub-catchment, especially areas included in min-catchments A and B. The least connected areas are found in the middle of the sub-catchment.

Figure 7.3 shows which areas are most likely to be susceptible to soil erosion based on topographic factors and land cover. Usually, when land cover weightings are added into the SCIMAP model, the locations of areas most at risk of soil erosion change. Each land cover classification was scaled between 0 (low risk) to 1 (high risk) based upon its potential for producing soil erosion, arable was assigned 1 (maximum risk) where the land might be left bare for part of the year (Reaney et al., 2011). However, a visual inspection of the two figures, Figures 7.2 and 7.3 indicates that there are no big differences in the locations of high risk areas after the integration of land cover weightings into the SCIMAP modelling process. This can be attributed to the fact that in the Blackwater sub-catchment, arable land covers more than 80% of the total area.
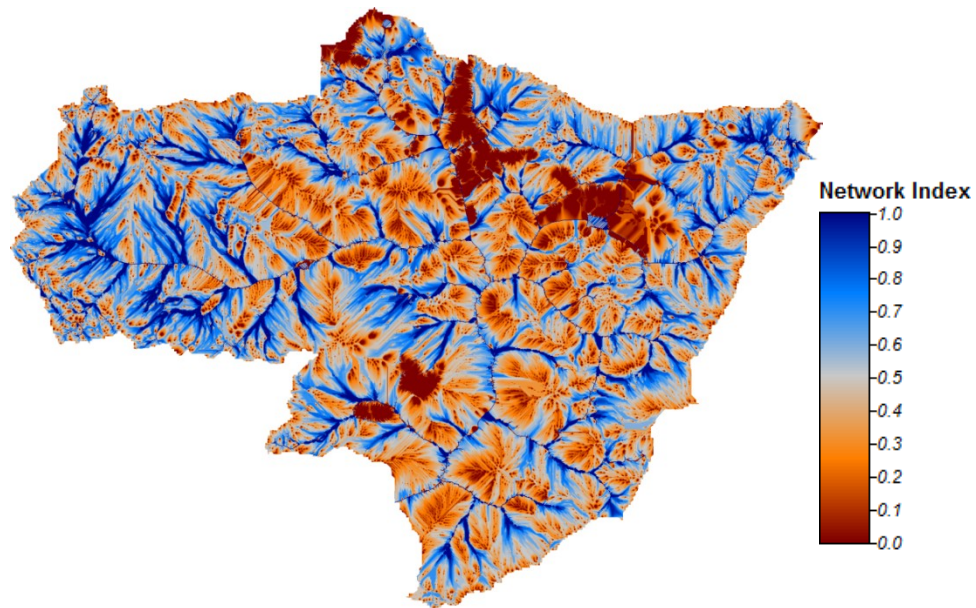
Figure 7.2: Network index values for the Blackwater catchment. The network index is used as representation of surface connectivity risk. Blue represents the highest potential connectivity and red the lowest.
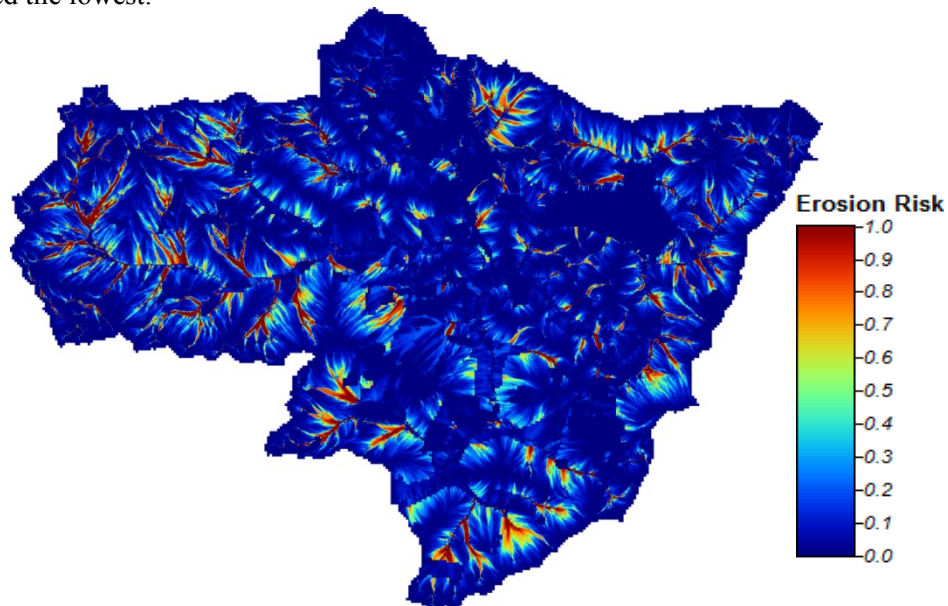
Figure 7.3: Blackwater sub-catchment potential pattern of surface erosion. Red is the highest relative risk, blue is the lowest.

The final stage of the SCIMAP modelling process adds a dilution effect to the accumulated risk to effectively give a risk concentration (Reaney et al., 2011). Risk at a location may not necessarily be transported through the hydrological network to the receiving areas and it is possible that a degree of risk may be diluted as a result of inputs of water from a large upslope contributing area. In Figure 7.4 the symbolisation runs from red (high risk)

through to green (low risk) in classes of one third of standard deviation of the mean of the risk value. In areas where this value is higher than the mean (red areas), the risk of pollution increases faster than it can be diluted thus the area is identified as having a risky input to it. Conversely, in locations where this value is less than the mean, the risk of pollution is less than the dilution potential thus these locations are classified as having lower risk inputs to the channels (Reaney et al., 2011).

Areas that are highlighted by SCIMAP as being at greatest risk of diffuse pollution are mainly located in the western parts of the sub-catchment, mini-catchments A and B (Figure 7.4). The agricultural areas surrounding the channels that run through the two mini-catchments are considered to be at a particular high risk of sediment loss. As discussed previously, these two mini-catchments are completely used for intensive farming. Thus, what is clear from the visual inspection of the figure is that the two mini-catchments A and B are highlighted as being most at risk of being critical source areas of surface soil erosion and consequently agricultural diffuse pollution. This appears to be due to the hydrological connectivity of these areas coupled with the presence of intensive arable farming. Other notable "hotspots" can be observed to the east of Heydon (mini-catchment C) and on the west of the sub-catchment. Locations with low risk are found at the upper reaches of the Heydon estate and in the middle of the sub-catchment where some patches of woodlands and large water bodies exist which are likely to contribute to lower erosion risk since they act to dilute risks from other sources in the catchment (Milledge et al., 2012).
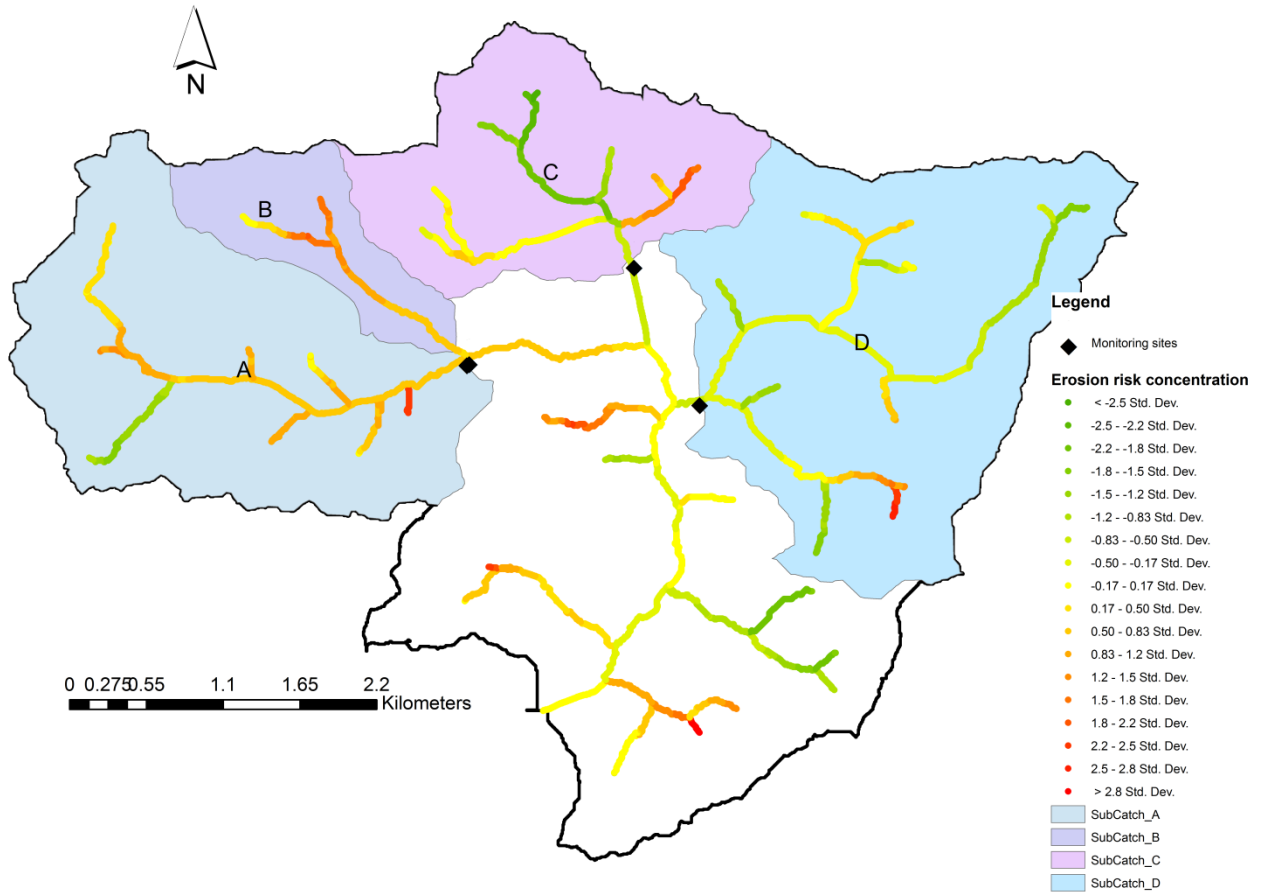
Figure 7.4: In channel risk mapping for the Blackwater sub-catchment, the accumulated risk weighted by the dilution potential. Areas in red show where there is more diffuse pollution risk than water to dilute the risk and green areas show where there is a less risk.

Figure 7.5 shows mini-catchments A and B overlaid with the field boundaries. Zooming in to mini-catchment scale provides a high resolution map of at risk areas in the channel network. As the two mini-catchments are dominated by arable farming, the model predicts that a high proportion of the two mini-catchments is susceptible to erosion. It also illustrates the predicted effects of in-stream dilution upon risk concentration as areas of high risk indicated by red tend to be diluted at the confluence with another channel.
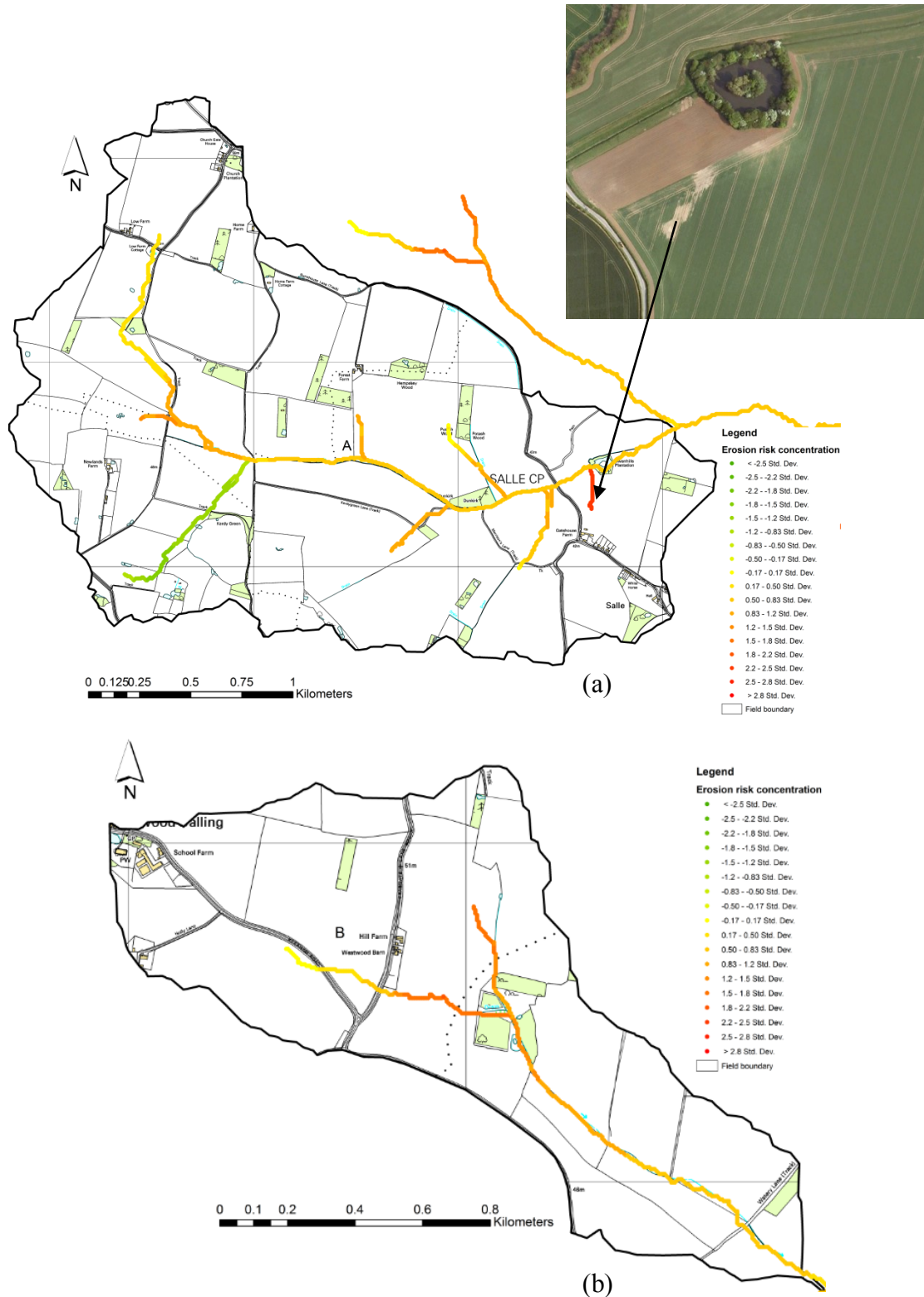
Figure 7.5: In channel risk mapping, the accumulated risk weighted by the dilution potential (a) mini-catchment A and (b) mini-catchment B. Areas in red show where there is more diffuse pollution risk than water to dilute the risk and green areas show where there is less risk.

7.2.4 SCIMAP Performance Assessment

The results obtained from applying the SCIMAP framework to the Blackwater sub-catchment can be assessed against spatial patterns of water quality data gathered from a series of monitoring stations operating as part of the Wensum DTC initiative. This allows an evaluation of the performance of SCIMAP in making spatial predictions and whether correlations can be identified between areas deemed to be most at risk of sediment pollution by SCIMAP and the records of turbidity (mini-catchments A, B, C and D were used in this assessment). Past research by Milledge et al. (2012) has successfully used water quality data to show that SCIMAP is able to reproduce observed water quality patterns across several UK catchments. Reaney et al. (2011) applied the SCIMAP model in River Eden catchment to understand the relationships between land cover, topography (hydrological connectivity) and spatially distributed salmon and fry data.

On a sub-catchment scale, results from the SCIMAP modelling framework show that mini-catchments A and B are generally at high risk of surface soil erosion (and therefore associated nutrient delivery via fine sediment) compared to C and D (Figure 7.3). Turbidity measures recorded at 30 minutes intervals at the outlet of each sub-catchment using an in-stream turbidity meter (Wensum Alliance, 2013) carried out by the Wensum DTC project from 2011 to 2013 support these predictions from the SCIMAP framework. The results from the turbidity measurements suggest that mini-catchments A and B have higher mean and median turbidity values compared to the other two mini-catchments. The mean turbidity values for mini-catchments A, B, C and D are 10.12, 8.53, 6.49 and 7.15 (NTU), respectively (Table 7.2). The lowest turbidity concentration measures were recorded for mini-catchment C with mean and median of 6.49 and 4.8 (NTU), respectively. These findings add support to the results produced by SCIMAP that these two mini-catchments (A and B) are most likely to be at greatest risk of agricultural diffuse pollution and C had the lowest risk (Table 7.2)

Numerical values from the final in-stream risk concentrations map allow for more assessment of SCIMAP performance in identifying parts of the landscape that generate risks (Table 7.2). These descriptive statistics from the SCIMAP final map allow for the comparison of the different mini-catchments with respect to their risk inputs to the channels, and the results were then compared with the water quality data. It is clear from the table that mini-catchments A and B had high mean and median values for fine sediment risk concentrations compared to the other two. Mini-catchment C had the lowest mean and median in-stream risk concentration, which is in agreement with the turbidity measures. The descriptive statistics of turbidity records from these mini-catchments are consisted with the SCIMAP results. The results from the water quality data (Table 7.2) suggest that mini-catchments A and B have higher mean and median turbidity values compared to those from C and D.

Table 7.2: Numerical values from the SCIMAP final risk map and the water quality data for mini-catchments A, B, C and D.

Mini-catchment	Area (ha)	SCIMAP Risk concentration		Water Quality Turbidity	
		Mean	Median	Mean	Median
A	537.9	0.15755	0.16726	10.12	7.3
B	133.7	0.18239	0.18101	8.53	5.9
C	352.1	0.10818	0.12813	6.49	4.8
D	661.4	0.11823	0.11744	7.15	5.1

Overall, SCIMAP results from the Blackwater sub-catchment support the viewpoint that a catchment dominated by arable farming is at some risk of sediment associated water quality problems (Yang et al., 2012). From the above discussion and on a mini-catchment scale, it can be concluded that SCIMAP framework was successful in identifying the areas at

major risk of sediment pollution and establishing a hierarchy of mini-catchments at risk.

Therefore, in terms of a catchment wide modelled output the results could be used by the

stakeholders to focus their attention on particular parts of a study area that are particularly

contributing to the sediment loss and thus diffuse pollution problems.

The methodology behind the SCIMAP framework has several limitations attached to

it, which can lead to a significant amount of inherent uncertainty attached to the model

predictions. A main limitation of the SCIMAP framework is that it does not account for the

effect of different soil types, which may significantly influence erodibility (Reaney et al.,

2011). Research has shown that differences in soil composition can quickly lead to variations

in levels of infiltration and overland flow (Heathwaite et al., 2005), which can indeed affect

the model predictions.

Furthermore, the framework does not differentiate between areas of different land use

due to the framework being based on land cover categories. Land cover differs from land use

in that it does not include management practices and is coarser in terms of categories. For

example, the arable category accounts for all the type of crops (cereals, root crops and

horticulture) which in fact differ in the percentage of ground cover throughout the growing

season and also in erosion risk (Defra, 2005). Thus, in the following sections, this weakness of

SCIMAP was addressed by using the Revised Universal Soil Loss Equation (RUSLE) and its

Crop Management Factor (C-factor) to evaluate the effect of different crop types on prediction of

soil erosion risks in the study catchment.

7.3 Universal Soil Loss Equation model (USLE/RUSLE)

The Universal Soil Loss Equation (USLE) (Wishmeier and Smith, 1978) and its later amended version the Revised Universal Soil Loss Equation (RUSLE) (Renard, 1997) are the most widely used methods to estimate soil erosion on a catchment scale (Kinnell, 2010; Csafordi et al. 2012; Drzewiecki et al. 2013; Shiferaw, 2011). The USLE/RUSLE has been described in detail in Section 2.4.3. RUSLE predicts the long-term average annual rate of soil erosion and the potential risk zones of erosion. Soil loss contributes to sediment yield and can contribute to agricultural diffuse source pollution in waterways (Drzewiecki et al. 2013; Boardman, 2013; Volk et al., 2010). Therefore, successful RUSLE calculations can contribute to an assessment of soil lost to watercourses as well as the identification of potential locations at high risk of soil erosion which can aid the local catchment managers and planners to improve land management (Prasuhn et al., 2013; Rickson, 2014).

Planning for soil and water conservation measures requires knowledge of the relation between the driving factors that cause soil erosion (e,g. the erosivity of rainfall, the slope of land, soil erodibility) and the factors that help to reduce such loss (e.g. vegetation cover, the conservation practices and measures). RUSLE can be used to compare several different erosional scenarios to assess and demonstrate the effect of changes in individual RUSLE parameters on the amount and spatial distribution of soil losses (Rulli et al., 2013).

7.3.1   RUSLE parameters

The RUSLE includes six factors. Their implementation in the Blackwater sub-catchment is discussed in the following sections.

7.3.1.1   Rainfall erosivity factor (R)

The rainfall erosivity factor (R factor) represents the erosion potential caused by rainfall (Kouli et al., 2008). It depends on the amount of precipitation within a region over a certain time period (Bargiel et al., 2013). The R factor was originally designed as an empirical measure to represent the averaged effect of annual rainfall. In an effort to estimate the R factor using monthly and annual rainfall data, Renard and Freimund (1994) proposed the use of both mean annual rainfall P and the Modified Fournier Index F (Arnoldus, 1980), where F is the sum of the monthly erosivity indicators. According to Drzewiecki et al. (2013) and Nigel and Rughooputh (2010) this is the most widely used method of estimating the rainfall erosivity factor. Ferro and Porto (1999) argued that even if F takes into account the seasonal variation in precipitation, analysing data on mean annual rainfall and the modified Fourmier index F for different European regions shows that the F index is strongly linearly correlated to the mean annual rainfall. Moreover, some studies (e.g. Lastoria et al., 2008; Drzewiecki et al. 2013) suggest that P and F are linearly correlated, thus making the added complications in the computation of F not necessary.

The F index, as proposed by Arnoldus (1980), is defined as:

$$\mathbf{F} = \sum_{j=1}^{12} \frac{p_j^2}{P}, \qquad \text{(Eq. 7.1)},$$

where pj, is the mean rainfall amount in mm for month j, and P is the annual precipitation total. Different authors have proposed different ways to retrieve R from P or F. Each method is optimized for a certain location, and as usual, with no guarantee that it will work if applied elsewhere (Lastoria et al., 2008). Therefore, to circumvent this problem, several equations have been used and the resulting rainfall erosivity indexes have been averaged. Table 7.3 below shows these equations and the references where they can be found.

Table 7.3 : Approximation R equations.

Author	Model
Arnoldus – linear (1980)	$R = (4.17 * F - 152) / 17.02$
Arnoldus – exponential (1977)	$R = 0.302 * F^{1.93}$
Renard and Freimun – F (1994)	$R = 0.739 * F^{1.847}$
Renard and Freimun – P (1994)	$R = 0.0483 * P^{1.61}$
Lo et al., (1985)	$R = 38.46 + 3.48 * P$
Yu and Rosewell (1977)	$R = 3.82 * F^{1.41}$

Sources: based on Lastoria et al. (2008)

R factor values were determined by averaging all R factor values obtained using all the equations above (Table 7.3) and using the precipitation data that were available from rain gauges in the Blackwater study area (Table 7.4) (Wensum Alliance, 2013). The calculated R factor values for the study area are 113.05 and 92.69 (US units) for the two farming years beginning in September 2011 and September 2012, respectively. Raster maps were generated in ArcGIS with pixel values of 113.05, 92.69 and a cell size of 5 x 5 m. Two other raster were generated with a cell size of 50 x 50 m (same resolution as OS50).

Table 7.4: Monthly precipitation records for Blackwater sub-catchment (mm).

Month	Marham LTA (mm) (data from Met Office)	Wensum monitoring stations	
	1981 - 2010	2011/12	2012/13
Sep	55.3	24.8	41.6
Oct	67.3	35.2	73.6
Nov	62.2	21.2	87.4
Dec	52.7	63.4	82.2
Jan	56.1	56.4	56.6
Feb	39.3	13.6	45.6
Mar	49.1	50.6	75
Apr	47.2	114.6	16.2
May	53.3	54	50.4
Jun	59.2	92.2	22.2
Jul	52.1	85.2	9.8
Aug	58.8	75	60.4
Sep			53.4
Oct			100.4

Sources: Wensum Alliance (2013)

7.3.1.2   Soil erodibility factor (K)

The soil erodibility factor (K factor) measures the susceptibility of soil particles or surface materials to detachment and transportation by the amount of rainfall and runoff input (Renard et al., 1997). Several parameters, namely soil texture, structure, permeability and organic matter content, determines the erodibility of a particular soil (Morgan, 2005). It is known that the most easily eroded soil particles are silt and very fine sand and the less erodible soil particles are aggregated soils because they are accrued together making them more resistible (Kim and Julien, 2006). Morgan (2005) argued that silt loams, loams, fine sands and sandy loams are those most susceptible to erosion.

In (R)USLE five important soil parameters, that is, % silt + very fine sand, % other coarse sand, % organic matter, structure and permeability are used as inputs in calculating soil erodibility (Wichmeier and Smith, 1978). However, the data in the National Soil Map (NatMap) (obtained via the Wensum DTC project from Cranfield University) includes details on texture, but not on permeability, structure and the percentage of silt and very fine sand information which are required in the traditional calculation. However, soil erodibility has also been satisfactorily described by K values derived directly from field measurements of erosion (Morgan, 2005). The index used by USLE, is an universally accepted erodibility index represents the average soil loss for a particular soil with a hypothetical slope length of 22.1 m with steepness of 9% (Table 7.5) (USLE: OMAFRA, 2012).

Inspection of Figure 7.6 indicates that four different soil types dominate the Blackwater sub-catchment. These types include deep loam, deep sandy, seasonally wet deep loam to clay and seasonally wet deep sand.   For this study, K factor values were obtained from Table 7.5, K values for different soil classes as used by USLE (USLE: OMAFRA, 2012; Gitas et al., 2009). After the soil map shapefile was added as a layer into ArcGIS, the soil map attribute table was edited by adding a new field of K values. The K factor used for deep loam

was 0.30, for deep sand was 0.13, for seasonally wet deep loam to clay was 0.20 and seasonally

wet deep sand was 0.04 (Figure 7.7). The map was in vector form and was converted to raster

form with cell size of 5 m and 50 m and reclassified based on K value of each soil class.
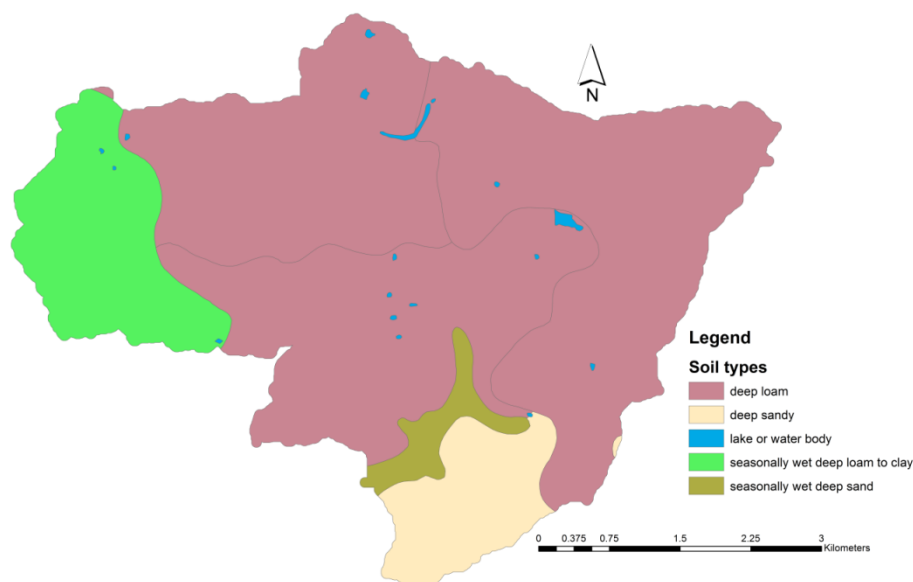
Figure 7.6: Soils map of the Blackwater sub-catchment indicating the different soil types

Table 7.5: K factor values for different soil classes as used by USLE

Textural Class	Average	Less than 2%	More than 2%
Clay	0.22	0.24	0.21
Clay Loam	0.30	0.33	0.28
Coarse Sandy Loam	0.07	- -	0.07
Fine Sand	0.08	0.09	0.06
Fine Sandy Loam	0.18	0.22	0.17
Heavy Clay	0.17	0.19	0.15
Loam	0.30	0.34	0.26
Loamy Fine Sand	0.11	0.15	0.09
Loamy Sand	0.04	0.05	0.04
Loamy Very Fine Sand	0.39	0.44	0.25
Sand	0.02	0.03	0.01
Sandy Clay Loam	0.20	- -	0.20
Sandy Loam	0.13	0.14	0.12
Silt Loam	0.38	0.41	0.37
Silty Clay	0.26	0.27	0.26
Silty Clay Loam	0.32	0.35	0.30
Very Fine Sand	0.43	0.46	0.37
Very Fine Sandy Loam	0.35	0.41	0.33

Sources: USLE: OMAFRA (2012), Gitas et al. (2009)
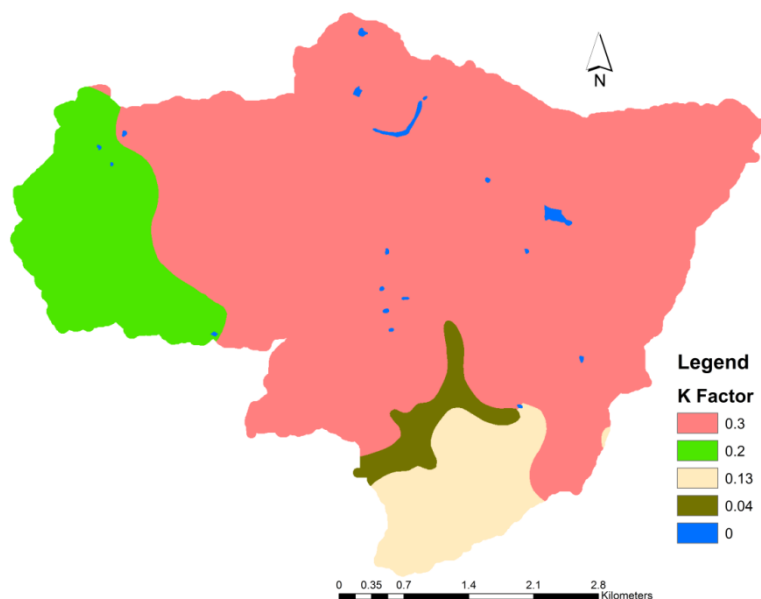
Figure 7.7: K factor raster map

7.3.1.3 Slope length and slope steepness factor (LS)

The topographic factor is a very important parameter in water soil erosion, since gravity force plays a decisive role in surface runoff. The specific effects of topography on soil erosion are estimated by the dimensionless LS factor in USLE, which combines the effects of a slope length factor (L) and a slope steepness factor (S) (Rabia, 2012). Slope steepness is the average gradient of slope between two specified points, usually expressed as a percentage. Slope length as defined by Smith and Wischmeier (1957) is the distance from the point of origin of overland flow to the point where either the slope gradient decreases enough that deposition begins, or the runoff water enters a well-defined channel that may be part of a stream network. In this study, the digital elevation models (DEM) of the study area with a cell size of 5 m (NEXTMap) and 50 m (OS50) were used for the calculation of the LS factor. According to Morgan (2005), in the USLE/RUSLE model, the appropriate value of LS can be obtained from nomographs or from the equation as defined by Wichmeier and Smith (1978) and Renard et al. (1997):

$$LS = [0.065 + 0.0456(S) + 0.006541(S)^2]\left(\frac{L}{constant}\right)^M \qquad \text{(Eq. 7.2)}$$

Where:

$S =$ slope steepness in %

$L =$ length of slope in metre

Constant =   22.1 m (72.5 ft)

$M =$ see Table 7.6

The value of L and S were derived from NEXTMap DEM. To calculate the L value, a flow accumulation raster was derived from the DEM after conducting Fill and Flow Direction processes in ArcGIS 10 (Kamaludin et al., 2013).

$$L = (Flow\ accumulation * DEM\ resolution) \qquad \text{(Kamaludin et al., 2013)}.$$

By substituting L value, LS equation will be:

$$LS = [0.065 + 0.0456(S) + 0.006541(S)^2]\left(\frac{(FlowAcc*DEM\ resolution)}{22.1}\right)^M \qquad \text{(Eq. 7.3)}$$

Slope (%) (Figure 7.8) was also directly derived from the DEM using ArcGIS. The value of M varies from 0.2-0.5 depending on the slope as shown in Table 7.6 (OMAFRA, 2012).

Table 7.6: M values for LS factor

M value	Slope (%)
0.5	>5
0.4	3-5
0.3	1-3
0.2	<1

Sources: Drzewieki et al. (2013), OMAFRA (2012)

Finally, the ArcGIS Raster Calculator function was used to input the modified

equation 7.3 to compute the LS factor (Figure 7.8). Slope of the DEM as a percent and flow

accumulation were employed to implement equation 7.3. DEM resolution of 5m and 50 m
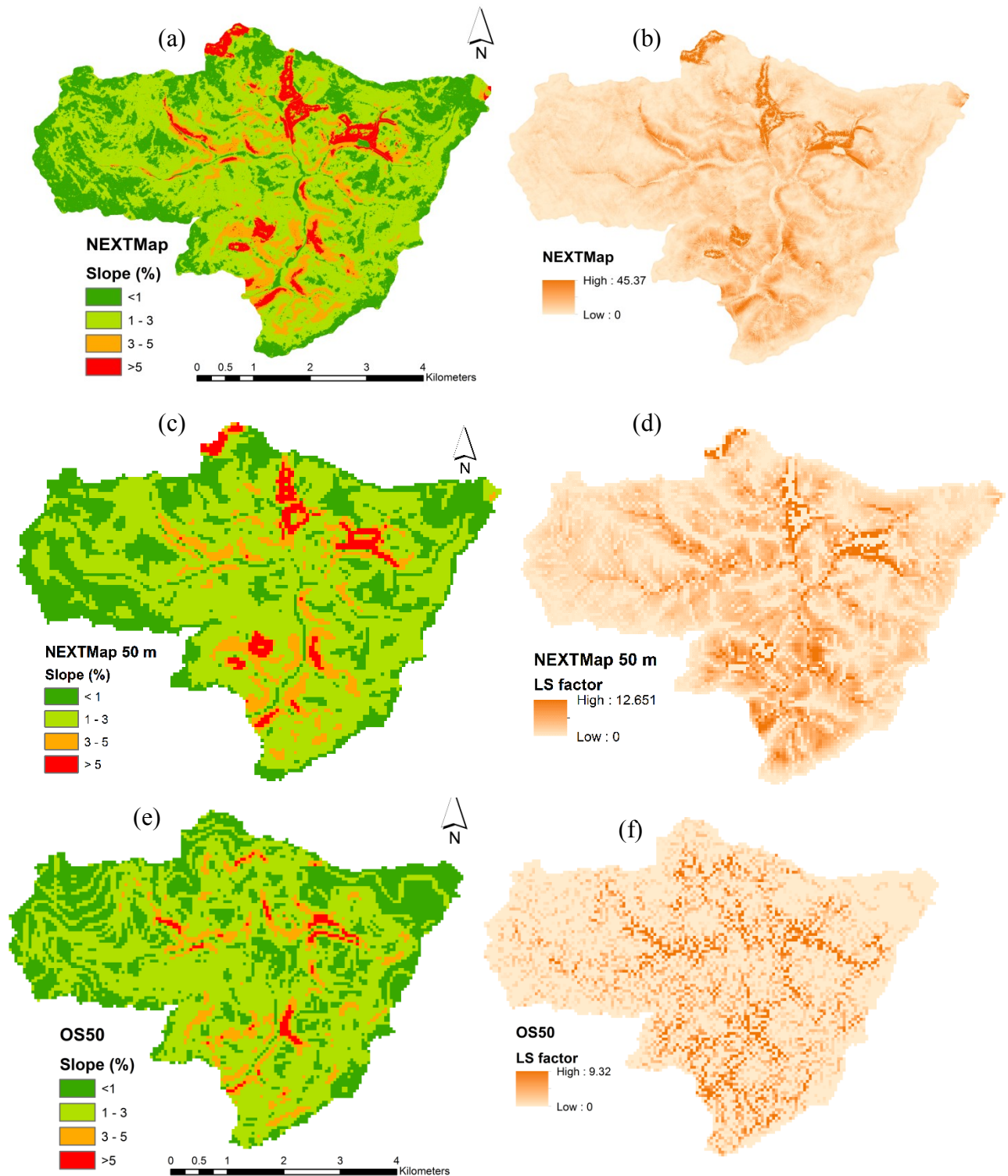
Figure 7.8: Slope (%) (a) and LS-factor (b) from NEXTMap 5m data, (c) and (d) from NEXTMap resampled to 50 m, (e) and (f) from OS50 m data. It is clear that LS-factor is strongly influenced by cell size.

7.3.1.4 Crop management factor (C)

The Crop Management Factor (C) represents the effect of vegetation and management on soil erosion rates. This dimensionless factor measures the ratio of soil loss for a specific crop with given cover management conditions to the soil loss under reference conditions "clean-tilled continuous fallow conditions" (Rabia, 2012). Under clean-tilled, continuous fallow, the value of C-factor is equal to one, and applying the USLE to these conditions will give the maximum possible amount of soil loss from any particular field. The amount of protective coverage of a crop for the surface of the soil influences the soil erosion rate. A C value is lower when there is more coverage of a crop for the soil surface resulting in less soil erosion (Renard et al., 1997). Therefore, as the vegetation cover increases, the soil loss decreases. For this reason, the C-factor is probably the most important factor within the USLE as it is the factor that can be varied most easily by either changing the crop or the cropping conditions.

Since soil loss varies with the percentage of the crop cover, it is necessary to take account of changes during the year to arrive at an annual value. According to Morgan (2005) and Wischmeier and Smith (1978) for arable farming, the year is divided into periods corresponding to different stages of crop growth. These are divided into five distinct growth stages and defined as: (1) fallow, ploughing to seedbed establishment; (2) secondary tillage for seedbed formation to 10 per cent crop cover; (3) establishment, 10 – 50 per cent crop cover; (4) development, 50 – 75 per cent crop cover; (5) maturity, 75 per cent crop cover to harvest. A sixth period can be considered (Morgan, 2005) for the residue after harvesting where three options are available: leaving the residue without seeding; leaving the residue and seeding; or removing the residue and leaving the ground bare.

Calculation of the C-factor using the method described above requires detailed information which does not always exist. For instance, its exact calculation needs an accurate record of the rotation and cultivation practices (Lastoria et al., 2008). The C-factor is one of the hardest factors to define due to the difficulties and expense involved in obtaining the required data. Thus, in such cases it has been suggested that the C-factor values can be assigned within the range of values cited in the literature allocated on the basis of identified cover types and weighted percentage of cover (Csafordi et al., 2012; Hui et al., 2010; Lastoria et al., 2008; Lee, 2004; Ligonja and Shrestha, 2013; Morgan, 2005; Sharma et al., 2011; Smitha and Sobha, 2011).

Some studies, however, have applied remote sensing data to develop values for the C-factor by classifying land cover categories and land use units (Csafordi et al., 2012). Ahmet (2010), Gitas et al (2009) and Kouli et al (2008) have used mid resolution satellite image (e.g. Landsat TM) to estimate the C-factor values by applying the Normalised Difference Vegetation Index (NDVI). The NDVI was used to estimate the C-factor because NDVI can express the condition of vegetation at different stages of growth (Gitas et al., 2009). Schonbrodt et al. (2010) calculated the C-factor using the fractional vegetation cover (FVC), as a function of the NDVI, based on Landsat-TM images and used C-factor values from literature assigned to each specific land use class from a classification based on Landsat-TM 2007 as reference. Other studies have used the satellite images to derived the land use/land cover map and then each of the land use/land cover categories has been assigned a value for the C-factor based on the values cited in literature (Lastoria et al., 2008; Lu et al., 2004; Pandey et al., 2007; Sharma et al,. 2011). Examples of some studies that have adopted remote sensing data to calculate C-factor values are listed in Table 7.7 below.

Table 7.7: Summary of other methods for estimating C-factor value using remotely sensed images.

Reference	Method of estimating C-factor
Bargiel et al., 2013, Poland	Land cover classification based on high resolution radar images.
Lu et al., 2004, Rondonia, Brazil	Remote-sensing Classification image. C-factor was estimated based on the fraction images from Spectral Mixture Analysis (SMA) of Landsat ETM+ image.
Ma et al., 2003, China	Greenness index
Ahmet, 2010, Turky	NDVI $\quad C = 1.02 - 1.21 * NDVI$
Gitas et al., 2009, Greece, Kouli et al., 2008, Greece, Van der Knijff et al., 1999, Itali, and Van der Knijff et al., 2000, Europe	NDVI $\quad C = e^{\left(-\alpha\left((NDVI)/(\beta - NDVI)\right)\right)}$

α, β : Parameters that determine the shape of the NDVI-C curve. According to Van der Knijff et al. (1999, 2000) an α-value of 2 and a β-value of 1 seem to give reasonable results.

7.3.1.4.1 C-factor values for crops in the Blackwater sub-catchment

Having a C-factor value range (from high to low risk depending on the productivity) for each crop in the study area, the accurate estimation of the annual average C-factor value for each crop is primarily based on information on crop rotations and the crop cover percentage on each stage of growth (Wall et al., 2002). Within the Blackwater sub-catchment a variety of crops are grown, each of which is planted and harvested at different times of the year and grows at a different rate. A typical farming year in the UK usually starts in September of one year and finishes in August the following year (farm-direct.co.uk). Based on information obtained from several sources, sowing and harvesting dates for a selection of crops grown in the Blackwater sub-catchment are reported in Table 7.7 below.

Table 7.7: Typical sowing and harvesting dates for a selection of crops grown in the UK.

Crop	Planted	Harvested
Winter Wheat	October	August
Winter Barley	September	July / August
Spring Barley	March / April	August
Oilseed Rape	August	July
Maize	May	September / October
Sugar beet	March / April	September to Christmas
Potatoes	April	August through October
Vining Peas (green harvest)	March to early June	From June until October
Vining Beans (green harvest)	March – April – May	within 15 weeks
Winter Beans Dried	October	September
Spring Beans Dried	March	September/October

Sources: based on Defra, (2005), UKAgriculture.com, Twining and Clark, (2009).

It is known that the amount of time arable land is bare and the growth rates of crops both influence soil erosion risk. For example, maize is harvested in the autumn and then fields of bare soil are often left exposed to autumn and winter rainfall which will significantly increase the soil erosion risk (Inman, 2006). Moreover, soil erosion risk at a point will be affected not only by the crop cover of the year in question, but also by past land use and land cover. Due to data availability from farm records available via the Wensum DTC project the two farming years of 2011/12 to 2012/13 were chosen for investigation. Example data of crop rotations for three years in fields within the study area is reported in Table 7.8 below.

Table 7.8: An example of three year crop rotations for some fields in the study area

Field Name	2010-2011	2011-2012	2012-2013
100 Acres	Dwarf French Beans Winter Oilseed Rape	Winter Wheat Winter Wheat	Winter Barley
11 Acres	Spring Barley	Spring Barley	Winter Barley
14 Acres	Spring Barley	Spring Barley	sugar beet
8 Acres & Long Meadow	Winter Barley	Winter Oilseed Rape	Winter Wheat
24 Acres	Winter barley	Winter Oilseed Rape	Winter Wheat
4 Acres	Spring Barley	Spring Barley	sugar beet
40 Acres	Spring barley	Winter Barley	Forage Maize Spring Barley
60 Acres	Winter wheat	Winter Barley	Winter Oilseed Rape
64 Acres	Winter Barley	Winter Barley	sugar beet
70 Acres	Winter Barley	Spring Barley Winter Barley	Winter Barley
Homefield & Meadow	Spring Barley	Spring Field Beans Winter Oilseed Rape	Winter Wheat
Long Meadow	Winter Barley	Spring Field Beans	Winter Wheat
Next House	Grass Ley	Grass Ley	Grass Ley

Source: Wensum DTC (2013).

As mentioned previously, the C-factor value depends on vegetation type, stage of growth and crop cover percentage at each stage (Gitas et al., 2009). However, the crop cover percentage varies significantly over the year depending on factors such as: the crop type (winter barley and oilseed rape are generally established earlier than winter wheat), the rate of the growth for each different crop (oilseed rape is known to experience a period of very rapid growth between May and June whereas winter wheat grows at a much more constant rate over the course of the year), and also the climate of the area (temperature) which affects the duration of all crop development phases (Defra, 2005; HGCA: the wheat growth guide, 2008).

The method that is suggested by Morgan (2005) and Wischmeier and Smith (1978) for estimating the C-factor value using the six crop stage periods (mentioned above) is very useful because it considers the percentage of crop cover at each stage of growth during the

whole farming year. However, information about the timing of each crop stage development and the percentage of crop cover at each stage during the farming year are not routinely collected by farms in the study area. Moreover, length of the respective periods usually varies a lot with crop, farms, climate and management (Morgan, 2005; Wischmeier and Smith, 1978). Thus, as this information was not available, the C-factor calculation method discussed above was not used for the estimation of the C values in our study.

Alternatively, as has been widely used in other research, the C-factor can be attributed to all the occurring land use types according to the values cited in the literature (Hui et al., 2010; Lastoria et al., 2008; Lu et al., 2004; Ligonja and Shrestha, 2013; Pandey et al., 2007; Sharma et al,. 2011). Therefore, a range of the C-factor values that are reported in the literature from all over the world, especially Europe, USA and Canada, were collected (Table 7.9). The median values were then chosen and allocated to each corresponding land use class occurring in the study area (Table 7.10).

Table 7.9: Crop management factor (C-factor) for different land use/land cover categories cited in the literature.

Reference	Crop type										
	Maize	Sugar Beet	Peas	Beans	Potatoes	Wheat	Barley	Oilseed Rape	Grass	Woodland	Urban
Bargiel et al. (2013), Poland	0.68	-	-	-	0.58	-	-	-	-	-	-
Drzewiecki et al. (2013), Poland	0.22	0.22	0.22	0.22	0.22	0.15ww-0.18sw	0.15wb-0.18sb	0.15wr-0.18sr	-	-	-
Fernandez et al. (2003) Lawyers Creek Watershed, Idaho	-	-	-	-	-	0.234	0.05sb	-	-	-	-
Friedli (2006), Germany (No-Tillage)	0.119	-	0.08	0.054	0.097	0.092	0.028	-	-	-	-
Gonzales Inca C. (2009), Peru	-	-	-	0.5	0.56	0.26	0.35	-	-	-	-
Kinnell (2005), Bethany, Missouri	-	-	-	-	-	0.11	-	-	-	-	-
Morgan (2005)	0.2-0.9	-	-	-	0.2-0.5	0.1-0.4	-	-	0.01	0.001	0.0
MUNLV NRW (2007), Germany	0.5	-	-	-	0.47	0.1	0.06wb	0.11	-	-	-
Owusu (2012), Ghana	0.63	-	-	-	-	-	-	-	-	-	-
Thuringian State Institute of Agriculture (TLL), Germany	0.35	0.32	0.2	0.2	0.29	0.12	0.07wb-0.15sb	0.07	-	-	-
Suri et al. (2002), Slovakia	0.6	0.44	0.3	0.3	0.6	0.13	0.13sb	0.22	-	-	-
Svetla Rousseva, 2003, Bulgaria	0.5	-	-	-	0.69	0.28	-	-	-	-	-
Wall et al. (2002), Alberta ,Prairie region, Canada	0.57	0.5	0.48	0.48	0.42	0.34	0.32	0.3	-	-	-

Table 7.10: The median of the C-factor values for each crop reported in Table 7.9 above.

	C-factor
Crop type	Median
Maize	0.53
Potatoes	0.45
Sugar beet	0.38
Beans	0.26
Peas	0.22
Winter Wheat	0.165
Oilseed rape	0.165
Spring Barley	0.15
Winter Barley	0.11
Grass	0.01
Woodland	0.001
Urban	0
Water bodies	0

The relative order of crops according to the associated erosion risk (high to low) when the median values were selected (Table 7.10 above) is consistent with the relative order of the C values calculated by Suri et al. (2002) (Table 7.11 below). These values have been used in several nationwide soil erosion assessments in EU member states such as the Sustainable Agriculture and Soil Conservation (SoCo) project, 2009.

Table 7.11: C-factor values for main crop groups from Suri et al. (2002).

Crops	**C-factor**
Sunflower	0.65
Grain Maize	0.6
Potatoes	0.6
Vegetables	0.5
Forage maize	0.45
Sugar beet	0.44
Legumes	0.3
Other crops	0.3
Oil rape	0.22
Several year forage crops	0.15
Cereals	0.13
One year forage crops	0.10

Therefore, from the above discussion the C factor values reported in Table 7.10 are considered realistic and were used in this study. Figures 7.9 and 7.10 illustrate the C factor distribution for the farming years of 2011/12 and 2012/13 respectively. However, as mentioned before, determination of the C-factor value for agricultural crops required detailed research about the pattern of anti-erosion protection offered by each crop at different stages of growth and the reduction in erosion caused by surface cover. In addition, previous cropping and management practices should be taken into account as well as monthly changes of the rainfall erosivity factor. In some countries, C-factor values resulting from such research for the most popular crops and crop rotation practices are tabulated. For conditions in the UK, this kind of information describing the full crop rotations has not yet been elaborated. These are the reasons behind the assumptions in assigning C-factor values for each crop in this study.
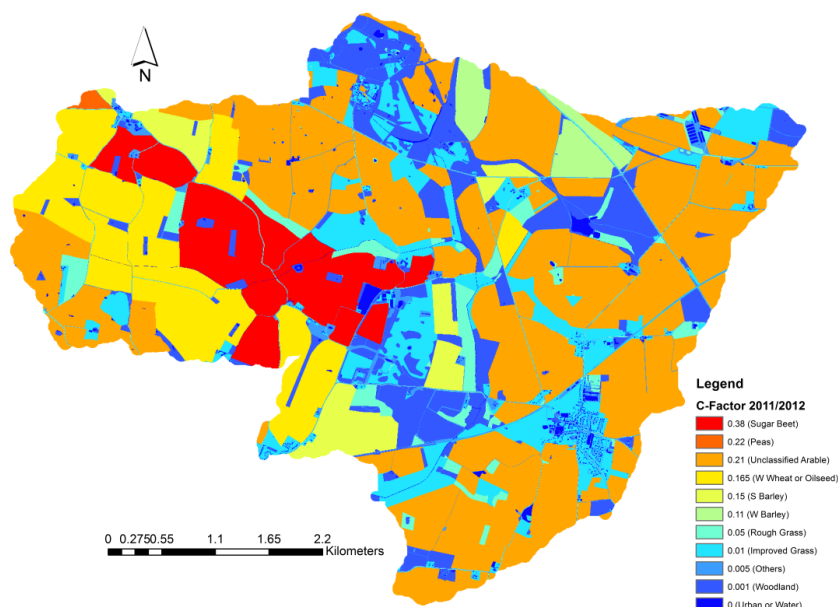
Figure 7.9: C factor raster map (5 x 5 m) for the farming year of 2011/12
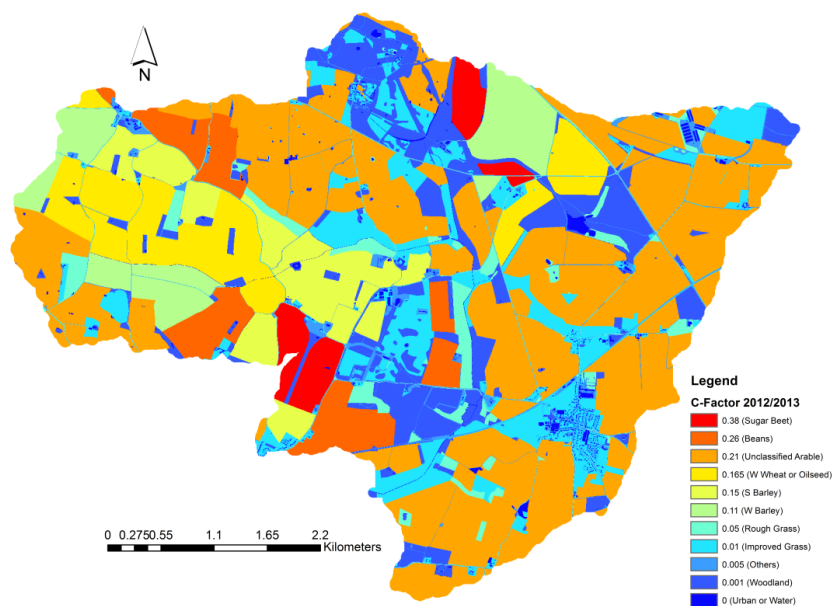
Figure 7.10: C factor raster map (5 x 5 m) for the farming year of 2012/13

7.3.1.5 Support practice factor (P)

The support practice factor (P), as defined by Wischmeier and Smith (1978), is the ratio of soil loss with a specific support practice to the corresponding loss with up and down slope cultivation. This factor considers any practice applied by humans to reduce erosion degree and soil loss amount deriving from water erosion processes. Therefore, the P value is equal to 1 when the land is ploughed directly down slope. This is also known as the worst practice. A P value is lower and less than one when the adopted conservation practice reduces soil erosion (Renard et al., 1997). Support practices (P) are designed to reduce erosion by slowing the rate of runoff water, thereby reducing its transport capacity and erosive power. The most common practices usually include cross slope cultivation, contour farming, strip cropping, terracing (Wall et al., 2002). It has been argued that the P factor is the most difficult factor to be determined and the least reliable of the USLE input factors (Hui et al., 2010). The values of P-factor based on the most used basic support practices in USLE/RUSLE (Wall et al., 2002; Wischmeier and Smith,1978) are shown in Table 7.12 below.

Table 7.12: P Factor Data.

Support Practice	P Factor
Up & down slope	1.0
Cross slope	0.75
Contour farming	0.50
Strip cropping, cross slope	0.37
Strip cropping, contour	0.25

Source: Gitas et al. (2009), OMAFRA, (2012),
Wall et al. (2002)

For the study area, according to Hughes (2012), cross slope cultivation is used in the Wensum catchment. Moreover, in some parts of the study area (Salle farm), the Entry Level Scheme (ELS) allows for a six metre margin alongside all water courses on cultivated land and also contour ploughing is adopted in areas where greatest run off risks are likely to occur (Wensum Alliance, 2013; Hiscock, 2011). Therefore, and according to Table 7.12, the P factor for the cultivated land was chosen to be the average value of 0.75 (cross slope) and 0.50 (contour farming) which is 0.625. Due to the lack of more information about the cultivation methods in the study area this value was used for all cropland in this study to begin with (later in this study, the influence of different cultivation methods on soil losses has been analysed, Section 7.3.6). Other lands such as forest and urban were assigned to one because there are no support practices (Drzewiecki et al., 2013; Lee, 2004), whereas water was allocated a 0.01 P factor (Ligonja and Shrestha, 2013; Teh, 2011). Figure 7.11 illustrates the P factor distribution in the Blackwater sub-catchment.
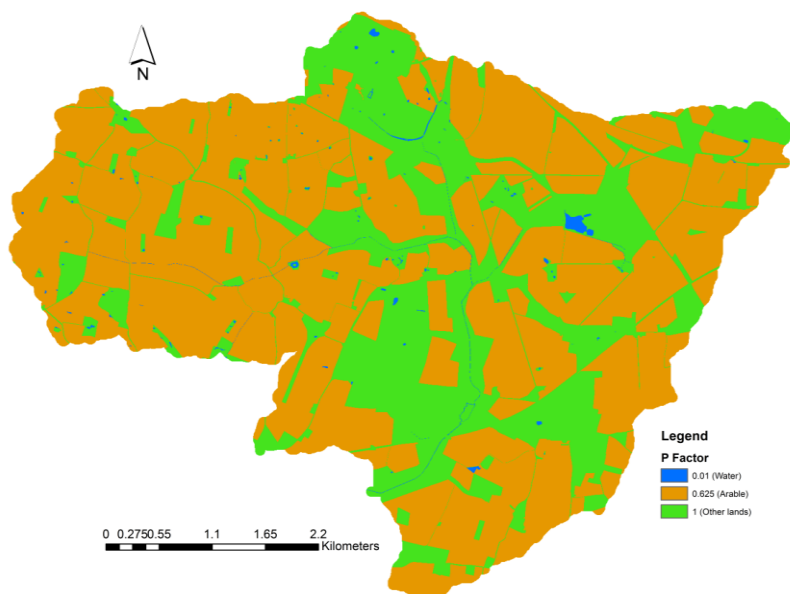
Figure 7.11: P factor raster map (5 x 5 m)

7.3.2 Production of USLE maps

In this study, the RUSLE was applied in a GIS environment to determine the average annual soil loss and its distribution in the Blackwater sub-catchment using two different DEMs with different spatial resolutions (5m and 50m). First of all, the RUSLE parameters determined for the study area were converted into raster maps using the cell size defined by each DEM (5m for NEXTMap and 50m for OS50). Then, all these parameters, the erosivity factor (R), soil erodibilty factor (K), topography factor (LS), cover management factor (C) and support practice factor (P), were multiplied using the Raster Calculator tool of ArcGIS for the two farming years of 2011/12 and 2012/13. In other word, the final RUSLE soil erosion risk estimation map using each DEM was produced by multiplying corresponding grid cells from each of the five factor maps as defined in the RUSLE (Eq. 2.2, Chapter 2).

7.3.3 Results

As the RUSLE was applied for two different seasons, the value of crop management factor (C) changed according to the crop rotation used in the study area and also the erosivity factor (R) which depends on rainfall intensity and amount during each season. The other three RUSLE perameters (LS, K and P) remained constant. Moreover, when a different DEM was used, the LS factor changed as the local slope and aspect values alter (Zhang et al., 2008). Thus, the result of RUSLE implimentation in the raster geographic domain for the two seasons comprised the following:

- Two maps of soil erosion risk (in tonnes/ha/year) for the study area, one for each farming year (2011/12 and 2012/13).

- Two tables, one is where the area (in hectares) covered by every class of erosion risk severity is presented and the other represents area (in hectares) and minimum, maximum and mean soil erosion risk (in tonnes/ha/year) for each land use category.

Initially, the erosion maps gave each individual cell's original value of soil erosion risk as derived from the implementation of RUSLE equation. However, in order to obtain a better view and understanding and at the same time be able to compare risks between the different seasons for each class of erosion risk severity or each land use category, these original values were classified into six classes of severity based on the soil loss tolerance (1 tonne/ha) suggested by Morgan (2005) and also classification from other relevant studies (e.g. Bargiel et al. 2013; Cerdan et al. 2010; OMAFRA, 2012; Tatzlaff et al. 2013; Verheijen et al. 2009). They were finally presented in a colour scheme of green (low risk) to red (high risk) in all the maps.

7.3.3.1   NEXTMap data

7.3.3.1.1   Farming year 2011/12
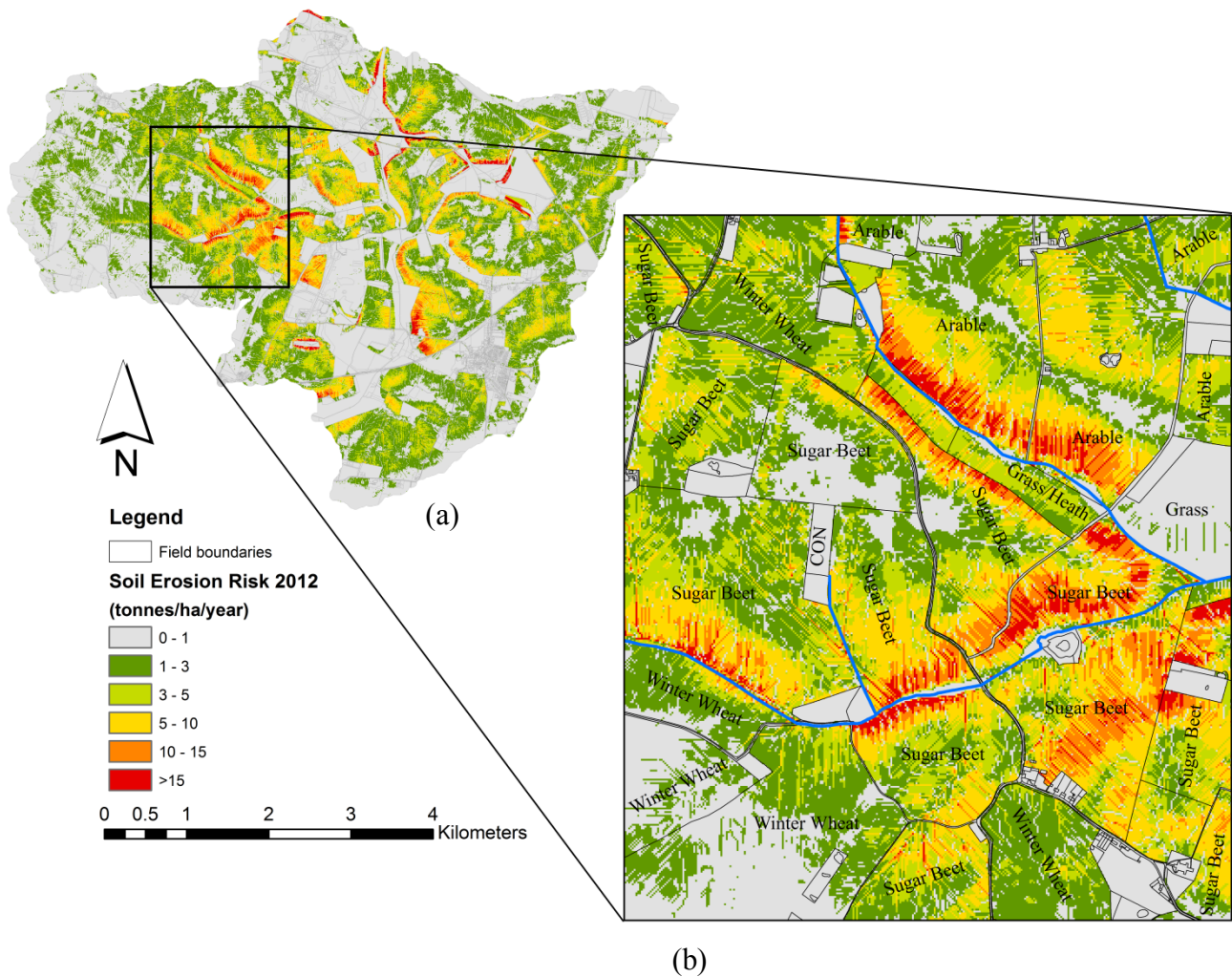
Figure 7.12: Soil erosion risk map for Blackwater sub-catchment. Farming year 2011/12 - NEXTMap

Table 7.13: Assessed soil erosion intensities for Blackwater study area. Farming year 2011/12 – NEXTMap

Soil erosion risk (tonne/ha/year)	Area (ha)	Share of total area (%)	Erosion risk category
0-1	2366.065	87.86	Very Low
>1-3	230.6575	8.57	Low
>3-5	59.6625	2.22	Medium
>5-10	28.825	1.07	High
>10-15	4.775	0.18	Very High
>15	2.8875	0.11	Extreme

Table 7.14: The annual soil loss rates based on the land use for
Blackwater study area. Farming year 2011/12 – NEXTMap

Crop	Area (ha)	Share of total area (%)	Soil erosion risk (tonne/ha/year)		
			Min	Max	Mean
Arable	1836.06	68.18	0.00	200.05	2.35
Grass	409.54	15.21	0.00	107.73	1.97
Others	77.70	2.89	0.00	7.44	0.16
Woodland	335.89	12.47	0.00	3.45	0.04
Urban	19.83	0.73	0.00	0.00	0.00
Water	13.76	0.52	0.00	0.00	0.00

Figure 7.12 (a and b) and Tables 7.13 and 7.14 present the annual soil loss rates for the Blackwater sub-catchment for the farming year of 2011/12 using the 5m spatial resolution DEM (NEXTMap). These maps offer a quick overview of the soil erosion rate caused by sheet and rill erosion for the study area. These maps also reveal the spatial locations of the high soil erosion risk areas. Based on this analysis, the amount of soil loss in the sub-catchment varies from 0 to 200.05 (tonne/ha/yr) due to variation in soil erodibility (K), slope (LS) and crop management (C) factors. As shown in the figures and tables, the highest mean value of the annual soil erosion rate calculated in the Blackwater were obtained for arable land with 2.35 (tonne/ha/yr), whilst the lowest contributors of soil erosion are urban and water bodies with mean value of zero (tonne/ha/yr). In general, it is unreasonable to assume that urban areas will have a zero soil loss contribution, however, urban areas represent less than 0.7% (19.83 ha) of the total area of the sub-catchment and therefore have insignificant impact on the total soil erosion, thus this result is acceptable. It should be noted that the C-factor value for urban land use category was assumed to be zero (Table 7.10). The enlarged sub-catchment section shown in Figure 7.12b reveals that the soil erosion risk is typically greater along the relatively steep slope areas along the river at the edges of adjacent crop fields. Agricultural land on flat terrain, grass and woodland are shown to be the least vulnerable to

soil erosion, apart from the other land cover (urban and water) which gave the value of zero soil erosion.

The results show that, the very low class of erosion risk severity (0 to1 tonne/ha/year) occupies 87.88% of the study area (Table 7.13), these areas are usually arable with very low slope gradient (low LS), grass, woodland, urban and water bodies. High and very high classes occupy only about 1.20% of the study area and are found in the areas with combinations of greater inclinations (large values of LS), in comparison with other areas, and cropped with crops associated with a high erosion risk (higher C value) such as sugar beet (Figure 7.12b). Evans (2002) has argued that, sugar beet is one of the crops that causes high rates of erosion risk. These results are in agreement with findings reported by Andrade et al. (2010) and Hoyos (2005). Generally speaking, steeper slopes have a greater potential to erode wherever they coincide with croplands which in turn increases the soil erosion risk (Volk et al., 2010). Thus, topography played a secondary role, since on steep slopes (higher LS values), soil erosion was predicted to be very low under grass and woodlands, but high under croplands. These results are consistent with Mati et al (2000), who proposed that on steep slopes, erosion was very low under natural forests and grasslands, but high under cultivated land. Hoyos (2005) also conclude that regardless of the topography and erodiblity, low erosion occurred in areas under forest, shrub and pasture. Therefore, arable lands are more susceptible to erosion because they are repeatedly tilled and often are left bare between the planting of different crops (crop rotations).

The maps show particularly well the influence of land use (C factor) and topography (LS factor) on erosion risk rates, however, although there is an effect of soil erodibility (K factor) and conservation support practices (P factor) on soil loss estimation, they are spatially difficult to differentiate for the following reasons. First, the Blackwater sub-catchment is dominated by one soil type (deep coarse loamy soil), roughly covering 80% of

the sub-catchment area (Figure 7.6). A small part to the west boundary of the sub-catchment

is covered by clay loam soil with gentle topography which favours mostly low erosion rates.

Secondly, regarding the conservation practices (P factor), under arable land the P-factor was

assumed to be constant by adopting a combined cross slope and contour farming practice on

all croplands across the sub-catchment (P = 0.625) (see Section 3.7.1.5).

7.3.3.1.2 Farming year 2012/13

To evaluate the effect of crop rotations (C factor) and rainfall erosivity (R factor)

between different seasons on soil erosion rates, the LS, K and P factors remained the same

while the C and R factors for the farming year of 2012/13 were used. Results are presented in

Figures 7.13 (a and b) and Tables 7.15 and 7.16. It is clear from the figures and tables that

mapping where erosion took place in the sub-catchment and estimating rates of erosion for the

areas affected showed that, compared to rates obtained for the year of 2011/12, the areas

categorized as very low soil erosion rate slightly increased, from 87.86 to 91.97 % out of the

total sub-catchment area (Tables 7.13 and 7.15). Moreover, the maximum soil erosion rate

decreased from 200.05 tonne/ha/yr for the farming year of 2011/12 to 185.91 tonne/ha/yr for

the farming year of 2012/13.

When looking into the comparison results obtained for the two different seasons, the

influence of the crop rotations (lower C values compared to the previous season) is evident.

As the data indicate (Table 7.10), there is no doubt that woodlands and well managed

grasslands protect the soil better and cause less erosion than seasonal crops. Crops like maize,

potatoes or sugar beet are known to cause more erosion than wheat, barley or oilseed rape

(Boardman et al., 2009; Defra, 2005; Evans, 2002). In this study, when the arable land use for

some fields was changed from sugar beet in season 2011/12 to winter wheat and spring barley

in the following season (2012/13) (Figures 7.12b and 7.13b), it is clear that the severity of soil

erosion risk was decreased in these fields. Furthermore, in our study, the values of C factor ranges from zero to 0.53 during both seasons, but their spatial distributions are different because of changes in the land use according to the crop rotation system. According to Table 7.10, sugar beet has a C value of 0.38, which is relatively high in comparison to those for winter wheat (0.165) and spring barley (0.15). Thus, targeting highly erodible cropland by changing from higher risk cultivation (i.e. maize, potatoes or sugar beet) to lower risk activities (i.e. wheat, barley or oilseed rape) would have the potential to reduce the annual soil loss rate (Boardman et al., 2009; Inman, 2006; Schonbrodt et al., 2010). However, it should be kept in mind that there was an assumption in allocating C factor values for each crop in this study. As discussed previously, since there are no studies available that describe them in the UK, the C factor values generated in this study were within range of values cited in the literature especially from Europe, USA and Canada.

Table 7.15: Assessed soil erosion intensities for Blackwater study area. Farming year 2012/13 – NEXTMap

Soil erosion risk (tonne/ha/year)	Area (ha)	Share of total area (%)	Erosion risk category
0-1	2476.73	91.97	Very Low
>1-3	165.83	6.16	Low
>3-5	29.92	1.11	Medium
>5-10	13.68	0.51	High
>10-15	3.12	0.12	Very High
>15	3.59	0.13	Extreme

Table 7.16: The annual soil loss rates based on the land use for Blackwater study area. Farming year 2012/13 – NEXTMap

Land use	Area (ha)	Share of total area (%)	Soil erosion risk (tonne/ha/year)		
			Min	Max	Mean
Arable	1840.51	68.35	0.00	185.91	2.30
Grass	405.09	15.04	0.00	88.32	1.59
Others	77.70	2.89	0.00	6.10	0.13
Woodland	335.89	12.47	0.00	2.83	0.04
Urban	19.83	0.73	0.00	0.00	0.00
Water	13.76	0.52	0.00	0.00	0.00
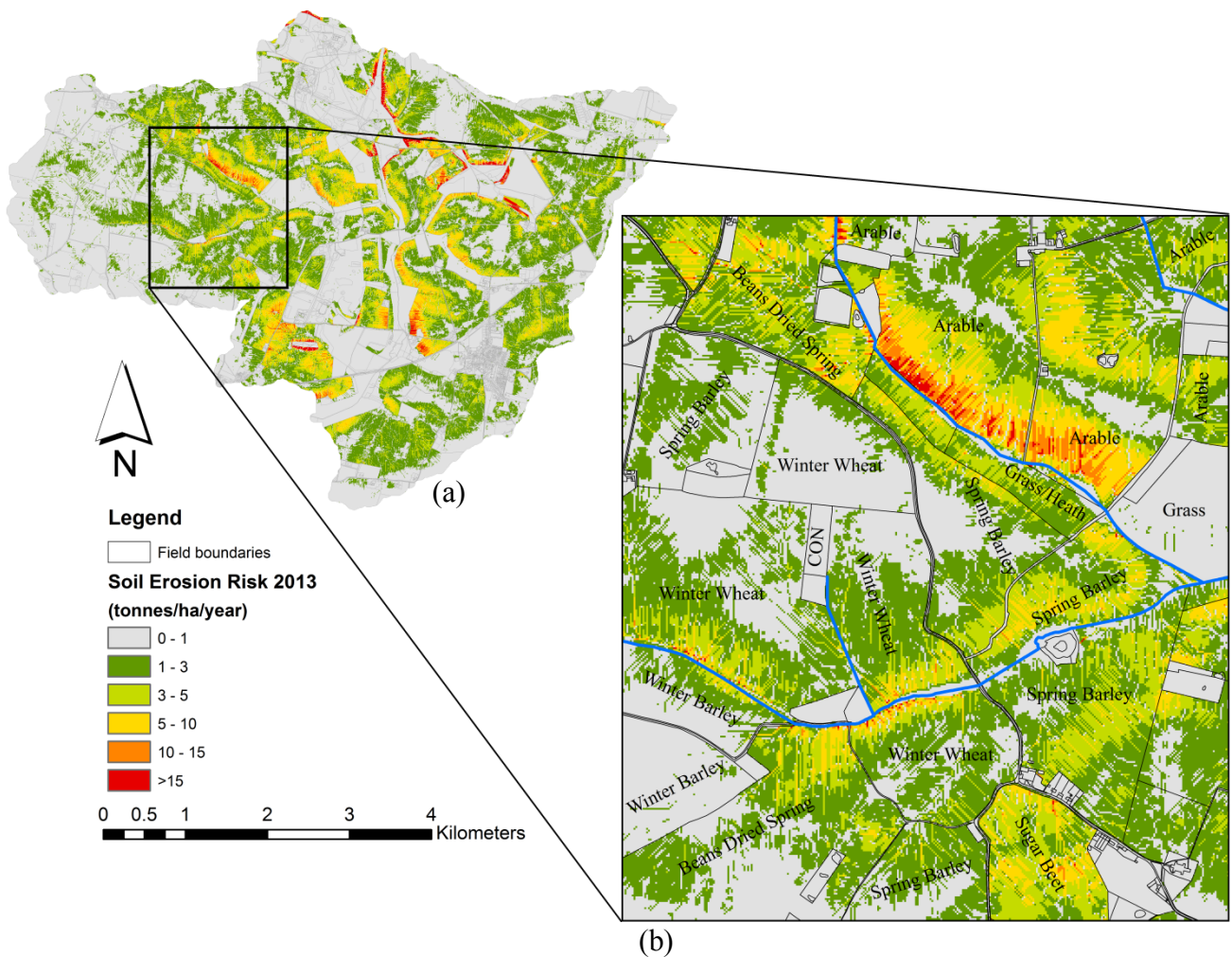
Figure 7.13: Soil erosion risk map for Blackwater sub-catchment. Farming year of 2012/13 - NEXTMap

In addition to the observed effect of crop rotation on the soil loss erosion risk between the two seasons, the effect of the difference in the rainfall erosivity factor (R) should be considered. It has been argued that there is a close correlation between the rainfall characteristics and soil loss (Pandey et al., 2007). Thus, an increase in the rainfall intensity and amount is generally accompanied by an increase in soil erosion. Therefore, the higher value of R factor (113.05) for the season of 2011/12 compared to 92.69 for the season of 2012/13 also makes a contribution to the higher estimates of soil erosion risk in the sub-catchment during the 2011/12 season. For example, the estimated amount of soil that was eroded from the entire sub-catchment was 2782.11 (metric ton/yr) for season 2011/12 and 2650.64 (metric ton/yr) for season 2012/13 (Table 7.17). This can be attributed to the effect of crop rotations (C factor) as well as the effect of the relatively high mean annual rainfall during the first season.

Table 7.17: Estimated amount of soil eroded from the entire Blackwater catchment for the two seasons

	Estimated soil losses from the whole sub-catchment (metric ton/yr)		
Season	R-factor	NEXTMap	OS50
2011/12	113.05	2782.11	1341.59
2012/13	92.69	2650.644	1311.685

However, it should be noted that rainfall erosivity (R factor) is an estimated value that depends on the amount of precipitation within the sub-catchment over the whole farming year. In other word, according to the R-values obtained, on average, season 2011/12 (R = 113.05) is wetter than season 2012/13 (R = 92.69), but actually there were months in the second season were associated with heavy rainfall. For example; the rainfall level in September, October, November and December for season 2012/13 was as much as twice the rainfall amount in the same months for the first season (Table 7.4). Thus, the average monthly rainfall over the autumn and the winter months of season 2012/13 is higher than that for the

first season, those months where the ground was likely to be bare. The effect of these differences in rainfall on the soil loss was not considered as the R factor was calculated based on an annual rainfall erosivity indicator which is originally based on the sum of monthly rainfall index (Section 7.3.1.1) for the whole farming year (Nigel and Rughooputh, 2010). This is a drawback of the RUSLE as it is not feasible to estimate soil loss for individual storm events and was primarily designed for calculating long-term average annual rates of erosion (Csafordi et al., 2012).

7.3.3.2   OS50 data

7.3.3.2.1   Farming year 2011/12

Figure 7.14 and Tables 7.18 and 7.19 illustrate the results of the RUSLE analysis of the Blackwater sub-catchment for the farming year of 2011\12 using the 50 m resolution DEM (OS50), whereas Figure 15 and Tables 7.20 and 7.21 present the results for season 2012\13. In general, the spatial distribution of the soil erosion risk in the Blackwater sub-catchment that was obtained using the 50 m resolution DEM follows the same pattern that was achieved when the higher resolution DEM (5 m) was used. However, maximum and mean values of the soil loss rates for each land use category are much lower compared to the same values that were obtained when the higher resolution DEM was used. For example, the average annual soil erosion loss from arable land is 1.19 tonne/ha/yr, but soil loss may range from zero to 83.31 tonne/ha/yr, due to variation in crop management (C), topographic (LS) and, with lesser effect, soil erodibility (K) factors (Table 7.19). These values were much higher when NEXTMap data were used (Table 7.14 and 7.16). Molnar and Julien (1998) compared soil loss erosion on different grid cell size and they concluded that large grid cell sizes underestimate soil losses because of the terrain slope effects.
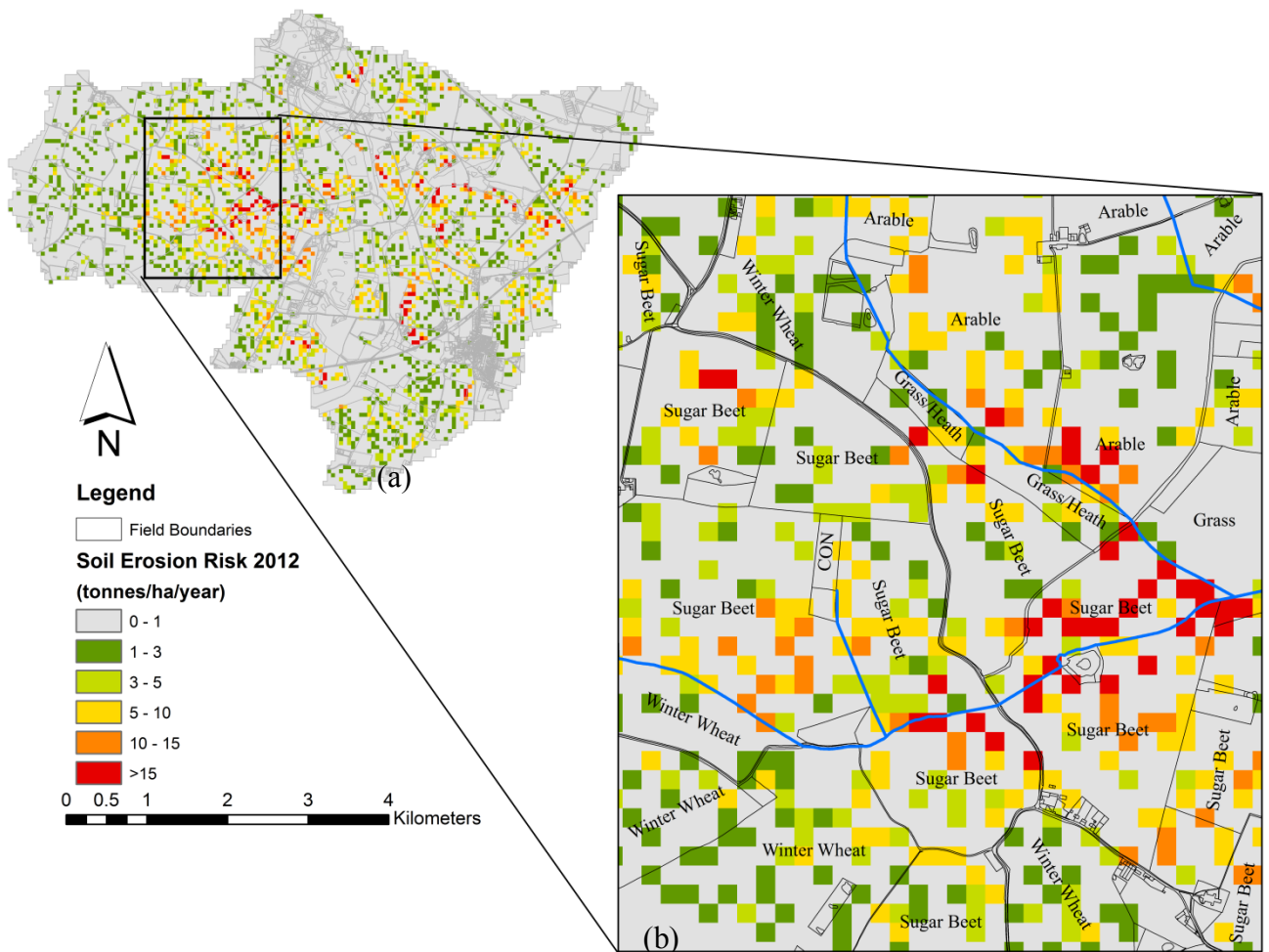
Figure 7.14: Soil erosion risk map for Blackwater sub-catchment. Farming year 2011/12 –

Table 7.18: Assessed soil erosion intensities. Farming year 2011/12 – OS50

Soil erosion risk (tonne/ha/year)	Area (ha)	Share of total area (%)	Erosion risk category
0-1	2400.5	92.60	Very Low
>1-3	111.25	4.29	Low
>3-5	47.25	1.82	Medium
>5-10	26.5	1.02	High
>10-15	4.5	0.17	Very High
>15	2.25	0.09	Extreme

Table 7.19: The annual soil loss rates based on the land use. Farming year 2011/12 – OS50

Land use	Area (ha)	Share of total area (%)	Soil erosion risk (tonne/ha/year)		
			Min	Max	Mean
Arable	1760.79	67.92	0.00	83.31	1.19
Grass	400.64	15.46	0.00	26.63	0.78
Others	74.87	2.88	0.00	0.87	0.04
Woodland	320.92	12.38	0.00	0.47	0.02
Urban	18.62	0.71	0.00	0.00	0.00
Water	16.59	0.64	0.00	0.00	0.00

7.3.3.2.2 Farming year 2012/13
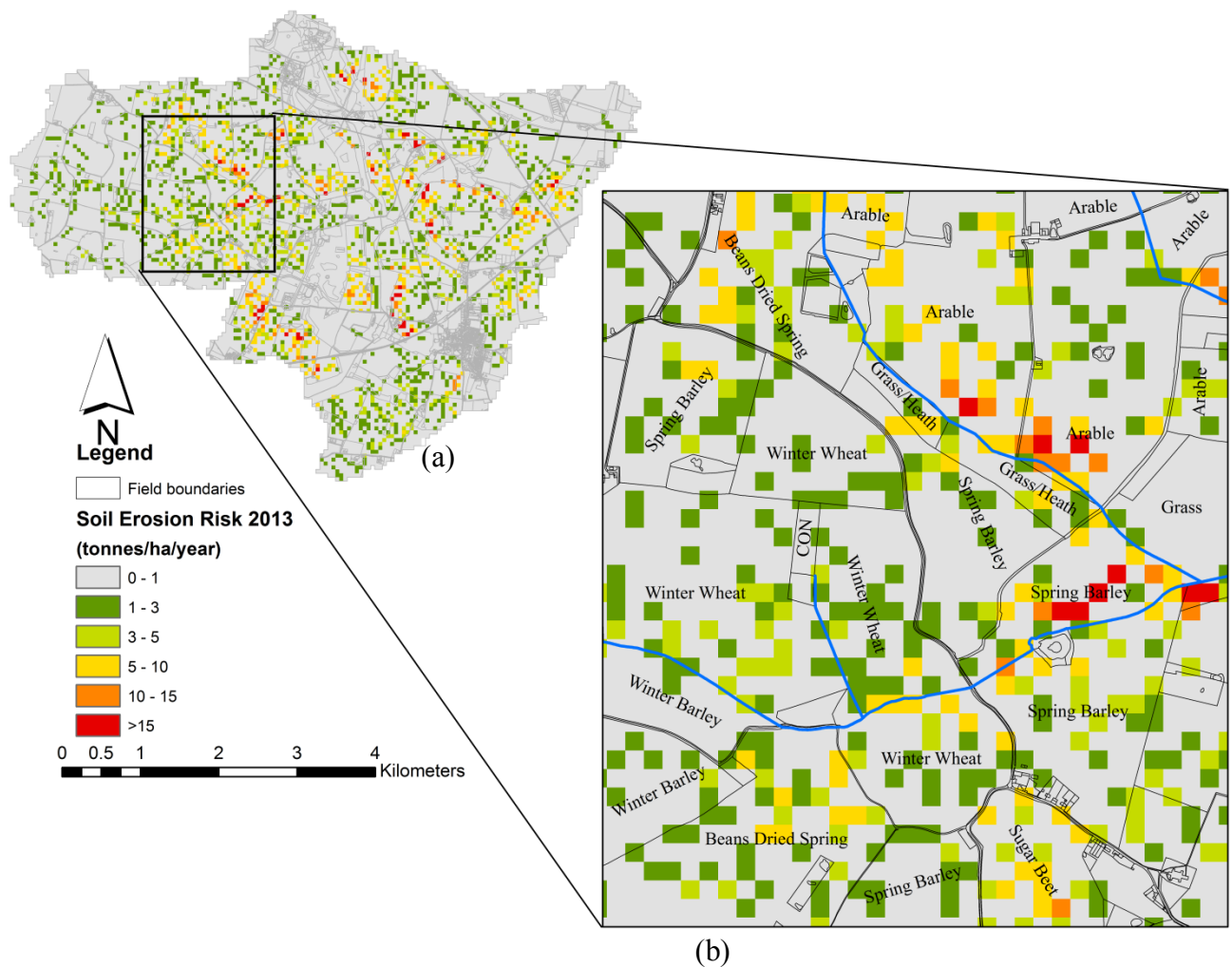
Figure 7.15: Soil erosion risk map for Blackwater sub-catchment. Farming year 2012/13 – OS50

Furthermore, it is clear from Figure 7.15 and Tables 7.20 and 7.21 that all values of the soil erosion rates, mean and maximum, for each land use category obtained for the season 2012\13 are slightly lower than those for season 2011\12. This could be attributed to the fact that season 2011\12 was overall wetter (R=113.05) than season 2012\13 (R= 92.69). However, some other factors could contribute to these findings such as the number of fields that were cropped with crops that are classified as highly susceptible to erosion e.g. sugar beet and potatoes (Defra, 2005) in each season.

Table7.20: Assessed soil erosion intensities. Farming year 2012/13 – OS50

Soil erosion risk (tonne/ha/year)	Area (ha)	Share of total area (%)	Erosion risk category
0-1	2450.25	94.52	Very Low
>1-3	92.5	3.57	Low
>3-5	31.5	1.22	Medium
>5-10	16.25	0.63	High
>10-15	1	0.04	Very High
>15	0.75	0.03	Extreme

Table 7.21: The annual soil loss rate based on the land use. Farming year 2012/13 – OS50

Land use	Area (ha)	Share of total area (%)	Soil erosion risk (tonne/ha/year)		
			Min	Max	Mean
Arable	1765.2	68.10	0.00	40.20	1.12
Grass	396.2	15.29	0.00	21.84	0.65
Others	74.9	2.88	0.00	0.71	0.04
Woodland	320.9	12.38	0.00	0.39	0.01
Urban	18.6	0.71	0.00	0.00	0.00
Water	16.6	0.64	0.00	0.00	0.00

7.3.3.3 NEXTMap data downsampled to a coarser resolution DEM (50 m)

To examine the impact of DEMs from the same source with different resolutions on soil erosion calculations, the NEXTMap 5-m data were resampled to a coarser resolution at 50-m grid scale. There are three commonly used DEM resampling methods, nearest neighbor, bilinear, and cubic interpolation methods. Previous research (Hail and Rientjes, 2005; Wu et al., 2005) concluded that methods of resampling do not significantly influence the quality of resampled DEMs. However, bilinear resampling technique is the most suggested method when using continuous data such as DEM, therefore it was used here (Usery et al., 2004).

Figure 7.16 and Tables 7.22 and 7.23 illustrate the results of the RUSLE analysis of the Blackwater sub-catchment for the farming year of 2011\12 using the 50 m resampled NEXTMap DEM (NEXTMap 50-m). In general, it is clear from the map that the spatial distribution of the soil erosion risk in the Blackwater sub-catchment obtained using the 50 m resolution DEM follows the same pattern that was generated when the higher resolution DEM (5 m) was used. However, maximum and mean values of the soil loss rates for each land use category are much lower compared to the same values that were obtained when the higher resolution DEM was used, but slightly higher than those obtained from the other 50-m resolution DEM (OS50 m) (Tables 7.19 and 7.23). The resampled 50-m NEXTMap DEM generated better predictions than the 50-m resolution OS DEM. The difference is probably due to the inherited differences in the resolution and quality of their original data sources used to create these two types of DEMs. The Ordnance Survey (OS50) DEM was developed mainly from 1:50,000 topographic maps with a relatively coarse resolution, while NEXTMap data were collected using airborne single-pass IFSAR platforms. Compared to OS50, as a more detailed original data source, the 50-m resampled NEXTMap data provide more detailed soil erosion predictions (see Figures 7.14 and 7.16) even with resampled lower resolution.

Similar conclusions have been drawn in previous studies such as Charrier and Li, (2012) and

Li and Wong, (2010).
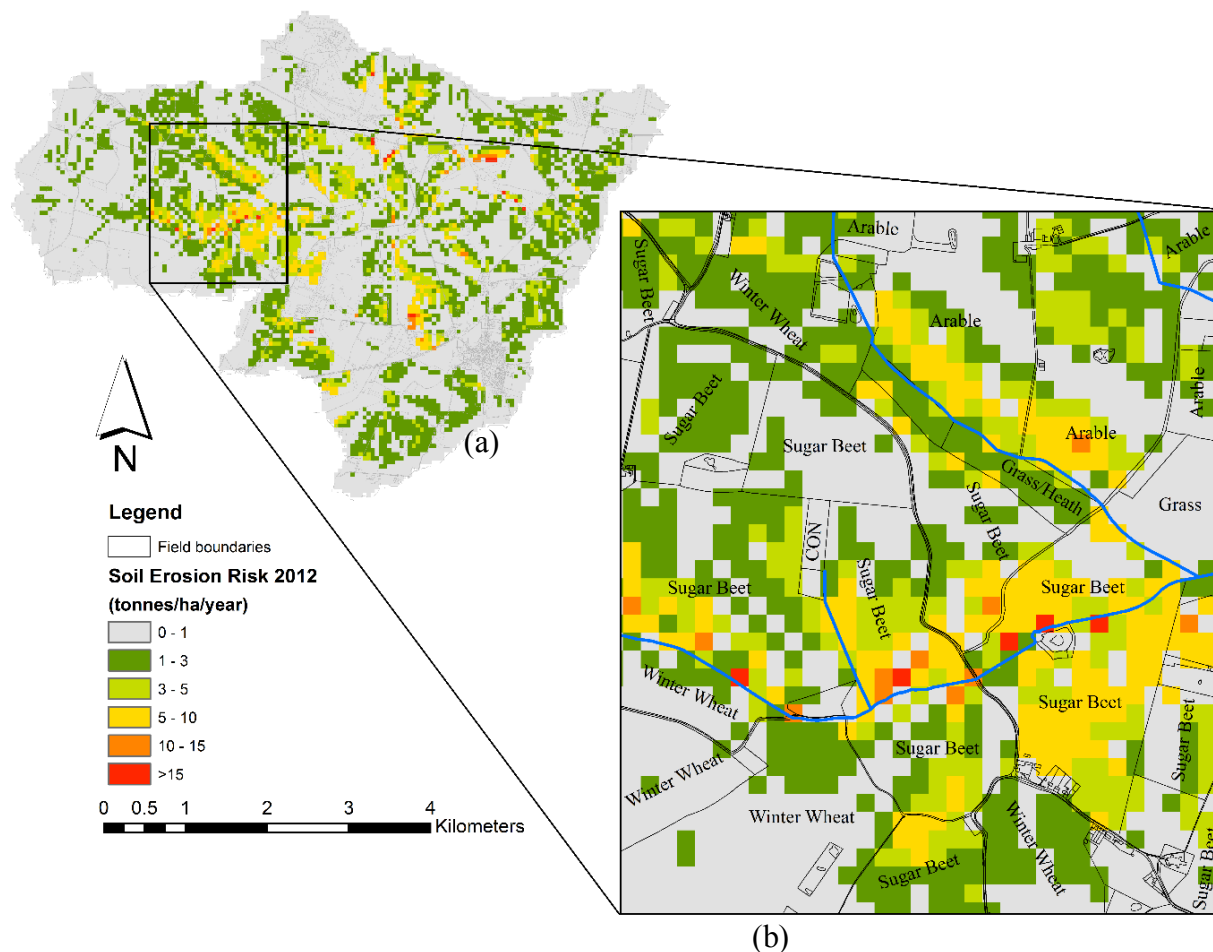
Figure 7.16: Soil erosion risk map for Blackwater sub-catchment. Farming year 2011/12 – NEXTMap 50-m

Table 7.22: Assessed soil erosion intensities. Farming year 2011/12 – NEXTMap 50-m

Soil erosion risk (tonne/ha/year)	Area (ha)	Share of total area (%)	Erosion risk category
0-1	2059.75	81.11	Very Low
>1-3	310.00	12.21	Low
>3-5	105.00	4.13	Medium
>5-10	53.25	2.10	High
>10-15	7.75	0.31	Very High
>15	3.75	0.15	Extreme 12

Table 7.23: The annual soil loss rates based on the land use. Farming year 2011/12 – NEXTMap 50-m

Crop	Area (ha)	Share of total area (%)	Soil erosion risk (tonne/ha/year) 12		
			Min	Max	Mean
Arable	1706.00	67.80	0.00	126.24	1.66
Grass	384.50	15.28	0.00	20.28	0.87
Others	71.00	2.82	0.00	4.20	0.24
Woodland	320.00	12.72	0.00	1.90	0.03
Urban	18.50	0.74	0.00	0.00	0.00
Water	16.25	0.65	0.00	0.00	0.00

7.3.4   Effect of DEM resolution on soil erosion

Three different digital elevation models (DEMs) with different spatial resolutions and different data sources (the NEXTMap 5-m data were resampled to 50-m resolution to evaluate the effect of DEM resolution separate from data source) were used to extract topographic parameters in erosion modelling. In general, the topographic features of the landscape have a great influence on the amount of soil loss, therefore different DEMs with various resolutions may produce diverse representations of topography that consequently result in different erosion risk predictions. As mentioned previously, in the USLE, effects of topography on soil erosion were characterised by the topography factor (LS) which could be obtained for each cell from the digital elevation model (DEM) (Wu et al., 2005). Figure 7.8 shows the slope and LS distributions obtained from the three DEMs. A visual examination indicates that DEM resolution does have profound effect on both slope and LS factor. It is obvious that changes in the resolution of the DEM affect the slopes and distribution of slopes and consequently values and distribution of LS factor within the sub-catchment. The maximum, average, and standard deviation of slope and LS values decrease as the DEM resolution becomes coarser. This

simply reinforces the fact that, a smoothing of the topographic features of the catchment occurs when DEM resolution is coarser (Cochrane and Flanagan, 2005).

It is clear from Table 7.24 that as the DEM resolution became coarser, the maximum, mean and standard deviation slope values generally decreased. The maximum slope value reduced substantially from 26.69^o for NEXTMap 5-m to 11.36^o for resampled NEXTMap data and to 5.29^o for OS50. In addition, the percentage of land with slope steepness greater than 3° decreased from 4.66% for NEXTMap 5-m to 3.07% for NEXTMap 50-m and to 1.13% for OS50. Indeed, maximum, mean and standard deviation of slope were shown to decrease as DEM cell size increased, similar to other findings in the literature (Martinez et al. 2010; Vaze et al 2010; Wu et al. 2008;; Zhang et al. 2008).Table 7.25 shows the effect of DEM spatial resolution on the LS factor. Apparently, maximum, mean and standard deviation of LS factor values decrease as the grid size increase. The maximum value of the LS factor declined dramatically from 45.369 to 12.65 from the two NEXTMap DEMs 5-m and 50-m respectively and to 9.324 from OS50 data. However, by simply inspecting Figure 7.8 and Tables 7.24-25, it is clear that results from 50-m resampled NEXTMap data are much better than those from the other 50-m resolution OS50 DEM for both slope and LS derivatives. When high resolution data (NEXTMap 5-m) were resampled to lower resolution (NEXTMap 50-m), their performances were degraded, but they perform reasonably well compare to the same resolution DEM (OS50) created from coarser source data. DEMs with same resolution but from different sources produced varied slope and LS statistics. These results confirm findings from earlier studies that different data sources of DEMs may produce more variability than DEMs of different resolution but from the same source (Baker et al., 2006; Charrier and Li, 2012; Li and Wong, 2010).

Table 7.24: Blackwater sub-catchment slope values for different resolutions.

Statistical Calculation	NEXTMap 5 m	NEXTMap 50 m	OS50
Minimum (°)	0	0	0
Maximum (°)	26.688	11.36	5.2867
Mean (°)	1.1998	1.05	0.8079
Standard Deviation (°)	1.4830	0.965	0.6684
% of slope >3°	4.66	3.07	1.13

Table 7.25: Blackwater sub-catchment LS values for different resolutions.

Statistical Calculation	NEXTMap 5 m	NEXTMap 50 m	OS50
Minimum	0	0	0
Maximum	45.369	12.65	9.324
Mean	0.4017	0.215	0.1976
Standard Deviation	0.780	0.376	0.4552

As mentioned before, the soil erosion from each cell estimated by RUSLE equation was obtained for the two different DEMs. During the process of soil erosion estimation, the soil type, rainfall erosivity, land use and conservation factor are similar throughout the sub-catchment while the topographic factor (LS) changes according to the DEM. The annual soil erosion risk results from NEXTMap 5-m are presented in Figure 7.12 and Tables 7.13 and 7.14, from OS50 in Figure 7.14 and Tables 7.18 and 7.19 and from the resampled NEXTMap 50-m in Figure 7.16 and Tables 7.22-23 for the farming season of 2011/12. In general, by using a DEM with a coarser resolution, areas categorized as very low erosion risk moderately increased, from 87.86 % to 92.60% of the total area, whereas those categorized as extreme erosion slightly decreased, from 0.11% to 0.09%. Moreover, the maximum soil erosion rate decreased from 200.05 (tonne/ha/yr) for the 5m resolution DEM to 126.24 and 83.16 (tonne/ha/yr) for the 50m resolution NEXTMap and OS respectivly, which proved the underestimation of erosion in coarser resolution as shown by Rojas et al. (2008), Wu et al.

(2005) and Zhang et al. (2008). Also by decreasing the DEM resolution, the average annual soil erosion rates of different land use/cover classes decreased, however, results from resampled NEXTMap are slightly higher than those from OS data due to the higher accuracy original source data as mentioned previously (Tables 7.14, 7.19 and 7.23).

Although, using two DEMs with different resolutions affected the output of the erosion model, the general pattern of the predicted soil erosion in coarser resolution was similar to that with finer resolution DEM. Figures 7.12b, 7.14b and 7.16b show that, there is a satisfactory agreement between the two erosion maps in capturing the areas under high erosion risk rates (see highlighted area). Overall, the analysis of erosion predictions and the slope and LS factor statistics revealed that the DEM with the coarser resolution generally underestimates soil erosion risks compared to the finer resolution one. In the RUSLE, effects of topography on soil erosion are characterised by the topographic factor (LS) that can be obtained from DEM and controlled by its resolution. Zhang et al. (2008) reported that DEM in coarse resolution only could preserve major relief features; therefore, it effects the soil erosion assessment. Wu et al. (2005) found that soil loss decreased with the increases of cell size. Although the resolution will affect all the topographic attributes, slope is probably the most important and has the greatest influence, especially when taking into account modelling of soil erosion risks. The resolution not only affects the topographic attributes from the DEM however, the variability of land use (C factor) and the support practices (P factor) classifications also have to be taken into account.

Clearly, the study shows that for larger DEM resolution, slopes decreased significantly and consequently both LS values in the RUSLE estimated erosion decreased, whilst at the same time higher resolution maintained steep slopes that have increased runoff quantities, which in turn has raised erosion estimates. In terms of determining the appropriate grid size for soil erosion modelling with the RUSLE, Wu et al. (2005) argued that it is difficult to

determine the best grid size due to the empirical nature of the RUSLE model. Also they add that when estimating soil erosion using a simple model like the RUSLE in the grid environment it is still hard to attain any adequate accuracy due to the empirical features and difficulties in parameterization. However, many studies have agreed that a smaller cell size would be more likely to provide a higher accuracy in the estimation of soil erosion (Prasuhn et al. 2013; Zhang et al. 2008; Cochrane and Flanagan 2005; Wu et al. 2005; Molnar and Julien 1998). Rojas et al (2008) concluded that soil erosion modelling using the RUSLE is best applied at a grid size close to the 22.1 m standard plot size of the USLE, the hillslope length on which it was based.

In this study, from a quantitative respect, it is difficult to suggest that a particular DEM has adequately represented an accurate estimation of soil loss in the study sub-catchment. In general, DEM resolution often influences estimated soil losses (Brazier et al., 2005), and DEMs that have sufficient resolution to detect small topography changes in low relief agricultural lands provide the opportunity to identify and prioritise the high-erosion risk areas (Prasuhn et al., 2013). Therefore, NEXTMap data, according to the outcome results, was believed to be more suitable for qualitatively representing the soil erosion risks. Wu et al. (2005) claimed that the smallest available grid size DEM should be selected for qualitative assessment of soil erosion risks. In addition, the lack of field measurements for the soil loss in the study area made quantitative comparisons between the output results from both DEMs impossible. Therefore, based upon the above discussion it appears that NEXTMap data is better for erosion prediction in the Blackwater sub-catchment, and thus will be used for further investigation of soil erosion scenarios in selected mini-catchments.

7.3.5   Validation of soil erosion results from the RUSLE

A validation of the erosion model results would require long-term measurements of sediment transport and water quality data (Volk et al., 2010). However, in the absence of such information some researchers have, alternatively, consulted reference values from the literature for comparable climate, soil and cropping conditions (Terzlaff et al., 2013). In this study, the validation of the RUSLE soil loss results was undertaken in three ways. Firstly, reference values from previous erosion risk studies in the UK were consulted. Secondly, the general trend in the total amount of soil estimated to be eroded from each of two mini-catchments A and B (Figure 7.17) was relatively compared with the water quality data (turbidity) recorded at the outlet of each catchment for farming years 2011/12 and 2012/13. Finally, the suspended sediment load of the two mini-catchments for the study period (seasons 2011/12 and 12/13) were estimated using the records of water discharge and the records of suspended sediment concentration derived from the continuous turbidity measurements. Then comparisons were made between the calculated sediment loads of the two mini-catchment with the results from the RUSLE and turbidity. These two mini-catchments were selected because of their water quality data and land use information availability.

7.3.5.1   USLE results compared to reference values from literature

Assessment of the risk of erosion in Britain has been aided by a series of case studies of particular sites or areas all based on field observation and measurement (Boardman, 2013). Most of these studies have reported, in general, relatively low rates of soil loss although in some cases erosion occurs to significant levels throughout the UK (Brazier, 2004). For example, in the Tamar catchment in South West England, it has been estimated that the gross erosion rate has reached 5.3 t/ha/year (Inman, 2006). Walling and Quine (1991) reported a net erosion rate from a sugar beet field at Rufford Forest Farm in Nottinghamshire of 10.5 t/ha/yr.

Brazier (2004) listed the results of soil erosion studies undertaken at different places in the UK and his data indicated that average soil erosion rates range from 0.22 to 4.89 t/ha/yr. Brazier (2004) also reported that the mean soil erosion for a field in east Norfolk was estimated to be 1.48 t/ha/yr. He also concluded that erosion rates averaged over a whole field are often less than 1.4 t/ha/yr, a threshold recognized as being acceptable by authors such as Evans (1981) and Morgan (1980). Cerdan et al. (2010) stated that mean sheet and rill erosion rate for the European area covered by arable land is about 3.6 t/ha/yr. In addition, Morgan (1985) argued that the erosion rates in the UK from cultivated land ranged from 0.1 to 3 t/ha/yr, and 10 to 40.50 t/ha/yr from bare soil. In general, as mentioned in the Environment Agency report (2004), the average annual soil losses from cultivated land are generally less than 5 t/ha but can occasionally exceed that.

As can be seen from the summary above, average annual soil losses from cultivated fields are generally less than 5 t/ha/yr. These reference values confirm the relatively correct magnitude of RUSLE results for the Blackwater sub-catchment. In the Blackwater, the rates of average erosion values in terms of crop types vary from 0.3 to 10.01 t/ha/yr (Table 26). It has been reported in the literature that there can be an overestimation of the soil loss results through (R)USLE modelling compared with field measurements (Bartsch et al. 2002; Evans 2002; Evans and Brazier 2005; Hui et al. 2010; Prasuhn et al. 2013), however, in general, the average of soil erosion values estimated by the RUSLE were considered realistic after comparison with the reference data from the series of the case studies throughout the UK.

Table 7.26: Rates of soil erosion in terms of crop types for min-catchments A and B in the Blackwater sub-catchment.

| | Mean soil erosion loss (tonne/ha/yr) | | | |
| | Mini-catchment A | | Mini-catchment B | |
Crop	Season 2011/12	Season 2012/13	Season 2011/12	Season 2012/13
Maize	1.03	0.85	-	-
Sugar Beet	4.03	3.45	4.19	10.01
Beans	-	1.38	-	2.804
Peas	0.42	-	-	-
Winter Wheat	0.97	1.13	2.937	1.286
Oilseed Rape	1.06	0.67	-	-
Spring Barley	0.30	1.25	1.705	1.356
Winter Barley	0.54	0.44	3.434	-

Note: These data are the results of implementing the RUSLE using the original factors data from the two mini-catchments A and B for the two seasons 2011/12 and 2012/13.

7.3.5.2 Relative comparison between the USLE results and water quality data

The second method of validating the RUSLE results for the Blackwater was to compare the general trend in the total amount of soil estimated to be eroded from mini-catchments A and B with the water quality data monitored at the outlet of each mini-catchment for seasons 2011/12 and 2012/13. These data were gathered from a series of automated monitoring stations and associated grab samples where variables such as turbidity and stage were measured (Wensum Alliance, 2013).

As indicated above, one of the most serious off-site environmental impacts associated with soil loss from agricultural land is the potential degradation of river water quality. In order to use water quality data in the validation of RUSLE results, the following discussion is divided into two approaches. In the first, turbidity measurements were averaged for each four months, as reported in Table 7.28 and illustrated in Figure 7.19 and then compared to the RUSLE results, in a relative way of comparison. The second approach involves the conversion of the turbidity record to one for suspended sediment concentrations, using a field-derived calibration relationship (see Appendix 1 for more details). Since turbidity can be

recorded continuously, it is possible to obtain a continuous record of sediment concentration. Wass et al. (1997) stated that it is generally expected that an adequate calibration relationship between suspended sediment and turbidity can be established. Stage data were also used to obtain discharge values according to stage-discharge relationship curves. The suspended sediment load of the two mini-catchments were then estimated using the record of water discharge and the calculated suspended sediment obtained from the above step. Sediment loads estimated of the two mini-catchments A and B for the two seasons are reported in Table 7.29 and depicted in Figure 7.20.

Because of the significant environmental impacts of sugar beet harvesting on soil and water, it was chosen to be used as the key crop to study the reliability of the RUSLE results in comparison with the water quality data. The land uses in the two mini-catchments for the two seasons are reported in Table 7.27. It is clear from the table that sugar beet was the dominant crop in mini-catchment A during the first season and in B for the second season. Furthermore, as can be seen from Figure 7.17, in both cases (catchment A season 2011/12 and catchment B season 2012/13) the fields where sugar beet was grown coincided with sites classified as at high risk on the basis of slope (LS) and also the majority of those fields are adjacent to the watercourses, which therefore increasing the erosion risk and the potential for delivery of the eroded sediment to the streams. As discussed previously, Defra (2005) provides a ranking of susceptible to erosion crops and includes potatoes, sugar beet and maize crops in the highest risk category. Table 7.27 and Figure 7.17 indicate that during the study periods, there were no potatoes, one maize field (coinciding with very gentle topography) and 32 sugar beet fields.

Table 7.27: Number of fields in terms of crop type in mini-catchments A and B for season 2011/12 and 2012/13.

	Number of fields occupied by each crop type			
	Mini-catchment A		**Mini-catchment B**	
Crop	**Season 2011/12**	**Season 2012/13**	**Season 2011/12**	**Season 2012/13**
Maize	1	1	0	0
Sugar Beet	21	1	3	7
Beans	0	3	0	3
Peas	1	0	0	0
Winter Wheat	9	11	3	2
Oilseed Rape	6	3	0	0
Spring Barley	2	16	3	4
Winter Barley	3	7	6	0
Total soil loss (tonne\year)	**278.72**	**254.11**	**143.25**	**162.989**
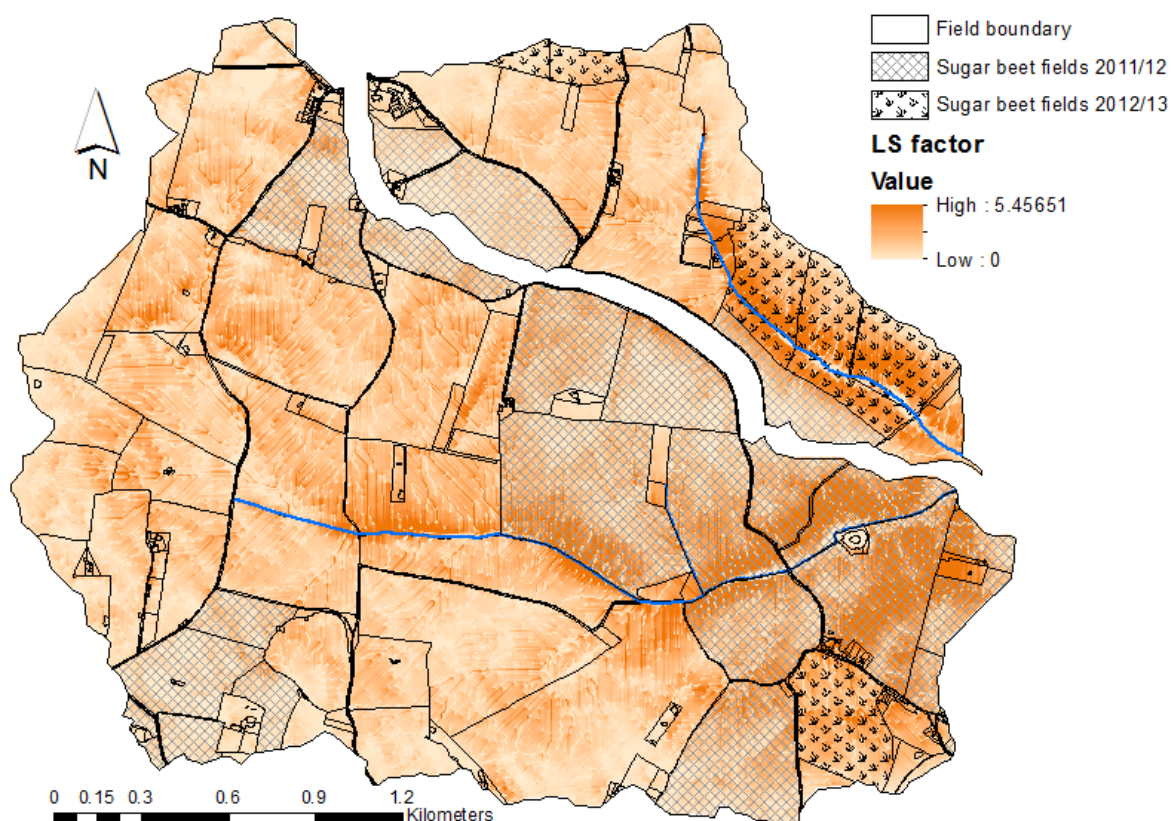
Figure 7.17: Sugar beet fields in mini-catchment A and B highlighted differently for each season

Sugar beet is usually drilled during spring (March/April) and harvested in the autumn (September/Christmas), but in some cases, it is also harvested until the end of February (Defra, 2010). During the process of sugar beet harvesting the soil is substantially disturbed and bare ground is left with ruts and wheelings that can channel water and lead to serious erosion (Defra, 2005). Therefore, rain coinciding with harvesting sugar beet can cause a lot of soil to leave the field. Given the fact that sugar beet tends to be harvested in the autumn until the late winter, it is often the case that harvesting takes place in wet conditions, autumn and winter rainfall events, which can result in extremely high rates of soil erosion taking place (Figure 7.18).

Figure 7.18: Impact of sugar beet harvesting on soil erosion. These photos were taken from Wood Dalling field on 27 November 2012. The right photo highlights the large suspended sediment concentration coming from a tributary due to sugar beet harvesting upstream.

The off-farm effects of sugar beet being sown during the spring of season 2011/12 will not appear on the adjacent watercourses until late autumn or even the winter of the next season 2012/13. Moreover, Walling and Amos (1999) demonstrated that eroded soil, mainly derived by winter rainfall events when arable fields were bare, was responsible for summer problem of turbidity, as sediments were progressively remobilised and deposited. As it was considered that the sugar beet was the main contributor to the soil erosion in the two mini-catchments, the amount of total soil estimated to be eroded from each catchment (RUSLE results) was relatively compared with the measurements of turbidity that were continuously recorded at each catchment outlet and to the sediment load estimated to come out from the two mini-catchments according to the water quality data. This type of comparison would also give an indication of the likely relationship between turbidity concentrations in the two rivers and the crop types that were grown in their catchments.

The total estimated soil loss by RUSLE from mini-catchment A for the season of 2011/12 was higher than that for the second season, 278.72 and 254.11 t/yr, respectively (Table 7.27). This was mainly attributed to the fact that sugar beet was the dominant crop in the first season, 21 fields (Table 7.27). The mean values of the turbidity measurements (averaged for each four months) for the periods from September to December 2012 and January to April 2013 (Season 2) are the highest among other periods for mini-catchment A, 13.55 and 14.56 (NTU), respectively (Table 7.28 and Figure 7.19). Nevertheless, the highest suspended sediment loads estimated to come out of the two mini-catchments happened during September to December 2012 (Table 7.29 and Figure 7.20). This can be attributed to the fact that sugar beet that was cropped in Season 1 was harvested in Season 2 during the period from September to December and sometimes up to February. These turbidity and suspended sediment load values are also higher than values for the same periods from mini-catchment B (Table 7.28). These results could be attributed to the fact that, in the spring of 2011, there

were 21 sugar beet fields in mini-catchment A and only 3 sugar beet fields in mini-catchment

B (Table 7.27). Thus, erosion was extensive where sugar beet was the dominant crop.

Table7.28: Descriptive statistics for turbidity measurements recorded at the outlet of sub-catchment A and B. the mean value is the average of each four months

		Rainfall (mm)		Turbidity (NTU)							
				Catchment A				Catchment B			
Months		Total	Aver.	Mean	STD	Min	Max	Mean	STD	Min	Max
Season 1	**Sep-11 to Dec-11**	144.6	36.15	**5.54**	5.72	0.9	69.6	**8.04**	4	2.2	66.6
	Jan-12 to Apr-12	235.2	58.8	**5.56**	8.63	1	141	**4.59**	3.25	0.9	46.8
	May-12 to Aug-12	306.4	76.6	**10.64**	8.99	1.7	97.5	**9.47**	6.4	0.1	58.24
Season 2	**Sep-12 to Dec-12**	284.8	71.2	**13.55**	11.91	2.9	96.2	**12.01**	16.8	0.1	246.5
	Jan-13 to Apr-13	193.4	48.35	**14.56**	18.07	4	293.1	**8.96**	12.49	1.5	167.6
	May-13 to Aug-13	144.2	36.05	**12.1**	15.62	4.2	246.8	**6.55**	16.09	1.4	193.3
	Sep-13 to Oct-13	153.8	76.9	**9.46**	10.25	2.1	192.3	**10.25**	12.71	2.4	199.1
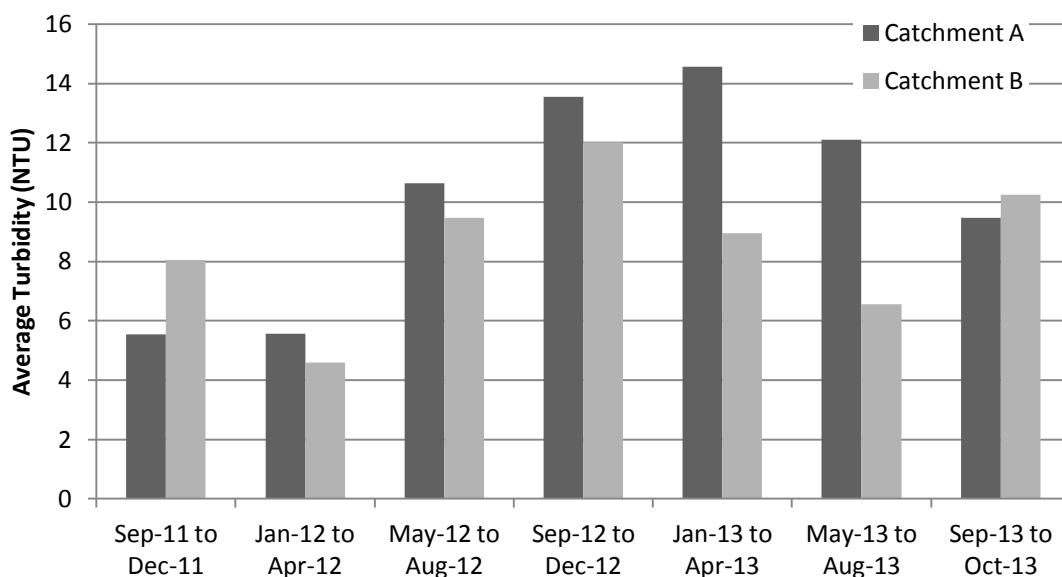
Figure 7.19: Turbidity mean values averaged for each four months

Table 7.29: Sediment load estimated according to turbidity measurements of mini-catchments A and B

			Catchment A			Catchment B		
	Moth	Rainfall (mm)	Sediment load (tonne)	4months total	Total Load	Sediment load (tonne)	4months total	Total Load
Season 1	Sep-11	24.8	0.233	0.931	5.713	0.266	1.062	4.138
	Oct-11	35.2	0.233			0.266		
	Nov-11	21.2	0.233			0.266		
	Dec-11	63.4	0.233			0.266		
	Jan-12	56.4	0.335	1.966		0.268	1.486	
	Feb-12	13.6	0.114			0.240		
	Mar-12	50.6	0.013			0.494		
	Apr-12	114.6	1.504			0.485		
	May-12	54	1.092	2.816		0.567	1.589	
	Jun-12	92.2	0.518			0.382		
	Jul-12	85.2	0.741			0.435		
	Aug-12	75	0.464			0.205		
Season 2	Sep-12	41.6	0.423	9.337	14.177	0.152	2.888	4.649
	Oct-12	73.6	1.513			0.674		
	Nov-12	87.4	4.490			1.300		
	Dec-12	82.2	2.910			0.761		
	Jan-13	56.6	0.542	4.528		0.241	1.217	
	Feb-13	45.6	1.243			0.131		
	Mar-13	75	2.585			0.636		
	Apr-13	16.2	0.157			0.210		
	May-13	50.4	0.138	0.312		0.143	0.544	
	Jun-13	22.2	0.054			0.113		
	Jul-13	11.2	0.021			0.148		
	Aug-13	60.4	0.099			0.140		
	Sep-13	53.4	0.110	0.361	0.361	0.056	0.266	0.266
	Oct-13	100.4	0.251			0.210		
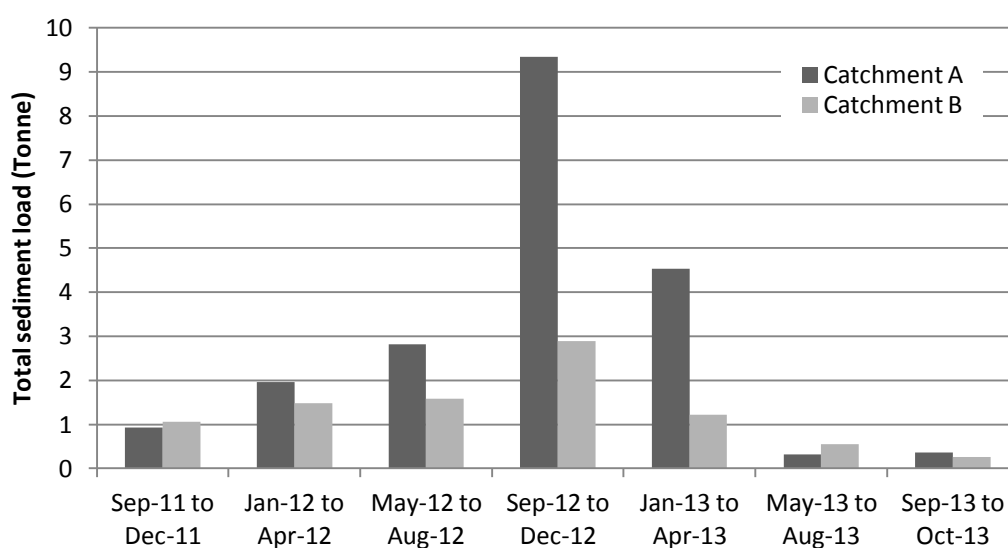
Figure 7.20: Sediment load of the two mini-catchments (A and B) for each four months

On the other hand, the net soil loss estimated to erode from mini-catchment B for the season of 2011/12 was lower than that for the second season, 143.25 and 162.989 t/yr, respectively (Table 7.27). Moreover, there was an increase in the mean turbidity value measured for B during the period from September to October 2013 compared to the value from A for the same period, 10.25 and 9.46 (NTU), respectively. Therefore, it can be suggested that the high number of sugar beet fields in mini-catchment B during the second season was an influence on that increase in the net soil loss from the catchment, and consequently in turbidity values (Table 7.28).

Turbidity values (Figure 7.19) and estimated suspended sediment loads (Figure 7.20) illustrate complementary facts. They are illustrating the issues about certain key events which can be important in terms of the overall sediment load. The big sediment loss that happened in the period from September to December 2012 was a result of a specific combination of factors, particularly harvesting a very risky crop (sugar beet) in heavy rain conditions (see Figure 7.18 for a good illustration). However, the RUSLE results do not reflect this. RUSLE assigned an annual weighting risk value to each land use category and did not consider what was going on in the fields during the crop harvesting process. The extent to which that risk is realised then depends on another factors, such as harvesting in heavy rain conditions. Therefore, RUSLE can be used to give an idea of potential risk of soil erosion, but not necessarily the complete picture of the realised risk.

Overall, the results obtained from the comparison of the river monitoring data and the RUSLE model output results for the two mini-catchments indicate that eroding sugar beet fields are an important source of sediment transported to the rivers. However, it should be recognized that not all the estimated soil loss came only from sugar beet fields, other crop fields also made significant contributions. Results presented in Table 7.26 indicates that

winter barley and winter wheat fields are estimated to yield an average annual soil loss of about 3.43 and 2.94 t/ha/yr, respectively.

Generally, the above discussion indicates that the RUSLE model can be successfully used for soil erosion risk estimation from croplands in the Blackwater sub-catchment. Moreover, the comparisons of the RUSLE annual mean soil erosion values in terms of crop types with the reference values from the literature for comparable cropping conditions confirm the relatively right magnitude of the model results. However, it should be noted that RUSLE produces undoubtedly errors in the prediction of soil erosion values as proved by some studies that compare USLE model results with values measured in the field (Boomer et al. 2008; van Rompaey et al. 2003). The large difference of the net soil estimated to erode from each mini-catchment between results from RUSLE and water quality data can be attributed to the following factors. First, as mentioned early in this section, RUSLE tends to overestimate the values of soil loss. Second, most eroded soil from hillslopes deposits within the catchment and only a portion of the sediment will reach streams or a catchment outlet (Morgan, 2005; Wu et al., 2005). Morgan (2005) also reported that the proportion of the sediment eroded from the land surface that discharges into the catchment outlet can vary from 3 to 90 per cent, decreasing with larger catchment area and lower average slope. Nevertheless, it has been suggested that RUSLE is highly suitable for identifying regions of higher possible soil loss qualitatively instead of providing quantitative values (Bargiel et al. 2013; van der Knijf et al. 2000; Wu et al. 2005).

7.3.6 Different Scenarios

Vegetation cover (C factor) and conservation support practices (P factor) are the main means of controlling soil erosion by water. The efficiency varies greatly with vegetation types, which are always related to land use patterns (Zhang et al., 2003) and the types of supporting cropland practices. The most commonly used practices are; cross slope, contour farming, strip cropping or terracing (Wall et al., 2002). Thus, impacts of changes in land use from the highly susceptible to erosion crops (e.g. sugar beet, potatoes or maize) to those classified as low erosion risk (Defra 2005), and changes in cultivation methods from cross slope to more effective tillage operations (e.g. contour and strip tillage cultivations) on the soil erosion risk can be analysed, simply by calculating the RUSLE with different empirical values for the individual factors. Therefore, to demonstrate the effect of changes in the C and P factors on the assessment of soil erosion risk, different scenarios were considered, and the results were compared to those that were obtained when the original data were used.

The first scenario (Table 7.30) was achieved by adopting different support practices (P-factor), contour farming (P = 0.5) for fields cropped with sugar beet or potatoes and strip cropping (P =0.37) for any other crops. A second scenario (Table 7.30) involved replacing highly susceptible to erosion crops (e.g. sugar beet, potatoes or maize) with moderately to less susceptible to erosion crops (e.g. wheat, barley or oilseed rape) according to the previous crop was planted in each field. These scenarios were applied to mini-catchments A and B (Figure 7.17) and for the two different seasons of 2011/12 and 2012/13.

Table 7.30: Descriptions of the different scenarios

Scenario	Description of Scenarios
1	Influence of tillage: change from cross slope tillage into contouring and strip cropping practices
2	Influence of changes in crop types: avoiding highly susceptible crops (potatoes, sugar beet and maize). Strip cropping practice was applied to all croplands

7.3.6.1   Season 2011/12

7.3.6.1.1   First scenario – different P values

Considering different supporting practices (P factor), a substantial reduction in soil losses were achieved when contouring and strip cropping practices were applied to the croplands, as expected. Figures 7.21b and 7.21b show the spatial distribution of the soil erosion intensity in mini-catchment A and B when the new P-factor values (Scenario 1) were used. Table 7.31 provides an overview of selected results. Both contour farming and strip tillage practices reduce the estimated amount of soil loss from mini-catchment A and B by more than 22% and 24%, respectively (Table 7.31). Combining both techniques which means managing all arable land in the two mini-catchment with either contour ploughing or strip tillage (sugar beet and potatoes cannot be cultivated with strip tillage) would result in an average soil erosion risk from each land use category less than the corresponding values from the original Scenario (P =0.625), (as discussed previously in Section 7.3.1.5, in normal cases cross slope farming was the dominant cultivation method used in Wensum catchment as well as contour ploughing at areas under greater risk of runoff). For example, the average annual soil loss from sugar beet fields was reduced from 4.03 tonne/ha/yr (Original Scenario) to 3.23 tonne/ha/yr when the improved P-factor values (Scenario 1) were used. These results demonstrate how soil protection measures can affect soil erosion rates.

When looking into the comparison of results for entire mini-catchments A and B, the influence of the new adopted P-factor values seems to be evident (Figure 7.23a and b). The results show that areas categorized as very low and low erosion moderately increased, whereas those categorized as very high and extreme erosion slightly decreased compared to the results obtained for original Scenario. For mini-catchment A, it can be seen from Figure 7.23a, that when contour farming and strip tillage practices were applied to the croplands, areas covered by the very low class of soil erosion risk increased from 411.9 ha (76.73% of the total area) to 442.43 ha (82.41% of the total area), and areas categorized as extreme erosion slightly decreased, from 0.21 ha (0.04% of the total area) to 0.10 ha (0.02% of the total catchment area). On other words, under Scenario 1, most of the area (82.41%) was predicted to suffer from very low erosion risk (0-1 tonne/ha/yr) and, in 0.02% of the catchment, the soil erosion was estimated to exceed >15 tonne/ha/yr. Almost the same pattern of results were obtained for mini-catchment B under Scenario1 (Figure 7.23b). Therefore, the soil erosion results that were obtained under this scenario clearly reveal the effectiveness and importance of conservation practices (contouring and strip cropping practices), and suggest that wider application could further reduce erosion. These support practices typically affect erosion by decreasing the erosive rate of rainfall and runoff (Fernandez et al., 2003; Jamshidi et al., 2013).

It is clear from the figures that the highest erosion risks are found at the parts of the catchment where relatively steep land (high LS factor values) was used to grow highly susceptible to erosion crops (e.g. sugar beet). The most vulnerable fields in the two mini-catchments according to the spatial distribution of the erosion risk severity categories were generally the fields that are adjacent to the watercourses, fields such as; Dunkirk, First Hempsky, Gatehouse Hyrne, Potash and Shed Field in mini-catchment A and Field House Meadow Big, Field House Meadow Small, Harrow, High Meadow, Rackety Barn and Shed

Field in mini-catchment B. All these fields were found to coincide with sites of high topographic factor values (LS) (see Figure 7.17). From Figures 7.21b and 7.22b, it is obvious that, even under Scenario 1 (using contour ploughing), at the fields where sugar beet coincided with sites classified as having high steep slopes (high LS values), the estimated mean soil erosion is still high. Therefore, at sites where steep slopes are observed, the highly susceptible crops (potatoes, sugar beet and maize) should be avoided unless other measures (including reduced-tillage and residual cover) are taken to control erosion (Boardman et al 2009; Fernandez et al 2003). According to Figures 7.21 and 7.22 in general, land use and slope gradient appear to be the major influences on the amount of soil losses in the catchments.

Season 2011\12

Figure 7.21: Soil erosion risk maps for mini-catchment A, (a) normal Scenario, (b) first level assessment of measures for soil erosion risk (Scenario one), by adopting different tillage practices, contour tillage (P =0.5) where sugar beet or potatoes occurred and strip tillage (P=0.37) for any other crop, (c) second level assessment of measures for soil erosion risk (Scenario two), by replacing any sugar beet, potatoes or maize crops with either wheat, barley or oilseed rape, according to the previous crop grown at the proposed field. Note: In scenario two, all fields were assumed to be cultivated with strip tillage.

Figure 7.22: Soil erosion risk maps for mini-catchment B, (a) normal Scenario, (b) first level assessment of measures for soil erosion risk (Scenario one), by adopting different tillage practices, contour tillage (P =0.5) where sugar beet or potatoes occurred and strip tillage (P=0.37) for any other crop, (c) second level assessment of measures for soil erosion risk (Scenario two), by replacing any sugar beet, potatoes or maize crops with either wheat, barley or oilseed rape, according to the previous crop grown at the proposed field. Note: In scenario two, all fields were assumed to be cultivated with strip tillage.

Table 7.31: Rates of soil erosion in mini-catchment A and B in terms of crop types based on the three scenarios.

	Season 2011\12					
	Mean soil erosion loss (tonne/ha/yr)					
	Mini-catchment A			Mini-catchment B		
Crop	Original Scenario	Scenario 1	Scenario 2	Original Scenario	Scenario 1	Scenario 2
Maize	1.03	0.61	-	-	-	-
Sugar Beet	4.03	3.23	-	4.19	3.352	-
Beans	-	-	0.21	-	-	-
Peas	0.42	0.25	0.25	-	-	-
Winter Wheat	0.97	0.58	0.58	2.937	1.739	1.739
Oilseed Rape	1.06	0.63	0.84	-	-	-
Spring Barley	0.30	0.18	0.18	1.705	1.009	1.009
Winter Barley	0.54	0.41	0.70	3.434	2.033	2.033
Total soil loss (tonne\year)	278.72	217.34	153.64	143.25	108.71	89.70
% of reduction		22.02%	44.88%		24.11%	37.38%

(a) (b)
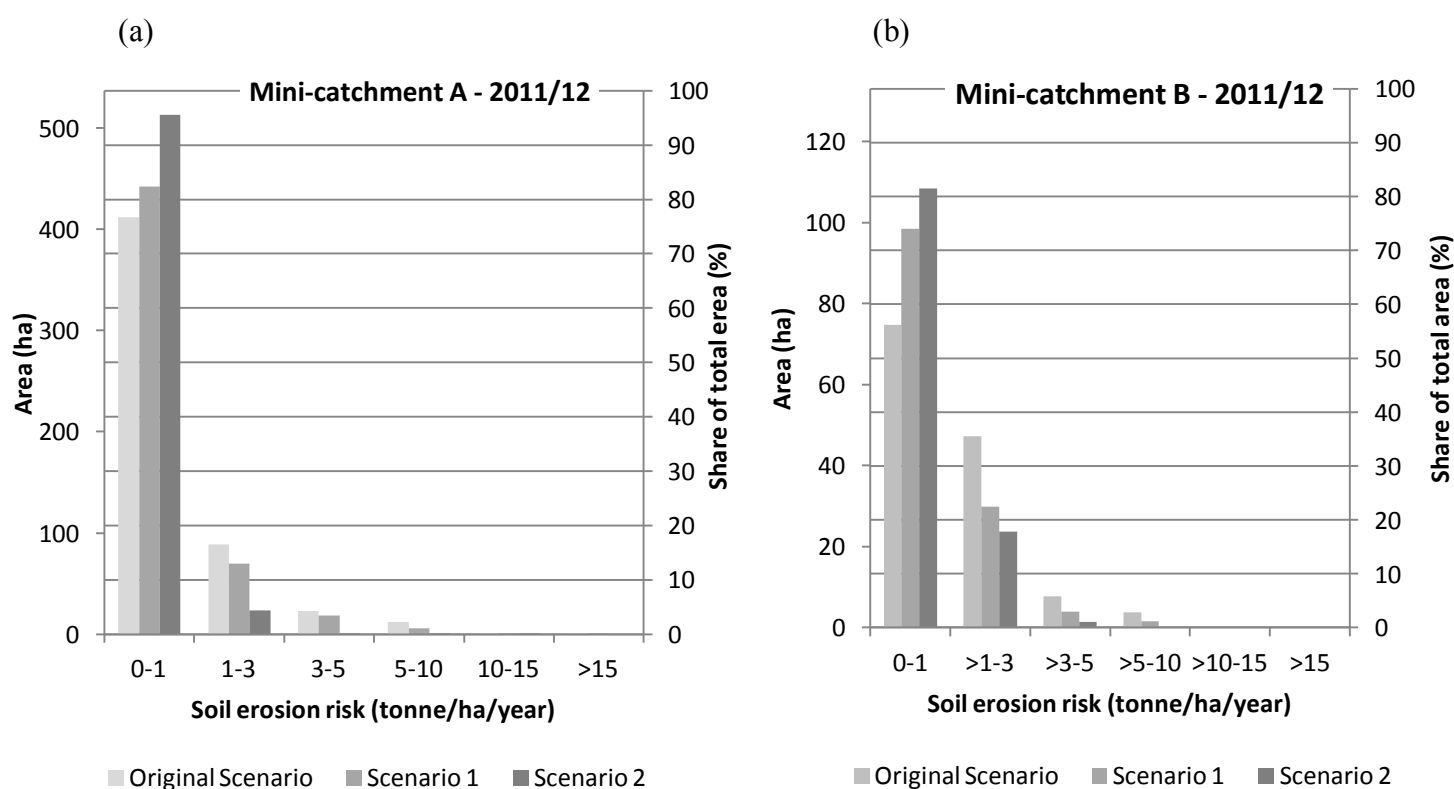
Figure 7.23: Areas occupied by each class of erosion severity (left Y axis) and their percentages from whole catchment area (right Y axis), according to the three scenarios adopted.

7.3.6.1.2 Second scenario – land use scenario (no potatoes, sugar beet or maize)

Figures 7.21c and 7.22c show the spatial distribution of the soil erosion intensity in mini-catchments A and B under Scenario 2. This approach was used to study potential impacts of changes in soil management as well as changes in crop rotation on the soil erosion rates. Different erosion risks are associated with different crop covers and Defra (2005) provides a ranking of susceptible land uses which includes potatoes, sugar beet and maize crops in the highest risk category. Thus, certain combinations of soil texture (K factor), slope (LS factor) and crop type (C factor) will lead to high risks of erosion (Boardman et al., 2009). From the previous results, it is clear that the high risks of soil erosion are associated with the crop of sugar beet. Therefore, in order to assess the effect of crop types on soil erosion risk, all highly susceptible to erosion land uses (potatoes, sugar beet or maize) were replaced by land uses (crops) classified as less susceptible to erosion (e.g. winter wheat, winter or spring barley and oilseed rape). In this scenario, which is assumed to be the best-scenario, the highly susceptible crops were avoided as well as applying strip cropping to all croplands in the catchments.

Figure 7.23(a and b) and Tables 7.31 illustrate the results for Scenario 2. Under this scenario, when the highly susceptible to erosion crops were avoided, substantial reduction in soil loss has been achieved. This scenario leads to an average erosion reduction by 44.88% and 37.38% for mini-catchments A and B, respectively, compared to the values from their original analyses and about 22.86% and 13.27% compared to Scenario 1 (Table 7.31). Therefore, by adopting feasible cropping management and soil erosion control practices (contouring and strip cropping practices) and avoiding crops highly susceptible to erosion the soil erosion risks in the two mini-catchments were significantly reduced. The variation in the mean soil erosion values in terms of each crop type between seasons is believed to be due to variation in soil erodibility (K), topography (LS) and rainfall erosivity factor (R) as well as

different erosion control practices (P) under the different scenarios. This result could be interpreted from the perspective that when a single crop was grown over many fields across the catchment, the overall estimated value of the mean soil loss from the whole fields would be affected by the variation in all of above mentioned factors (Fernandez et al., 2003; van Vliet et al., 1976).

For mini-catchments A and B, under the best scenario conditions (adopting strip cropping practice and avoiding highly susceptible to erosion crops), areas of the catchment categorized as very low and low erosion moderately increased, whereas areas categorized as very high and extreme erosion completely disappeared (zero values) compared to the results obtained for the other two scenarios (Figure 7.23a and b). Most of the area of mini-catchment A (95.57%) was predicted to suffer from very low erosion risk (0-1 tonne/ha/yr) compared to 76.73% and 82.41% for the original analysis and Scenario 1, respectively. 4.34% of the mini-catchment area was classified under low erosion risk according to Figure 7.23a, 0.07% as moderate erosion risk, 0.01% as high erosion risk, and 0% as very high to extreme erosion risk. Almost same results were obtained for mini-catchment B under this scenario (see Figure 7.23b). Overall, by adopting strip tillage practice and considering other land use, avoiding highly susceptible to erosion crops, a substantial reduction in soil loss has been achieved.

7.3.6.2   Season 2012/13

7.3.6.2.1   First scenario – different P values

Figure 7.24 presents the spatial distribution of the soil loss risk under Scenario 1 in the mini-catchment A for season 2012/13. A visual inspection of the figure indicates that the spatial extent of areas of the catchment suffered from soil erosion are much lower in season 2012/13 compared to the previous season (2011/12) under all scenarios. This result could be

interpreted from several perspectives. First, in mini-catchment A, during season 2012/13, there were only two fields cropped with crops which are classified as highly susceptible to erosion by (Defra, 2005), sugar beet and maize (there were 21 sugar beet fields in first season), and in addition, all were grown on level to gently sloping landscape which favours mostly low erosion rates. Second, the rainfall intensity for the whole farming year was relatively lower in season 2012/13 compared to the previous season. The rainfall erosivity factor (R), as calculated based on the sum of monthly erosivity index, was 113.05 for season 2011/12 and 95.32 for season 2012/13. Thus, this result indicates that lower predicted soil loss in season 2012/13 was a consequence of the relatively low amount of rainfall compared to the previous season. An increase in rainfall amount is generally accompanied by an increase in soil loss. Thus, this could be another reason of why soil loss was moderately lower in this season compared to the previous one. On the other hand, although on an average first season was considered to be wetter than second season, mini-catchment B experienced higher rates of soil loss in second season compared to the first one, due to the high number of sugar beet fields during this season.

However, as discussed previously, it is important to note that rainfall erosivity factor (R) is an estimated value across the whole farming year. In fact there are some months in the second season which were much wetter than their corresponding months in the first season and some of those months coincided with the bare ground periods, after harvesting, drilling and early growth phases on new crops (Table 7.4). Thus, by using an annual rainfall erosivity factor (R) some of these differences in the monthly rainfall intensities, which are likely to be quite important for sediment loss processes on the ground, are overlooked. Boardman et al. (2009) argued that erosion on bare fields varies from season to season depending on rainfall amount, intensity and timing

Under Scenario 1, most of the area of the mini-catchment (about 95 %) was considered to suffer from very low erosion risk, and 0% for areas classified as very high to extreme erosion risk (Figure 7.25a). Still, under Scenario 1 for season 2012/13, the highest annual mean soil erosion rate (reduced from 3.45 to 2.76 tonne/ha/yr) was estimated for sugar beet (Table 7.31). Despite adopting different cultivation method, the mean rate of soil losses estimated from sugar beet fields in mini-catchment B was relatively high (8.011t/ha/yr) (Table 7.31). The relatively high soil loss value can be attributed to the high LS factors, since most of the sugar beet fields coincided with sites classified at high risk in terms of topography (LS values) (Figure 7.17). Therefore, this results support the assertion that growing highly susceptible to erosion crops on high risk sites, sloping fields adjacent to water courses, would be best avoided (Boardman et al., 2009; Defra, 2005; Inman, 2006).

In season 2012/13, Scenario 1 lead to an average erosion reduction of about 18.41% and 21.76% from mini-catchments A and B, respectively, compared to their original scenarios. Further inspection of Figures 7.26a and b indicates that, in terms of erosion risk severity categories, if there are no high risk crops in the catchment at the first place, the cultivation method changes have little impact, but if there are high risk crops (i.e. sugar beet) there would be large differences in the area coved by each severity class. For example, the very low erosion risk category increased by only 5% in the case of mini-catchment A (Figure 7.26a), whereas the same category has increased by about 17% for B (Figure 7.26b).
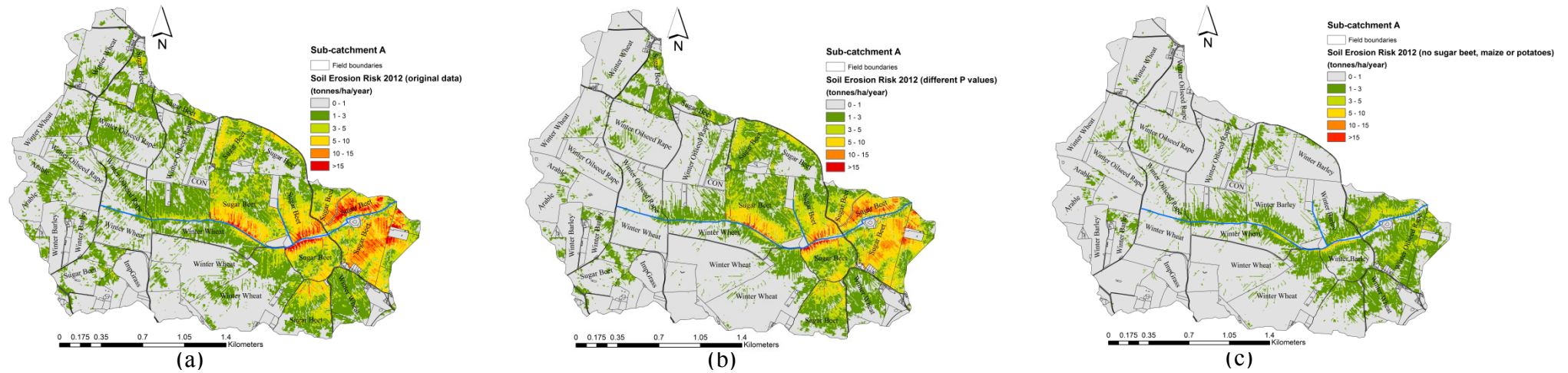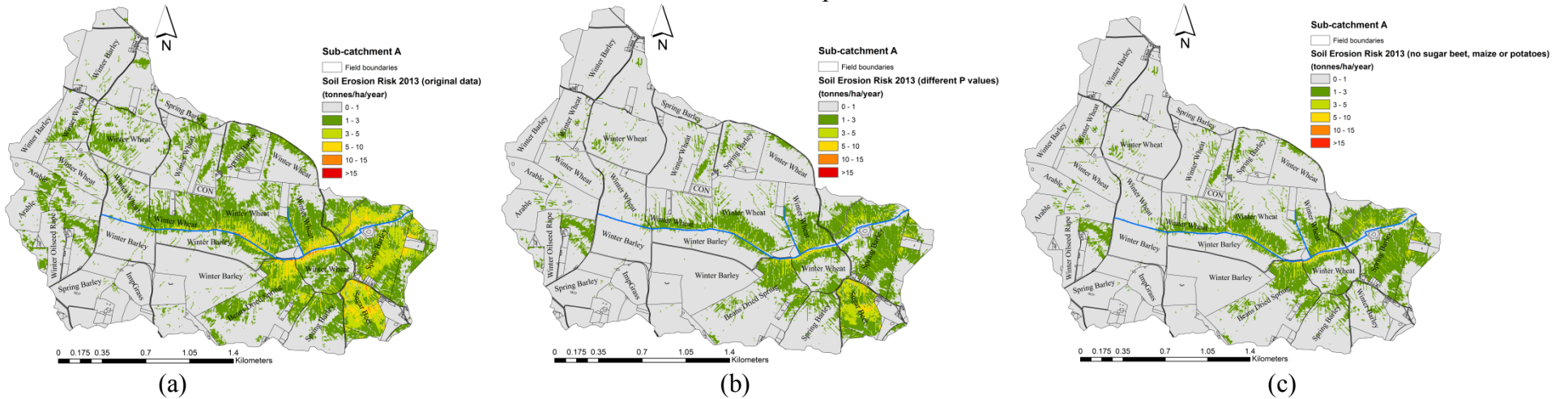
Figure 7.24: Soil erosion risk maps for mini-catchment A, (a) normal scenario, (b) first level assessment of measures for soil erosion risk (Scenario one), by adopting different tillage practices, contour tillage (P =0.5) where sugar beet or potatoes occurred and strip tillage (P=0.37) for any other crop, (c) second level assessment of measures for soil erosion risk (Scenario two), by replacing any sugar beet, potatoes or maize crops with either wheat, barley or oilseed rape, according to the previous crop grown at the proposed field. Note: In scenario two, all fields were assumed to be cultivated with strip tillage.
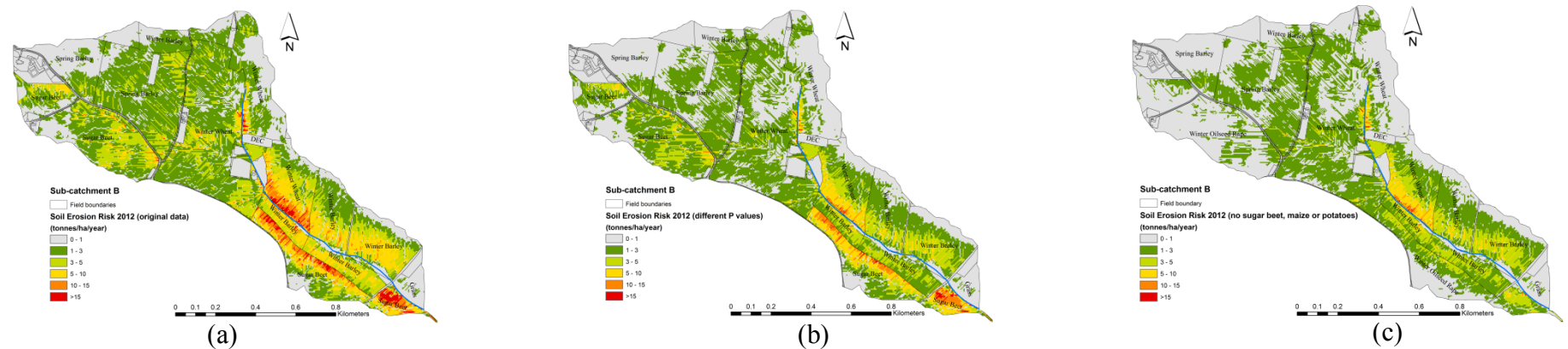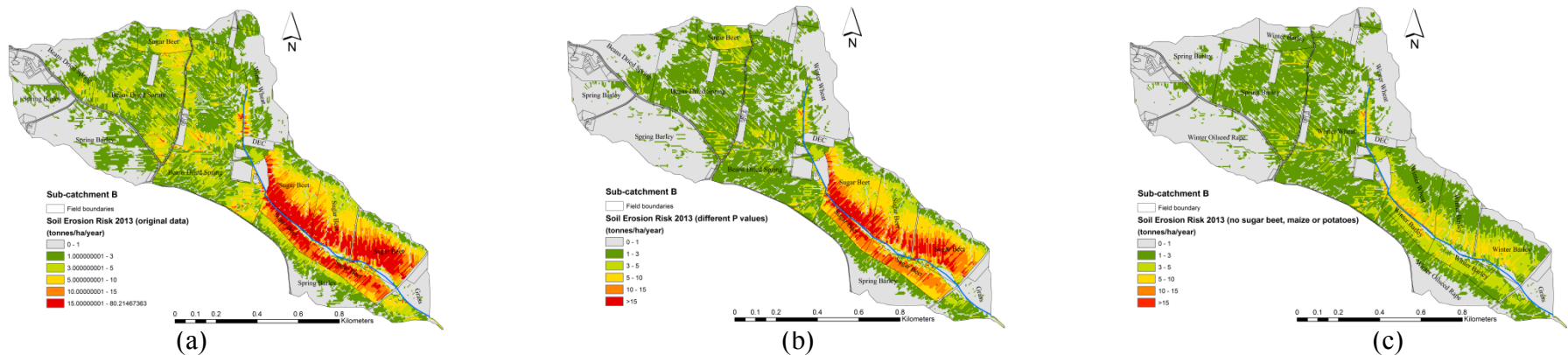

Figure 7.25: Soil erosion risk maps for mini-catchment B, (a) normal scenario, (b) first level assessment of measures for soil erosion risk (Scenario one), by adopting different tillage practices, contour tillage (P =0.5) where sugar beet or potatoes occurred and strip tillage (P=0.37) for any other crop, (c) second level assessment of measures for soil erosion risk (Scenario two), by replacing any sugar beet, potatoes or maize crops with either wheat, barley or oilseed rape, according to the previous crop grown at the proposed field. Note: In scenario two, all fields were assumed to be cultivated with strip tillage.

Table 7.32: Rates of soil erosion in mini-catchments A and B in terms of crop types based on the three scenarios.

|	Season 2012\13					
	Mean soil erosion loss (tonne/ha/yr)					
	Mini-catchment A			Mini-catchment B		
Crop	Original Scenario	Scenario 1	Scenario 2	Original Scenario	Scenario 1	Scenario 2
Maize	0.85	0.50	-	-	-	-
Sugar Beet	3.45	2.76	-	10.013	8.011	-
Beans	1.38	0.82	0.73	2.804	1.688	1.688
Peas	-	-	-	-	-	-
Winter Wheat	1.13	0.67	0.67	1.286	0.761	1.523
Oilseed Rape	0.67	0.51	0.47	-	-	2.619
Spring Barley	1.25	0.74	0.74	1.356	0.803	1.205
Winter Barley	0.44	0.26	0.30	-	-	-
Total soil loss (tonne\year)	254.11	207.33	147.74	162.989	127.53	92.195
% of reduction		18.41%	41.86%		21.76%	43.44%

(a)

(b)
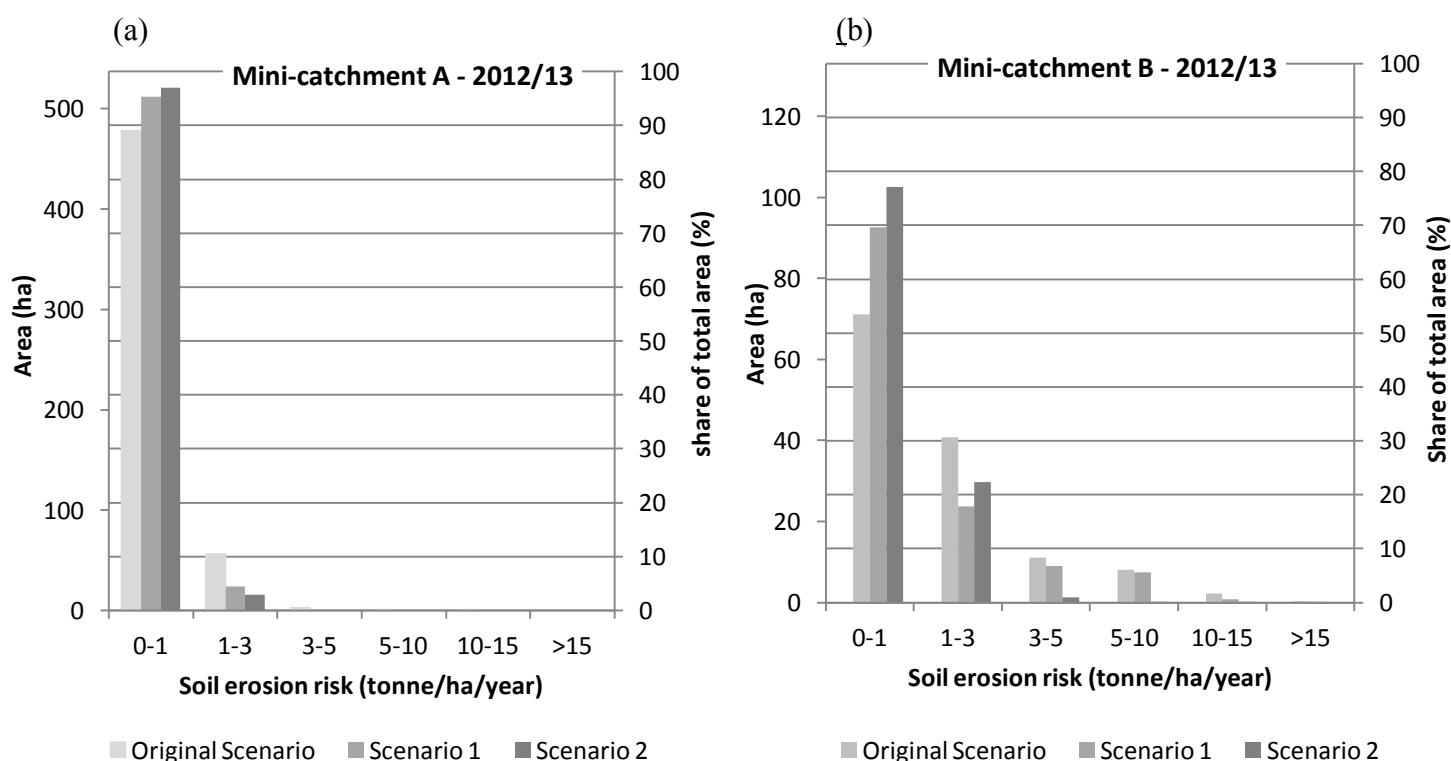
Figure 7.26: Areas occupied by each class of erosion severity (left y- axis) and their percentages from whole catchment area (right y-axis), according to the three scenarios adopted.

7.3.6.2.2   Second scenario – land use scenario (no sugar beet, potatoes or maize)

Figures 7.24c, 7.25c and 7.26 and Tables 7.31 present the results of the assessment of soil erosion risk in mini-catchments A and B under Scenario 2, season 2012/13. In general, the lowest/best soil erosion risks values obtained for mini-catchment A was achieved under Scenario 2 for the farming season of 2012/13. Results showed that under this scenario, the percent of land in the very low erosion category largely increased (97.03% of the total area) while that in the very high to extreme categories decreased (0%) (Figure 7.26a). The average annual amount of eroded soil from the mini-catchment was found to be about 147.74 (tonne/yr) with about 41.86% reduction compared to the original analysis. The underlying reason for these results can be attributed to the fact that in parallel with the best scenario condition applied to the catchment (strip cropping and avoiding high risk crops) the rainfall erosivity factor (R) was relatively low compared to the previous season. Therefore, it appears that, depending on rainfall characteristics, many agricultural lands are at a high risk of soil erosion.

The impact of changes in cultivation methods and crop types on rates of soil erosion in mini-catchment B was really significant, since the sugar beet was the dominant crop during season 2012/13. Figure 7.26b illustrates that the area of the mini-catchment covered by very low erosion increased by about 25% compared to the original analysis. Moreover, a reduction in soil loss up to 43.44% was estimated when these combined erosion control practices (strip cropping practice and avoiding high risk crops) were implemented.

7.3.7   Summary and conclusion

It has been shown from the above discussion that, the integration of the RUSLE with raster GIS is of best use for land classification of soil erosion risks. Although many

assumptions were made in this study, the erosion rate values obtained were reasonable when compared to measured soil losses cited in the literature from fields at different sites around the UK. In addition, the relative comparisons of turbidity measurements measured at the outlets of the mini-catchments A and B to the RUSLE results for each catchment confirmed the realistic RUSLE output results.

Two DEMs from different sources at various spatial resolutions were analysed for their reliability for soil erosion modelling with RUSLE. It was difficult to quantitatively compare their soil loss results because of the lack of field based soil loss measurements in the study area. In this study, the highest resolution DEM, NEXTMap (5m), was found to be the most realistic at qualitatively identifying regions of higher possible soil loss risk. This is because when the coarser DEM was used erosion processes may not be adequately represented due to possible significant loss of spatial variability represented by the LS factor in the RUSLE. However, although using DEM data in different resolutions and from different sources affected the output results of the erosion model, the large-scale patterns of predicted soil erosion at coarser resolution were similar to those with the finer resolution DEM.

The strength of the RUSLE model is in identifying the relative spatial differences of erosion risk rather than on exact values (Hoyos, 2005). Therefore, the resulting erosion risk patterns should indicate which factors are more or less influential and under what conditions. Thus, in order to understand the effects of changes in some factors, the RUSLE was implemented using different scenarios; the influence of different support practices (Scenario 1) and the influence of changes in land uses (Scenario 2). Results showed that even under first scenario (contour farming practice for sugar beet fields), the mean annual soil loss from sugar beet fields is still very high compared to other crops. This was interpreted as a consequence of the current spatial distribution of the sugar beet fields across the catchment (especially season 2011/12 for mini-catchment A and season 2012/13 for B) where the majority of the

sugar beet fields coincided with sloping fields (higher LS values) which were also adjacent to water courses (Figure 7.13). Inman (2006) discussed some of the causes of soil erosion on agriculture land in England and Wales and he suggested that one of the key activities that encourage soil erosion is the growing highly susceptible crops on inappropriate land. As mentioned previously, certain combinations of soil texture, slope and crop type can lead to high risks of erosion (Boardman et al., 2009). Therefore, adopting additional cropping management and erosion control practices (including for example; reduced-tillage or residue cover) and targeting areas with high risk of erosion should help to further reduce soil erosion risks (Boardman et al., 2009; Defra, 2005; Fernandez et al., 2000; Inman, 2006; Volk et al., 2010). Nevertheless, as advised by Defra (2005), for any areas with a substantial erosion risk the situation can be completely avoided by keeping these areas under permanent grass or woodland.

Modelling the effect of land use changes (Scenario 2) on the soil erosion risks indicated that the erosion potential of the mini-catchments would decrease as a result of converting highly susceptible to erosion crops to those classified as low risk crops. Chambers and Garwood (2000) argued that in order to minimize erosion risks on susceptible sites it is important that soil conservation practices are used, such as ensuring that low susceptible to erosion crops are grown on particularly high risk fields, and where practically possible, avoiding compaction and wheelings. Boardman et al. (2009) also concluded that successful conservation schemes require a multi-method approach combining land use change and anti-erosion management measures. Consistent with this, the best results in this study were achieved under Scenario 2, where highly susceptible to erosion crops were avoided and strip tillage practice was applied to all croplands.

7.4 SCIMAP vs RUSLE

In this study two different approaches (SCIMAP and RUSLE) were used to predict soil erosion risks in the Backwater sub-catchment, therefore, it is useful to compare their predictions. Figure 7.27 (a and b) illustrates areas at high risk of erosion based on SCIMAP and RUSLE. It is clear from the maps that the spatial distribution of SCIMAP and RUSLE predictions of areas at high risk of soil erosion is quite different. The result from SCIMAP indicates that a high proportion of the Blackwater sub-catchment is susceptible to erosion (Figure 7.27a). As discussed earlier, due to the catchment wide predominance of arable farming and as a result of the risk weighting specified to arable land use (100% risk), the model considered that a significant proportion of the catchment area is at risk of soil erosion. However, a closer look at the erosion risk map indicated that the areas deemed to be most at risk are those in the highest headwater parts of the catchment where high risks of connectivity are combined with arable land (see figure 7.27a, mini-catchments A and B).

On the other hand, RUSLE results indicate that only particular parts of the sub-catchment are found to be at high risk of soil erosion. Further inspection of Figure 7.27b reveals that those areas with the highest severity of soil erosion were often predicted to be at areas on steep lands (high LS) coincident with high risk land uses. As opposed to the results form SCIMAP, areas classified as having a high risk of erosion in the RUSLE approach have been interestingly shifted to the parts of the sub-catchment where sites classified as at high risk on the bases of soil types and slopes coincided with highly susceptible to erosion land cover (Figure 7.27b).

Therefore, results of this study lead to the observation that, in a small lowland catchment that is almost covered by arable land, SCIMAP tends to predict that the areas susceptible to hydrological connectivity and under the influence of arable farming are those

areas at high risk of soil erosion and results suggest that large proportions of the study catchment at risk of erosion. Whereas in the RUSLE approach, only parts of the catchment where sites are classified as at high risk on the basis of soil types and slopes coinciding with highly susceptible to erosion land cover are classified as risky areas. These areas are usually the sites on sloping fields adjacent to watercourses. Thus, this strongly suggests that, in SCIMAP, landuse is the key controlling factor in determining risky areas within the Blackwater sub-catchment. On the other hand, for RUSLE modelling, risky areas were determined at locations where three or more factors coincided, vulnerable soil, steeper slope (high LS value) and high risk crop (C factor).

Despite the differences between SCIMAP and RUSLE in their spatial predictions of areas at high risk of soil erosion described above, there is an agreement between the two approaches in that mini-catchments A and B are more at high risk of agricultural diffuse pollution compared to the other parts of the sub-catchment. It should be acknowledged that RUSLE is an empirically-based model used in the science of soil erosion to provide predictions of average soil loss over long periods of time. Results from this model can be used to target specific combinations of soil type, land use and slope that lead to significant soil erosion, enabling mitigation process to be implemented. Brazier (2013) argued that the use of models such as the RUSLE to predict the medium to long-term effects of soil erosion can provide the means to target areas where soil erosion exceeds a given tolerance levels. SCIMAP takes a different approach and operates in a risk-based framework rather than on a net loss prediction basis. As discussed earlier in this chapter, SCIMAP works with the spatial pattern of land cover, hydrological connectivity (topography) and rainfall data to calculate map based predictions of where risk is generated, connected and concentrated within the catchment. These maps are used to trace back across the catchment to where the risk sources are probably located (Reaney et al., 2011). Thus, SCIMAP appears to have good potential to

be used at least as a tool for the identification of critical source areas across a catchment

(Hahn et al., 2013).
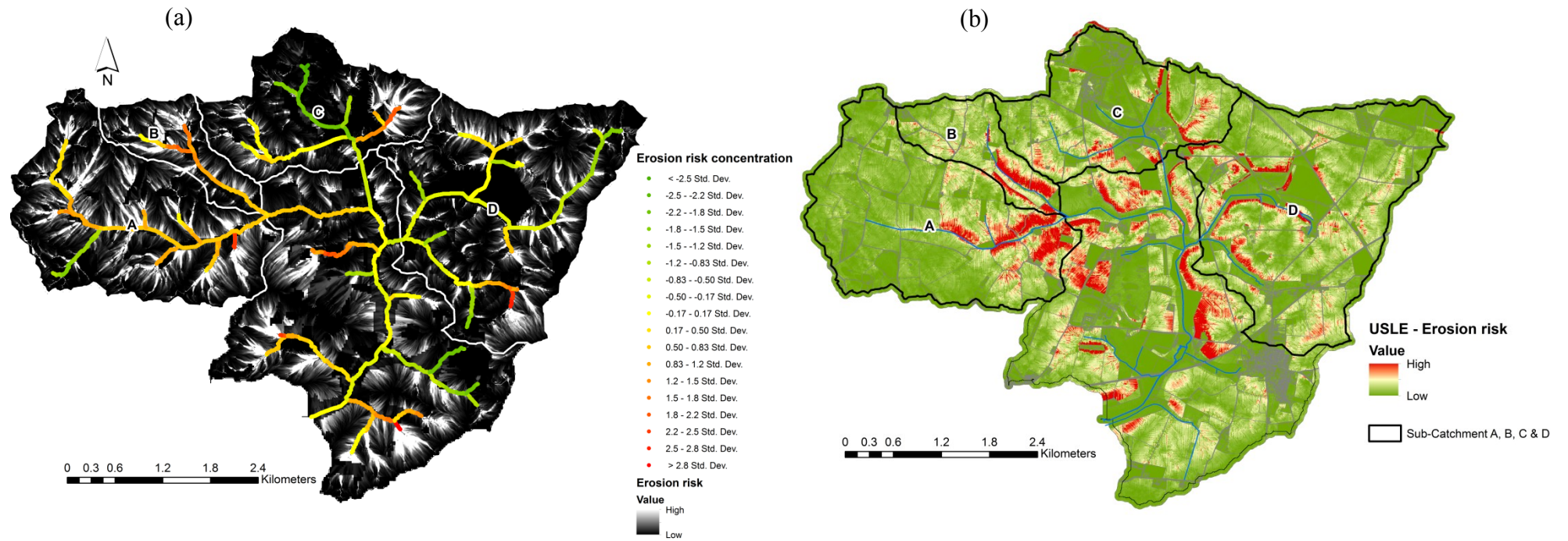
Figure 7.27: Blackwater sub-catchment models showing areas at high risk of erosion based on (a) SCIMAP and (b) RUSLE.

7.5 Chapter conclusions

This chapter has applied a diffuse pollution risk-based modelling approach (SCIMAP) and a soil erosion risk estimation model (RUSLE) to the Blackwater sub-catchment using two DEMs from different sources at different resolutions, NEXTMap 5m and OS Landform Panorama 50m. The results indicated that both models were indeed sensitive to the data resolution. The highest resolution NEXTMap DEM was found to be more realistic than the courser OS50m DEM, especially for the SCIMAP approach. Therefore, due to the overall poorer performance of the OS Landform Panorama 50m DEM, it is not recommended as the DEM of choice for soil erosion and diffuse pollution modelling in the Blackwater sub-catchment. However, for the soil erosion analysis it should be noted that the resampled NEXTMap 50-m performed slightly better than the OS 50-m and that is believed to be be due to the higher quality original source data.

The results from SCIMAP suggest that the dominance of arable farming in the Blackwater sub-catchment results in large proportions of the study area estimated as at risk of erosion. This can be attributed to the fact that in SCIMAP analysis is based on land cover category. This does not differentiate between different crops inside the arable category, which in fact vary greatly in terms of erosion risk, and instead assigned the highest risk weighting value (%100 risk) to any arable land cover (Reaney et al., 2011). In future, to overcome this weakness of the SCIMAP approach and to enable an assessment of variations in the effect of different crops upon erodibility (weighting risk), the internationally accepted RUSLE Crop Management Factor (C-factor) should be used. As a result, SCIMAP could then can be used to produce a catchment-wide risk map where the effects of different crop types would be considered. Another limitation of the SCIMAP approach compared to RUSLE is the omission of the effect of soil types on soil loss prediction processes. To overcome this drawback, the

effects of soil type upon erodibility can be consider by developing a combined land cover and soil type risk map which can be incorporated into the SCIMAP model.

The comparison of the predictions obtained with the two models indicates that the locations and extent of high erosion risk areas in the Blackwater sub-catchment were more dependent on land cover in the SCIMAP framework and on soil type, slope (topography) and crop type in the RUSLE model. In terms of the in-stream sediment risk, SCIMAP results indicated that mini-catchments A and B are especially at risk. These two mini-catchments were also represented by RUSLE as areas prone to high risk of soil erosion. Therefore, according to the results from both models, it can be inferred that the two mini-catchments A and B are considered to be the most likely source of sediment diffuse pollution in the Blackwater sub-catchment. Thus, soil erosion on arable land is definitely a problem in these two mini-catchments. Significantly, these results are supported by the real time measurements of water quality at the outlet of each mini-catchment, as discussed earlier in this chapter. Thus, with these findings from both models, management interventions can be focused and priority should be given to areas of high risks within these two mini-catchments.

However, the real strength of the RUSLE model over SCIMAP is that different erosion scenarios can be analysed and compared with each other (Ranzi et al. 2012; Rulli et al. 2013; Terranova et al. 2009). In this study, by comparing different scenarios, the effectiveness of some anti-erosion practices (changes in the C and P factors) has been highlighted. The comparisons of the scenarios (the effects of land use changes and anti-erosion management measures on soil erosion) provide a useful basis for the definition of prevention and control measures by organisations responsible for soil and water resources management. For example, a scenario of implementing best management practices on steep, vulnerable soil will help to examine the effectiveness of the scenario in minimising soil losses, which, in turn limits sediment deliver to a water body.

Overall, based on the above discussion, it is clear that in a GIS environment the RUSLE can be applied to determine field-scale soil loss quantitatively and spatially, and then to predict erosion hazard over a larger catchment. The combined RUSLE/GIS approach was useful for describing areas that are vulnerable to soil erosion, enabling immediate conservation planning. The study yielded useful soil erosion risk thematic maps for the Blackwater sub-catchment and some of its mini-catchments in more detail, where hot spot locations of soil erosion risk were identified. Those maps can be important for authorities (e.g. such as a River Trust) to plan future land use alternatives and to apply specific soil conservation practices at the identified high risk locations.

However, it should be noted that many assumptions were involved in applying RUSLE in the Blackwater sub-catchment. Since detailed data for the calculation of the K and C factors were not available, these parameters were estimated from the literature. The uncertainties regarding data sources for these factors as well as those associated with the DEM data may introduce larger uncertainties in soil erosion estimates. Undoubtedly, (R)USLE produces errors in the prediction of soil erosion values as proved by studies that compare RUSLE/USLE estimated values with ones observed in the field (Bartsch et al. 2002; Boomer et al. 2008; Evans 2002; Evans and Brazier 2005: Prasuhn et al. 2013; van Rompaey et al. 2003). Therefore, often RUSLE/USLE is more suitable for identifying soil erosion risk areas qualitatively rather than providing quantitative values (Bargiel et al. 2013; van der Knijf et al. 2000; Wu et al. 2005). Nevertheless, these data are indispensable for conservation policies that need qualitative erosion assessment in relation to soil protection and water quality management.

Chapter 8

Conclusions

8.1 Overview

DEM-based modelling of watershed processes has become increasingly popular in environmental research, for example hydrological and geomorphology studies, mainly due to the advances in availability and efficiency of DEMs to represent topographic properties of catchments, such as slope, field slope length and channel network. This research has investigated the accuracies and uncertainties associated with different digital elevation datasets derived from different sources and explored the implications of their use in hydrological analysis and catchment management applications in a UK lowland river catchment. The research then studied the effect of DEM sources and resolutions on extracted stream networks and catchment boundaries as well as the implications of using these different DEMs for soil erosion and diffuse pollution modelling in the Blackwater sub-catchment, one of the five priority sub-catchments of the larger River Wensum catchment in Norfolk.

Achieving good ecological and chemical status for English rivers is an important objective of the Water Framework Directive (WFD, 2000); intensive agricultural activities have the potential to work against this objective. Research has shown that Blackwater sub-catchment is a high risk area for sediment loss and its associated diffuse pollutant inputs as a result of intensive arable farming (Sear et al., 2006; Wensum Alliance, 2013). Previous research (e.g. Boardman et al., 2009; Collins et al., 2009; Defra, 2005) has called for a move

towards better agricultural land management practices (such as land use changes and anti-erosion management measures) aiming to minimise soil disturbance and reduce soil erosion as a source of sediments. The effectiveness of these measures can be investigated by projecting scenarios of land use changes and changes in cultivation methods using soil erosion modelling frameworks (e.g. RUSLE). However, little research has focused on investigating the effectiveness of these scenarios in the context of risk-assessment for specific sites. Therefore, one of the research objectives was to use RUSLE to examine the risk of soil losses under different scenarios of land use changes and different land cultivation practices.

This chapter first summarises the main findings of the research. In the latter part of this chapter the implications for catchment management are discussed and recommendations for future research are made.

8.2 Findings

8.2.1 Objective 1

To evaluate the accuracy of different DEM datasets representing the same region and surface type but derived from different sources.

In this study, the quality of seven elevation datasets: ASTER, SRTM, Bluesky DTM, LandMap DTM, NEXTMap DTM, Ordnance Survey Landform and Ordnance Survey Panorama over an area of 225 sq km in the River Wensum catchment has been investigated. The results from the quality comparisons in terms of slope and elevation descriptive statistics and histograms, cross-sectional profiles, and analytical shading relief images revealed the following findings. The results showed the presence of artifacts in most DEM datasets (Chapter 4, Section 4.3.4). Some artifacts occurred on the surface of a certain morphometry.

The remote sensing methods such as IFSAR and ASTER capture the earth surface and required filtering. The ASTER GDEM 1 elevation dataset was found to contain anomalies and artifacts that degrade its overall accuracy. It has a lot of pit artifacts where the elevation is considerably lower than the surrounding terrain. The LandMap DTM (25 m) was a noisy elevation dataset. The data contains a lot of spurious pits, spikes and stripe-effects artifacts occurred with high frequency. To a lesser extent, the examined relief-shaded images of the NEXTMap DTM revealed some artifacts caused by woodland cover that were not completely removed during the process of converting from DSM to DTM. In the case of contour based DEMs, visual inspection of the shaded relief maps revealed that striping and flat hill-tops along contours are present in the OS contour based DTMs (especially OS 10m). Similar artifacts associated with the contour data are discussed in several studies such as Carrara et al. (1997), Desmet (1997) and Wise et al. (2008).

The coarser DEM, SRTM 90 m, performed better than both LandMap and ASTER apart from the fact that elevation values were overestimated in areas covered by woodlands. Results of horizontal profiling (Chapter 4, Section 4.3.3) indicated that SRTM data represented surface elevations quite similarly to results from the higher resolution DEMs: Bluesky, NEXTMap, Ordnance Survey Profile and Ordnance Survey Panorama for all land cover types, but if significant vegetation is present the elevation values are usually overestimated. In contrast, results of the horizontal profiling showed that elevations from ASTER and LandMap were consistently lower than those of other datasets. Moreover, they showed the lowest mean elevation values compared with the other datasets. This is in line with results of previous studies (Forkuor and Maathuis, 2012; Lin et al., 2013; Slater et al., 2009). In addition, according to the slope statistics, the ASTER and LandMap data were found to have about only 62.7 and 63.5% of their areas having slopes less than or equal to 3°, respectively. These results are in counterintuitive with findings from the higher accuracy

DEMs (NEXTMap and Bluesky) where approximately 90% of their areas have slopes of 0 - 3°. In a related study, Collins et al. (2013) reported that approximately 98% of the area represented by Wensum catchment has a median slope of 0 to 3°.

Vertical accuracy is the most important factor to be considered when a DEM is used. The most common practice to assess the accuracy of a DEM is to generate statistical measures, such as RMSE, mean error and standard deviation. This assessment was carried out by verification of each DEM against a number of higher accuracy spot heights. This approach is a common method of accuracy assessment in many applications. The results discussed in Chapter 4, Section 4.3.5.3 clearly show that the ASTER and LandMap elevation datasets produced the worst results on most statistical measures (minimum, mean, RMSE and std.dev) in comparison with other elevation datasets. The analyses also revealed that SRTM has a higher vertical accuracy (in terms of RMSE) than both ASTER and LandMap datasets. Among all the DEMs used in this study, the OS 10m data were found to be the most accurate based on the comparison against the higher accuracy reference data. It has the highest vertical accuracy (RMSE = 0.5987 m) and this can be attributed to the fact that OS 10m DEM and the reference data are products of the same organisation, the Ordnance Survey.

In this part of the study, the findings suggested that both ASTER and LandMap elevation datasets performed very poorly in the Wensum area. METI and NASA acknowledged that ASTER GDEM 1 is research grade due to the presence of certain residual anomalies and artifacts in the data that may affect the accuracy of the product and hinder its effective utilization for certain applications. Bluesky 5m (photogrammetry) and NEXTMap 5m (IFSAR) elevation datasets were found to be the most accurate and thus the most realistic approximation of the real surface amongst the selected DEMs. The performance of the other three DEMs, OS 10m, OS 50m and SRTM 90m in comparison to the results from the finer resolution DEMs and also against the higher accuracy reference data suggests that these

DEMs provide good approximations of the real ground surface and thus were considered suitable for inclusion in further stages of this research.

8.2.2   Objective 2

To determine an appropriate threshold value (flow accumulation threshold) that can be used to accurately delineate channel networks in the Blackwater sub-catchment.

Accurate delineation of the surface pathways of water movement on the catchment landscape is a vital component for many catchment-based natural resource management issues. Processes and phenomena determined by small local variations in topography such as concentration of overland flow for surface water modelling are likely to be modelled differently according to the type of DEM used. The quality of these DEM-derived hydrological features is sensitive to DEM accuracy (Burrough and McDonnell 1998). Channel network extraction models often simulate transitions from hillslope to channelized flow based on a contributing area threshold calculated from the DEM. Different values of the contributing drainage area threshold produced radically different stream networks. The main part of this section of the study (Chapter 5, Section 5.2.3) was devoted to examining the effect of DEM source and resolution in identifying the point of transition where diffuse (hillside) erosion terminates and fluvial (stream) erosion initiates as a result of concentrated surface flow using the relationship between contributing drainage area and local slope (Montgomery and Foufoula-Georiou, 1993; Ijjasz-Vasquez and Bras, 1995; Tarolli and Dalla Fontana, 2009) for the Blackwater sub-catchment.

Results from this study revealed that the higher resolution DEMs (Bluesky and NEXTMap) are more appropriate for extracting various hydrological and geomorphological process domains on the arable lowland of the Blackwater sub-catchment. It was found that from the area-slope plots for the different five DEMs, only Bluesky and NEXTMap DEMs

were able to depict the different inflection points that enabled the distinction between the various geomorphic and hydrologic regimes, hillslopes, unchannelized, and channelized domains. These distinct flow path regimes defined by an area-slope relationship have been identified for different areas in the previous literature (e.g. Henkle et al., 2011; Ijjasz-Vasquez and Bras, 1995; McNamara et al., 1999; Montgomery and Foufoula-Georiou, 1993; Tarolli and Dalla-Fontana, 2009).

For the Blackwater sub-catchment and using the 5 m resolution DEMs (Bluesky and NEXTMap), plotting contributing area against local slope reveals trends in the relationship that signify physical changes in persistent sediment transport process domains. First, there was a break from positive to negative slope of the relationship at very low contributing area (0.000625 km², hillslope diffuse process). A break from negative to less negative gradient was found at larger contributing area (0.005 km², unchanneled valleys), and a break from less negative to more negative gradient was obtained at a larger contributing area (1.25 km²), attributed to where fluvial channel processes begin to persist (true streams). On the other hand, the findings indicated that none of the other three DEMs (OS 10m, OS 50m and SRTM 90m) were able to clearly capture any of these hillslope morphologic scaling regimes. In the case of OS 10m performance, the effect of the data source is clearly evident. The curvature in the diffusive region of the area-slope relationship is lost and the relationship is linear nearly over the entire domain (Chapter 5, Section 5.2.4, Figure 5.26C). This is believed to be attributed to the fact that the contour based DEMs usually exhibit a lot of artifacts such as; flat hill-tops, terraces along contours and striping. The contour based DEM poorly modelled the relatively flat terrain (such as the Blackwater sub-catchment) as artifacts occur in areas where contours are separated by a large distance (Carrara et al., 1997). Interestingly, despite the fact that OS Panorama (50m) is coarser than OS Landform Profile (10m) and originates from the

same data source, the performance of OS 50m was better in the area-slope relationship analysis for the Blackwater sub-catchment.

The examination of the area-slope relationship for the different DEMs demonstrates that as cell size increases, details in the area-slope relationship are lost. At a grid spacing of 10 m, 50 m and 90 m, the curvature in the diffusive region is lost as the data become more linear (Chapter 5, Section 5.2.4). Therefore, findings revealed that for the Blackwater sub-catchment a DEM of at least 5 m resolution is needed so that the area-slope relationship can be used as a tool to determine hillslope-to-channel partitioning. At any resolution larger than 5 m it appears that important hillslope details are lost. Consequently, it can be said that the area-slope relationship plot can provide a tool for determining a suitable DEM resolution for observing geomorphic processes (Hancock and Evans, 2006; Tarolli and Dalla-Fontana, 2009). According to the findings, for the Blackwater sub-catchment, DEMs with resolution of 5 m or finer need to be used to accurately identify the dominant geomorphic processes and distinct flow path regimes.

8.2.3   Objective 3

Quantitatively comparing the positional accuracy of drainage networks derived from different DEMs.

Accurate delineations of stream networks and catchment boundaries are important for hydrological modelling and catchment resource management studies. Using the highest resolution data available is always advised, however, this thesis provides a measure of how much variation might be introduced into the delineated stream network and catchment boundaries when different DEMs are used. Several factors influence the accuracy of stream network delineations in areas with low relief due to the occurrence of artifacts and the lack of sufficient details in DEM representations of the terrain. The third objective of this research

was to evaluate and compare positional accuracy as well as assess selected hydrological parameters (stream order, number of streams in each order, stream lengths and catchment area) of drainage networks delineated in the Blackwater sub-catchment from NEXTMap, Bluesky, OS 50 and SRTM DEMs against a higher accuracy reference network (Chapter 6). The main interest, however, was in comparison of the positional accuracy of different stream networks extracted first, directly from the original DEMs and second, from DEMs after the simulation of DEM errors. Two methods for quantitatively evaluating and comparing such extractions were used, horizontal RMSE and different buffer zones (epsilon band) around the reference network.

The results obtained from all the methods used in this study revealed that DEM spatial resolution and data source type were important factors that influenced the extent and positional accuracy of the extracted stream networks. The horizontal RMSE was found to increase with the cell size. The results showed that differences in the distance between the modelled stream network and the reference network tended to be smaller with a finer resolution in both the horizontal RMSE and epsilon band buffer approaches. This meant that stream networks extracted from Bluesky and NEXTMap DEMs were closer to the reference network. Further, the effect of data source and processing methods for generating DEMs was also apparent, where the 5 m resolution NEXTMap data offered a better horizontal RMSE value of 22.36 m, as opposed to 30.01 m from the other 5m resolution data, Bluesky. This was believed to be due to the effect of the data source type, the method of processing the original data to create the DEM and other post-processing activities (e.g. DSM to DTM).

Results from this analysis also show that the performance of the DEMs is better after the simulation of DEM errors (error propagation). Findings suggested that using Monte Carlo simulations with alternative DEM realizations produced by adding random error surfaces onto the original DEM (unconditional simulation of error) and then deriving most probable stream

networks improved the accuracy of extracted stream networks, compared to those extracted from the original DEMs. The derivation of the most probable stream networks showed a better spatial matching between these networks and the reference network. Thus, the use of DEM realizations with modelled error seems to give more reliable results that minimise the uncertainty due to errors in the original DEM (Gatziolis and Fried, 2004; Poggio and Soille, 2011: Raaflaub and Collins, 2006).

Overall, in this study, the results obtained suggested that the major factors affecting the positional accuracy of derived stream networks are the DEM resolution, and to lesser extent data source, processing and post-processing techniques. NEXTMap data offers better results compared with the other elevation datasets, however, the differences between NEXTMap and Bluesky derived stream networks were not substantial, in some respects the Bluesky data performed well and similar to NEXTMap. Generally, the results discussed in this section (objective 3) strongly suggest that, for the purpose of modelling stream networks in the Blackwater sub-catchment, NEXTMap is the best input DEM data and using Monte Carlo simulation to identify the most probable stream network is also worthwhile.

8.2.4 Objective 4

To conduct an assessment of soil erosion and diffuse pollution risks in the study catchment using different DEMs. A particular focus of this investigation was to identify the locations (or sub-catchments) of high risk soil erosion areas within the study catchment using RUSLE and SCIMAP modelling techniques.

The main objective of this section of the research was to investigate the current diffuse sediment pollution risks and soil erosion problems associated with arable cultivation in Blackwater sub-catchment using two different modelling approaches. The diffuse pollution risk modelling framework (SCIMAP) and a model for long-term average annual soil erosion

prediction (RUSLE) were applied to the Blackwater sub-catchment using two different DEMs, NEXTMap 5m and OS 50m. The findings indicated that both modelling approaches were indeed sensitive to the data resolution. The highest resolution NEXTMap DEM was found to be more realistic than the coarser OS50m DEM, particularly in the case of the SCIMAP approach. Therefore, the following discussion is based on the results from using NEXTMap data as the surface representation into SCIMAP and the RUSLE.

Not all the areas contribute equally to the delivery of diffuse pollutants to the drainage network and the observed water quality problems. Hence, the identification of critical source areas (CSAs) is crucial for management to be targeted at the most appropriate locations (Heathwaite, 2010). The basis of the SCIMAP analysis is the consideration of both the probability of a part of the catchment landscape generating a risk and then that risk reaching the waterways (Lane et al., 2006). The analysis of the intermediate layers from applying the SCIAMP model to the Blackwater sub-catchment showed that large proportions of the sub-catchment were assessed as at risk of diffuse pollution. This was attributed to the fact that most of the sub-catchment area is used for intensive arable farming which is considered by SCIMAP as having the highest risk weight (100% risk) (Chapter 7, Section 7.2.3.1).

However, the in-stream risk concentration results, where the dilution effect was considered, indicated that the areas at greatest risk of diffuse pollution were mainly located in the western parts of the sub-catchment, mini-catchments A and B. These two mini-catchment were highlighted as being most at risk of being critical source areas of surface soil erosion and consequently agricultural diffuse pollution. Furthermore, these findings were supported by the water quality data gathered by the DTC Wensum project at the outlet of each mini-catchment. The high risk in these two mini-catchments was attributed to the interactions between high levels of hydrological connectivity and highly susceptible to erosion land use. Therefore, in

this instance, it is these areas where conservation soil management activities would be best targeted in order to minimise sediment erosion risk.

In the second part of objective 4, it was demonstrated that the use of RUSLE in a GIS environment for modelling soil erosion can provide a very sound base for the effective estimation and visualisation of soil erosion risks in the Blackwater sub-catchment. In order to understand the soil erosion problems associated with arable cultivation in the study area, this section sought to quantify the magnitude of the soil erosion rates and spatially identify parts of the sub-catchment prone to higher risk of erosion associated with crops cultivation using the RUSLE. Generally, although assumptions had to be made in the computation of the soil erodibility (K) and crop management (C) factors, the soil erosion rate values obtained were reasonable when compared to measured soil loss rates cited in the literature from fields at different sites around the UK (Chapter 7, Section 7.3.5). However, estimated soil loss rates were still higher than soil erosion tolerance (Verheijen et al., 2009) and also than field measurements (Brazier, 2004).

As many studies show, RUSLE often overestimate soil erosion rates. Generally this is attributed to the empirical nature of the model and to the fact that it is based on experimental plot data (Evans and Brazier, 2005). As previously stated, a shortcoming of USLE/RUSLE models is that they do not predict sediment deposition. Thus, the model predicts erosion universally, even where deposition may occur, therefore, at a catchment scale, it is likely that the model will tend to overestimate erosion (Warren et al., 2005). In addition, the accuracy of the predicted soil loss will depend on how well the parameter values that are used for sub-factor calculations describe the physical and management conditions on the ground. An error in the selection of a factor value will produce an equivalent error in soil loss estimates. For instance, in this study quite general assumptions had to be made for the values of the crop

management (C) and soil erodibility (K) factors. One of these was that the effect of the crop factor that was assumed to be constant throughout the seasons.

Sugar beet cultivation has been identified as a key cause of soil loss and consequently stream pollution in the study area. Findings obtained from the comparison of the river monitoring data and the RUSLE model output results for mini-catchments A and B indicated that eroding sugar beet fields were an important source of sediment transported to the rivers. Results highlighted that sugar beet can be very risky crop if it is harvested in the wrong conditions, such as during or after heavy rainfall. In the context of sugar beet cultivation in the Blackwater sub-catchment, mini-catchment A had the largest areas cropped with sugar beet in season 2011/12, 21 fields in total. According to the water quality data, this study suggested that the potentially high rate of soil erosion associated with sugar beet fields after harvest was the main source of increased sediment inputs to the streams in the Blackwater sub-catchment. The findings also indicated that values of high turbidity and sediment load measured at the outlet of mini-catchment A during the period from September 2012 to April 2013 (Table 7.26 and 7.27) were consistent with harvesting of sugar beet fields planted in the previous 2011/12 season.

In considering the wider implications of the results outlined above, it is important to highlight the need for some protective measures on sugar beet (or potatoes and maize) cultivation in the Blackwater sub-catchment, which appear to increase the potential for high rates of soil loss and sediment delivery to watercourses. As noted in Chapter 7, most of the area of sugar beet cultivation in the Blackwater sub-catchment occurs on fields that are characterized by relatively steep topography and soils (e.g. deep loam) that are particularly susceptible to erosion. In addition, many sugar beet fields are located relatively close to watercourses. These factors are likely to increase the erosion risk and the efficiency of sediment delivery to watercourses.

RUSLE has the capacity to allow the impact of changing factors influencing soil erosion to be analysed. In this case the soil type, rainfall and topography were treated as unchanged parameters, while vegetation effects (C-factor) were altered by changing the crop types that were grown and the support practices (P factor) were modified by adopting more effective erosion control practices. The observed results from these scenarios indicated that the most effective reductions in soil erosion were achieved when the highly susceptible to erosion crops (e.g. sugar beet) were avoided and a strip tillage practice was applied to arable crop land across the whole sub-catchment. Important findings from this part of the research were that the effectiveness of conservation practices (contouring and strip tillage) in comparison to conventional management (cross slope tillage) in controlling soil erosion is site specific, and is affected by changes in slope gradient and the crop types grown. Results show that sugar beet fields coinciding with sloping landscapes still generated high rates of soil loss even when the cultivation practice was changed from cross slope tillage to contour ploughing (Chapter 7, Table 7.29). Therefore, individual site assessments are needed, where additional crop management and erosion control practices (for example; reduced-tillage or residue cover) can be implemented for further reduction in soil erosion risks.

Results from these different scenarios provide means that can be used to isolate and describe areas that are vulnerable to soil erosion (which in turn are the most likely sources of pollution), allowing immediate application of soil conservation management. These scenarios are important instrument for policy making to develop soil conservation strategies with multiple criteria for sustainable land management. The risk maps and erosion information can also help enhance discussions between farmers and agencies responsible for catchment scale land and water management and, potentially, agreement on mutually acceptable mitigation measures.

8.3 Implications and Recommendations

8.3.1 Data implications

Modelling overland flow is very dependent on parameters such as slope and aspect which are sensitive to micro changes in topography. In our study, from the collection of DEMs examined, the NEXTMap 5m DTM was found to be the best representation of the topography of the Wensum catchment. As stated before, the Wensum catchment is typical of much land in eastern and southern England in terms of topography and drainage systems. Therefore, the findings of this research are relevant to the problems that occur when working with DEM data at many UK lowland catchment settings. According to our findings, a DEM with 5 metre grid resolution (or finer) is recommended to avoid possible errors when modelling the hydrological processes for such lowland catchment.

It is important to note that elevation data availability has changed since this research started. For example, ASTER GDEM data have been improved with the release of the GDEM2 version in late 2011. It has been stated that the overall accuracy of GDEM2 was improved by the removal of voids and anomalies so that it is approximately three meters more accurate than GDEM1 (ASTER Validation Team, 2011; Meyer et al., 2012; Suwandana et al., 2012). In addition, Ordnance Survey has recently (mid 2013) introduced new sets of elevation data. The Land-form Panorama (OS50) has been superseded by the new OS terrain 50 product, which has been verified to be 4 m RMSE. This data is an open source product which enable users to access a source with consistently maintained height content for the whole of Great Britain (Ordnance Survey, 2013a). Another completely new Ordnance Survey product is OS Terrain 5. This offers 5 metre grid and 5 metre contour options within the one product (Ordnance Survey, 2013b). Certainly according to the findings of this research, one of the

greatest improvements in catchment management applications would be to make data such as OS Terrain 5 freely available to organisations such as river trusts.

Moreover, the Environment Agency has recently made its collection of LiDAR data much more readily available for non-commercial use. As yet, however, these data do not cover all part of the country, including a stripe through the middle of the Blackwater study area. Nevertheless, these data may well provide a valuable resource for organisations such as river trusts in the future (Environmental Agency, 2014).

8.3.2 Error modelling implications

It has been recognized in the literature that even though summary statistics are easy to calculate and interpret, they provide only a global, and thus a limited picture of DEM uncertainty (Fisher and Tate, 2006; Kraus et al., 2004; Wechsler and Kroll, 2006; Wise, 1998). Assessment of the elevation alone is also less informative than the consideration of the derived hydrological parameters. Findings from Chapter 6 show that error modelling is very important in DEM uncertainty and DEM error propagation modelling. Creating multiple equally probable realisations of random error surfaces, extracting stream networks by using these different terrain surfaces as inputs to the flow routing model and then obtaining the most probable stream network produced more robust results compared to the networks extracted from the original DEMs. Therefore, it is important that error modelling techniques are more routinely employed by GIS users, particularly where the fitness for purpose of a data source is not well-established.

8.3.3 Implications for catchment management

The findings from this study have implications for current land management agendas in the River Wensum area and in the Blackwater sub-catchment in particular. There is

evidence in the literature and from water quality data that the Blackwater sub-catchment is at risk of soil erosion problems. This study has shown that in a GIS environment and using a 5m resolution DEM (NEXTMap) the RUSLE can be applied to determine field-scale soil loss quantitatively and spatially, to predict erosion hazards across the catchment. The study presents an example of a model-based estimation of the mean annual long-term risk of soil erosion in the catchment. Based on the model results, which should be interpreted as risk potentials rather than precise numbers, delineation and ranking of sub-areas (or sub-catchments) vulnerable to soil erosion becomes feasible. Therefore, these measured and modelled data of soil erosion risks can be used to aid farmers and other agencies in defining those areas where soil erosion is important and thus where their monitoring policy and mitigation measures should be directed.

The findings presented in this thesis show that GIS-based applications have great potential as a support for catchment management. GIS modelling tools that can be used to test and trial alternative management options and solutions (e.g. different scenarios in soil loss assessment) are particularly helpful in simulating future environmental improvement measures. These advances of GIS analysis are also dependent on the availability of accurate input data, particularly elevation data.

To our knowledge, the GIS capability in most river trusts is quite limited and often does not extend beyond basic mapping. To take advantage of the recent improvements in data availability (e.g. access to LiDAR) additional training and technical support are likely to be needed to extend their routine use of GIS from the descriptive to the more analytical.

8.3.4 Limitations and recommendations for future work

The main aim of this study was to understand accuracies and uncertainties associated with different digital elevation datasets derived from different sources and to explore the

implications of their use in hydrological analysis and catchment management applications in the Blackwater sub-catchment of the River Wensum. In answering this aim through the set of objectives summarised above, the following topics have been identified for further work.

8.3.4.1   DEM accuracy assessment

The limitations of the research on DEM quality are mainly related to the availability of reference DEM data of higher order accuracy. It would have been appropriate to have reference DEMs created using techniques such as high resolution LiDAR data (i.e. 2 metre LiDAR data). The reference data used were a set of spot heights collected from higher accuracy topographic maps (Chapter 4, Section 4.3.5.1) and the locations of these spot heights was mainly based on the existing road network across the study area, which contributed to limitations in the spatial distribution of these heights.

For the DEM error propagation analysis, conditional stochastic simulation (Hunter and Goodchild, 1995) could have been implemented and the outputs compared with the results from the unconditional method used in this study. Conditioning the simulation model allows consideration of spatial autocorrelation between neighbouring error values which might produce less variation in the topographic parameters compared with uncorrelated error (Raaflaub and Collins, 2006).

8.3.4.2   SCIMAP

The methodology behind the SCIMAP framework has several limitations attached to it, which could lead to a significant amount of inherent uncertainty in the model predictions. A main limitation of the SCIMAP framework is that it does not account for the effect of different soil types, which may significantly influence erodibility (Reaney et al., 2011). Research has shown that differences in soil composition can quickly lead to variations in levels of infiltration and overland flow (Heathwaite et al., 2005), which indeed can affect the

model predictions. To overcome this drawback, the effects of soil type upon erodibility could be considered by developing a combined land cover and soil type risk map to be incorporated into the SCIMAP model.

Furthermore, the framework does not differentiate between areas of different land use due to the framework being based on land cover categories. Land cover differs from land use in that it does not include management practices and is coarser in terms of categories. For example, the arable category accounts for all the type of crops (arable cereals and arable horticulture), which in fact differ in the percentage of ground cover throughout the whole growing season (Defra, 2005). Therefore, assuming that the arable category stays constant over the course of a year is not necessarily the case, as crop cover will vary during the growing season and also between different seasons. Thus, to overcome this weakness of SCIMAP approach and to enable an assessment of variations in the effect of different crops upon erodibility (weighting risk), the internationally accepted USLE Crop Management Factor (C-factor) can be used. The C-factor has been discussed in detail in Section 7.3.1.4.

8.3.4.3 RUSLE

In order to further develop the results obtained from this research using the RUSLE, several suggestions for future studies are made here. To improve the quality of erosion modelling results, the methods of estimation of RUSLE factor values should be improved. As mentioned earlier in this thesis, there were many assumptions behind computation of the crop cover management factor (C) and soil erodibility (K) factors. Since detailed data for the calculation of the K and C factors were not available these parameters were estimated from the literature. The uncertainties regarding data sources for these factors may introduce larger uncertainties in soil erosion estimates.

In this study, the coarse data (NatMap) used to obtain K values, despite details on texture, lacked information with respect to the permeability, structure and the percentage of silt and very fine sand information, which are required in the traditional calculations. Therefore, literature values previously calculated based on texture were used. This is not optimal as the k factor is also dependent on local organic matter, permeability and structure. The K factor could be considerably improved within the study area if further research was undertaken. The results would be most accurate if soil samples were taken from the sub-catchment landscape and then analysed for soil structure, permeability, organic matter and texture including percentages of silt, fine sand and clay.

As stated before, the C factor in RUSLE reflecting the effect of vegetation on soil erosion by water is one of the most important factors for estimating soil erosion rates. In this study, each type of crop occurred within the study area was assigned a yearly C value obtained from range of values cited in the literature especially from Europe, USA and Canada (Chapter 7, Section 7.3.1.4). To improve the calculation of C factor, detailed information for individual crops would be required. Information about the cultivation methods and crop rotations in the study area and knowledge about the ground cover percentage at each growth stage are vital to quantify the C factor. In other words, the C factor has to represent the changing conditions of the crop throughout the period of study. This can also necessitate calculations on land use in previous years so that the full effect of crop rotations is known. Therefore, extensive field visits to assess the degree of each crop cover within the study area for the period of study would be required first. Nevertheless, aerial photographs and high resolution satellite remote sensing images are also seen as valuable tool for vegetation cover mapping (Drzewiecki et al., 2013; Vrieling, 2006; Zhang et al., 2011).

Some other limitations of RULSE can be summarised as: it is not feasible to estimate soil loss for individual storm events and it was primarily designed for calculating long-term

average annual rates of erosion (Csafordi et al., 2012); it does not account for gully or stream-channel erosion (Gitas et al., 2009); it generates results usually higher than field based estimates (Bartsch et al., 2002; Evans, 2002; Evans and Brazier, 2005; Hui et al., 2010; Prasuhn et al., 2013) and it does not estimate deposition and sediment yield at a downslope locations (Pandy et al., 2007; Renard et al., 1991).

8.4 Concluding statement

The thesis has enhanced understanding of the properties of different DEMs with varying resolutions and generated from contrasting data sources and of the impacts of these differences on hydrological analysis and catchment management applications. Much remains to be done, but it is hoped that this thesis provides guidance to local catchment managers and organisations such as river trusts about the best use of DEM datasets in developing catchment understanding and future plans.

References

Anderson, D. and Ames, D. (2011). A Method for Extracting Stream Channel Flow Paths from LiDAR Point Cloud Data. *Journal of Spatial Hydrology*, 11(1).

Anderson, E., Thompson, J. and Austin, R. (2005). LIDAR density and linear interpolator effects on elevation estimates. *International Journal of Remote Sensing*, 26(18), pp.3889--3900.

Andrade, O., Kappas, M. and Erasmi, S. (2010). Assessment of erosion hazard in Torres municipality of Lara State (Venezuela) based on GIS. *Interciencia*, 35(5), p.348.

Arnoldus, H., Boodt, M., Gabriels, D. and others, (1980). An approximation of the rainfall factor in the Universal Soil Loss Equation. *Assessment of erosion.*, pp.127--132.

Asok, S. and Sobha, V. (2011). Spatial Information Technology as a tool for soil erosion assessment using USLE-A study in the Shendurney Wild Life Sanctuary, South Kerala, India. *International Journal of Environmental Sciences*, 1(7), pp.1978--2003.

ASTER Validation Team, (2009). *ASTER global DEM validation summary report*. Published by the ASTER GDEM Validation Team: METI, NASA and USGS in cooperation with NGA 523 and other colloborators. June 2009, 28 pages.

ASTER Validation Team, (2011). *ASTER Global Digital Elevation Model Version 2 - Summary of Validation Results*. NASA Land Processes Distributed Active Archive Center and the Joint Japan-US ASTER Science Team.

Atkinson, D., Deadman, P., Dudycha, D. and Traynor, S. (2005). Multi-criteria evaluation and least cost path analysis for an arctic all-weather road. *Applied Geography*, 25(4), pp.287--307.

Atkinson, P. and Foody, G. (2002). Uncertainty in remote sensing and GIS: fundamentals. *Uncertainty in remote sensing and GIS*, pp.1--18.

Baker, M., Weller, D. and Jordan, T. (2006). Comparison of Automated Watershed Delineations: Effects on land cover areas, percentages, and relationships to nutrient discharge. *Photogrammetric Engineering & Remote Sensing*, 72(2), pp.159-168.

Bandara, K., Samarakoon, L., Shrestha, R. and Kamiya, Y. (2011). Automated generation of digital terrain model using point clouds of digital surface model in forest area. *Remote Sensing*, 3(5), pp.845--858.

Bargiel, D., Herrmann, S. and Jadczyszyn, J. (2013). Using high-resolution radar images to determine vegetation cover for soil erosion assessments. *Journal of environmental management*, 124, pp.82--90.

Bartsch, K., van Miegroet, H., Boettinger, J. and Dobrwolski, J. (2002). Using empirical erosion models and GIS to determine erosion risk at Camp Williams. *Journal of Soil and Water Conservation*, 57, pp.29--37.

Benson, D., Fritsch, O., Cook, H. and Schmid, M. (2014). Evaluating participation in WFD river basin management in England and Wales: Processes, communities, outputs and outcomes. *Land Use Policy*, 38, pp.213--222.

Bizuwerk, A., Taddese, G. and Getahum, Y. (2008). Application of GIS for Modeling Soil Loss Rate in Awash Basin, Ethiopia. *International Livestock Research Institute (ILRI)*.

Blanchard, S., Rogan, J. and Woodcock, D. (2010). Geomorphic change analysis using ASTER and SRTM digital elevation models in central Massachusetts, USA. *GIScience & Remote Sensing*, 47(1), pp.1--24.

Bland, J. and Altman, D. (1986). Statistical methods for assessing agreement between two methods of clinical measurement. *The Lancet*, 327(8476), pp.307-310.

Blaszczynski, J. (2001). Regional Sheet and Rill Soil Erosion Prediction with the Revised Universal Soil Loss Equation (RUSLE). *GIS Interface. Resource Notes No.46*.

Boardman, J. (2013). Soil Erosion in Britain: Updating the Record. *Agriculture*, 3(3), pp.418--442.

Boardman, J., Shepheard, M., Walker, E. and Foster, I. (2009). Soil erosion and risk-assessment for on- and off-farm impacts: A test case using the Midhurst area, West Sussex, UK. *Journal of Environmental Management*, 90(8), pp.2578-2588.

Boomer, K., Weller, D. and Jordan, T. (2008). Empirical models based on the universal soil loss equation fail to predict sediment discharges from Chesapeake Bay catchments. *Journal of Environmental Quality*, 37(1), pp.79--89.

Brazier, R. (2004). Quantifying soil erosion by water in the UK: a review of monitoring and modelling approaches. *Progress in Physical Geography*, 28(3), pp.340--365.

Brazier, R. (2013). Hillslope Soil Erosion Modeling. *Treatise on Geomorphology, Academic Press, San Diego,CA*, 2, pp.135 - 146.

Burrough, P. (1986). *Principles of geographical information systems for land resources assessment*. Oxford [Oxfordshire]: Clarendon Press.

Burrough, P., McDonnell, R. and Burrough, P. (1998). *Principles of geographical information systems*. Oxford: Oxford University Press.

Carlisle, B. (2005). Modelling the spatial distribution of DEM error. *Transactions in GIS*, 9(4), pp.521--540.

Carrara, A., Bitelli, G. and Carla, R. (1997). Comparison of techniques for generating digital terrain models from contour lines. *International Journal of Geographical Information Science*, 11(5), pp.451--473.

Cerdan, O., Govers, G., Le Bissonnais, Y., Van Oost, K., Poesen, J., Saby, N., Gobin, A., Vacca, A., Quinton, J., Auerswald, K. and others, (2010). Rates and spatial variations of soil erosion in Europe: a study based on erosion plot data. *Geomorphology*, 122(1), pp.167--177.

Chambers, B. and Garwood, T. (2000). Monitoring of water erosion on arable farms in England and Wales. 1990--94. *Soil Use and Management*, 16(2), pp.93--99.

Chang, K. and Tsai, B. (1991). The effect of DEM resolution on slope and aspect mapping. *Cartography and Geographic Information Systems*, 18(1), pp.69--77.

Chapman, P., Kay, P., Mitchell, G. and Pitts, C. (2014). Surface water quality. In: J. Holden, ed., *Water Resources: An integrated approach*, 1st ed. London: Routledge, pp.79 -- 122.

Charrier, R. and Li, Y. (2012). Assessing resolution and source effects of digital elevation models on automated floodplain delineation: A case study from the Camp Creek

Watershed, Missouri. *Applied Geography*, 34, pp.38--46.

Chaubey, I., Cotter, A., Costello, T. and Soerens, T. (2005). Effect of DEM data resolution on SWAT output uncertainty. *Hydrological Processes*, 19(3), pp.621--628.

Chirico, P. (2004). An evaluation of SRTM, ASTER and contour based DEMs in the Caribbean region. *Proceedings of the URISA 2004 Caribbean GIS conference. Barbados: URISA.*.

Choi, Y., Park, H., Sunwoo, C. and Clarke, K. (2009). Multi-criteria evaluation and least-cost path analysis for optimal haulage routing of dump trucks in large scale open-pit mines. *International Journal of Geographical Information Science*, 23(12), pp.1541--1567.

Chrisman, N. (1982). A theory of cartographic error and its measurement in digital databases. In: *AutoCarto 5*. Bethesda, MD, pp.159--68.

Chrisman, N. (1991). The error component in spatial data. *Geographical information systems*, 1, pp.165--174.

Chrysoulakis, N., Abrams, M., Kamarianakis, Y. and Stanislawski, M. (2011). Validation of ASTER GDEM for the area of Greece. *Photogrammetric Engineering & Remote Sensing*, 77(2), pp.157--165.

Clarke, S. and Burnett, K. (2003). Comparison of digital elevation models for aquatic data development. *Photogrammetric Engineering & Remote Sensing*, 69(12), pp.1367--1375.

Cochrane, T. and Flanagan, D. (2005). Effect of DEM resolutions in the runoff and soil loss predictions of the WEPP watershed model. *University of Canterbury. Natural Resources Engineering*.

Collins, A., Anthony, S., Hawley, J. and Turner, T. (2009). The potential impact of projected change in farming by 2015 on the importance of the agricultural sector as a sediment source in England and Wales. *Catena*, 79(3), pp.243--250.

Collins, A., Zhang, Y., Hickinbotham, R., Bailey, G., Darlington, S., Grenfell, S., Evans, R. and Blackwell, M. (2013). Contemporary fine-grained bed sediment sources across the River Wensum Demonstration Test Catchment, UK. *Hydrological Processes*, 27(6), pp.857--884.

Collischonn, W. and Pilar, J. (2000). A direction dependent least-cost-path algorithm for roads and canals. *International Journal of Geographical Information Science*, 14(4), pp.397--406.

Colombo, R., Vogt, J., Soille, P., Paracchini, M. and de Jager, A. (2007). Deriving river networks and catchments at the European scale from medium resolution digital elevation data. *Catena*, 70(3), pp.296--305.

Coombes, M., Curini, A., Howard Keeble, A., Green, T. and Soar, P. (2007). *River Wensum Restoration Strategy*. Natural England Research Reports, Number 024.

Cooper, R., Krueger, T., Hiscock, K. and Rawlins, B. (2014). High-temporal resolution fluvial sediment source fingerprinting with uncertainty: a Bayesian approach. *Earth Surface Processes and Landforms*.

Costa-Cabral, M. and Burges, S. (1994). Digital elevation model networks (DEMON): A model of flow over hillslopes for computation of contributing and dispersal areas. *Water resources research*, 30(6), pp.1681--1692.

Csafordi, P., Podor, A., Bug, J. and Gribovsyki, Z. (2012). Soil Erosion Analysis in a Small Forested Catchment Supported by ArcGIS Model Builder. *Acta Silvatica et Lignaria Hungarica*, 8(1), pp.39--55.

Da Ros, D. and Borga, M. (1997). Use of digital elevation model data for the derivation of the geomorphological instantaneous unit hydrograph. *Hydrological processes*, 11(1), pp.13--33.

Darnell, A., Lovett, A., Barclay, J. and Herd, R. (2010). An application-driven approach to terrain model construction. *International Journal of Geographical Information Science*, 24(8), pp.1171--1191.

Darnell, A., Tate, N. and Brunsdon, C. (2008). Improving user assessment of error implications in digital elevation models. *Computers, Environment and Urban Systems*, 32(4), pp.268--277.

Datta, P. and Schack-Kirchner, H. (2010). Erosion relevant topographical parameters derived from different DEMs - A comparative study from the Indian Lesser Himalayas. *Remote Sensing*, 2(8), pp.1941--1961.

Defra, (2002). *Directing the flow Priorities for future water policy*. London: Department for Environment, Food and Rural Affairs.

Defra, (2005). *Controlling Soil Erosion: a Manual for the Assessment and Management of Agricultural Land at Risk of Water Erosion in Lowland England*. London: Department for Environment, Food and Rural Affairs.

Defra, (2009). *Safeguarding our Soils: A Strategy for England*. London: Department for Environment, Food and Rural Affairs.

Defra, (2010). *Fertiliser Handbook*. London: Department for Environment, Food and Rural Affairs.

Defra, (2013). *Catchment based approach: improving the quality of our water environment*. London: Department for Environment, Food and Rural Affairs.

Desmet, P. and Govers, G. (1996). Comparison of routing algorithms for digital elevation models and their implications for predicting ephemeral gullies. *International Journal of Geographical Information Science*, 10(3), pp.311--331.

Desmet, P., Poesen, J., Govers, G. and Vandaele, K. (1999). Importance of slope gradient and contributing area for optimal prediction of the initiation and trajectory of ephemeral gullies. *CATENA*, 37(3-4), pp.377-392.

DLR, (2014). *DLR Portal - DLR*. [online] Available at: http://www.dlr.de/ [Accessed 5 Mar. 2014].

Do, H., Limet, S. and Melin, E. (2011). Parallel computing flow accumulation in large Digital Elevation Models. *Procedia Computer Science*, 4, pp.2277--2286.

Dobos, E. and Daroussin, J. (2005). The derivation of the potential drainage density Index (PDD). *In Dobos et al. 2005. An SRTM-based procedure to delineate SOTER terrain units on 1:1 and 1:5 million scales. EUR 21571 EN, 55pp. Office of Official Publications of the European Communities, Luxemburg.*.

Dowman, I. (2004). Integration of LIDAR and IFSAR for mapping. *International Archives of Photogrammetry and Remote Sensing*, 35(B2), pp.90--100.

Drzewiecki, W., Wkezyk, P., Pierzchalski, M. and Szafranska, B. (2013). Quantitative and

Qualitative Assessment of Soil Erosion Risk in Malopolska (Poland), Supported by an Object-Based Analysis of High-Resolution Satellite Images. *Pure and Applied Geophysics*, pp.1--29.

Ebdon, D. (1978). *Statistics in Geography: A Practical Approach*. Oxford: Blackwell.

Ehlschlaeger, C. and Goodchild, M. (1994). Dealing with uncertainty in categorical coverage maps: defining, visualizing, and managing errors. 1(2), pp.101--106.

El-Sheimy, N., Valeo, C. and Habib, A. (2005). *Digital terrain modeling*. Boston: Artech House.

ENTEC, (2012). *Defra Wensum Demonstration Test Catchment: Conceptual and Numerical Catchment Modelling*. Doc Reg No. 26982rr016, Abbey Foregate, Shrewsbury.

Environment Agency, (2004). *Model Procedures for the Management of Land Contamination*. Bristol: Environment Agency September 2004.

Environmental Agency, (2014). *LIDAR data, aerial LIDAR, height data, DSM and DTM from Geomatics Group*. [online] Geomatics-group.co.uk. Available at: http://www.geomatics-group.co.uk/GeoCMS/Products/LIDAR.aspx [Accessed 4 Aug. 2014].

Evans, R. (1981). Assessments of Soil Erosion and Peat Wastage for Parts of East Anglia, England, a Field Visit. In: R. Morgan, ed., *Soil Conservation: Problems and Prospects*, 1st ed. Chichester, UK: Wiley, pp.521--530.

Evans, R. (2002). An alternative way to assess water erosion of cultivated land - field-based measurements: and analysis of some results. *Applied Geography*, 22(2), pp.187--207.

Evans, R. (2010). Runoff and soil erosion in arable Britain: changes in perception and policy since 1945. *Environmental Science & Policy*, 13(2), pp.141--149.

Evans, R. and Brazier, R. (2005). Evaluation of modelled spatially distributed predictions of soil erosion by water versus field-based assessments. *Environmental Science & Policy*, 8(5), pp.493--501.

Farr, T., Rosen, P., Caro, E., Crippen, R., Duren, R., Hensley, S., Kobrick, M., Paller, M., Rodriguez, E., Roth, L. and others, (2007). The shuttle radar topography mission. *Reviews of geophysics*, 45(2).

Fernandez, C., Wu, J., McCool, D. and Stockle, C. (2003). Estimating water erosion and sediment yield with GIS, RUSLE, and SEDD. *Journal of Soil and Water Conservation*, 58(3), pp.128--136.

Ferrier, R. and Jenkins, A. (2010). The catchment management concept. In: R. Ferrier and A. Jenkins, ed., *Handbook of catchment management*, 1st ed. Chichester, UK: Wiley-Blackwell, pp.1--17.

Ferro, V., Porto, P. and Yu, B. (1999). A comparative study of rainfall erosivity estimation for southern Italy and southeastern Australia. *Hydrological sciences journal*, 44(1), pp.3--24.

FGDC, (1998). Geospatial Positioning Accuracy Standards Part 3: National Standard for Spatial Data Accuracy. *Reston, VA: US Federal Geographic Data Committee*. [online] Available at: htpp://www.fgdc.gov/FGDC-standards projects/accuracy/part3/chapter3.

Field, A. (2009). *Discovering statistics using SPSS*. 3rd ed. London: Sage Publications.

Fisher, P. (1998). Improved modeling of elevation error with geostatistics. *GeoInformatica*, 2(3), pp.215--233.

Fisher, P. and Tate, N. (2006). Causes and consequences of error in digital elevation models. *Progress in Physical Geography*, 30(4), pp.467--489.

Foody, G. and Atkinson, P. (2002). *Uncertainty in remote sensing and GIS*. Hoboken, NJ: J. Wiley.

Forkuor, G. and Maathuis, B. (2012). Comparison of SRTM and ASTER Derived Digital Elevation Models over Two Regions in Ghana - Implications for Hydrological and Environmental Modeling. *Studies on Environmental and Applied Geomorphology*, pp.219--240.

Friedli, S. (2006). Digital soil erosion hazard map of Switzerland in acres grid - with special emphasis on agricultural land; CDE University of Bern.

Gallant, J. and Hutchinson, M. (1996). Towards an Understanding of Landscape Scale and Structure. In: *Third International Conference/Workshop on Integrating GIS and Environmental Modeling*. Santa Barbara: National Center for Geographical Information and Analysis.

Gallego, J., Fernandez, V. and Velez, J. (2010). Uncertainty in the extracted drainage network associated to the applied DEM correction method: Implementation of a new DEM correction approach. In: *Proceedings of the Accuracy 2010 Symposium*. Leicester, UK, pp.209-212.

Gamache, M. (2004). Free and low cost datasets for international mountain cartography. *Proceedings, 4th ICA Mountain Cartography Workshop, Vall de Nuria, Catalonia, Spain, 2004.*

Gandolfi, C. and Bischetti, G. (1997). Influence of the drainage network identification method on geomorphological properties and hydrological response. *Hydrological Processes*, 11(4), pp.353--375.

Gatziolis, D. and Fried, J. (2004). Adding Gaussian noise to inaccurate digital elevation models improves spatial fidelity of derived drainage networks. *Water resources research*, 40(2).

Gehrke, S. and Uebbing, R. (2011). Quantification of turbulence for airborne line-scanner images. In: *ASPRS 2011 Annual Conference*. Milwaukee, Wisconsin.

Gitas, I., Douros, K., Minakou, C., Silleos, G., Karydas, C. and others, (2009). Multi-temporal soil erosion risk assessment in N. Chalkidiki using a modified usle raster model. *EARSeL eProceedings*, 8(1), pp.40--52.

Goncalves, J. and Oliveira, A. (2004). Accuracy analysis of DEMs derived from ASTER imagery. *International Archives of Photogrammetry and Remote Sensing*, 35, pp.168--172.

Gonga-Saholiariliva, N., Gunnell, Y., Petit, C. and Mering, C. (2011). Techniques for quantifying the accuracy of gridded elevation models and for mapping uncertainty in digital terrain analysis. *Progress in Physical Geography*, 35(6), pp.739--764.

Gonzales Inca, C. (2009). *Assessing the Land Cover and Land Use Change and Its Impact on Watershed Services in a Tropical Andean Watershed of Peru*. A Master's Thesis. University of Jyvaskyla.

Goodchild, M. (1993). Data models and data quality: problems and prospects. *Environmental modeling with GIS*, pp.94--103.

Goodchild, M. (2009). Geographic information systems and science: today and tomorrow. *Procedia Earth and Planetary Science*, 1(1), pp.1037-1043.

Goodchild, M. and Hunter, G. (1997). A simple positional accuracy measure for linear features. *International Journal of Geographical Information Science*, 11(3), pp.299--306.

Gordon, N., McMahon, T., Finlayson, B., Gippel, C. and Nathan, R. (2004). *Stream Hydrology: An Introduction for Ecologist*. 2nd ed. Chichester, West Sussex, England: Wiley.

Gorokhovich, Y. and Voustianiouk, A. (2006). Accuracy assessment of the processed SRTM-based elevation data by CGIAR using field data from USA and Thailand and its relation to the terrain characteristics. *Remote Sensing of Environment*, 104(4), pp.409--415.

Hahn, C., Prasuhn, V., Stamm, C., Milledge, D. and Schulin, R. (2013). A comparison of three simple approaches to identify critical areas for runoff and dissolved reactive phosphorus losses. *Hydrology and Earth System Sciences Discussions*, 10(11), pp.14495--14534.

Haile, T. and Rientjes, T. (2005). Effects of LIDAR DEM resolution in flood modeling: a model sensitivity study for the City of Tegucigalpa, Honduras. In: *Proceedings of ISPRS WG III/3, III/4, V/3 workshop, "Laser scanning 2005",*. Enschede, The Netherlands.

Hancock, G. and Evans, K. (2006). Channel head location and characteristics using digital elevation models. *Earth Surface Processes and Landforms*, 31(7), pp.809--824.

Harris, G. and Heathwaite, A. (2005). Inadmissible evidence: knowledge and prediction in land and riverscapes. *Journal of hydrology*, 304(1), pp.3--19.

Haygarth, P., Condron, L., Heathwaite, A., Turner, B. and Harris, G. (2005). The phosphorus transfer continuum: Linking source to impact with an interdisciplinary and multi-scaled approach. *Science of the Total Environment*, 344(1), pp.5--14.

Heathwaite, A. (2010). Multiple stressors on water availability at global to catchment scales: understanding human impact on nutrient cycles to protect water quality and water availability in the long term. *Freshwater Biology*, 55(s1), pp.241--257.

Heathwaite, A., Quinn, P. and Hewett, C. (2005). Modelling and managing critical source

areas of diffuse pollution from agricultural land using flow connectivity simulation. *Journal of Hydrology*, 304(1), pp.446--461.

Hebeler, F. and Purves, R. (2009). The influence of elevation uncertainty on derivation of topographic indices. *Geomorphology*, 111(1), pp.4--16.

Heine, R., Lant, C. and Sengupta, R. (2004). Development and comparison of approaches for automated mapping of stream channel networks. *Annals of the Association of American Geographers*, 94(3), pp.477--490.

Hengl, T. and Reuter, H. (2008). *Geomorphometry: Concepts, Software, Applications*. Amsterdam: Elsevier.

Hengl, T., Grohmann, C., Biv, Conrad, O. and Lobo, A. (2009). SAGA vs GRASS: a comparative analysis of the two open source desktop GIS for the automated analysis of elevation data. *Proceedings of Geomorphometry*.

Hengl, T., Heuvelink, G. and Van Loon, E. (2010). On the uncertainty of stream networks derived from elevation data: the error propagation approach. *Hydrology & Earth System Sciences Discussions*, 7(1).

Henkle, J., Wohl, E. and Beckman, N. (2011). Locations of channel heads in the semiarid Colorado Front Range, USA. *Geomorphology*, 129(3), pp.309--319.

Hensley, S., Munjy, R. and Rosen, P. (2007). Interferometric Synthetic Aperture Radar (IFSAR). In: D. Maune, ed., *Digital Elevation Model Technologies and Applications: The DEM Users Manual*, 2nd ed. Bethesda, Md: American Society for Photogrammetry and Remote Sensing, pp.141 - 194.

HGCA, (2008). *The wheat growth guide*. HGCA.

Hirt, C., Filmer, M. and Featherstone, W. (2010). Comparison and validation of the recent freely available ASTER-GDEM ver1, SRTM ver4. 1 and GEODATA DEM-9S ver3 digital elevation models over Australia. *Australian Journal of Earth Sciences*, 57(3), pp.337--347.

Hiscock, K. (2011). *Catchment science and the Wensum Demonstration Test Catchment Project, UK-China Sustainable Agriculture Innovation Network Workshop 18 March 2011*.

Hiscock, K., Lister, D., Boar, R. and Green, F. (2001). An integrated assessment of long-term changes in the hydrology of three lowland rivers in eastern England. *Journal of environmental management*, 61(3), pp.195--214.

Hodgson, M., Jensen, J., Schmidt, L., Schill, S. and Davis, B. (2003). An evaluation of LIDAR-and IFSAR-derived digital elevation models in leaf-on conditions with USGS Level 1 and Level 2 DEMs. *Remote Sensing of Environment*, 84(2), pp.295--308.

Hogg, S. (1982). Sheetfloods, sheetwash, sheetflow, or ... ?. *Earth-Science Reviews*, 18(1), pp.59-76.

Hohle, J. and Hohle, M. (2009). Accuracy assessment of digital elevation models by means of robust statistical methods. *ISPRS Journal of Photogrammetry and Remote Sensing*, 64(4), pp.398--406.

Holden, J. (2014). *Water Resources: An integrated approach*. London: Routledge.

Holmes, K., Chadwick, O. and Kyriakidis, P. (2000). Error in a USGS 30-meter digital elevation model and its impact on terrain modeling. *Journal of Hydrology*, 233(1), pp.154--173.

Hooke, J. (2003). Coarse sediment connectivity in river channel systems: a conceptual framework and methodology. *Geomorphology*, 56(1), pp.79--94.

Hoyos, N. (2005). Spatial modeling of soil erosion potential in a tropical watershed of the Colombian Andes. *Catena*, 63(1), pp.85--108.

Huggel, C., Schneider, D., Miranda, P., Delgado Granados, H. and KÃÃb, A. (2008). Evaluation of ASTER and SRTM DEM data for lahar modeling: A case study on lahars from Popocatepetl Volcano, Mexico. *Journal of Volcanology and Geothermal Research*, 170(1-2), pp.99-110.

Hui, L., Xiaoling, C., Lim, K., Xiaobin, C. and Sagong, M. (2010). Assessment of soil erosion and sediment yield in Liao watershed, Jiangxi Province, China, Using USLE, GIS, and RS. *Journal of Earth Science*, 21(6), pp.941--953.

Hunter, G. and Goodchild, M. (1995). Dealing with error in a spatial database: A simple case study. *Photogrammetric Engineering and Remote Sensing*, 61(5), pp.529--537.

Hunter, G. and Goodchild, M. (1997). Modeling the uncertainty of slope and aspect estimates derived from spatial databases. *Geographical Analysis*, 29(1), pp.35--49.

Ijjasz-Vasquez, E. and Bras, R. (1995). Scaling regimes of local slope versus contributing area in digital elevation models. *Geomorphology*, 12(4), pp.299--311.

Illian, J., Penttinen, A., Stoyan, H. and Stoyan, D. (2008). *Statistical analysis and modelling of spatial point patterns*. Chichester, England: John Wiley.

Inman, A. (2006). *Soil erosion in England and Wales: causes, consequences and policy options for dealing with the problem*. Surrey: WWF - UK.

Intermap Technologies, (2011). *NEXTMap Data: digital terrain models, digital surface models | Intermap*. [online] Intermap. Available at: http://www.intermap.com/data/nextmap [Accessed 8 Sep. 2011].

Intermap, (2004). *Intermap Product Handbook and Quick Start Guide*. v3.3. Englewood: Intermap Technologies, Inc.

Intermap, (2010). *Intermap Product Handbook and Quick Start Guide*. Standard Edition v4.4.1. Denver: Intermap Technologies Inc.

Jamshidi, R., Dragovich, D. and Webb, A. (2013). Estimating catchment-scale annual soil loss in managed native eucalypt forests, Australia. *Forest Ecology and Management*, 304, pp.20--32.

Jarvis, A., Reuter, H., Nelson, A. and Guevara, E. (2008). Hole-filled SRTM for the globe Version 4. *available from the CGIAR-CSI SRTM 90m Database (http://srtm. csi. cgiar. org)*.

Jenson, S. and Domingue, J. (1988). Extracting topographic structure from digital elevation data for geographic information system analysis. *Photogrammetric engineering and remote sensing*, 54(11), pp.1593--1600.

Joowon, P. (2011). *Comparison of the Positional Accuracy of Stream Mapping Methods: Considering the Effects of Minimum Contributing Area and Spectral Data*. PhD. UMI.

Jordan, G. (2007). Digital Terrain Analysis in a GIS Environment: Concepts and Development. In: R. Peckham and G. Jordan, ed., *Digital Terrain Modelling*, 1st ed.

Berlin: Springer, pp.1--39.

Kallis, G. and Butler, D. (2001). The EU water framework directive: measures and implications. *Water Policy*, 3(2), pp.125-142.

Kamaludin, H., Lihan, T., Rahman, Z., Mustapha, M., Idris, W. and Rahim, S. (2013). Integration of remote sensing, RUSLE and GIS to model potential soil loss and sediment yield (SY). *Hydrology & Earth System Sciences Discussions*, 10(4).

Karaburun, A. (2010). Estimation of C factor for soil erosion modeling using NDVI in Buyukcekmece watershed. *Ozean journal of applied sciences*, 3(1), pp.77--85.

Kenny, F. and Matthews, B. (2005). A methodology for aligning raster flow direction data with photogrammetrically mapped hydrology. *Computers & Geosciences*, 31(6), pp.768--779.

Khan, U., Sharma, A. and Tuteja, N. (2009). A new approach for delineation of hydrologic response units in large catchments. In: *18th world IMACS / MODSIM Congress*. Cairns, Australia 13 - 17 July 2009.

Khan, U., Tuteja, N. and Sharma, A. (2013). Delineating hydrologic response units in large upland catchments and its evaluation using soil moisture simulations. *Environmental Modelling & Software*, 46, pp.142--154.

Kienzle, S. (2004). The effect of DEM raster resolution on first order, second order and compound terrain derivatives. *Transactions in GIS*, 8(1), pp.83--111.

Kim, H. and Julien, P. (2006). Soil erosion modeling using RUSLE and GIS on the Imha watershed. *Water Engineering Research*, 7(1), pp.29-41.

Kinnell, P. (2005). Raindrop-impact-induced erosion processes and prediction: a review. *Hydrological processes*, 19(14), pp.2815--2844.

Kinnell, P. (2010). Event soil loss, runoff and the Universal Soil Loss Equation family of models: A review. *Journal of Hydrology*, 385(1), pp.384--397.

Kouli, M., Soupios, P. and Vallianatos, F. (2009). Soil erosion prediction using the revised universal soil loss equation (RUSLE) in a GIS framework, Chania, Northwestern Crete, Greece. *Environmental geology*, 57(3), pp.483--497.

Kraus, K., Briese, C., Attwenger, M. and Pfeifer, N. (2004). Quality measures for digital terrain models. In Altan, O. (ed.) International Society for Photogrammetry and Remote Sensing XXth Congress Proceedings, Vol. XXXV.Part B/2 (2004) ISPRS, Istanbul, pp. 113-118.

Krieger, G., Moreira, A., Fiedler, H., Hajnsek, I., Werner, M., Younis, M. and Zink, M. (2007). TanDEM-X: A Satellite Formation for High-Resolution SAR Interferometry. *IEEE Trans. Geosci. Remote Sensing*, 45(11), pp.3317-3341.

Kuleli, T. (2009). Quantitative analysis of shoreline changes at the Mediterranean Coast in Turkey. *Environmental Monitoring and Assessment*, 167(1-4), pp.387-397.

LaLonde, T., Shortridge, A. and Messina, J. (2010). The Influence of Land Cover on Shuttle Radar Topography Mission (SRTM) Elevations in Low-relief Areas. *Transactions in GIS*, 14(4), pp.461--479.

Landmap, (2011). *Landmap - Spatial Discovery*. [online] Available at: http://www.landmap.ac.uk/ [Accessed 9 Sep. 2011].

Landmap, (2014). *Bluesky 5m resolution Digital Terrain Model (DTM) for England and Wales*. NERC Earth Observation Data Centre.

Lane, S., Brookes, C., Louise Heathwaite, A. and Reaney, S. (2006). Surveillant science: challenges for the management of rural environments emerging from the new generation diffuse pollution models. *Journal of Agricultural Economics*, 57(2), pp.239--257.

Larocque, A. (2013). Universal Soil Loss Equation (USLE). *Encyclopedia of Natural Hazards*, pp.1062--1062.

Lastoria, B., Miserocchi, F., Lanciani, A. and Monacelli, G. (2008). An estimated erosion map for the Aterno-Pescara river Basin. *European Water*, 21(22), pp.29--39.

Lee, G. and Lee, K. (2006). Scaling effect for estimating soil loss in the RUSLE model using remotely sensed geospatial data in Korea. *Hydrology & Earth System Sciences Discussions*, 3(1).

Lee, J. and Stucky, D. (1998). On applying viewshed analysis for determining least-cost paths on digital elevation models. *International Journal of Geographical Information Science*, 12(8), pp.891--905.

Lee, J. and Wong, D. (2001). *Statistical analysis with ArcView GIS*. New York: John Wiley.

Lee, S. (2004). Soil erosion assessment and its verification using the universal soil loss equation and geographic information system: a case study at Boun, Korea. *Environmental Geology*, 45(4), pp.457--465.

Li, J. and Wong, D. (2010). Effects of DEM sources on hydrologic applications. *Computers, Environment and urban systems*, 34(3), pp.251--261.

Li, X., Temant, J. and Lawrence, G. (2004). Three-dimensional mapping with airborne IFSAR based STAR technology – Intermap's experiences. Istanbul, Turkey: Proceedings of XXth ISPRS Congress, 12-23 July, 2004.

Li, Z. (1992). Variation of the accuracy of digital terrain models with sampling interval. *The Photogrammetric Record*, 14(79), pp.113--128.

Li, Z., Zhu, Q. and Gold, C. (2005). *Digital terrain modeling: Principles and Methodology*. New York: CRC Press.

Ligonja, P. and Shrestha, R. (2013). Soil erosion assessment in Kondoa eroded area in Tanzania Using Universal Soil Loss Equation, Geographic Information Systems and Socioeconomic approach. *Land Degradation & Development*.

Lim, K., Sagong, M. and others, (2010). Assessment of soil erosion and sediment yield in Liao watershed, Jiangxi Province, China, Using USLE, GIS, and RS. *Journal of Earth Science*, 21(6), pp.941--953.

Lin, K., Zhang, Q. and Chen, X. (2010). An evaluation of impacts of DEM resolution and parameter correlation on TOPMODEL modeling uncertainty. *Journal of hydrology*, 394(3), pp.370--383.

Lin, S., Jing, C., Coles, N., Chaplot, V., Moore, N. and Wu, J. (2013). Evaluating DEM source and resolution uncertainties in the Soil and Water Assessment Tool. *Stochastic Environmental Research and Risk Assessment*, 27(1), pp.209--221.

Lin, W., Chou, W., Lin, C., Huang, P. and Tsai, J. (2006). Automated suitable drainage network extraction from digital elevation models in Taiwan's upstream watersheds. *Hydrological Processes*, 20(2), pp.289--306.

Lindsay, J. (2006). Sensitivity of channel mapping techniques to uncertainty in digital elevation data. *International Journal of Geographical Information Science*, 20(6), pp.669--692.

Lindsay, J. and Evans, M. (2008). The influence of elevation error on the morphometrics of channel networks extracted from DEMs and the implications for hydrological modelling. *Hydrological Processes*, 22(11), pp.1588--1603.

Ling, F., Zhang, Q. and Wang, C. (2005). Comparison of SRTM Data with other DEM sources in Hydrological Researches. In: *International Symposium on Remote Sensing of Environment, June 20--24*. St Petersburg, Russia.

Liu, X. and Bian, L. (2008). Accuracy Assessment of DEM Slope Algorithms Related to Spatial Autocorrelation of DEM Errors. In: Q. Zhou, B. Lees and G. Tang, ed., *Advances in Digital Terrain Analysis*, 1st ed. Berlin: Springer, pp.307 - 322.

Liu, X. and Zhang, Z. (2011). Drainage network extraction using LiDAR-derived DEM in volcanic plains. *Area*, 43(1), pp.42--52.

Liu, Y. (2008). An evaluation on the data quality of SRTM- DEM at the alpine and Plateau area, north-western of china. *The International Archives of the Photogrammetry. Remote Sensing and Spatial Inform*, 37(B1), pp.1123--1128.

Longley, P., Goodchild, M., Maguire, D. and Rhind, D. (2005). *Geographical information systems and science*. 2nd ed. Chichester: Wiley.

Lovett, A. and Appleton, K. (2008). *GIS for environmental decision-making*. Boca Raton: CRC Press.

Lu, D., Li, G., Valladares, G. and Batistella, M. (2004). Mapping soil erosion risk in Rondonia, Brazilian Amazonia: using RUSLE, remote sensing and GIS. *Land Degradation & Development*, 15(5), pp.499--512.

Lunetta, R. and Lyon, J. (2004). *Remote sensing and GIS accuracy assessment*. Boca Raton, Fla.: CRC Press.

Lyon, J. (2003). *GIS for water resources and watershed management*. London: Taylor & Francis.

Maidment, D. (2002). *Arc Hydro: GIS for Water Resources*. Redlands, Calif.: ESRI Press.

Mainstone, C., Dils, R. and Withers, P. (2008). Controlling sediment and phosphorus transfer to receiving waters--a strategic management perspective for England and Wales. *Journal of Hydrology*, 350(3), pp.131--143.

Mantelli, L., Barbosa, J. and Bitencourt, M. (2011). Assessing ecological risk through automated drainage extraction and watershed delineation. *Ecological Informatics*, 6(5), pp.325--331.

Marechal, D. and Holman, I. (2004). Comparison of hydrologic simulations using regionalised and catchment-calibrated parameter sets for three catchments in England. *Cranfield University at Silsoe Institute of Water and Environment*, p.116.

Martinez, C., Hancock, G., Kalma, J., Wells, T. and Boland, L. (2010). An assessment of digital elevation models and their ability to capture geomorphic and hydrologic properties at the catchment scale. *International Journal of Remote Sensing*, 31(23), pp.6239--6257.

Martz, L. and Garbrecht, J. (1995). Automated recognition of valley lines and drainage networks from grid digital elevation models: A review and a new method - Comment. *Journal of Hydrology*, 167(1), pp.393--396.

Mati, B., Morgan, R., Gichuki, F., Quinton, J., Brewer, T. and Liniger, H. (2000). Assessment of erosion hazard with the USLE and GIS: A case study of the Upper Ewaso Ng'iro North basin of Kenya. *International Journal of Applied Earth Observation and Geoinformation*, 2(2), pp.78--86.

Maune, D. (2007). *Digital elevation model technologies and applications*. Bethesda, Md.: American Society for Photogrammetry and Remote Sensing.

McDougall, K., Liu, X., Basnet, B. and Apan, A. (2008). Digital elevation model accuracy requirements for catchment management. *Proceedings of Queensland Spatial Conference Gold Coast, Queensland, Australia*.

McGonigle, D., Burke, S., Collins, A., Gartner, R., Haft, M., Harris, R., Haygarth, P., Hedges, M., Hiscock, K. and Lovett, A. (2014). Developing Demonstration Test Catchments as a platform for transdisciplinary land management research in England and Wales.

Environmental Science: Processes & Impacts.

McMaster, K. (2002). Effects of digital elevation model resolution on derived stream network positions. *Water Resources Research*, 38(4), pp.13--1.

McNamara, J., Kane, D. and Hinzman, L. (1999). An analysis of an arctic channel network using a digital elevation model. *Geomorphology*, 29(3), pp.339--353.

McNamara, J., Ziegler, A., Wood, S. and Vogler, J. (2006). Channel head locations with respect to geomorphologic thresholds derived from a digital elevation model: A case study in northern Thailand. *Forest ecology and management*, 224(1), pp.147--156.

Mercer, B. (2004). DEMs created from airborne IFSAR--an update. *In Proceedings of ISPRS Commission II Symposium. Istanbul*.

Mercuri, P., Engel, B. and Johannsen, C. (2006). Evaluation and accuracy assessment of high-resolution IFSAR DEMs in low-relief areas. *International journal of remote sensing*, 27(13), pp.2767--2786.

Metz, M., Mitasova, H. and Harmon, R. (2011). Efficient extraction of drainage networks from massive, radar-based elevation models with least cost path search. *Hydrology and Earth System Sciences*, 15(2), pp.667--678.

Meyer, D., Tachikawa, T., Abrams, M., Crippen, R., Krieger, T., Gesch, D. and Carabajal, C. (2012). Summary of the Validation of the Second Version of the Aster Gdem. *ISPRS-International Archives of the Photogrammetry, Remote Sensing and Spatial Information Sciences*, 1, pp.291--293.

Milledge, D., Lane, S., Heathwaite, A. and Reaney, S. (2012). A Monte Carlo approach to the inverse problem of diffuse pollution risk in agricultural catchments. *Science of the Total Environment*, 433, pp.434--449.

Mokrech, M., Nicholls, R., Richards, J., Henriques, C., Holman, I. and Shackley, S. (2008). Regional impact assessment of flooding under future climate and socio-economic scenarios for East Anglia and North West England. *Climatic Change*, 90(1-2), pp.31--55.

Molnar, D. and Julien, P. (1998). Estimation of upland erosion using GIS. *Computers & Geosciences*, 24(2), pp.183--192.

Montgomery, D. and Foufoula-Georgiou, E. (1993). Channel network source representation using digital elevation models. *Water Resources Research*, 29(12), pp.3925--3934.

Moore, I., Grayson, R. and Ladson, A. (1991). Digital terrain modelling: a review of hydrological, geomorphological, and biological applications. *Hydrological processes*, 5(1), pp.3--30.

Morgan, R. (1980). Soil erosion and conservation in Britain. *Progress in Physical Geography*, (4), pp.25 - 47.

Morgan, R. (1985). Soil erosion measurement and soil conservation research in cultivated areas of the UK. *Geographical journal*, 151(1), pp.11--20.

Morgan, R. (2005). *Soil erosion and conservation*. 3rd ed. Malden, MA: Blackwell Pub.

Muller, J., Morley, J., Walker, A., Kitmitto, K., Mitchell, K., Smith, A., Barnes, J., Keenan, R., Cross, P., Dowman, I. and Quarmby, N. (2000). The LANDMAP project for the automated creation and validation of multi-resolution orthorectified satellite image products and a 1â€• DEM of the British Isles from ERS tandem SAR interferometry. In: *Adding Value to Remotely Sensed Data. Proceedings of the 26th Annual Conference of the Remote Sensing Society*. RSS2000, pp.12--14.

Munafo, M., Cecchi, G., Baiocco, F. and Mancini, L. (2005). River pollution from non-point sources: a new simplified method of assessment. *Journal of Environmental Management*, 77(2), pp.93--98.

Munlv, N. (2007). Bodenerosion durch Wasser, Ursachen, Bedeutung und Umgang in der landwirtschaftlichen Praxis von NRW.

Murphy, P., Ogilvie, J., Meng, F. and Arp, P. (2008). Stream network modelling using lidar and photogrammetric digital elevation models: a comparison and field verification. *Hydrological Processes*, 22(12), pp.1747--1754.

Nelson, A., Reuter, H. and Gessler, P. (2009). DEM production methods and siurces. In: T. Hengl and H. Reuter, ed., *Geomorphometry: Concepts, Software, Applications*, 1st ed. Amsterdam: Elsevier, pp.65 - 85.

Nigel, R. and Rughooputh, S. (2010). Soil erosion risk mapping with new datasets: An improved identification and prioritisation of high erosion risk areas. *Catena*, 82(3),

pp.191--205.

Nikolakopoulos, K., Kamaratakis, E. and Chrysoulakis, N. (2006). SRTM vs ASTER elevation products. Comparison for two regions in Crete, Greece. *International Journal of Remote Sensing*, 27(21), pp.4819--4838.

O'Callaghan, J. and Mark, D. (1984). The extraction of drainage networks from digital elevation data. *Computer vision, graphics, and image processing*, 28(3), pp.323--344.

OECD, (2012). *Water Quality and Agricultural: Meeting the Policy Challenge*. OECD Studies on Water, OECD Piblishing.

Oksanen, J. and Sarjakoski, T. (2005). Error propagation of DEM-based surface derivatives. *Computers & Geosciences*, 31(8), pp.1015--1027.

OMAFRA, (2012). *Universal Soil Loss Equation (USLE)*. Order No. 12-051. OMAFRA.

Ordnance Survey, (2009a). *OS MasterMap Topography Layer, user guide and technical specification*. v1.8. December 2009 Ordnance Survey, Southampton.

Ordnance Survey, (2009b). *OS VectorMap Local, user guide and technical specification*. v1.1. September 2009 Ordnance Survey, Southampton.

Ordnance Survey, (2010a). *Landform panorama user guide and technical specification*. v5.1. December 2010 Ordnance Survey, Southampton.

Ordnance Survey, (2010b). *Landform Profile user guide and technical specification*. v5.2. December 2010 Ordnance Survey, Southampton.

Ordnance Survey, (2013a). *OS Terrain 5 User guide and technical specification*. v1.1. July 2013 Ordnance Survey, Southampton.

Ordnance Survey, (2013b). *OS Terrain 50 User guide and technical specification*. v1.0. April 2013 Ordnance Survey, Southampton.

Orlandini, S., Tarolli, P., Moretti, G. and Dalla Fontana, G. (2011). On the prediction of channel heads in a complex alpine terrain using gridded elevation data. *Water Resources Research*, 47(2).

Owens, P. and Collins, A. (2006). *Soil erosion and sediment redistribution in river*

catchments: Measurement, Modelling and Management. Wallingford, UK: CABI Pub.

Owusu, G. (2013). A GIS-Based Estimation of Soil Loss in the Densu Basin in Ghana. *West African Journal of Applied Ecology*, 20(2), pp.41--51.

Paik, K. (2008). Global search algorithm for nondispersive flow path extraction. *Journal of Geophysical Research: Earth Surface (2003--2012)*, 113(F4).

Pandey, A., Chowdary, V. and Mal, B. (2007). Identification of critical erosion prone areas in the small agricultural watershed using USLE, GIS and remote sensing. *Water resources management*, 21(4), pp.729--746.

Parveen, R. and Kumar, U. (2012). Integrated Approach of Universal Soil Loss Equation (USLE) and Geographical Information System (GIS) for Soil Loss Risk Assessment in Upper South Koel Basin, Jharkhand. *Journal of Geographic Information System*, 4, p.588.

Paz, A., Collischonn, W., Risso, A. and Mendes, C. (2008). Errors in river lengths derived from raster digital elevation models. *Computers & Geosciences*, 34(11), pp.1584--1596.

Peckham, R. and Jordan, G. (2007). *Digital terrain modelling: Development and Applications in a Policy Support Environment*. Berlin: Springer.

Penas, F., Fernandez, F., Calvo, M., Barquin, J. and Pedraz, L. (2011). Influence of data sources and processing methods on theoretical river network quality. *Limnetica*, 30(2), pp.197--216.

Podobnikar, T. (2009). Methods for visual quality assessment of a digital terrain model. *SAPI EN. S. Surveys and Perspectives Integrating Environment and Society*, 2(2), p.19.

Poggio, L. and Soille, P. (2011). A probabilistic approach to river network detection in digital elevation models. *Catena*, 87(3), pp.341--350.

Posen, P., Hutchins, M., Lovett, A. and Davies, H. (2011). Identifying the catchment size at which robust estimations of agricultural land use can be made, and implications for diffuse pollution modelling. *Applied Geography*, 31(3), pp.919--929.

Prasuhn, V., Liniger, H., Gisler, S., Herweg, K., C, inas, A. and Cl'ement, J. (2013). A high-resolution soil erosion risk map of Switzerland as strategic policy support system. *Land*

use policy, 32, pp.281--291.

Prato, T. and Herath, G. (2007). Multiple-criteria decision analysis for integrated catchment management. *Ecological Economics*, 63(2), pp.627--632.

Quinn, P., Beven, K., Chevallier, P. and Planchon, O. (1991). The prediction of hillslope flow paths for distributed hydrological modelling using digital terrain models. *Hydrological processes*, 5(1), pp.59--79.

Raaflaub, L. and Collins, M. (2006). The effect of error in gridded digital elevation models on the estimation of topographic parameters. *Environmental Modelling & Software*, 21(5), pp.710--732.

Rabia, R. (2012). Mapping Soil Erosion Risk Using Rusle, Gis and Remote Sensing Techniques. In: *The 4th International Congress of ECSSS, EUROSOIL 2012*. soil science for the benefit of mankind and environment, 2-6 June, Bari, Italy.

Rabia, R. and Harb, A. (2012). Mapping Soil Erosion Risk Using RUSLE, GIS and Remote Sensing Techniques. p.1082.

Rabus, B., Eineder, M., Roth, A. and Bamler, R. (2003). The shuttle radar topography missionâ€"a new class of digital elevation models acquired by spaceborne radar. *ISPRS Journal of Photogrammetry and Remote Sensing*, 57(4), pp.241--262.

Ranzi, R., Le, T. and Rulli, M. (2012). A RUSLE approach to model suspended sediment load in the Lo river (Vietnam): Effects of reservoirs and land use changes. *Journal of Hydrology*, 422, pp.17--29.

Ravibabu, M. and Jain, K. (2008). Digital Elevation Model Accuracy Aspects. *Journal of Applied Sciences*, 8(1).

Rawlins, B. (2011). *A pilot study to assess soil spectroscopic methods for mapping key topsoil properties in the Blackwater sub-catchments (Wensum DTC)*. British Geological Survey Internal Report, OR/11/053.

Rayburg, S., Thoms, M. and Neave, M. (2009). A comparison of digital elevation models generated from different data sources. *Geomorphology*, 106(3), pp.261--270.

Reaney, S. (2014). *What are the scale and data requirements for SCIMAP?*. [online]

SCIMAP - Diffuse Pollution Risk Mapping. Available at: http://www.scimap.org.uk/2014/02/what-are-the-scale-and-data-requirements-for-scimap/ [Accessed 5 Jul. 2014].

Reaney, S., Lane, S., Heathwaite, A. and Dugdale, L. (2011). Risk-based modelling of diffuse land use impacts from rural landscapes upon salmonid fry abundance. *Ecological Modelling*, 222(4), pp.1016--1029.

Renard, K. and Freimund, J. (1994). Using monthly precipitation data to estimate the R-factor in the revised USLE. *Journal of hydrology*, 157(1), pp.287--306.

Renard, K., Foster, G., Weesies, G. and Porter, J. (1991). RUSLE: Revised universal soil loss equation. *Journal of soil and Water Conservation*, 46(1), pp.30--33.

Renard, K., Foster, G., Weesies, G., McCool, D., Yoder, D. and others, (1997). Predicting soil erosion by water: a guide to conservation planning with the revised universal soil loss equation (RUSLE). *Agriculture Handbook (Washington)*, (703).

Reuter, H., Nelson, A. and Jarvis, A. (2007). An evaluation of void-filling interpolation methods for SRTM data. *International Journal of Geographical Information Science*, 21(9), pp.983--1008.

Reuter, H., Nelson, A., Strobl, P., Mehl, W. and Jarvis, A. (2009). A first assessment of Aster GDEM tiles for absolute accuracy, relative accuracy and terrain parameters. *Geoscience and Remote Sensing Symposium,2009 IEEE International,IGARSS 2009*, (5), pp.240 - 243.

Rickson, R. (2014). Can control of soil erosion mitigate water pollution by sediments?. *Science of The Total Environment*, 468, pp.1187--1197.

Rodriguez, E., Morris, C. and Belz, J. (2006). A global assessment of the SRTM performance. *Photogrammetric Engineering & Remote Sensing*, 72(3), pp.249--260.

Rojas, R., Velleux, M., Julien, P. and Johnson, B. (2008). Grid scale effects on watershed soil erosion models. *Journal of Hydrologic Engineering*, 13(9), pp.793--802.

Romkens, M., Helming, K. and Prasad, S. (2002). Soil erosion under different rainfall intensities, surface roughness, and soil water regimes. *Catena*, 46(2), pp.103--123.

Rousseva, S. (2004). Ideas for Physical Interpretation of the USLE. *N. Poushkarov Research Institute for Soil Science and Agroecology, Sofia, Bulgaria.*

Rulli, M., Offeddu, L. and Santini, M. (2013). Modeling post-fire water erosion mitigation strategies. *Hydrology and Earth System Sciences*, 17(6), pp.2323--2337.

Schauble, H., Marinoni, O. and Hinderer, M. (2008). A GIS-based method to calculate flow accumulation by considering dams and their specific operation time. *Computers & Geosciences*, 34(6), pp.635--646.

Schonbrodt, S., Saumer, P., Behrens, T., Seeber, C. and Scholten, T. (2010). Assessing the USLE crop and management factor C for soil erosion modeling in a large mountainous watershed in Central China. *Journal of Earth Science*, 21(6), pp.835--845.

Schumann, G., Matgen, P., Cutler, M., Black, A., Hoffmann, L. and Pfister, L. (2008). Comparison of remotely sensed water stages from LiDAR, topographic contours and SRTM. *ISPRS journal of photogrammetry and remote sensing*, 63(3), pp.283--296.

Schwanghart, W., Groom, G., Kuhn, N. and Heckrath, G. (2013). Flow network derivation from a high resolution DEM in a low relief, agrarian landscape. *Earth Surf. Process. Landforms*.

SCIMAP, (2013). *SCIMAP - Diffuse Pollution Risk Mapping*. [online] Available at: http://www.scimap.org.uk/ [Accessed 7 May 2013].

Scott, K., Quist, J. and Bakker, C. (2009). Co-design, social practices and sustainable innovation: involving users in a living lab exploratory study on bathing. In: *Joing actions on climate change conference*.

Sear, D., Newson, M., Old, J. and Hill, C. (2006). *Geomorphological appraisal of the River Wensum Special Area of Conservation*. English Nature Research Reports, Number 685.

Sharma, A., Tiwari, K. and Bhadoria, P. (2011a). Determining the optimum cell size of digital elevation model for hydrologic application. *Journal of earth system science*, 120(4), pp.573--582.

Sharma, A., Tiwari, K. and Bhadoria, P. (2011b). Effect of land use land cover change on soil erosion potential in an agricultural watershed. *Environmental monitoring and assessment*, 173(1-4), pp.789--801.

Shen, Z., Chen, L., Ding, X., Hong, Q. and Liu, R. (2013). Long-term variation (1960--2003) and causal factors of non-point-source nitrogen and phosphorus in the upper reach of the Yangtze River. *Journal of hazardous materials*, 252, pp.45--56.

Sheshukov, A. (2015). Predicting location and length of ephemeral gullies with a process-based Topographic Index model. *Proc. IAHS*, 367, pp.93-98.

Shiferaw, A. (2011). Estimating soil loss rates for soil conservation planning in the Borena Woreda of South Wollo Highlands, Ethiopia. *Journal of Sustainable Development in Africa*, 13(3), pp.87--106.

Slater, J., Heady, B., Kroenung, G., Curtis, J., Haase, D., Hoegemann, C. and Kevin, T. (2009). *Evaluation of the New ASTER Global Digital Elevation Model*. Available online at: http://earth-info.nga.mil/GandG/elevation/.

Smith, D. and Wischmeier, W. (1957). Factors affecting sheet and rill erosion. *Transactions, American Geophysical Union*, 38, pp.889--896.

Smith, H., Blackstock, K., Wall, G. and Jeffrey, P. (2014). River basin management, development planning, and opportunities for debate around limits to growth. *Journal of Hydrology, http://dx.doi.org/10.1016/j.jhydrol.2014.04.022*.

Smith, M. (2010). Digital elevation models for research: UK datasets, copyright and derived products. *Geological Society, London, Special Publications*, 345(1), pp.129-133.

Smith, M., Rose, J. and Booth, S. (2006). Geomorphological mapping of glacial landforms from remotely sensed data: An evaluation of the principal data sources and an assessment of their quality. *Geomorphology*, 76(1), pp.148--165.

Soille, P. (2007). From Mathematical Morphology to Morphological Terrain Features. In: R. Peckham and G. Jordan, ed., *Digital Terrain Modelling*, 1st ed. Berlin: Springer, pp.45 - 66.

Soille, P., Vogt, J. and Colombo, R. (2003). Carving and adaptive drainage enforcement of grid digital elevation models. *Water Resources Research*, 39(12), p.1366.

Sonneveld, B. and Nearing, M. (2003). A nonparametric/parametric analysis of the Universal Soil Loss Equation. *Catena*, 52(1), pp.9--21.

Sorensen, R. and Seibert, J. (2007). Effects of DEM resolution on the calculation of topographical indices: TWI and its components. *Journal of Hydrology*, 347(1), pp.79--89.

Stocking, M., O'Riordan, T. and others, (1995). Soil erosion and land degradation. *Environmental science for environmental management.*, pp.223--242.

Strahler, A. (1952). Hypsometric (area-altitude) analysis of erosional topography. *Geological Society of America Bulletin*, 63(11), p.1117.

Sun, G., Ranson, K., Kharuk, V. and Kovacs, K. (2003). Validation of surface height from shuttle radar topography mission using shuttle laser altimeter. *Remote Sensing of Environment*, 88(4), pp.401--411.

Suri, M., Cebecauer, T., Hofierka, J. and Fulajtar, E. (2002). Soil erosion assessment of Slovakia at a regional scale using GIS. *Ecology (Bratislava)*, 21(4), pp.404 - 422.

Suwandana, E., Kawamura, K., Sakuno, Y., Kustiyanto, E. and Raharjo, B. (2012). Evaluation of ASTER GDEM2 in comparison with GDEM1, SRTM DEM and topographic-map-derived DEM using inundation area analysis and RTK-dGPS data. *Remote Sensing*, 4(8), pp.2419--2431.

Tang, C. and Liu, C. (2009). Surface water hydrologic simulation of Qingshuijiang Watershed based on SRTM DEM. *Journal Of Liaoning Technical University (Natural Science Edition)*, 28(4), pp.652-655.

Tarboton, D. (1997). A new method for the determination of flow directions and upslope areas in grid digital elevation data. *Water Resources Research*, 33(2), pp.309 - 319.

Tarboton, D., Bras, R. and Rodriguez-Iturbe, I. (1992). A physical basis for drainage density. *Geomorphology*, 5(1), pp.59--76.

Tarboton, D., Bras, R. and Rodriguez-Iturbe, I. (1991). On the extraction of channel networks from digital elevation data. *Hydrological processes*, 5(1), pp.81--100.

Tarolli, P. and Dalla Fontana, G. (2009). Hillslope-to-valley transition morphology: New opportunities from high resolution DTMs. *Geomorphology*, 113(1), pp.47--56.

Teh, S. (2011). *Soil Erosion Modeling using RUSLE and GIS on Cameron Highlands,*

Malaysia for Hydropower Development. A Master´s thesis. RES | The School for Renewable Energy Science.

Terranova, O., Antronico, L., Coscarelli, R. and Iaquinta, P. (2009). Soil erosion risk scenarios in the Mediterranean environment using RUSLE and GIS: an application model for Calabria (southern Italy). *Geomorphology*, 112(3), pp.228--245.

Tetzlaff, B., Friedrich, K., Vorderbrugge, T., Vereecken, H. and Wendland, F. (2013). Distributed modelling of mean annual soil erosion and sediment delivery rates to surface waters. *Catena*, 102, pp.13--20.

Thieler, E., Himmelstoss, E., Zichichi, J. and Ergul, A. (2009). *Digital Shoreline Analysis System (DSAS) version 4.0 - An ArcGIS extension for calculating shoreline change*. U.S. Geological Survey Open-File Report 2008-1278.

Thomas, J., Joseph, S., Thrivikramji, K. and Arunkumar, K. (2014). Sensitivity of digital elevation models: The scenario from two tropical mountain river basins of the Western Ghats, India. *Geoscience Frontiers*, 5(6), pp.893-909.

Thompson, J., Bell, J. and Butler, C. (2001). Digital elevation model resolution: effects on terrain attribute calculation and quantitative soil-landscape modeling. *Geoderma*, 100(1), pp.67--89.

Thuringian State Institute of Agriculture, (2013). *C-factor table - project*. [online] Tll.de. Available at: http://www.tll.de/verstola/content/verstola/methodik/dabag/c-faktor/c-tabelle.html [Accessed Sep. 2013].

Tighe, M. and Chamberlain, D. (2009). Accuracy Comparison of the SRTM, ASTER, NED, NEXTMAP USA Digital Terrain Model over Several USA Study Sites. *ASPRS/MAPPS 2009 Fall Conference November 16-19, 2009 San Antonia, Texas*.

Toutin, T. (2008). ASTER DEMs for geomatic and geoscientific applications: a review. *International Journal of Remote Sensing*, 29(7), pp.1855--1875.

Toy, T., Foster, G. and Renard, K. (2002). *Soil erosion: processes, prediction, measurement and control*. New York: John Wiley & Sons.

Tribe, A. (1992). Automated recognition of valley lines and drainage networks from grid digital elevation models: a review and a new method. *Journal of Hydrology*, 139(1),

pp.263--293.

Trowbridge, S. (2014). *A Comparison of Digital Elevation Models to Accurately Predict Stream Locations*. A Master's thesis. University of Nebraska.

Turcotte, R., Fortin, J., Rousseau, A., Massicotte, S. and Villeneuve, J. (2001). Determination of the drainage structure of a watershed using a digital elevation model and a digital river and lake network. *Journal of Hydrology*, 240(3), pp.225--242.

Twining, S. and Clarke, J. (2009). Future of UK winter oilseed rape production. *Crop Protection Association Agricultural Industries Confederation: ADAS*, 14.

UK Agriculture, (2013). *UK agriculture, farming, food, the countryside*. [online] Available at: http://www.ukagriculture.com/ [Accessed 9 Sep. 2014].

Urai, M., Tachikawa, T. and Fujisada, H. (2012). Data acquisition strategies for ASTER global DEM generation. *ISPRS Annals of Photogrammetry, Remote Sensing and Spatial Information Sciences*, I-4, pp.199--202.

Usery, E., Finn, M., Scheidt, D., Ruhl, S., Beard, T. and Bearden, M. (2004). Geospatial data resampling and resolution effects on watershed modeling: A case study using the agricultural non-point source pollution model. *Journal of Geographical Systems*, 6(3), pp.289--306.

van der Knijff, J., Jones, R. and Montanarella, L. (1999). Soil erosion risk assessment in Italy. *European Soil Bureau, EUR 19022 EN*, p.52.

van der Knijff, J., Jones, R. and Montanarella, L. (2000). Soil erosion risk assessment in Europe. European Soil Bureau. *EUR 19044 EN*, p.36.

Van Rompaey, A., Bazzoff, P., Montanarella, R. and Govers, L. (2003). Validation of soil erosion risk assessments in Italy. *European Soil Bureau Research Report No. 12, EUR 20676EN. Office for Official Publications of the European Communities, Luxembourg*, p.25.

Vaze, J., Teng, J. and Spencer, G. (2010). Impact of DEM accuracy and resolution on topographic indices. *Environmental Modelling & Software*, 25(10), pp.1086--1098.

Verheijen, F., Jones, R., Rickson, R. and Smith, C. (2009). Tolerable versus actual soil

erosion rates in Europe. *Earth-Science Reviews*, 94(1), pp.23--38.

Vianello, A., Cavalli, M. and Tarolli, P. (2009). LiDAR-derived slopes for headwater channel network analysis. *Catena*, 76(2), pp.97--106.

Vieux, B. (1993). DEM aggregation and smoothing effects on surface runoff modeling. *Journal of Computing in Civil Engineering*, 7(3), pp.310--338.

Vieux, B. (2005). *Distributed hydrologic modeling using GIS*. 2nd ed. Dordrecht: Kluwer.

Vliet, L., Wall, G. and Dickinson, W. (1976). Effects of agricultural land use on potential sheet erosion losses in southern Ontario. *Canadian Journal of Soil Science*, 56(4), pp.443--451.

Vogt, J., Colombo, R. and Bertolo, F. (2003). Deriving drainage networks and catchment boundaries: a new methodology combining digital elevation data and environmental characteristics. *Geomorphology*, 53(3), pp.281--298.

Volk, M., Moller, M. and Wurbs, D. (2010). A pragmatic approach for soil erosion risk assessment within policy hierarchies. *Land Use Policy*, 27(4), pp.997--1009.

Vrieling, A. (2006). Satellite remote sensing for water erosion assessment: A review. *Catena*, 65(1), pp.2--18.

Wall, G., Coote, D. and Pringle, E. (2002). *RUSLEFAC - Revised Universal Soil Loss Equation for Application in Canada: A Handbook for Estimating Soil Loss from Water Erosion in Canada*. Ottawa: Research Branch, Agriculture and Agri-Food Canada.

Walling, D. and Amos, C. (1999). Source, storage and mobilisation of fine sediment in a chalk stream system. *Hydrological processes*, 13(3), pp.323--340.

Walling, D. and Quine, T. (1991). Use of 137Cs measurements to investigate soil erosion on arable fields in the UK: potential applications and limitations. *Journal of Soil Science*, 42(1), pp.147--165.

Walling, D., Collins, A., Jones, P., Leeks, G. and Old, G. (2006). Establishing fine-grained sediment budgets for the Pang and Lambourn LOCAR catchments, UK. *Journal of Hydrology*, 330(1), pp.126--141.

Wang, L. and Liu, H. (2006). An efficient method for identifying and filling surface

depressions in digital elevation models for hydrologic analysis and modelling. *International Journal of Geographical Information Science*, 20(2), pp.193--213.

Wang, X. and Yin, Z. (1998). A comparison of drainage networks derived from digital elevation models at two scales. *Journal of Hydrology*, 210(1), pp.221--241.

Warren, S., Hohmann, M., Auerswald, K. and Mitasova, H. (2004). An evaluation of methods to determine slope using digital elevation data. *Catena*, 58(3), pp.215--233.

Warren, S., Mitasova, H., Hohmann, M., Landsberger, S., Iskander, F., Ruzycki, T. and Senseman, G. (2005). Validation of a 3-D enhancement of the Universal Soil Loss Equation for prediction of soil erosion and sediment deposition. *Catena*, 64(2), pp.281--296.

Wass, P., Marks, S., Finch, J., Leeks, G. and Ingram, J. (1997). Monitoring and preliminary interpretation of in-river turbidity and remote sensed imagery for suspended sediment transport studies in the Humber catchment. *Science of the Total Environment*, 194, pp.263--283.

Wechsler, S. (2007). Uncertainties associated with digital elevation models for hydrologic applications: a review. *Hydrology & Earth System Sciences*, 11(4), pp.1481--1500.

Wechsler, S. and Kroll, C. (2006). Quantifying DEM uncertainty and its effect on topographic parameters. *Photogrammetric Engineering and Remote Sensing*, 72(9), p.1081.

Weng, Q. (2002). Quantifying uncertainty of digital elevation models derived from topographic maps. *Springer*, pp.403--418.

Wensum Alliance, (2013). *River Wensum Demonstration Test Catchment Project | Wensum Alliance*. [online] Available at: http://www.wensumalliance.org.uk [Accessed 11 Mar. 2013].

Weydahl, D., Sagstuen, J., Dick, O. and Ronning, H. (2007). SRTM DEM accuracy assessment over vegetated areas in Norway. *International Journal of Remote Sensing*, 28(16), pp.3513--3527.

Widayati, A., Lusiana, B., Suyamto, D. and Verbist, B. (2004). Uncertainty and effects of resolution of digital elevation model and its derived features: case study of Sumberjaya, Sumatera, Indonesia. *Int. Arch. of Photogrammetry and Remote Sensing*, 35, pp.1013--

1018.

Wilson, J. (2012). Digital terrain modeling. *Geomorphology*, 137(1), pp.107--121.

Wilson, J. and Gallant, J. (2000). *Terrain analysis: Principles and Applications*. New York: Wiley.

Wilson, J., Aggett, G., Deng, Y. and Lam, C. (2008). Water in the Landscape: A Review of Contemporary Flow Routing Algorithms. In: Q. Zhou, B. Lees and G. Tang, ed., *Advances in Digital Terrain Analysis*, 1st ed. Berlin: Springer, pp.213 - 236.

Wischmeier, W. and Smith, D. (1978). Predicting rainfall erosion losses: A guide to conservation planning. *Agricultural Handbook 537. U.S. Department of Agriculture, Science and Education Administration, Washington, DC*.

Wise, S. (1998). Digital terrain models - traps for the unwary. In Proceedings of the 3rd International Conference on GeoComputation '98 .University of Bristol, UK, pp. 1--18.

Wise, S. (2000). Assessing the quality for hydrological applications of digital elevation models derived from contours. *Hydrological processes*, 14(11-12), pp.1909--1929.

Wise, S. (2007). Effect of differing DEM creation methods on the results from a hydrological model. *Computers & Geosciences*, 33(10), pp.1351--1365.

Wise, S. (2008). The Accuracy of Gridded Digital Elevation Models Interpolated to Higher Resolution. In: *GIS Research UK 2008 16th Annual Conference*. Manchester Metropolitan University.

Wolock, D. and McCabe, G. (1995). Comparison of single and multiple flow direction algorithms for computing topographic parameters in TOPMODEL. *Water Resources Research*, 31(5), pp.1315--1324.

Wu, S., Li, J. and Huang, G. (2005). An evaluation of grid size uncertainty in empirical soil loss modeling with digital elevation models. *Environmental Modeling & Assessment*, 10(1), pp.33--42.

Wu, S., Li, J. and Huang, G. (2007). Modeling the effects of elevation data resolution on the performance of topography-based watershed runoff simulation. *Environmental Modelling & Software*, 22(9), pp.1250--1260.

Wu, S., Li, J. and Huang, G. (2008a). A study on DEM-derived primary topographic attributes for hydrologic applications: sensitivity to elevation data resolution. *Applied Geography*, 28(3), pp.210--223.

Wu, S., Li, J. and Huang, G. (2008b). Characterization and evaluation of elevation data uncertainty in water resources modeling with GIS. *Water resources management*, 22(8), pp.959--972.

Yang, M., Li, X., Hu, Y. and He, X. (2012). Assessing effects of landscape pattern on sediment yield using sediment delivery distributed model and a landscape indicator. *Ecological Indicators*, 22, pp.38--52.

Zandbergen, P. (2006). The effect of cell resolution on depressions in digital elevation models. *Applied GIS*, 2(1), pp.4(1)-4(16).

Zhang, J. and Goodchild, M. (2002). *Uncertainty in geographical information*. London: Taylor & Francis.

Zhang, J., Chang, K. and Wu, J. (2008). Effects of DEM resolution and source on soil erosion modelling: a case study using the WEPP model. *International Journal of Geographical Information Science*, 22(8), pp.925--942.

Zhang, W. and Montgomery, D. (1994). Digital elevation model grid size, landscape representation, and hydrologic simulations. *Water resources research*, 30(4), pp.1019--1028.

Zhang, W., Zhang, Z., Liu, F., Qiao, Z. and Hu, S. (2011). Estimation of the USLE cover and management factor C using satellite remote sensing: A review. *IEEE Conference Publications, 19th International Conference on Geoinformatics*, pp.1--5.

Zhang, X., Drake, N., Wainwright, J. and Mulligan, M. (1999). Comparison of slope estimates from low resolution DEMs: scaling issues and a fractal method for their solution. *Earth Surface Processes and Landforms*, 24(9), pp.763--779.

Zhang, X., Zhang, Y., Wen, A. and Feng, M. (2003). Assessment of soil losses on cultivated land by using the 137Cs technique in the Upper Yangtze River Basin of China. *Soil and Tillage Research*, 69(1), pp.99--106.

Zhou, Q. and Liu, X. (2004). Analysis of errors of derived slope and aspect related to DEM

data properties. *Computers & Geosciences*, 30(4), pp.369--378.

Zhou, Q. and Liu, X. (2008). Assessing Uncertainties in Derived Slope and Aspect from a Grid DEM. In: Q. Zhou, B. Lees and G. Tang, ed., *Advances in Digital Terrain Analysis*, 1st ed. Berlin: springer, pp.279 - 306.

Zhou, Q., Lees, B. and Tang, G. (2008). *Advances in digital terrain analysis*. Berlin: Springer-Verlag.

APPENDIX 1: Suspended Sediment – Turbidity Relationship

Stage - Discharge Relationship: mini-catchment A

$y = 0.3946x^{2.4868}$
$R^2 = 0.9779$

$y = 0.237x - 0.0405$
$R^2 = 0.9747$

◆ EM

Suspended Solids-Turbidity Relationship: Site A

$y = 1.3966x$
$R^2 = 0.762$

$y = 1.4735x^{0.9798}$
$R^2 = 0.8578$
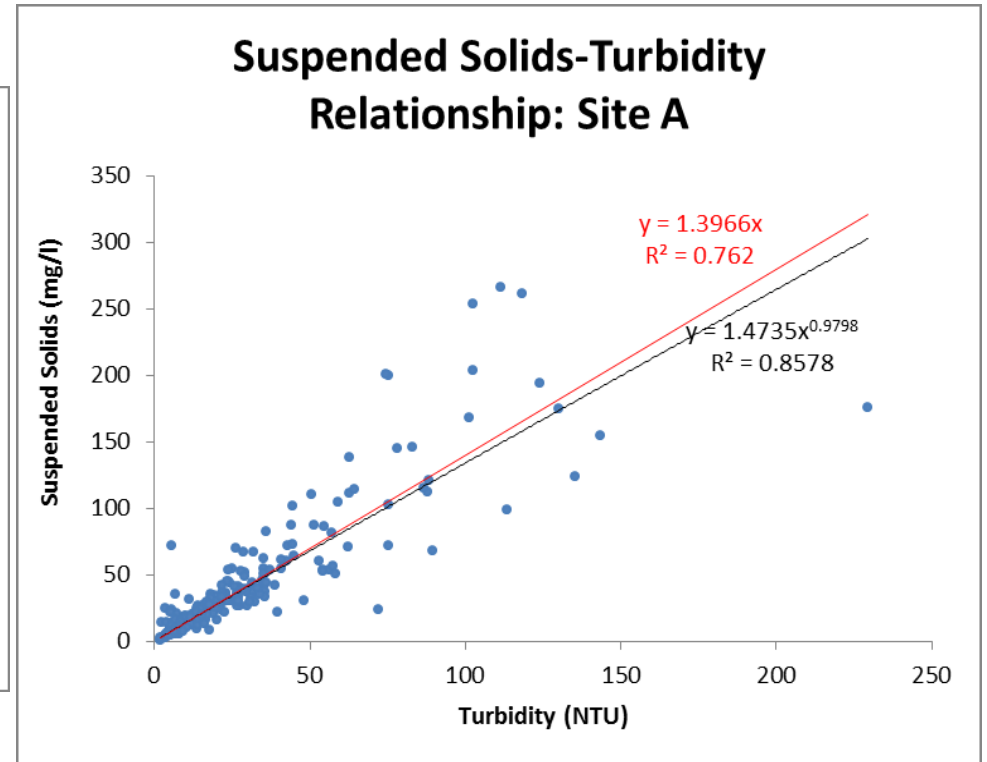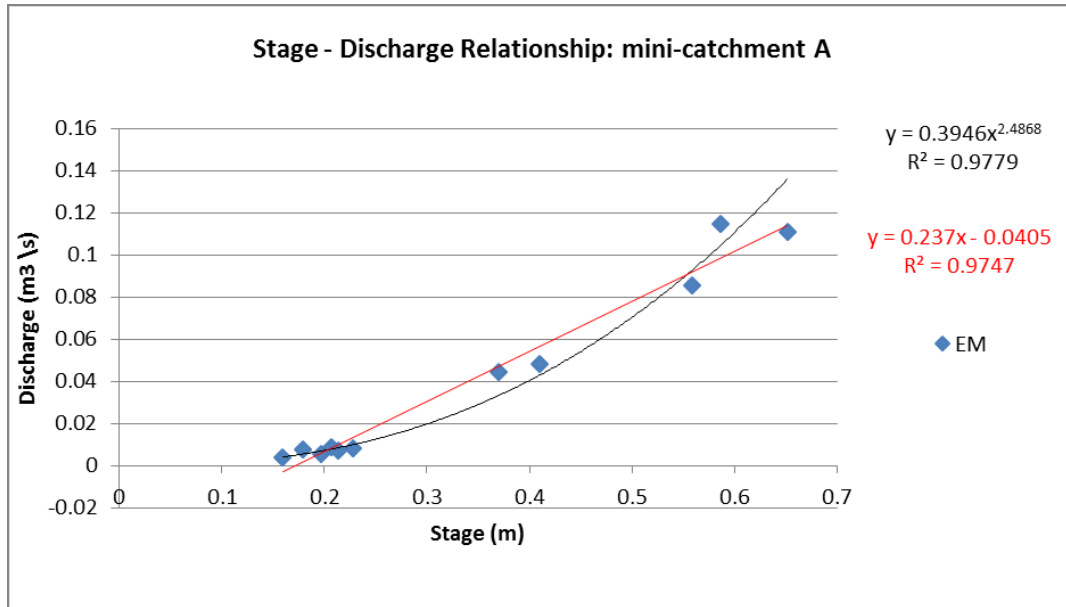
Conversion of Turbidity to TSS and Stage to Discharge and then the calculation of total sediment loss for April 2012, mini-catchment A										
Date/time	Stage (m)	Discharge (m3/s)	Discharge (l/s)	Turbidity	TSS (mg/l)	Filter	Load (kg/hour)	Total Load (kg)	Total load (tonne)
01/04/2012 00:00	0.20788	0.007937683	7.9376825	6.8	9.639230662	1	0.275447349	1503.527109	1.503527109
01/04/2012 01:00	0.20788	0.007937683	7.9376825	7	9.916928906	1	0.283382759		
01/04/2012 02:00	0.20788	0.007937683	7.9376825	3.5	5.02837907	1	0.143689236		
01/04/2012 03:00	0.20665	0.0078214	7.821400009	4.3	6.152087914	1	0.173224586		
01/04/2012 04:00	0.20665	0.0078214	7.821400009	3.7	5.309751416	1	0.149506883		
01/04/2012 05:00	0.20299	0.007481437	7.481437024	3.7	5.309751416	1	0.143008455		
01/04/2012 06:00	0.20421	0.007593755	7.593754939	4	5.731239003	1	0.156677848		
01/04/2012 07:00	0.20482	0.00765029	7.650289506	3	4.323480908	1	0.11907317		
01/04/2012 08:00	0.20604	0.007764112	7.764111678	3.1	4.464638786	1	0.124790235		
01/04/2012 09:00	0.20452	0.007622454	7.62245429	5.3	7.550846423	1	0.207201534		
01/04/2012 11:00	0.20604	0.007764112	7.764111678	4.7	6.712304061	1	0.187614282		
01/04/2012 12:00	0.20726	0.00787894	7.878940321	3.9	5.590816551	1	0.158578956		
01/04/2012 13:00	0.20971	0.008112591	8.11259058	4.5	6.432321767	1	0.187858055		
01/04/2012 14:00	0.20604	0.007764112	7.764111678	3.2	4.605704697	1	0.12873314		
01/04/2012 15:00	0.20757	0.007908279	7.908278802	2.6	3.757863723	1	0.106985642		
⋮	⋮	⋮	⋮	⋮	⋮	⋮	⋮		
30/04/2012 16:00	0.66667	0.143965602	143.9656021	7.4	10.47184919	1	5.427309866		
30/04/2012 17:00	0.66361	0.142327931	142.3279306	4.5	6.432321767	1	3.295796566		
30/04/2012 18:00	0.65324	0.136861106	136.8611061	4.2	6.011872963	1	2.962049701		
30/04/2012 19:00	0.64591	0.133073884	133.0738836	5.5	7.829923219	1	3.751049847		
30/04/2012 20:00	0.64072	0.130430681	130.4306808	4.5	6.432321767	1	3.020299587		
30/04/2012 21:00	0.63339	0.126751477	126.7514765	4.4	6.292237006	1	2.871181192		
30/04/2012 22:00	0.62882	0.124489407	124.4894072	4.3	6.152087914	1	2.757131198		
30/04/2012 23:00	0.62515	0.122690427	122.690427	3.9	5.590816551	1	2.469382811		